Synthesis, characterization and evaluation of antibacterial, antidiabetic and toxicological profiles of newly-derived therapeutic agents

by

Ramesh Gannimani

Dissertation presented for the degree of

Doctor of Philosophy (Biochemistry)

at

University of KwaZulu-Natal

School of Life Sciences

College of Agriculture, Engineering and Science

February 2016

Supervisor: Dr Patrick Govender

Co-Supervisor: Dr Karen Pillay

DECLARATIONS

Form EX1-5

COLLEGE OF AGRICULTURE, ENGINEERING AND SCIENCE

DECLARATION 1 - PLAGIARISM

I, Ramesh Gannimani declare that

1. The research reported in this thesis, except where otherwise indicated, is my original research.

2. This thesis has not been submitted for any degree or examination at any other university.

3. This thesis does not contain other persons' data, pictures, graphs or other information, unless specifically acknowledged as being sourced from other persons.

4. This thesis does not contain other persons' writing, unless specifically acknowledged as being sourced from other researchers. Where other written sources have been quoted, then:

a. Their words have been re-written but the general information attributed to them has been referenced

b. Where their exact words have been used, then their writing has been placed in italics and inside quotation marks, and referenced.

5. This thesis does not contain text, graphics or tables copied and pasted from the Internet, unless specifically acknowledged, and the source being detailed in the thesis and in the References sections.

Signed G. Ramesh

……

Declaration Plagiarism 22/05/08 FHDR Approved

COLLEGE OF AGRICULTURE, ENGINEERING AND SCIENCE

DECLARATION 2 - PUBLICATIONS

Publication 1

Ramesh Gannimani, Amanda Perumal, Suresh Babu Naidu Krishna, Sershen, Karen Muthusamy, Ajay Mishra, Patrick Govender. **Synthesis of silver and gold nanoparticles using aqueous seed extract of *Portorhus longifolia* as a green reducing agent and evaluation of antibacterial activity**. *Digest Journal of Nanomaterials and Biostructures,* 9, 4, (2014), 1669-1679.

Contributions: The candidate conceptualized the research plan, synthesized and characterized the nanoparticles, and compiled the initial manuscript. Ramesh Gannimani and Amanda Perumal used scanning electron microscopy for morphological characterization of nanoparticles. The candidate together with Suresh Babu Naidu performed the antibacterial studies. All other authors fulfilled the role of supervisor.

Publication 2

Ramesh Gannimani, Amanda Perumal, Muthusamy Ramesh, Karen Pillay, Mahmoud E. Soliman and Patrick Govender. **Antipyrine–gamma cyclodextrin inclusion complex: Molecular modeling, preparation, characterization and cytotoxicity studies***, Journal of Molecular Structure*, 1089 (2015) 38–47.

Contributions: The candidate conceptualized the research idea, synthesized and characterized inclusion complex, and prepared the initial version of the paper. The candidate and Amanda Perumal generated the cytotoxicity data. In addition, Ramesh Gannimani collaborated with Muthusamy Ramesh for the computational modelling aspect of this paper. All other co-authors fulfilled a supervisory role.

Publication 3

Ramesh Gannimani, Muthusamy Ramesh, Sphamandla Mtambo, Karen Pillay, Mahmoud E. Soliman and Patrick Govender, **γ-Cyclodextrin capped silver nanoparticles for molecular recognition and enhancement of antibacterial activity of chloramphenicol**, *Journal of Inorganic Biochemistry,* 157 (2016) 15–24

Contributions: The candidate conceptualized the research strategy, synthesized and characterized all the compounds, and prepared the paper. Muthusamy Ramesh assisted Ramesh Gannimani with the computational studies presented in this paper. In addition, the candidate together with Sphamandla Mtambo finalized the antibacterial studies. All other co-authors fulfilled a supervisory role.

Publication in Preparation 1

Ramesh Gannimani, Karen Pillay and Patrick Govender. **Investigation of 3, 5-dicyanopyridine scaffolds as antidiabetic and antibacterial agents** is being prepared for submission to the journal of *Medicinal Chemistry Research*.

Contributions: The candidate conceptualized the research strategy, synthesis, characterization of all the compounds, antibacterial and antidiabetic analysis and, preparation of the final manuscript. In addition, the candidate together with Sphamandla Mtambo finalized the antibacterial studies. All other co-authors fulfilled a supervisory role.

Publication in Preparation 2

Ramesh Gannimani, Karen Pillay, Patrick Govender. **Pharmaceutical salts of fluoroquinolones with quinic acid,** is being prepared for submission to the *Journal of Pharmaceutical and Biomedical Analysis*.

Contributions: The candidate conceptualized the research strategy, synthesis, characterization of the compounds, cytotoxicity analysis and preparation of the final manuscript. All other co-authors fulfilled a supervisory role.

Signed:…….. Date:22/08/2016……..

I, Dr Patrick Govender as supervisor of the PhD study hereby consent to the submission of this PhD Thesis.

Signed: Date: 22/08/2016

SUMMARY

Therapeutic agents are an integral part of life as we are faced with a myriad of health problems that range from inherent conditions such as diabetes to being afflicted by invading organisms such as bacteria. A major drawback of current pharmaceutical agents to treat these conditions is that they have a limited timescale as they become ineffective due to toxicity and in the case of bacterial infection, resistance often develops. To counteract this scenario, pharmaceutical research is faced with the arduous task of continuously developing cost-effective therapeutic agents that display high bio-efficacies against these pathologies.

The advent of nanoscience has broadened the area of drug discovery research. The exceptional physicochemical properties of nanoparticles make them one of the most interesting and promising agents in medicine. Nanomedicine based on noble metal nanoparticles have attracted much interest recently and there is a demand for the new biocompatible nanoparticle with pharmaceutical applications. Metal nanoparticles in combination with plant extracts have gained much importance for medicinal application. For this reason, we explored the synthesis of silver and gold nanoparticles using medicinal plants indigenous to South Africa, and their application as antibacterial agents. Silver and gold nanoparticles were synthesized using an aqueous seed extract of *Protorhus longifolia* as both reducing and capping agent. The nanoparticles were characterized and evaluated for antibacterial properties against both Gram-positive and -negative bacteria. The nanoparticles displayed antibacterial activity against *Escherichia coli* (ATCC 35218), *Klebsiella pneumoniae* (ATCC 700603), *Staphylococcus aureus* (ATCC 43300) and *Pseudomonas aeruginosa* (ATCC 27853).

Heterocyclic molecules belonging to the class pyridine with 2-amino-4-aryl-6-sulfanyl substitution pattern has drawn much attention currently for a variety of biological activities. Considering the importance of these pyridine compounds in the medical field, we have synthesized several pyridine molecules in a one pot multi-component approach. These compounds were screened for their antibacterial potential but did not show good activity. However, since this class of compounds has also been shown to have promise as α-glucosidase inhibitors, they were tested for antidiabetic properties. Among the derivatives that were prepared, compounds containing aromatic substitution at position 6 of the pyridine ring were found to be potential α-glucosidase inhibitors. In support of the enzymatic inhibition data, molecular docking studies with the α-glucosidase enzyme also confirmed that best affinity towards the enzyme occurred when there was aromatic substitution at position 6 of the pyridine ring instead of the aliphatic substitution. Importantly, this study is the first to report 2-amino-

4-aryl-6-sulfanyl pyridine compounds as potential α-glucosidase inhibitors and thereby provides a viable avenue in the generation of new antidiabetic compounds.

Drug discovery is expensive and time-consuming field. Finding new drug candidates is not enough as many potential drug candidates with attractive bioactivities are deemed unsuitable as feasible mainstream therapeutic agents, due to their poor pharmaceutical properties such as poor solubility, permeability and tolerability. Hence, along with the discovery and development of new drugs, focusing on novel strategies promotes rapid implementation of modified drugs developed from current candidates that have become ineffective through microbial resistance.

Cyclodextrins (CD) and their derivatives are important pharmaceutical excipients which can decrease side effects of drugs by encapsulating them in a sugar skeleton. We studied the inclusion phenomena of chloramphenicol with different cyclodextrins using molecular docking and molecular dynamics to identify the most suitable polymer for their encapsulation. Chloramphenicol was found to form stronger inclusion complexes with γ-CD than α-CD and β-CD. Encapsulation phenomena of chloramphenicol with γ-CD, a nanocomposite constituting of chloramphenicol and γ-CD capped silver nanoparticles was synthesized. The surface enhanced Raman spectroscopy (SERS) data confirmed the molecular recognition of chloramphenicol by cyclodextrin capped silver nanoparticles. The stability of the nanoparticle before and after loading with the drug chloramphenicol was determined from zeta potential analysis. The antibacterial activities displayed against *Pseudomonas aeruginosa* (ATCC 27853), *Enterococcus faecalis* (ATCC 5129), *Klebsiella pneumoniae* (ATCC 700603) and *Staphylococcus aureus* (ATCC 43300) confirmed the synergistic antibacterial effect of chloramphenicol with γ-cyclodextrin capped silver nanoparticles. The data seems to suggest that organic inorganic hybrid molecules obtained by loading chloramphenicol on cyclodextrin capped nanoparticles by means of non-covalent interactions enhances the antibacterial activity of chloramphenicol. Importantly, this combination strategy resulted in the use of lower concentrations of chloramphenicol thereby minimizing its side effects.

In a proof of concept approach given that cyclodextrin complexion has been shown to result in controlled release which directly affects drug efficacy, inclusion phenomena of the anti-inflammatory drug antipyrine, with different cyclodextrins was studied by computational and experimental methods. The supramolecular inclusion complexes of these drugs with γ-CD were prepared by a freeze-drying method and characterized using solid state characterization techniques such as thermogravimetric analysis, differential scanning calorimetry, X-ray diffraction, Fourier transform infrared spectroscopy (FTIR) and scanning electron microscopy

(SEM). We were also able to prove the phenomena of inclusion complexation using NMR techniques. Results from 1H NMR and 2D NOESY studies supported the mode of inclusion phenomenon obtained from theoretical calculations. In addition, we were able to show that the antipyrine inclusion complex is nontoxic against the mammalian MDCK-1 cell line.

Solubility of a therapeutic agent is another important factor which contributes to its pharmacokinetic properties such as absorption and bioavailability. The solubility of weakly basic or acidic drug substances can be increased by converting the therapeutic molecules to salts using various organic and inorganic counter ions. The use of organic counter ions is preferred in that they can simultaneously increase the solubility and transport of drug substances across the absorbing membrane. In this research work we also synthesized novel organic salts of ciprofloxacin and norfloxacin using biocompatible quinic acid. The salts were characterized by spectroscopic techniques like FTIR-ATR, NMR and mass spectrometry followed by thermal analysis (DSC and TGA) and X-ray diffraction. Solubility and octanol-water partition coefficients were analyzed. The cytotoxicity studies using the VERO cell lines indicated that salts were biocompatible. This study contributes to the importance of salt formation chemistry in the pharmaceutical applications in terms of rational design and development of innovative salt forms of drug candidates to overcome solubility issues while limiting toxic side effects.

ACKNOWLEDGEMENTS

I wish to express my sincere gratitude and appreciation to the following people and institutions:

I express my sincere thanks to ***Dr. Patrick Govender*** for giving me the great opportunity to work in his research group. I thank him very much for always having an open door for me, for standing by me during all hardships, for many valuable advices and constructive criticism throughout my research work.

I extend my sincere thanks to my co supervisor ***Dr. Karen Pillay*** for providing sufficient support with manuscript and thesis writing and for many valuable discussions throughout my research work.

My sincere thanks to University of KwaZulu-Natal for providing necessary laboratory facilities to carry out this work

It was a great pleasure working with ***Njabulo, Spha, Lethu, Shaun, Mellissa, Kamini, Jerushka*** and ***Anushka***. Thank you all for all the assistance and friendly environment.

I express my special thanks to ***Mr. Dinesh Jagganath***, ***Mrs Nirasha Nundkumar***, ***Mr. Dilip Jagjivan, Mr. Neal Keith Broomhead, Mr. Gregory Moodley***, ***Mr. Miler Nundkumar, and Mr. Raj Sumaro*** for all their valuable support, throughout the course of this work.

I would like to take the opportunity to thank ***Dr. Jaya Lakkakula, Dr. Swamy, Dr. Ramesh Niadu, Dr. Suhas Ramesh, Dr. Mahadev, Dr. Ramakrishna, Dr. Raana and Dr. Ram Gopal*** for sharing knowledge, answering my queries and for the encouragement to fulfill my research work.

I am pleased to thank all my friends ***Mahesh, Ganesh, Pramod, Suhas, Deeksha, Mayur, Jaipal*** who extended their support, encouragement, and appreciation throughout my research work.

I would like to extend special appreciation to my parents, ***Mr. Krishnamurthy G and Mrs. Ratnam*** for their endless support, love and selfless sacrifices.

Finally, I would like to acknowledge almighty God for giving me the strength and courage to successfully finish this journey.

PREFACE

This dissertation is presented as a compilation of seven chapters.

Chapter 1	**Introduction**
Chapter 2	**Literature Review**
Chapter 3	**Synthesis and antibacterial activity of silver and gold nanoparticles produced using aqueous seed extract of *protorhus longifolia* as a reducing agent**
Chapter 4	**Investigation of 3, 5-Dicyanopyridine scaffolds as antidiabetic and antibacterial agents**
Chapter 5	**γ-cyclodextrin capped silver nanoparticles for molecular recognition and enhancement of antibacterial activity of Chloramphenicol**
Chapter 6	**Quinic acid based organic salts of ciprofloxacin and norfloxacin: Synthesis, characterization and cytotoxicity studies**
Chapter 7	**General Discussion and Conclusion**
Appendix 1	**Antipyrine-gamma cyclodextrin inclusion complex: Molecular modeling, preparation, characterization and cytotoxic studies**
Appendix 2	**Supplementary information for Chapter 4**
Appendix 3	**Supplementary information for Chapter 6**

CONTENTS

ABBREVIATIONS

AgNPs	Silver nanoparticle
AuNPs	Gold nanoparticles
AMBER	Assisted model building with energy refinement
AM1	Austin model 1
ANOVA	One-way analysis of variance
ATCC	American Type Culture Collection
ATR-FTIR	Attenuated total reflectance-Fourier transform infrared
CCD	Charged couple device
CMP	Chloramphenicol
CD	Cyclodextrin
CDs	Cyclodextrins
α-CD	alpha cyclodextrin
β-CD	beta cyclodextrin
γ-CD	gamma cyclodextrin
CDAgNPs	Cyclodextrin capped silver nanoparticles
^{13}C NMR	Carbon-13 nuclear magnetic resonance spectroscopy
°C	Degrees Celsius
CDCl3	Deuterated chloroform
COSY	Correlated nuclear magnetic resonance spectroscopy
DSC	Differential scanning calorimetry
d	Doublet
dd	Double doublet
DLS	Dynamic light scattering
DMSO	Dimethyl sulfoxide
DMSO-d6	Deuterated dimethyl sulfoxide
2D NMR	Two-dimensional nuclear magnetic resonance
EDX	Energy dispersive X-ray analysis
FTIR	Fourier transform infrared spectroscopy
h	hour
HSQC	Heteronuclear single quantum coherence
HCl	Hydrochloric acid
HMBC	Heteronuclear multiple bond coherence

HNO_3	Nitric acid
HRMS	High resolution mass spectrometry
HRTEM	High resolution transmission electron microscopy
HSQC	Heteronuclear multiple quantum coherence
^1H NMR	Proton nuclear magnetic resonance spectroscopy
m	Multiplet
MCF-7	Human adenocarcinoma cells
MDCK	Madin Darby canine kidney epithelial cells
MD	Molecular dynamics
MIC	Minimum inhibitory concentration
MM–PBSA	Molecular mechanics–Poisson–Boltzmann surface Area
µL	Micro-liters
µM	Micro Molar
mL	Milliliters
MS	Mass spectra
MTT	3-(4,5-dimethylthiazol-2-yl)-2,5-diphenyltetrazolium bromide
NMR	Nuclear magnetic resonance
NOESY	Nuclear overhauser effect spectroscopy
NCCLS	National committee for clinical laboratory standards
PBS	Phosphate buffer saline
P-XRD	Powder X-ray diffraction
PDB	Protein data bank
RMSD	Root mean square deviation
s	Singlet
SEM	Scanning electron microscopy
SAED	Selected area diffraction
t	Triplet
TEM	Transmission electron microscopy
TLC	Thin Layer chromatography
TGA	Thermogravimetric analysis
UV	Ultraviolet spectroscopy
WHO	World health organization

LIST OF FIGURES

LIST OF TABLES

Chapter 1

INTRODUCTION AND PROJECT AIMS

1 Introduction and Project Aims

1.1 Introduction

The need for novel pharmaceutical compounds to treat human diseases is ever increasing [1], and medicinal compounds can be compiled from a variety of sources. Plant materials are the traditional sources of medicinal compounds [2]. Designing, synthesizing and creating a library of the compounds in the laboratory is another commonly used approach in identifying novel compounds [3]. Along with the development of new medicines, finding new strategies to improve the current existing treatments is an important aspect of modern drug discovery research [4]. In view of the cost and strain involved in the new drug development, modern drug discovery research is increasingly focusing on further modifying, improving and finding new formulation of existing pharmacologically active compounds [4, 5]. The approach is attractive and helpful in quick development of new treatments. This thesis aims to identify new potentially promising sources for medical applications and finding new formulation strategies for the improvement of existing therapies.

1.2 Objectives and scope of study

The central aim of this study was to develop novel and/or improve currently available antibacterial pharmaceutical candidates. The main objectives of this research study are as follows:

a. Green synthesis of silver and gold nanoparticles (AgNPs and AuNPs respectively) capped with phytochemicals extracted from a South African indigenous medicinal plant, and their evaluation as antibacterial agents.
b. Synthesis of multi-substituted pyridine derivatives bearing a 2-amino-4-aryl-6-sulfanyl substitution pattern via a one-pot reaction approach and evaluation of their antibacterial activities. Since similar molecules have shown good antidiabetic properties, these molecules were also investigated foe their α-glucosidase inhibitory activity.
c. Synthesis of and study of chloramphenicol-loaded, cyclodextrin capped silver nanomaterials as an innovative method for the improvement of antibacterial efficacy of chloramphenicol. The multi-spectrum versatility of this strategy to improve other pre-existing pharmaceutical preparations was assessed using the anti-inflammatory agent antipyrine.

d. Synthesis of quinic acid based organic salts of fluoroquinolones to improve their pharmacological properties as antibacterial agents.

This thesis is divided into seven chapters, including this introductory **Chapter 1.** In **Chapter 2**, a detailed literature review is presented.

Chapter 3 describes the synthesis of silver and gold nanoparticles from the aqueous seed extract of *Protorhus longifolia* and evaluation of their antibacterial activity. These nanoparticles that bear natural medicinal compounds capped to their surfaces, showed potential antibacterial activity against bacterial species *Escherichia coli* (ATCC 35218), *Klebsiella pneumoniae* (ATCC 700603), *Staphylococcus aureus* (ATCC 43300) and *Pseudomonas aeruginosa* (ATCC 27853). Novel plant-derived nanomaterials generated in this study, could provide antibacterial treatments with additional benefits, such as lower toxicity and high potential for combating drug-resistant diseases. This aspect of the study was published in the *Digest Journal of Nanomaterials and Biostructures* [6].

Chapter 4 reports on the synthesis of a novel class of medicinally useful heterocyclic compounds. The synthesized 3,5-dicyanopyridines were characterized by IR, NMR and HRMS. Inhibition of α-glucosidase and the antibacterial activities of the molecules were then evaluated. Although no antibacterial activity was detected, interestingly five of the nine compounds showed good inhibition of α-glucosidase which was closely aligned to the commercially available inhibitor, acarbose. Compounds were studied for their binding affinity for the active site of α-glucosidase enzyme. Computational modeling studies revealed that the newly designed heterocycles were effective in binding to the active site of α-glucosidase thereby providing a seemingly useful synthetic pathway that may yield even more potent anti-diabetic molecules.

Chapter 5 describes the application of cyclodextrins in the conjugation and formulation of the antibacterial drug chloramphenicol with silver nanoparticles. Cyclodextrins, which an important class of supramolecules capable of encapsulating hydrophobic drugs into their cavities; provide novel applications in pharmaceutical fields in improving the therapeutic value of drug substances. In this study, a suitable cyclodextrin that encapsulates chloramphenicol was selected using a combination approach that includes molecular docking, semi-empirical and molecular dynamics. Based on the docking score and binding free energies γ-cyclodextrin

inclusion complexes of chloramphenicol were found to be more stable as compared to α- and β-cyclodextrin inclusion complex of chloramphenicol. In addition γ-cyclodextrin capped silver nanoparticles were synthesized and used to generate a nanocomposite with chloramphenicol. The nanocomposite has produced synergistic antibacterial effect against *Pseudomonas aeruginosa* (ATCC 27853), *Enterococcus faecalis* (ATCC 5129), *Klebsiella pneumoniae* (ATCC 700603) and *Staphylococcus aureus* (ATCC 43300). This aspect of the research study was published in *Journal of Inorganic Biochemistry* [7].

In addition, since cyclodextrin complexion has been shown to result in controlled release that directly affects drug efficacy, inclusion phenomena of the anti-inflammatory drug antipyrine with different cyclodextrins was studied by computational and experimental methods. Interestingly, the inclusion complex was found to be non-toxic towards the MDCK-1 cell line, highlighting its potentially safe pharmaceutical application. The aspects of this research have been accepted for publication in *Journal of Molecular Structure* [8] and presented as additional work in this thesis as **Appendix 1**.

Chapter 6 highlights the importance of salt formation chemistry in the pharmaceutical industry. The solubility of the pharmaceutical substances is a key determinant of its bioavailability. Many novel pharmaceutically active compounds fail at clinical trials due to limited solubility. In chapter 6 we demonstrated the application of quinic acid in increasing the solubility of antibacterial drugs ciprofloxacin and norfloxacin by salt formation chemistry. The novelty aspect of this study is that organic salts generated have increased the solubility of the drug substances whilst keeping their lipophilicity higher when compared to their respective salts with inorganic acids. Thus we propose higher membrane permeability of the organic salts based on ion pairing mechanism. Additionally, it was found that quinic acid was not toxic and when used as a counter ion did not increase the toxicity of drug substances. Hence we also propose further studies for development of new combination therapy based on salt formation chemistry.

Finally, **Chapter 7** presents a general discussion, conclusion, and ideas on future research concepts.

1.3 References

[1] J. Bérdy, Thoughts and facts about antibiotics: where we are now and where we are heading, The Journal of Antibiotics, 65 (2012) 385-395.

[2] M.J. Balunas, A.D. Kinghorn, Drug discovery from medicinal plants, Life Sciences, 78 (2005) 431-441.

[3] S. Jain, I. Rathish, R. Sankaran, A review on current industrial trends for synthesis of medicinal compounds, International Journal of Pharmacy and Pharmaceutical Science, 5 (2013) 33-45.

[4] T.T. Ashburn, K.B. Thor, Drug repositioning: identifying and developing new uses for existing drugs, Nature reviews Drug Discovery, 3 (2004) 673-683.

[5] S. Kalepu, V. Nekkanti, Insoluble drug delivery strategies: review of recent advances and business prospects, Acta Pharmaceutica Sinica B, 5 (2015) 442-453.

[6] R. Gannimani, A. Perumal, S. Krishna, Sershen, K. Muthusamy, A. Mishra, P. Govender, Synthesis and antibacterial activity of silver and gold nanoparticles produced using aqueous seed extract of *protorhus longifolia* as a reducing agent, Digest Journal of Nanomaterials and Biostructures, 9 (2014) 1669-1679.

[7] R. Gannimani, M. Ramesh, S. Mtambo, K. Pillay, M.E. Soliman, P. Govender, γ-cyclodextrin capped silver nanoparticles for molecular recognition and enhancement of antibacterial activity of chloramphenicol, Journal of Inorganic Biochemistry, 157 (2016) 15-24.

[8] R. Gannimani, A. Perumal, M. Ramesh, K. Pillay, M.E. Soliman, P. Govender, Antipyrine–gamma cyclodextrin inclusion complex: Molecular modeling, preparation, characterization and cytotoxicity studies, Journal of Molecular Structure, 1089 (2015) 38-47.

Chapter 2

LITERATURE REVIEW

2 Literature Review

2.1 Introduction

In recent years, an increase in the incidence of both communicable and non-communicable diseases has become a major health concern [1]. Communicable or contagious diseases are a group of diseases mainly originating from infectious microbial organisms such as bacteria, fungi and viruses and are transmissible directly (from person to person) or indirectly (by a vector). Non-communicable diseases (NCDs) which cannot transfer from person to person include a wide range of ailments such as diabetes, heart disease, cancer and chronic lung diseases mostly affecting different organs of the body [2]. In 2013 an estimated 6.4 million deaths were reported due to infectious diseases and 39 million deaths were due to non-infectious causes. Further, 5.8 million deaths due to infectious diseases and 83 million deaths due to NCDs is expected by 2050 [3].

Another report suggests that NCDs are the leading cause of death worldwide accounting for nearly 63% of all deaths globally in 2008 [4]. There also exists a link between infectious and non-infectious diseases and often prevalence of one kind of disease encourages the onset of other diseases. For example, the prevalence of diabetes increases the chance for *Mycobacterium tuberculosis* infection [5]. Similarly, people infected with HIV and who are on long-term antiretroviral treatment are at higher risk of non-infectious metabolic disorders such as cardiac, renal, gastrointestinal, neurological and psychiatric diseases [6]. In addition, viral infections such as hepatitis B and C have been reported to predispose cancer [7].

Thus both communicable and non-communicable diseases pose a significant burden on global healthcare management systems and society. To meet these ever-pressing challenges demands that continuous investment and research into developing cost-effective treatment protocols are sustained. This literature study strives to provide an all-inclusive account of two medically orientated threats namely bacterial infections and diabetes.

2.2 Bacterial infections

Several bacterial species are becoming an increasingly important cause of invasive infection worldwide [8]. According to the World Health Organization (WHO) reports, 1.5 million people died in 2014 of *Mycobacterium tuberculosis* infections and 48 000 were infected with multidrug-resistance tuberculosis [9]. The other major bacterial infections causing great number of morbidity and mortality worldwide [8]. There is a rapid emergence of bacterial resistance to most of the mainstream antibiotics, creating ineffective therapeutic agents and also making the process of drug discovery more difficult [10]. It is worth noting that despite continuous efforts by global pharmaceutical companies, only two new classes of antibiotics viz oxazolidinone (linezolid) and cyclic lipopeptide (daptomycin) have been introduced into the market in the last decade [11, 12]. Hence, there is a constant and more focused effort needed for the rapid discovery of novel scaffolds to compete with the emergence of bacterial resistance.

2.2.1 Antibiotic scaffolds

Most antibiotics available at present mainly target five bacterial processes such as cell wall biosynthesis (β-lactams, vanomycin, daptomycin), translation (tetracyclines, aminoglycosides, chloramphenicol, oxazolidinones, macrolides, streptogramins, fusidic acid), folic acid biosynthesis (sulfonamides), transcription (rifamycins) and DNA replication (quinolones) [13, 14]. **Fig. 2.1** represents different classes of antibiotics that are either naturally derived or chemically synthesized. Depending on the mode of action, antibiotics are classified as bactericidal (β-lactams, flouroquinolones) since they kill bacteria by disrupting cell wall and bacteriostatic (chloramphenicol, macrolides) as they are responsible for halting bacterial replication by interfering with cell metabolism.

2.2.2 Antibiotic resistance

The antibiotic resistance is increasing globally and many infections are becoming untreatable [10]. As mentioned in 2.2.1 above sections, most of the antibiotics target only five cellular processes in the bacteria, and this limited spectrum of targets contributes to the easy and rapid development of antibiotic resistance [15]. The overuse and misuse of antibiotics is an additional factor contributing to the development of antibiotic resistance [16].

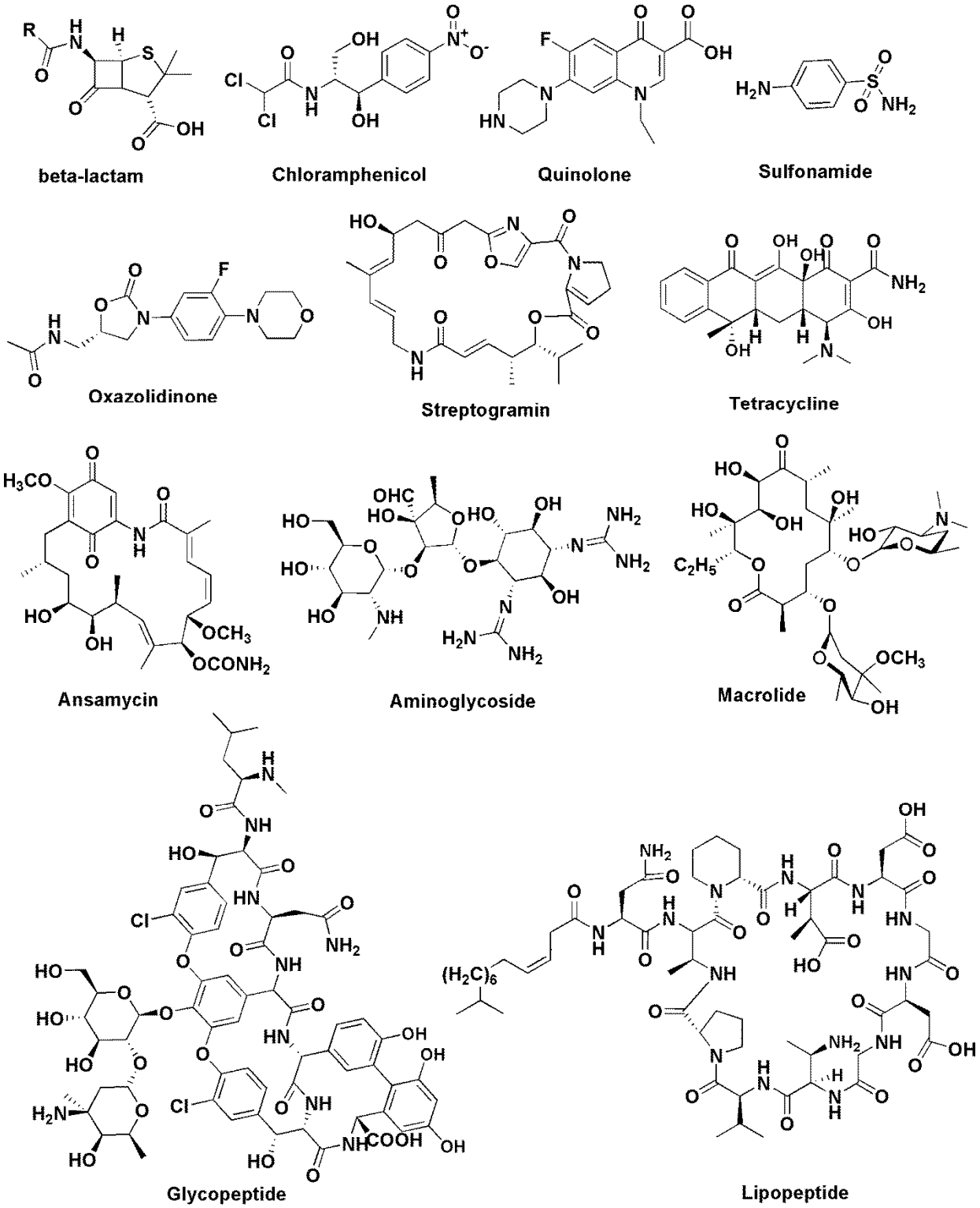

Figure 2.1 General structure of the different classes of antibiotics [17].

Some bacteria are naturally resistant to antibiotics, while others acquire resistance by different mechanisms such as mutations in genes, acquisition of new gene elements encoding for

defensive enzymes and proteins, down regulation of porins that allow the influx of the antibiotics, acquisition of efflux pumps to prevent accumulation of the antibiotic inside the bacteria, and altered cell wall synthesis processes so that antibiotics no longer interfere [18].

Mutations in DNA gyrase enzymes, gyrA and gyrB, results in resistance towards quinolones in *E. coli* and *S. pneumoniae* [19, 20]. Mutations affecting the RNA polymerase β subunit have resulted in the *E.coli* resistance toward rifampicin [21]. Exogenous horizontal gene transmission of resistance elements to human pathogenic *S. aureus* from soil bacteria belonging to the class *Streptomyces* genus is believed to have contributed to *S. aureus* resistance toward vancomycin [22]. Acquisition of the gene expressing β-lactamase resulted in the resistance to β-lactam antibiotics *via* the enzymatic hydrolysis of β-lactam antibiotics mechanism in the members of the *Enterobacteriaceae* and *S. aureus* family [23, 24]. Down regulation of genes at transcriptional level that are responsible for the expression of porin OprD, prevented penetration of carbapenems in *P. aeruginosa* [25] and over expression of the MexXY efflux pump was found to be associated with fluoroquinolone resistance in *P. aeruginosa* clinical isolates [25]. In response to presence of antibiotics, bacteria also express a variety of enzymes such as group transferases (acyltransferases, acetyltransferases, phosphotransferases, thioltransferases, nucleotidyltransferases, glycosyltransferase), redox enzymes, epoxidases, esterases, etc. which can effectively modify and degrade the antibiotics thereby preventing them from binding to their targets [26]. A report by Shi et al. suggest that resistance to aminoglycosides was due to the aminoglycoside-kinase mediated transfer of a phosphate group to a hydroxyl nucleophile on the aminoglycoside [27]. Different types of chloramphenicol acetyltransferases have been found to be responsible for the inactivation of chloramphenicol [28]. Similarly, evolution of several multidrug resistant strains of *Mycobacterium tuberculosis*, *P. aeruginosa* , *Acinetobacter baumannii*, and *K. pneumoniae* against most of the potent drugs like rifampicin, isoniazid, β-lacatams, ethambutol and fluoroquinolones by various mechanisms has compromised the effectiveness of this class of antibiotics [8, 29].

2.2.3 Toxicity and limitations of antibiotics

The antibiotics belonging to the class aminoglycosides can accumulate in the epithelial cells causing nephrotoxicity, followed by renal impairment [30], whilst the use of the broad-spectrum antibiotic chloramphenicol is limited by its bone marrow toxicity [31]. Tetracyclines were found to compete with calcium for incorporation into bone, hence unsafe for consumption by children and pregnant women [32]. Fluoroquinolones and β-lactams have been shown to cause serious side effects in the central nervous system and cardiovascular system [33, 34]. Streptogramins are associated with side effects such as headache, arthralgias and myalgias [35], and macrolides have been linked to ototoxicity via damage to the cochlea [36]. Thus the use of antibiotics is restricted due to their toxicity.

2.3 Diabetes mellitus

Diabetes is one of the most common non-communicable metabolic disorders, characterized by increased blood glucose levels as a consequence of insulin deficiency or insulin resistance [37]. Both the impaired insulin level or defective insulin action leads to the derangements in the catabolism and anabolism of carbohydrates, lipids and proteins; resulting in heterogeneous disorders such as hyperglycemia and glucose intolerance [38]. When left untreated, diabetes leads to more serious consequences such as visual impairment and possibly blindness, cardiovascular disease, renal failure and even premature death [38]. The prevalence of diabetes in all age groups of both developed and developing countries is increasing at an alarming rate and is expected to raise to epidemic proportions by 2030 [39].

2.3.1 Classification

Diabetes mellitus has been mainly classified into four types based on its etiology and clinical presentation [38]. Type-I diabetes also called juvenile diabetes is insulin dependent and occurs mainly in children due to the destruction of insulin producing pancreatic *beta* cells by *beta*-cell specific autoimmune processes [40, 41]. Type-II diabetes is also called non-insulin dependent diabetes, and is a manifestation of insulin resistance and deficiency [38], whilst gestational diabetes is a temporary clinical condition in pregnant women [38]. Other types of diabetes may occur due to various reasons such as genetic defects, surgical causes, use of drugs, etc. [38]. Type-I and II diabetes are most prevalent, and epidemiology suggest that 5-10% of the diabetic population is of type-I while type-II accounts for 80-90% of the diabetic population [42].

Type-II diabetes mellitus is the most prevalent in modern society since the modern life style of inappropriate diet, inadequate levels of physical activity and obesity are the main contributing factors for onset of type II diabetes mellitus [43]. Other reasons for prevalence of type II diabetes include body cell resistance to insulin, increased hepatic glucose production, lowered insulin-mediated glucose transport, and impaired *beta* cell functioning [43].

2.3.2 Biochemistry of diabetes

Diabetes is directly linked to defects in glucose metabolism, the primary source of energy for respiring cells [44]. Insulin, a polypeptide hormone synthesized within the *beta* cells of the islets of Langerhans in the pancreas, plays an important role in regulating blood glucose levels [44]. The main events of carbohydrate metabolism such as glucose transport across muscle and adipocyte cell membranes, regulation of hepatic glycogen synthesis, and inhibition of glycogenolysis and gluconeogenesis are controlled by insulin [45]. Insulin binds to receptor sites on the peripheral side of the cell membrane and mediates the transport of glucose into respiring cells [45, 46]. Insulin regulates the catabolism and anabolism of glucose and thus have a controlling effect on both glycolysis and glycogenesis [46]. The end result of all these events is a reduction in blood glucose concentration [46]. The optimum concentration of insulin in the blood stream is critical in maintaining glucose homeostasis and in clearing the postprandial glucose load [47]. Insufficient amounts of insulin or poor cellular response to insulin as well as defective insulin leads to improper handling of glucose by the body cells or inappropriate glucose storage in the liver and muscles. This ultimately leads to persistent high levels of blood glucose resulting in the condition called hyperglycemia [47]. As hyperglycemia persists, the body cells become devoid of glucose, which forces the cells to seek alternative energy sources, and cells turn to ketogenesis a process that makes use of fatty acids stored in adipose tissue [47]. The excess glucose from the blood and ketone bodies generated in ketogenesis or fatty acid catabolism are excreted via urine, thereby leading to glycosuria and ketonuria, which characterizes diabetes mellitus [48]. The excess ketone bodies in the blood can result in ketoacidosis [48], and if left untreated, coma and death can follow [48]. The chronic hyperglycemia arising from diabetes mellitus accompanies long-term damage, dysfunction, and failure of various organs, especially the eyes, kidneys, nerves, heart, and blood vessels [48].

2.3.3 Managing diabetes

Diabetes can be managed by healthy eating, regular physical activity and medication [49]. Controlled diet combined with physical activity can help in establishing metabolic control and bringing down blood glucose levels in cases of early stage of diabetes [49]. However, in most cases lifelong maintenance of blood glucose levels using exogenous insulin and pharmacotherapy is required [50]. For type-I diabetes, multiple daily insulin injections or a continuous infusion of insulin is given. For type-II diabetes, along with insulin supply, other approaches to control hyperglycemia and enhance insulin secretion are required [51]. There are several antidiabetic medications commercially available which target different metabolic processes. These therapeutic agents can be broadly classified as insulin secretion enhancers (sulfonylureas and meglitinides), hepatic gluconogenesis suppressors (biguanides), insulin sensitizers (thiazolidinediones rosiglitazone and pioglitazone), α-glucosidase inhibitors (acarbose, voglibose and miglitol), dipeptidyl-peptidase IV inhibitors (omarigliptin, gemigliptin, trelagliptin), and sodium–glucose co-transporter 2 inhibitors (empagliflozin, canagliflozin) [50]. **Fig. 2.2** represents the different classes of antidiabetic medication currently in use.

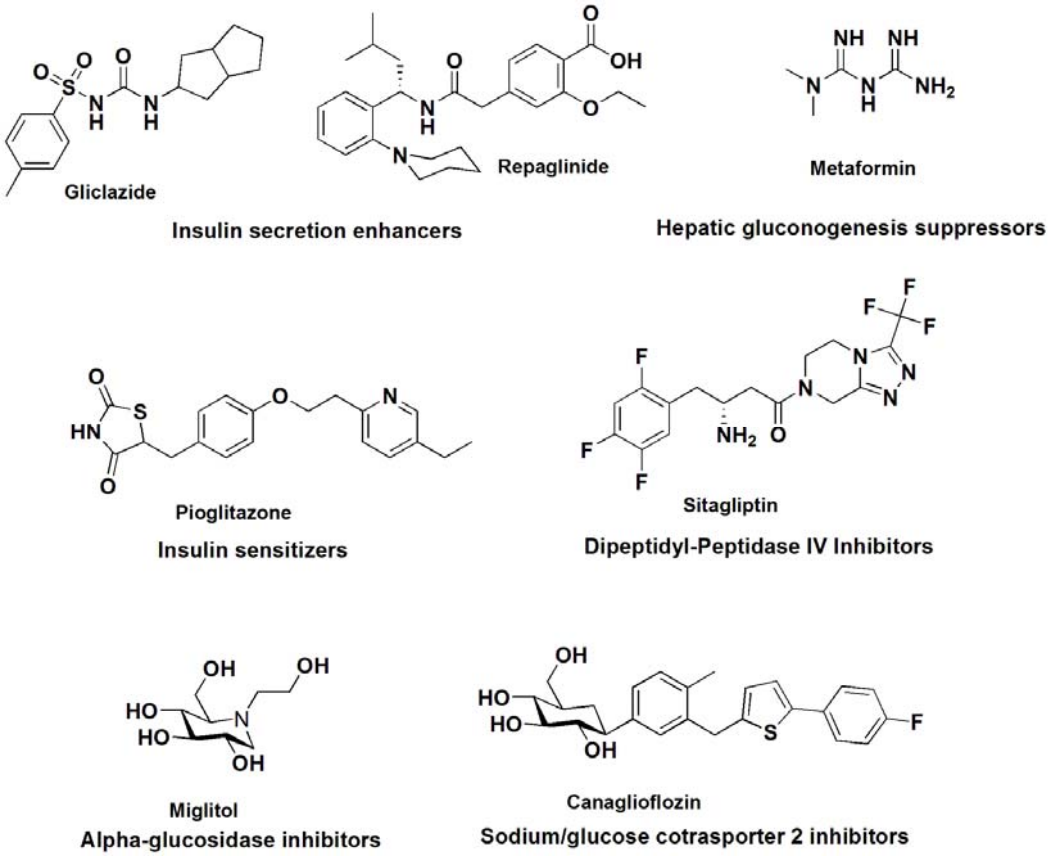

Figure 2.2 Major classes of antidiabetic medications.

2.3.4 Toxicity and limitations of anti-diabetic medication

Antidiabetic drugs such as sulfonylureas and meglitinides may lead to weight gain, hypoglycemia and decreased kidney function [52]. Further, sulfonylureas are only useful in people with type-II diabetes whose *beta* cells still produce insulin [53]. Biguanides cannot be used in patients with renal impairment due to its side effect of lactic acidosis, and buformin and phenformin which belong to this class have been withdrawn from the market [54]. The risk of other side effects of metformin such as diarrhea, dyspepsia, weight gain and hypoglycemia increases when taken in combination with sulfonylureas [54]. Insulin sensitizers cause weight gain, fluid retention, and anemia that increases heart disease and bone fractures [55]. Pioglitizone, an insulin sensitizer increases the risk of bladder cancer [56]. Side effects of dipeptidyl-peptidase IV inhibitors include nasopharyngitis, headache, nausea, heart failure, hypersensitivity, skin reactions and joint pains [57]. Gastrointestinal problems (flatulence and diarrhea) are commonly observed with α-glucosidase inhibitors, also their use is limited in patients with significant renal impairment [58, 59]. Sodium–glucose cotransporter 2 inhibitors are associated with treatment-emergent adverse events such as urinary tract and genital infections, back pain, polyuria, dysuria, and dyslipidemia [60].

Thus there is a significant need for the discovery and development of safer medicinal compounds with novel scaffolds to ensure that treatments are available for both multi-drug resistant bacteria species and diabetes mellitus. The limitation to the current treatment is that some of them are expensive and harbor adverse effects on patients. Hence there is a need for new viable chemotherapies. Drug discovery is a vast area of research and bringing new therapeutic agents into the market involves strategic compilation of thousands of different compounds from a variety of sources and their biological testing in high throughput screening. The traditional approach of drug discovery involves the isolation of bioactive compounds from the plant origin or to design and chemically synthesize novel organic or inorganic pharmaceuticals in the laboratory. Among the different kinds of medicinal compounds, aromatic functionalized heterocycles are excellent scaffolds and indispensable for preparing diversity-oriented compounds for medicinal and pharmaceutical applications. There is a compelling need to synthesize and evaluate more heterocycles for various biological applications. Recently, nanomaterials have drawn much attention in the medical field [61]. Due to their unique size and shape-dependent optical properties, metal-nanoparticles have found potential applications in medicine and hence there is a high demand for biodegradable materials

that are compatible with biomedical applications [61]. The organic-inorganic hybrid materials or nanocomposites can be generated by combination of organic drugs and inorganic metal nanoparticle for potential therapeutic applications [62].

2.4 Heterocyclic molecules

Heterocyclic molecules form the largest class of organic compounds which are present in many natural products, biomolecules, and a wide variety of drugs. Pyridines are an important class of six membered nitrogen-containing aromatic heterocycle present in numerous derivatives of biological relevance and pharmacologically significant compounds [63]. Pyridines exhibit a broad range of biological activity such as antimicrobial, anti-inflammatory, anti-asthmatic, antidepressant, antidiabetic, inhibiting acetylcholinesterase, treating hypertension or hypotension, inhibiting HIV protease, preventing or inducing apoptosis, act as Ca^{2+} channel blockers, hepato-protective and show antitumor properties [64-67]. Pyridines are also utilized in agrochemistry for their herbicide, insecticide, and antifungal properties [68]. Pyridine-derived organic materials and polymers have applications in organic photovoltaic devices [69] and organic light-emitting devices [70]. Pyridines like DMAP have been used as organocatalysts and several pyridine metal chelates have been used as efficient organometallic catalysts in organic synthesis [71, 72]. Thus, the pyridine nucleus occupies an important position in many pharmaceutical, agrochemical and material products.

Diversifications in the functional group or pharmacophore substitutions at different positions of the pyridine core have produced numerous compound libraries with diverse biological activity. Of particular note, 3,5-dicyanopyridines represent an important class of medicinally privileged heterocyclic scaffold [73]. In this class, particularly 2-amino-4-aryl-6-sulfanyl substitution **(Fig. 2.3)** pattern has drawn much attention currently for a variety of biological activity [74]. These multi-substituted pyridine compounds exhibit a broad range of biological activities such as anti-bacterial, antiprion, antihepatitis B virus, and anticancer [74]. Additionally, a few compounds of this class have been recognized as highly selective agonists for adenosine receptors and are recommended for the development of new medication for the treatment of Parkinson's disease, hypoxia/ischemia, epilepsy, kidney disease, and Creutzfeldt–Jacob disease [75].

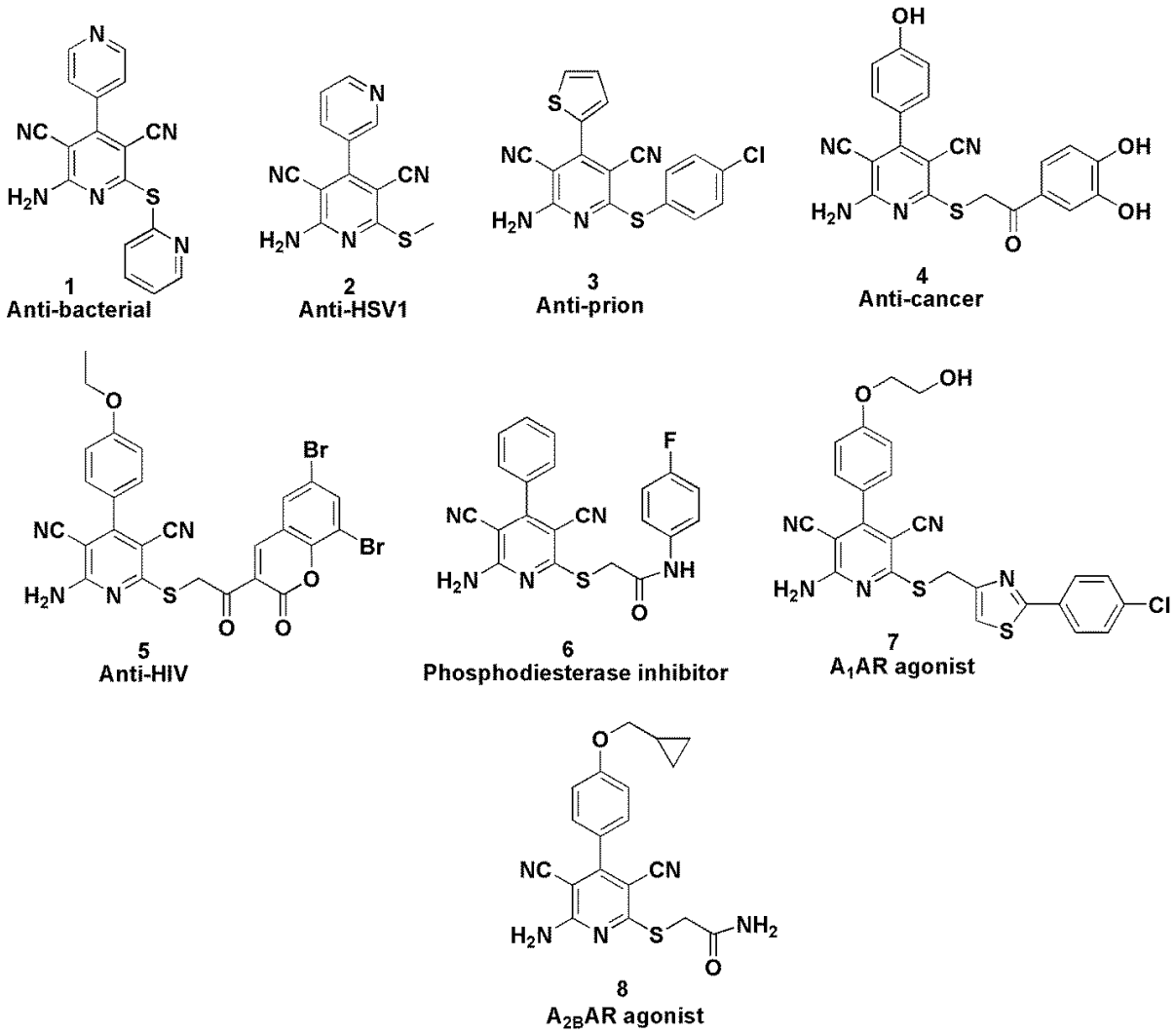

Figure 2.3 Structural representation of some medicinally useful 2-amino-3,5-dicyano-6-sulfanyl pyridines scaffolds.

Fig. 2.3 demonstrates some medicinally useful 2-amino-3,5-dicyano-6-sulfanyl pyridine scaffolds that are used against a wide range of biological targets. Potent antibacterial activity of several pyridine-3,5-dicarbonitrile derivatives of type **1 (Fig. 2.3)** against both gram-positive and gram-negative bacterial strains have been reported [76-78]. Compounds of type **2 (Fig. 2.3)** were found to be potential anti–HSV1 agents **[79]**. Perrier et al. and May et al. demonstrated the compounds of type **3 (Fig. 2.3)** to bind cell-surface glycosylphosphatidylinositol-anchored proteins and prevent their post-translational conversion to protease resistant isoforms, thus helping to prevent prion induced neurodegenerative diseases [80-82]. Based on structure-based drug discovery, Bowman et al. proposed that compounds of the type **4 (Fig. 2.3)** can be good

anticancer agents [83]. Pharmacophore model analysis by Deng et al. confirmed that compound **5 (Fig. 2.3)** is a potent HIV-1 integrase inhibitor [84], and compound **6 (Fig. 2.3)** was found to be a phosphodiesterase inhibitor and hence used as potent drug for the treatment of cardiovascular diseases [85].

The 2-amino-3,5-dicyano-6-sulfanyl pyridines have been used as selective non-ribose agonists for the adenosine receptor [86]. Adenosine receptors **(AR)** play an important role in signal transduction across the membrane and hence are described as potential targets in the treatment of cardiovascular diseases (angina pectoris, atrial fibrillation, infarct), metabolic diseases (diabetes, dyslipidemia), Parkinson's disease, hypoxia/ischemia, asthma, kidney disease, epilepsy and cancer [87-90]. Due to their agonist activity, 2-amino-3,5-dicyano-6-sulfanyl pyridines have found application in treatment of various ailments. For example, Capadenoson 7 **(Fig. 2.3),** a selective adenosine A_1 AR agonist, acts as an anti-anginal agent [91, 92]. Lee et al. discovered that the A_1 AR subtype agonists reduce the nephrotoxic effects of aminoglycosides by controlling renal drug accumulation [93]. Substituted 2-thio-3,5-dicyano-4-phenyl-6-aminopyridine compounds of the formula **7 (Fig. 2.3)** are adenosine A_1 receptor agonists which may be used in combination with aminoglycosides for the protection of kidney from toxic effects caused by aminoglycosides during treatment of infectious diseases in humans [94]. BAY60-6583 compound type 8 **(Fig. 2.3)** is reported to mediate anti-inflammatory, kidney-protective, cardio-protective effects by specifically binding to A_{2B} subtype adenosine receptors [95]. Structurally similar compounds aminocyanopyridines have shown mitogen activated protein kinase-activated protein kinase-2 inhibition and thus possess application in the treatment of autoimmune diseases and cancer [96]. In addition, it has recently been shown that similar heterocyclic compounds could be an attractive class of corrosion inhibitors [97] and thus have industrial application as well.

2.4.1 Synthesis of 2-amino-3,5-dicyano-6-sulfanyl pyridines

Synthesis of 3,5-dicyanopyridine scaffolds can be carried out under many different reaction conditions using various catalysts. One of the most facile and convenient procedures is one-pot, three-component condensation between aldehyde, malononitrile, and a thiol to make the 3,5-dicyanopyridine core. This multicomponent method is very rapid and economical due to the commercial availability of the starting materials. The reaction has been carried out in the presence of a wide variety of catalysts like organic bases (Et_3N, DABCO, piperidine, morpholine, thiomorpholine, pyrrolidine, N,N-DIPEA, pyridine, 2,4,6-collidine, DMAP, aniline, N-methylaniline, N,N-dimethylaniline, and N,N-diethylaniline) [98, 99], inorganic

bases (K_2CO_3) [100], Lewis acids ($Sc(OTf)_3$, $ZnCl_2$) [101, 102], ionic liquids [103, 104] and boric acid [98]. Nanoparticles of SnO [105], TiO_2 [106], CaO [107], Fe_2O_3 [108], ZnO [109] and SiO_2 [110], have also been reported to effectively catalyze the multicomponent reaction for the synthesis of 2-amino-3,5-dicyano-6-sulfanyl pyridines.

The reaction mechanism for this multicomponent condensation has been proposed to proceed via Michael addition onto Knoevenagel adduct [75, 111] **(Fig. 2.4)**. Initially, in a base catalyzed condensation reaction between the aldehyde and one equivalent of malononitrile, formation of Knoevenagel adducts 1 **(Fig. 2.4**) takes place. This reaction is followed by the nucleophilic addition of the thiol group to the unsaturated carbon of one of the nitrile groups of Knoevenagel adduct resulting in intermediate **2** (**Fig. 2.4**). 1,4-Michael addition of the second equivalent of malononitrile on the intermediate followed by immediate cyclisation and tautomerization gives 1,4-dihydropyridine intermediate **5** (**Fig. 2.4**). This undergoes aromatisation via oxidation to yield sterically accessible pyridine-3,5-dicarbonitrile as the final product.

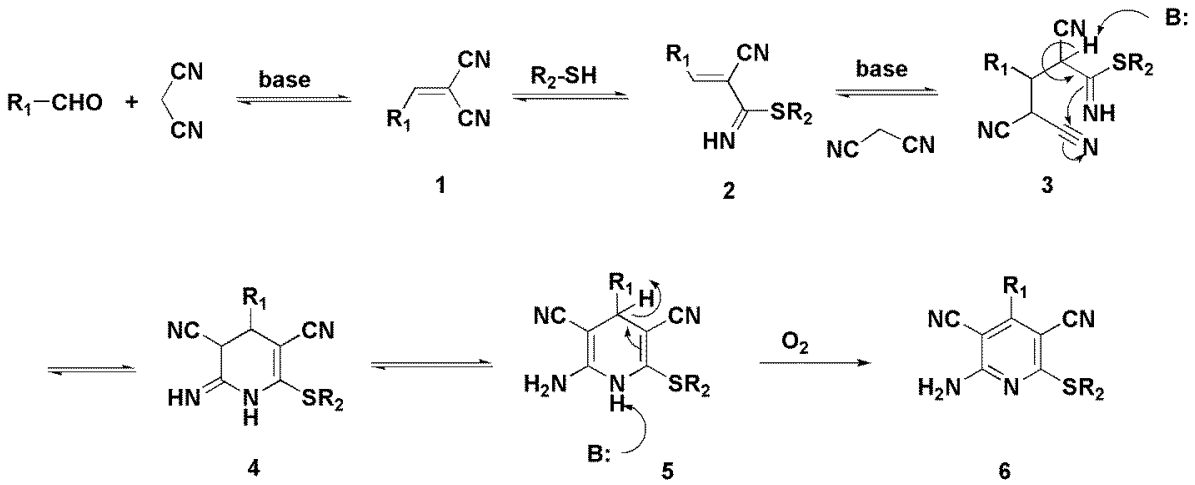

Figure 2.4 Reported mechanism for the synthesis of pyridine-3, 5-dicarbonitriles [111].

In view of the medicinal importance of pyridine- 3,5-dicarbonitriles and our continued interest in the development of new medicinally important compounds, in this research work, we discuss the synthesis and evaluation of 2-thio-3,5-dicyano-4-aryl-6-aminopyridines as antidiabetic and antibacterial agents. We used relatively simple base-catalyzed reaction for the synthesis of 2-thio-3,5-dicyano-4-aryl-6-aminopyridine compounds using commercially available malononitrile, different substituted benzaldehydes, and thiols as starting material. Inexpensive and readily available triethylamine was used as the catalyst and ethanol was used as the solvent.

2.5 Nanotechnology as a platform for the development of novel therapeutics

Nanoparticles are any material with nanoscale dimensions of the order of 100 nm or less [112]. When the materials are miniaturized to nanoscale, they behave differently than the bulk one and often exhibit significantly novel and improved physical, chemical, and biological properties based exclusively on their size and morphology [112]. The new and improved materials generated by using nanotechnology, prompt new developments in the fields of electronics, catalysis, imaging and medicine [113]. Thus, the field of nanotechnology has become a very active area of research in modern science, attracting attention of researchers from almost every field of science [113].

2.5.1 Silver and gold nanoparticles

Although extensive research in nanoscience and nanotechnology has only started recently, the use of nanoscale gold and silver particles from the ancient time is well documented. Stained glass artisans were created by trapping silver and gold in the glass matrix and this is one of the most documented example of nanotechnology known in history [114]. Ancient ceramic technology used gold nanoparticles to get metallic luster on ceramics and this can be traced back to the 9^{th} - 17^{th} century [114]. The use of noble metals and their derivatives for medicinal purposes has evolved from the ancient times. The Vedic period in ancient India witnessed the use of mixtures of gold powder (known as 'Bhasma') and herbs to improve immunity to fight against anemia, asthma and muscle weakness [115]. In China, ailments such as smallpox, skin ulcers and measles were treated using gold compounds. Various types of silver compounds such as silver powder, silver oxide and silver zeolite have been in use from ancient times as antimicrobial agents [116]. Recently, much progress has been made in nanotechnology and silver nanoparticles (AgNPs) and gold nanoparticles (AuNPs) have become more valuable with a wide range of applications [117].

Nanoparticles possess a high percentage of atoms present on the surface, and hence higher surface area to volume ratio compared to the bulk materials [114] which makes the nanoparticle behave differently from bulk materials. The nanoparticle state is considered as the intermediate state, between atomic/molecular state and bulk state and hence their unusual properties cannot be explained by using either quantum mechanics or classical physics [118]. The optical, magnetic and electrical properties of nanoparticles strongly depend on the size and shape of the particles and can be altered by controlling their geometry [118]. Hence, study of the synthesis

and application of novel nanoparticles is very attractive and highly focused within the last decades [114]. Metal nanoparticles are one of the most wide-spread and diverse among the different types of nanoparticles [119]. Amongst them, AgNPs and AuNPs are well known and have numerous applications in electronics, catalysis, imaging and medicine [120].

2.5.2 Therapeutic properties and applications of silver and gold nanoparticles

Recently there has been significant progress in the design and study of metal-derived nanomaterials for therapeutic and biomedical applications [121]. Particularly, noble metals with their intrinsic properties such as resistance to corrosion, thermal stability and decreased toxicity have attracted much attention. When reduced to nanosize, the noble metals acquire special characteristics such as high surface-to-volume ratio and tunable broad optical properties prompting their versatile application in diagnostics and therapeutics [121]. The AgNPs and AuNPs which can be easily prepared and attached to various biomolecules have a wide range of applications in the fields of diagnostics, surgery and medicine [122].

The optical properties of both AgNPs and AuNPs can be tuned to desirable wavelengths by controlling their size, shape and composition on their surface. Moreover, nanoparticles can efficiently absorb and convert light or radiofrequencies into heat. These unique properties enable nanoparticles to be used for imaging and photo-thermal applications [123]. Also, facile surface chemistry of nanoparticles allow the functionalization of the surface with moieties such as antibodies, peptides, nucleic acids and therapeutic agents, so that the bio-conjugated metal-nanoparticles can be used for specific purposes [123].

2.5.3 Antimicrobial properties

The broad-spectrum antimicrobial activities of metal-nanoparticles against bacteria, fungi, and virus is well known [124]. The unique physicochemical properties of noble metal-nanoparticles together with their high surface area-to-volume ratios are contributing factors towards their effective antimicrobial activity [124]. In addition, the production of nanoparticles is cost effective and unlike the classical antibiotics, metal-nanoparticles are less prone to resistance as they attack multiple sites on the microorganism [124]. As more and more multidrug-resistant bacterial strains are emerging, there is a high demand for new antibiotics with novel modes of action. Therefore, AgNPS and AuNPs have become an attractive source of drug candidates [124].

Several mechanisms have been proposed for the antibacterial activity of metal-nanoparticles. The main events involved in the mechanism of action are: production of reactive oxygen species that damage cellular components, cell membrane destruction and increased permeability, and denaturation of proteins and nucleic acids thus disrupting replication and enzyme activity [125]. The antimicrobial effects of AgNPs were most extensively studied and different mechanisms have been proposed to explain the high antimicrobial activity of AgNPs. According to the chemiosmotic mechanism proposed by Dibrov et al., low concentrations of Ag^+ induces massive proton leakage through the *Vibrio cholerae* membrane, which results in cell death [126]. A case study on *E. coli* as a model for gram-negative bacteria by Sondi et al. confirms that AgNPs damaged the cell membrane of *E. coli* by forming pits in the cell wall of the bacteria, while the AgNPs were found to accumulate in the bacterial membrane [127]. Similarly, Amro et al. suggest that metal depletion causes irregular-shaped pits in the outer membrane releasing lipopolysaccharides, resulting in altered membrane permeability and cell death [128]. Mechanistic studies on *E. coli* and *S. aureus* by Feng et al. revealed that silver ion released from the nanoparticles bind to the functional groups of DNA and proteins causing their denaturation and cell death [129, 130]. Kim et al. proposed the free radical mechanism wherein free radicals generated by AgNPs induced cell membrane damage [131]. Nagy et al. proposed that the antibacterial mechanism of AgNPs is due to the exhaustion of the antioxidant capacity of the cell. In response to silver ions released from AgNPs/zeolite composite, upregulation of several antioxidant genes as well as genes coding for metal transport, metal reduction, and ATPase pumps was observed in *S. aureus* and *E. coli*, confirming oxidative stress driven cell death [132]. Owing to their antibacterial properties, silver-impregnated bacteriostatic water filters (NATURE2 G45-VC40) have been in use for safe drinking water and swimming pool filters [133]. Several colloidal nanosilver algaecides (Algaedyn, MicroSilver BG-R) are also commercially available and can safely be used as disinfectants even in high amounts [133].

AuNPs are relatively less toxic than their silver counterparts, but fewer studies were performed with regard to their antibacterial properties. AuNPs when irradiated with focused laser pulses of suitable wavelength, were able to kill bacteria [134] and Li et al. reported that biocompatible cationic and hydrophobic functionalized AuNPs effectively suppressed growth of multi-drug resistant bacteria [135]. Poly-allylamine hydrochloride coated anionic AuNPs were reported to cause *E. coli* cell lysis, revealing that cationic coated AuNPs are more toxic than anionic coated ones [136]. Anti-protein A antibody conjugated AuNPs were employed to kill the gram-positive bacterium *S. aureus* by means of laser-induced overheating effects [137]. AuNPs conjugated

with the antibiotics ampicillin, kanamycin and streptomycin produced synergistic antibacterial effects against *E. coli*, *M. luteus* and *S. aureus* [138]. Thus, it can be concluded that AuNPs can be promising potential antibiotic agents for treating serious bacterial infections, but which have minimal side effects.

2.5.4 Tumor targeting

Classical therapies for cancer are plagued by severe side effects such as toxicity, due to their inability to differentiate between cancerous and normal cells [139]. Hence, therapies differentiating and targeting malignant cells are of high importance in medicine. The potential therapeutic application of noble metal-nanoparticles represents an attractive platform for cancer therapy in a wide variety of targets. AuNPs have been shown to bind to heparin-binding glycoproteins thereby inhibiting their subsequent signaling events [140], a passive anticancer targeting mechanism that demonstrates the intrinsic anticancer properties of the AuNPs [140]. Nanoparticles can easily be functionalized with a variety of hydrophobic and hydrophilic biological molecules such as polyethylene glycol, antibodies, peptides and nucleic acids to specifically target extracellular and intracellular pathways, and thus their antitumor action can be actively directed towards a particular target [141]. AgNPs were found to be potentially cytotoxic against acute myeloid leukemia (AML) cells, as well as the human breast cancer cells MDA-MB-231 and MCF-7 [142-144], and their cytotoxicty involved a similar mechanism of action to that of their antibacterial activity [145].

AuNPs conjugated with epidermal growth factor receptor antibody (anti-EGFR) were used for the selective photothermal therapy (PTT) of human epithelial cancer cells, A431 [146]. VEGF antibody attached AuNPs induced a higher level of apoptosis in B-chronic lymphocytic leukemia cells when compared to free AuNPs and antibodies [147]. A9 RNA aptamer conjugated multifunctional AuNPs were successfully used for surface-enhanced Raman scattering (SERS) based photo thermal therapy of LNCaP prostate cancer cells [148].

Thermal ablation or hyperthermia is a method of tumor targeting, where nanoparticles are used to heat up the cancerous cells beyond their temperature tolerance limits [149]. Due to surface plasmon resonance (SPR), nanoparticles have the capacity to absorb light and convert the absorbed light into localized heat which can be employed for photothermal therapy [149]. When the temperature increases above 42°C, cell viability is strongly reduced and at even high

temperatures denaturation of proteins, apoptosis and tissue ablation can occur. Monoclonal antibodies (anti-HER2) conjugated to gold nanocages were used to induce a near-infrared region based photo thermal therapy for breast cancer cells (SK-BR-3) targeting their over expressed epidermal growth factor receptors (EGFR) [150].

Most of the clinically used organic drug molecules used in the treatment of cancer are low molecular weight compounds that can readily diffuse into both cancerous and healthy tissues [139, 151]. A consequence of this is the severe side effects in healthy cells and reduced efficacy at the target site [139]. Nanoparticles can be used as vectors to achieve targeted delivery and optimized bio-distribution of drugs in cancer cells/tissue. Dhar et al. demonstrated that a Pt(IV) complex, which is normally inactive, can be made active against several cancer cell lines when attached to polyvalent oligonucleotide gold nanoparticle conjugates [152]. AuNPs have also been used as vehicles for the delivery of the anticancer drug paclitaxel [153]. AuNPs have shown potential as intracellular delivery vehicles for antisense oligonucleotides [154] and for therapeutic siRNA by providing protection against RNAses [147]. Simultaneous imaging and therapy of breast cancer *in vitro* using silica-gold nano shells has also been reported [155]. Thus, noble metal-nanoparticles have theranostic application since they are being explored simultaneously as diagnostic and therapeutic tools. To achieve desired effects in therapy, it is critical to use rationally designed and engineered NPs that can be targeted to tissues of interest.

2.5.5 Diagnostics and imaging

Surface plasmon resonance is the characteristic property of all metal nanoparticles since the interaction of radiation with the free electron on the metal surface causes them to oscillate [156]. SPR originates when the photons resonate with the free electrons on the metal particle surface at a certain wavelength [156]. Various factors such as dielectric constant of the metal and medium, size, shape and capping of the organic molecule present on the surface of the nanoparticles influence SPR [156]. SPR can be observed in UV-Vis spectroscopy for AgNPs and AuNPs, which qualifies them for application in sensing, diagnostics and as optical materials. SPR oscillation also strongly enhances their light absorption and scattering properties (Rayleigh and Raman) of metal nanoparticles, which can be exploited in cancer imaging technology [157].

Diagnostic applications of nanoparticles are focused on early disease detection, visualization and quantification of the patho-physiological abnormalities, and image-guided therapy and treatment [151]. Conventional diagnosis and imaging techniques using organic dyes have drawbacks like short imaging times due to rapid renal clearance, renal toxicity, and vascular permeation [158]. Also poor photo-stability, low quantum yields and low detection sensitivity necessitates high dosage radiation which could damage the healthy tissue [151]. Noble metal-nanoparticles based imaging probes, good contrast enhancement and diagnostic agents help in improving the site-specificity and sensitivity of diagnostic imaging [151].

In general, nanoparticle-based imaging probes consist of a targeting agent or vehicle functionalized on its surface which helps to locate disease biomarkers tagged on the cell surface to enable imaging ability and specificity [159]. The diagnostic ability integrated with therapeutic properties of nanoparticles enables their application for theranostic purposes. Another advantage associated with noble metal-nonmaterial derived imaging probes is that they can be used with multiple imaging modalities to yield complementary information compared to any single imaging technique [159].

Colloidal AuNPs, which are relatively non-cytotoxic are used as important imaging agents in biomedical applications. AuNPs are promising imaging and diagnostic agents for cancer due to their property of absorbing light in the visible and near-infra red range [160]. For example, poly (amidoamine) dendrimers entrapped AuNPs were used to target folate receptors on human epithelial carcinoma cells and their fluorescence imaging was conducted using fluorescence isothiocyanate (FITC) [161]. Gold nanorods conjugated to anti-epidermal growth factor receptor (anti-EGFR) monoclonal antibodies have been used for dark field light-scattering imaging of two malignant oral epithelial cell lines, HOC-313 clone-8 and HSC-3n [162]. Anti-epidermal growth factor receptor (EGFR) conjugated colloidal AuNPs were used for early diagnosis of oral cancer based on their surface plasmon resonance [163]. Kim et al. demonstrated that PEG-coated AuNPs are useful as computed tomography contrast agents for a blood pool and hepatoma imaging [164]. Optical biosensors were developed using triangular AgNPs for the system for binding the antigen ADDL, a putative Alzheimer's disease pathogen and anti-ADDL antibodies. This system was developed by Duyne et al. and helped in the diagnosis of Alzheimer's disease [165]. Thus AgNPs and AuNPs have shown great promise as molecular imaging probes.

2.5.6 Biosensors

AgNPs and AuNPs based nano-biosensors are of great interest in various applications such as environmental protection, biotechnology and food safety. Sugar-coated AuNPs were able to detect low concentrations (10 pg/mL) of plant proteinous toxin, ricin and hybrid Au–Ag nanoparticles were able to sense 0.1 ng/mL of *S. aureus* enterotoxin B, a potential application for the detection of toxins in food safety [166, 167].

AgNPs based biosensors for fast monitoring of penicillin with immobilization of penicillinase enzyme by physical adsorption method was recently developed by Sistani et al. [168]. Wei et al. used AgNPs for sensing in enzymatic assays of calf intestine alkaline phosphatase (CIAP), dephosphorylating adenosine triphosphate (ATP) and protein kinase A (PKA) [169]. Using this method, the activity of enzymes and inhibitors could be determined. Chen et al. described oligonucleotide functionalized AgNPs and AuNPs for the detection of DNA, based on surface enhanced resonance Raman scattering assay [170]. Ag@Au bimetallic nanoparticles based biosensors developed by Ghodselahi et al. showed a good response to low concentration of DNA and has a short response time [171].

2.5.7 General methods for the synthesis of silver and gold nanoparticles

Many different approaches have been developed for the synthesis of AgNPs and AuNPs of different sizes and shapes. These methods can be broadly classified into two main types, the top-down and the bottom-up approach.

2.5.7.1 Top-down approach

This approach involves the miniaturization of the bulk material to nanostructure by using different techniques and subsequent stabilization of the resulting nanoscale particles by capping agents. The most commonly used methods in this approach are mechanical grinding, evaporation-condensation and laser ablation. The absence of impurities and chemical contamination are advantages of this method [172, 173].

Mechanical grinding is the oldest method and involves milling of bulk materials in mechanical attrition devices to highly crystalline nanomaterials [174]. The disadvantage of this method is that the nanoparticles synthesized contain crystal defects at the surface, due to large strain imparted to particles during the milling process [173].

In the evaporation-condensation method and laser ablation method, bulk metal is heated or ablated by absorbed pulsed laser beam energy in a liquid medium and the vaporized metal condenses to generate nanoparticles. The size and shape of nanoparticles generated by these methods mainly depends on the optical property of the metal, laser wavelength, duration of laser impulse used, and presence of surfactants in the medium [175]. Synthesis of both AgNPs and AuNPs by this method has been reported [175-177]. The disadvantage of these methods is the requirement of highly expensive and cumbersome equipment for the generation of high temperatures and high power laser beams.

2.5.7.2 Bottom-up approach

In this approach, the reduction of various metal ions leads to the formation of atoms, and the atoms (building blocks of the nanoparticles) agglomerate into oligomeric clusters which eventually convert into colloidal nanoparticle structures. The reduction of metal ions can be performed by chemical, thermal [178], microwave [179], sonochemical [180], electrochemical [181] and photochemical reduction [182] methods using different salts. A large variety of additives such as donor ligands, polymers, and surfactants, are used in these processes to guide the nucleation, growth control and stabilization of the resulting nanoparticles. Silver and gold nanoparticles with different morphology can be obtained using these methods by varying parameters such as, precursor salt, reducing agent and stabilizing agent. The most commonly used additives are polymers (polyvinyl pyrrolidone), surfactants (sodium dodecylsulfate), dendrimers, and biomolecules such as DNA, sugars, proteins, peptides, and amino acids [183].

2.5.7.2.1 Chemical reduction

Chemical reduction is the most frequently applied method for the generation of AgNPs and AuNPs. The synthesis of nanoparticles by this approach is typically carried out using a metal precursor, a reducing agent and a stabilizing additive. Chemical reduction by organic and inorganic reducing agents of Ag^+ and Au^+ ions to the metallic Ag^0 and Au^0, followed by agglomeration of the atoms to clusters (nucleation and growth) lead to the formation of nanoparticles. Most commonly used reducing agents are sodium borohydride, sodium citrates, ascorbates, and hydrazine [184-188]. The size and shape of the resulting nanoparticles depends on reaction parameters such as concentration, pH and temperature.

The chemical methods for the synthesis of nanoparticles are rapid and can be conducted in large scale, but the problem with most of the chemical methods is that they involve the use of toxic and hazardous chemicals such as $NaBH_4$, and N_2H_4; thus limiting the application of nanoparticles in the medical field. Also, poor control on growth, shape and stability of these nanoparticles necessitates the addition of stabilizing agents. Furthermore, there is evidence to suggest that chemically synthesized nanoparticles cause adverse effects on humans, animals, plants, and the environment [189, 190].

2.5.7.2.2 Biological methods for the synthesis of nanoparticles

Many chemical and physical methods that are available for the synthesis of nanoparticles often require energy intensive processes such as high temperatures and pressure, toxic radiation, and expensive equipment thus making them less feasible [191]. Also, the biomedical applications of nanoparticles synthesized by chemical methods are limited due to the toxic chemicals adsorbed on their surfaces. To overcome these problems, current studies are embarking on the use of green biological methods for nanoparticle synthesis. The merits of these methods involve lower reaction temperatures, less cumbersome reaction processes, and non-pure starting materials may be used, all of which result in cheaper maintenance. Both prokaryotic and eukaryotic organisms have been demonstrated to have strong potential for metallic nanoparticle synthesis and nanoparticles obtained from these sources have been evaluated for a wide range of applications.

The silver resistant bacteria *P. stutzeri A259*, was the first bacterial strain found with capacity to form AgNPs from Ag+ ions using its naturally-occurring protective pathway against silver ions toxicity [192]. Intracellular AuNPs synthesis by the bacterial species *P. boryanum, G. ferrireducens,* and *S. algae* is also reported [193]. Extracellular synthesis of AgNPs by *B. subtilis, B. megatherium, E. coli, E. cloacae* and AuNPs by *R. capsulata, S. maltophilia* has also been reported in literature [194].

One example of a eukaryotic nanoparticle producer is the fungus *Phoma*, which produces AgNPs that exhibit antibacterial properties and these are also employed as catalysts in the oil industry [195]. *F. oxysporum* produces nanoparticles of Ag, Au, Pt, Zr, Cd, Pb and Ti [194, 196], and intracellular bioreduction of gold ions by *V. luteoalbum* occurred at lower pH values resulted in the formation of smaller and uniformly spherical-shaped AuNPs.

Many plants have been successfully used for efficient and rapid extracellular synthesis of AgNPs and AuNPs. Plant mediated green synthesis of AgNPs using *Emblica officinalis* fruit extract and *Rhizophora mucronata* leaf buds and their application as antibacterial agents has been discussed [197, 198]. The AgNPs and AuNPs synthesized by using *Butea monosperma* leaf extract for potential application for cancer therapeutics has been reported by Patra et al. [199]. Megarajan et al. reported the photosynthesis of AuNPs using phytoproteins of spinach leaves, and their application as catalysts for the degradation of an azo dye, methyl orange [200].

The mechanism involved in both intracellular and extracellular synthesis of nanoparticles is not well understood. However, it is hypothesized that enzymes and other biomolecules such as polypeptides, proteins, lipid, flavonoids, terpenoides, ascorbic acids, polyphenols, etc. have the main role in the reductive reactions used by various organisms [194]. For instance, extracellular synthesis of AgNPs by white rot fungus, *Phaenerochaete chrysosporium* was proposed to initiate by chemical functional groups such as carboxylate anion, carboxyl and peptide bond of proteins, and hydroxyl of saccharides present on the cell wall surface [201]. The synthesis of AuNPs by *Fusarium oxysporum* was proposed to be catalyzed by hydrogenase and NADH-dependent reductase [202]. Similarly, biosynthesis of AuNPs by laccase enzyme isolated from *Paraconiothyrium Variabile* has been reported [203]. Bhattacharjee et al. highlighted the dipeptide- and tripeptide-mediated reduction of $HAuCl_4$ to colloidal AuNPs [204]. In yet another similar study, a chemically reducing potential around the metal cluster was generated due to the interaction with the peptide, and this was expected to drive the reduction of silver and gold ions to AgNPs and AuNPs respectively [205]. Although these hypothetical mechanisms explain nanoparticle formation in biological systems, a detailed study is needed to clarify the processes.

Many species of bacteria, fungi and algae have the natural ability to produce nanoparticles, and faster growth rates of these organisms can be exploited for large scale synthesis of nanoparticles. However, maintaining the microbial culture is a tedious process. Nanoparticle synthesis using plant extracts is relatively more economical, energy efficient and cost effective. Plant extracts are highly convenient due to short reaction times and easy availability of different plant materials like leaves that can be harvested without removing the plant from the wild. Green synthesized nanoparticles therefore have significant value in medicine due to their biocompatibility [191].

2.6 Hypothesis of the study

Since 3,5-dicyanopyridines bearing the 2-amino-4-aryl-6-sulfanyl substitution pattern present in many pharmaceutically important compounds exhibited a wide variety of biological activity including antimicrobial and anticancer activity; molecules containing this core structure can be synthesized and evaluated for more novel biological applications. Recently metal nanoparticles have gained high importance in drug delivery, sensing, imaging and chemotherapy medicine due to their unique physical and biological properties. Thus, exploring more of them would help to find novel therapeutic agents. The function of hybrid molecules for better therapeutic properties and to combat drug resistance has become an important subject of study in the field of medicinal chemistry [206]. The hybrid molecules or materials can be generated by organic-organic or organic-inorganic combination [62, 206]. Organic–inorganic hybrid materials are generated using organic and inorganic components either in the form of homogeneous systems derived from miscible organic and inorganic components, or in the form of heterogeneous systems as nanocomposites [62]. In organic-inorganic hybrids, the association between the constituents can be either in the form of chemical covalent linkage or mere physical adsorption forces such as van der Waals forces [62, 207, 208]. The co-existence of two different molecules with entirely different modes of action in the form of hybrid molecules produce synergistic effects and thus offer advantages such as dosage compliance, minimized toxicity, and overcoming drug resistance when compared to the parent counterparts [209]. Hence the synthesis and evaluation of drug conjugated nanoparticles as organic-inorganic hybrid molecules for their antibacterial properties is interesting.

Developing novel medication without compromising on safety and efficacy is both an expensive and time consuming process in the pharmaceutical industry [210]. There are thus a large number of drugs that are withdrawn at the clinical trial stage, due to their poor pharmaceutical properties such as poor solubility, permeability and tolerability, and also rapid metabolism and elimination from the body. Hence along with the discovery and development of new drugs, focus must also be on novel strategies to improve current therapies. Modification of existing drugs in terms of improved formulation such as salt formation, inclusion complexation, repurposing and repositioning to further improve the therapeutic value of current chemotherapies will help in more rapid development of treatments.

In conclusion, the main objective of this this PhD research study was to synthesize and evaluate novel pharmaceutical candidates that can be used against microbial infections and diabetes.

2.7 References

[1] C.D. Mathers, D. Loncar, Projections of global mortality and burden of disease from 2002 to 2030, PLOS Medicine, 3 (2006) e442.

[2] T. Muka, D. Imo, L. Jaspers, V. Colpani, L. Chaker, S.J. van der Lee, S. Mendis, R. Chowdhury, W.M. Bramer, A. Falla, The global impact of non-communicable diseases on healthcare spending and national income: a systematic review, European Journal of Epidemiology, 30 (2015) 251-277.

[3] C. Dye, After 2015: infectious diseases in a new era of health and development, Philosophical Transactions of the Royal Society B: Biological Sciences, 369 (2014) 20130426.

[4] A. Alwan, D.R. MacLean, L.M. Riley, E.T. d'Espaignet, C.D. Mathers, G.A. Stevens, D. Bettcher, Monitoring and surveillance of chronic non-communicable diseases: progress and capacity in high-burden countries, The Lancet, 376 (2010) 1861-1868.

[5] C. Dye, B. Bourdin Trunz, K. Lonnroth, G. Roglic, B.G. Williams, Nutrition, diabetes and tuberculosis in the epidemiological transition, PLOS One, 6 (2011) e21161.

[6] S.G. Deeks, A.N. Phillips, Clinical review: HIV infection, antiretroviral treatment, ageing, and non-AIDS related morbidity, British Medical Journal, 338 (2009) 288-292.

[7] T. Swan, Hepatitis C drug development catapults onward, Clayden P, Harrington M, Swan T, et al.; i-Base/Treatment Action Group, (2013).

[8] R.J. Fair, Y. Tor, Antibiotics and bacterial resistance in the 21st century, Perspectives in Medicinal Chemistry, 6 (2014) 25.

[9] http://www.who.int/mediacentre/factsheets/fs104/en/, (2014).

[10] C.L. Ventola, The antibiotic resistance crisis: part 1: causes and threats, Pharmacy and Therapeutics, 40 (2015) 277.

[11] C. Walsh, Where will new antibiotics come from?, Nature Reviews Microbiology, 1 (2003) 65-70.

[12] S.J. Projan, Why is big Pharma getting out of antibacterial drug discovery?, Current Opinion in Microbiology, 6 (2003) 427-430.

[13] K.M. Overbye, J.F. Barrett, Antibiotics: where did we go wrong?, Drug Discovery Today, 10 (2005) 45-52.

[14] S.J. Projan, New (and not so new) antibacterial targets–from where and when will the novel drugs come?, Current Opinion in Pharmacology, 2 (2002) 513-522.

[15] A.E. Clatworthy, E. Pierson, D.T. Hung, Targeting virulence: a new paradigm for antimicrobial therapy, Nature Chemical Biology, 3 (2007) 541-548.

[16] C.A. Arias, B.E. Murray, Antibiotic-resistant bugs in the 21st century—a clinical super-challenge, New England Journal of Medicine, 360 (2009) 439-443.

[17] C.T. Walsh, T.A. Wencewicz, Prospects for new antibiotics: a molecule-centered perspective, The Journal of Antibiotics, 67 (2014) 7-22.

[18] J.M. Blair, M.A. Webber, A.J. Baylay, D.O. Ogbolu, L.J. Piddock, Molecular mechanisms of antibiotic resistance, Nature Reviews Microbiology, 13 (2015) 42-51.

[19] H. Yoshida, M. Bogaki, M. Nakamura, S. Nakamura, Quinolone resistance-determining region in the DNA gyrase gyrA gene of Escherichia coli, Antimicrobial Agents and Chemotherapy, 34 (1990) 1271-1272.

[20] X.-S. Pan, G. Yague, L.M. Fisher, Quinolone resistance mutations in Streptococcus pneumoniae GyrA and ParC proteins: mechanistic insights into quinolone action from enzymatic analysis, intracellular levels, and phenotypes of wild-type and mutant proteins, Antimicrobial Agents and Chemotherapy, 45 (2001) 3140-3147.

[21] D.J. Jin, C.A. Gross, Mapping and sequencing of mutations in the Escherichia colirpoB gene that lead to rifampicin resistance, Journal of Molecular Biology, 202 (1988) 45-58.

[22] A. Tomasz, Weapons of microbial drug resistance abound in soil flora, Science(Washington), 311 (2006) 342-343.

[23] J. Davies, Inactivation of antibiotics and the dissemination of resistance genes, Science, 264 (1994) 375-382.

[24] I. Brook, Beta-lactamase-producing bacteria and their role in infection, Reviews in Medical Microbiology, 16 (2005) 91-99.

[25] D.J. Wolter, N.D. Hanson, P.D. Lister, Insertional inactivation of oprD in clinical isolates of Pseudomonas aeruginosa leading to carbapenem resistance, FEMS Microbiology Letters, 236 (2004) 137-143.
[26] G.D. Wright, Bacterial resistance to antibiotics: enzymatic degradation and modification, Advanced Drug Delivery Reviews, 57 (2005) 1451-1470.
[27] K. Shi, S.J. Caldwell, D.H. Fong, A.M. Berghuis, Prospects for circumventing aminoglycoside kinase mediated antibiotic resistance, Frontiers in Cellular and Infection Microbiology, 3 (2013).
[28] S. Schwarz, C. Kehrenberg, B. Doublet, A. Cloeckaert, Molecular basis of bacterial resistance to chloramphenicol and florfenicol, FEMS Microbiology Reviews, 28 (2004) 519-542.
[29] K.D. Green, S. Garneau-Tsodikova, Resistance in tuberculosis: what do we know and where can we go, Frontiers in Microbiology, 4 (2013).
[30] M.-P. Mingeot-Leclercq, P.M. Tulkens, Aminoglycosides: nephrotoxicity, Antimicrobial Agents and Chemotherapy, 43 (1999) 1003-1012.
[31] A. Yunis, Chloramphenicol toxicity: 25 years of research, The American Journal of Medicine, 87 (1989) 44N-48N.
[32] P.J. Whalley, F.G. Martin, R.H. Adams, B. Combes, Disposition of tetracycline by pregnant women with acute pyelonephritis, Obstetrics & Gynecology, 36 (1970) 821-826.
[33] A. Sarro, G. Sarro, Adverse reactions to fluoroquinolones. An overview on mechanistic aspects, Current Medicinal Chemistry, 8 (2001) 371-384.
[34] M.F. Grill, R. Maganti, Cephalosporin-induced neurotoxicity: clinical manifestations, potential pathogenic mechanisms, and the role of electroencephalographic monitoring, Annals of Pharmacotherapy, 42 (2008) 1843-1850.
[35] M.F. Grill, R.K. Maganti, Neurotoxic effects associated with antibiotic use: management considerations, British Journal of Clinical Pharmacology, 72 (2011) 381-393.
[36] N. Principi, S. Esposito, Comparative tolerability of erythromycin and newer macrolide antibacterials in paediatric patients, Drug Safety, 20 (1999) 25-41.
[37] A.D. Association, Diagnosis and classification of diabetes mellitus, Diabetes Care, 36 (2013) S67-S74.
[38] D. Mellitus, Diagnosis and classification of diabetes mellitus, Diabetes care, 28 (2005) S37.
[39] S. Wild, G. Roglic, A. Green, R. Sicree, H. King, Global prevalence of diabetes estimates for the year 2000 and projections for 2030, Diabetes Care, 27 (2004) 1047-1053.
[40] A. Lernmark, A. Falorni, Immune phenomena and events in the islets in insulin-dependent diabetes mellitus, in, Blackwell Science: Oxford, 1997, pp. 15.11-15.23.
[41] D.B. Schranz, Å. Lernmark, Immunology in diabetes: an update, Diabetes/Metabolism Reviews, 14 (1998) 3-29.
[42] J.-W. Yoon, H.-S. Jun, Autoimmune destruction of pancreatic β cells, American Journal of Therapeutics, 12 (2005) 580-591.
[43] F.B. Hu, J.E. Manson, M.J. Stampfer, G. Colditz, S. Liu, C.G. Solomon, W.C. Willett, Diet, lifestyle, and the risk of type 2 diabetes mellitus in women, New England Journal of Medicine, 345 (2001) 790-797.
[44] C. Stehouwer, I. Ferreira, M. Kosakova, C. Palombo, Glucose metabolism, Diabetes and the Arterial Wall, (2015).
[45] M. Piero, G. Nzaro, J. Njagi, Diabetes mellitus-a devastating metabolic disorder, Asian Journal of Biomedical and Pharmaceutical Sciences, 5 (2015) 1.
[46] G. Wilcox, Insulin and insulin resistance, Clinical Biochemist Reviews, 26 (2005) 19.
[47] R.R. Wolfe, E.R. Nadel, J. Shaw, L.A. Stephenson, M.H. Wolfe, Role of changes in insulin and glucagon in glucose homeostasis in exercise, Journal of Clinical Investigation, 77 (1986) 900.
[48] E.A. Nyenwe, A.E. Kitabchi, The Evolution of Diabetic Ketoacidosis: An Update of its Etiology, Pathogenesis and Management, Metabolism, (2015) 507-521.
[49] U. Yoon, L.L. Kwok, A. Magkidis, Efficacy of lifestyle interventions in reducing diabetes incidence in patients with impaired glucose tolerance: a systematic review of randomized controlled trials, Metabolism, 62 (2013) 303-314.
[50] A.B. Olokoba, O.A. Obateru, L.B. Olokoba, Type 2 diabetes mellitus: a review of current trends, Oman Medical Journal, 27 (2012) 269-273.

[51] E.A. Nyenwe, T.W. Jerkins, G.E. Umpierrez, A.E. Kitabchi, Management of type 2 diabetes: evolving strategies for the treatment of patients with type 2 diabetes, Metabolism, 60 (2011) 1-23.
[52] D.M. Nathan, J.B. Buse, M.B. Davidson, E. Ferrannini, R.R. Holman, R. Sherwin, B. Zinman, Medical management of hyperglycemia in type 2 diabetes: a consensus algorithm for the initiation and adjustment of therapy a consensus statement of the American Diabetes Association and the European Association for the Study of Diabetes, Diabetes Care, 32 (2009) 193-203.
[53] S.E. Inzucchi, R.M. Bergenstal, J.B. Buse, M. Diamant, E. Ferrannini, M. Nauck, A.L. Peters, A. Tsapas, R. Wender, D.R. Matthews, Management of hyperglycemia in type 2 diabetes, 2015: a patient-centered approach: update to a position statement of the American Diabetes Association and the European Association for the Study of Diabetes, Diabetes Care, 38 (2015) 140-149.
[54] H. Nasri, M. Rafieian-Kopaei, Metformin: current knowledge, Journal of Research in Medical Sciences, 19 (2014).
[55] R.W. Nesto, D. Bell, R.O. Bonow, V. Fonseca, S.M. Grundy, E.S. Horton, M. Le Winter, D. Porte, C.F. Semenkovich, S. Smith, Thiazolidinedione use, fluid retention, and congestive heart failure a consensus statement from the American Heart Association and American Diabetes Association, Circulation, 108 (2003) 2941-2948.
[56] A. Neumann, A. Weill, P. Ricordeau, J. Fagot, F. Alla, H. Allemand, Pioglitazone and risk of bladder cancer among diabetic patients in France: a population-based cohort study, Diabetologia, 55 (2012) 1953-1962.
[57] R. Pathak, M. Barna Bridgeman, Dipeptidyl peptidase-4 (DPP-4) inhibitors in the management of diabetes, Pharmacy and Therapeutics, 35 (2010) 509.
[58] F.A. Van De Laar, P.L. Lucassen, R.P. Akkermans, E.H. Van De Lisdonk, G.E. Rutten, C. Van Weel, α-Glucosidase Inhibitors for Patients With Type 2 Diabetes Results from a Cochrane systematic review and meta-analysis, Diabetes Care, 28 (2005) 154-163.
[59] M. Alsahli, J.E. Gerich, Hypoglycemia in patients with diabetes and renal disease, Journal of Clinical Medicine, 4 (2015) 948-964.
[60] A. Ptaszynska, K.M. Johnsson, S.J. Parikh, T.W. de Bruin, A.M. Apanovitch, J.F. List, Safety profile of dapagliflozin for type 2 diabetes: pooled analysis of clinical studies for overall safety and rare events, Drug Safety, 37 (2014) 815-829.
[61] O.V. Salata, Applications of nanoparticles in biology and medicine, Journal of Nanobiotechnology, 2 (2004) 3.
[62] J.L. Vivero-Escoto, Y.-T. Huang, Inorganic-organic hybrid nanomaterials for therapeutic and diagnostic imaging applications, International Journal of Molecular Sciences, 12 (2011) 3888-3927.
[63] A. Chaubey, S. Pandeya, Pyridine: a versatile nucleuse in pharmaceutical field, Asian Journal of Pharmaceutical and Clinical Research, 4 (2011) 5-8.
[64] C.-M. Lu, Y.-L. Chen, H.-L. Chen, C.-A. Chen, P.-J. Lu, C.-N. Yang, C.-C. Tzeng, Synthesis and antiproliferative evaluation of certain indolo [3, 2-c] quinoline derivatives, Bioorganic & Medicinal Chemistry, 18 (2010) 1948-1957.
[65] G.M. Buckley, N. Cooper, R.J. Davenport, H.J. Dyke, F.P. Galleway, L. Gowers, A.F. Haughan, H.J. Kendall, C. Lowe, J.G. Montana, 7-Methoxyfuro [2, 3-c] pyridine-4-carboxamides as PDE4 Inhibitors: A Potential Treatment for Asthma, Bioorganic & Medicinal Chemistry Letters, 12 (2002) 509-512.
[66] D. O'Hagan, Pyrrole, pyrrolidine pyridine, piperidine, azepine and tropane alkaloids, Natural Product Reports, 14 (1997) 637-651.
[67] M. Horiuch, C. Murakami, N. Fukamiya, D. Yu, T.-H. Chen, K.F. Bastow, D.-C. Zhang, Y. Takaishi, Y. Imakura, K.-H. Lee, Tripfordines AC, Sesquiterpene Pyridine Alkaloids from Tripterygium w ilfordii, and Structure Anti-HIV Activity Relationships of Tripterygium Alkaloids, Journal of Natural Products, 69 (2006) 1271-1274.
[68] A.-Y. Guan, C.-L. Liu, X.-F. Sun, Y. Xie, Discovery of pyridine-based agrochemicals by using Intermediate Derivatization Methods, Bioorganic & Medicinal Chemistry, (2015).
[69] J. You, M.-F. Lo, W. Liu, T.-W. Ng, S.-L. Lai, P. Wang, C.-S. Lee, Synthesis and characterization of cyano-substituted pyridine derivatives for applications as exciton blockers in photovoltaic devices, Journal of Materials Chemistry, 22 (2012) 5107-5113.

[70] P.K. Koech, E. Polikarpov, J.E. Rainbolt, L. Cosimbescu, J.S. Swensen, A.L. Von Ruden, A.B. Padmaperuma, Synthesis and application of pyridine-based ambipolar hosts: control of charge balance in organic light-emitting devices by chemical structure modification, Organic Letters, 12 (2010) 5534-5537.
[71] S. Lin, X. Lu, Cationic Pd (II)/bipyridine-catalyzed conjugate addition of arylboronic acids to β, β-disubstituted enones: Construction of quaternary carbon centers, Organic Letters, 12 (2010) 2536-2539.
[72] N. De Rycke, F. Couty, O.R. David, Increasing the Reactivity of Nitrogen Catalysts, Chemistry-A European Journal, 17 (2011) 12852-12871.
[73] M.T. Cocco, C. Congiu, V. Lilliu, V. Onnis, Synthesis and in vitro antitumoral activity of new 3, 5-dicyanopyridine derivatives, Bioorganic & Medicinal Chemistry, 15 (2007) 1859-1867.
[74] U.V. Desai, M.A. Kulkarni, K.S. Pandit, A.M. Kulkarni, P.P. Wadgaonkar, A simple, economical, and environmentally benign protocol for the synthesis of 2-amino-3, 5-dicarbonitrile-6-sulfanylpyridines at ambient temperature, Green Chemistry Letters and Reviews, 7 (2014) 228-235.
[75] N.M. Evdokimov, A.S. Kireev, A.A. Yakovenko, M.Y. Antipin, I.V. Magedov, A. Kornienko, One-step synthesis of heterocyclic privileged medicinal scaffolds by a multicomponent reaction of malononitrile with aldehydes and thiols, The Journal of Organic Chemistry, 72 (2007) 3443-3453.
[76] M.B. Kanani, M.P. Patel, Synthesis and in vitro antimicrobial evaluation of novel 2-amino-6-(phenylthio)-4-(2-(phenylthio) quinolin-3-yl) pyridine-3, 5-dicarbonitriles, Medicinal Chemistry Research, 22 (2013) 2912-2920.
[77] J.A. Makawana, M.P. Patel, R.G. Patel, Synthesis and in vitro antimicrobial evaluation of penta-substituted pyridine derivatives bearing the quinoline nucleus, Medicinal Chemistry Research, 21 (2012) 616-623.
[78] L. Srinivasula Reddy, T. Ram Reddy, R.B. Mohan, A. Mahesh, Y. Lingappa, N.C. Gangi Reddy, An Efficient Green Multi-Component Reaction Strategy for the Synthesis of Highly Functionalised Pyridines and Evaluation of Their Antibacterial Activities, Chemical and Pharmaceutical Bulletin, 61 (2013) 1114-1120.
[79] A.H.H.E. Fawzy A. Attaby, Synthesis, Reactions, and Antiviral Activity of 6-Amino-2-thioxo-1,2-dihydro-3,4-bipyridine-3,5-dicarbonitrile Phosphorus, Sulfur and Silicon, 182 (2007) 695-709.
[80] K. Guo, R. Mutter, W. Heal, T.R. Reddy, H. Cope, S. Pratt, M.J. Thompson, B. Chen, Synthesis and evaluation of a focused library of pyridine dicarbonitriles against prion disease, European Journal of Medicinal Chemistry, 43 (2008) 93-106.
[81] B.C. May, J.A. Zorn, J. Witkop, J. Sherrill, A.C. Wallace, G. Legname, S.B. Prusiner, F.E. Cohen, Structure-activity relationship study of prion inhibition by 2-aminopyridine-3, 5-dicarbonitrile-based compounds: parallel synthesis, bioactivity, and in vitro pharmacokinetics, Journal of Medicinal Chemistry, 50 (2007) 65-73.
[82] V. Perrier, A.C. Wallace, K. Kaneko, J. Safar, S.B. Prusiner, F.E. Cohen, Mimicking dominant negative inhibition of prion replication through structure-based drug design, Proceedings of the National Academy of Sciences, 97 (2000) 6073-6078.
[83] A.L. Bowman, Z. Nikolovska-Coleska, H. Zhong, S. Wang, H.A. Carlson, Small molecule inhibitors of the MDM2-p53 interaction discovered by ensemble-based receptor models, Journal of the American Chemical Society, 129 (2007) 12809-12814.
[84] J. Deng, T. Sanchez, L.Q. Al-Mawsawi, R. Dayam, R.A. Yunes, A. Garofalo, M.B. Bolger, N. Neamati, Discovery of structurally diverse HIV-1 integrase inhibitors based on a chalcone pharmacophore, Bioorganic & Medicinal Chemistry, 15 (2007) 4985-5002.
[85] K. Yamazaki, N. Kusunose, K. Fujita, H. Sato, S. Asano, A. Dan, M. Kanaoka, Identification of phosphodiesterase-1 and 5 dual inhibitors by a ligand-based virtual screening optimized for lead evolution, Bioorganic & Medicinal Chemistry Letters, 16 (2006) 1371-1379.
[86] M.W. Beukers, L.C. Chang, J.K. von Frijtag Drabbe Künzel, T. Mulder-Krieger, R.F. Spanjersberg, J. Brussee, A.P. IJzerman, New, non-adenosine, high-potency agonists for the human adenosine A2B receptor with an improved selectivity profile compared to the reference agonist N-ethylcarboxamidoadenosine, Journal of Medicinal Chemistry, 47 (2004) 3707-3709.

[87] H. Johnston-Cox, A.S. Eisenstein, M. Koupenova, S. Carroll, K. Ravid, The macrophage A2B adenosine receptor regulates tissue insulin sensitivity, PLOS One (2014).
[88] K. Drew, T. Jinka, L. Bogren, I. Bailey, Z. Carlson, J. Olson, Methods and compositions for the treatment of ischemic injury to tissue using therapeutic hypothermia, in, US Patent 20,150,238,513, 2015.
[89] U. Rosentreter, R. Henning, M. Bauser, T. Krämer, A. Vaupel, W. Hübsch, K. Dembowsky, O. Salcher-Schraufstätter, J.-P. Stasch, T. Krahn, Substituted 2-thio-3, 5-dicyano-4-aryl-6-aminopyridines and the use thereof, in, Google Patents, 2006.
[90] T. Krahn, T. Krämer, U. Rosentreter, J.M. Downey, N. Solenkova, Use of substituted 2-thio-3, 5-dicyano-4-phenyl-6-aminopyridines for the treatment of reperfusion injury and reperfusion damage, in, Google Patents, 2006.
[91] J. Louvel, D. Guo, M. Soethoudt, T.A. Mocking, E.B. Lenselink, T. Mulder-Krieger, L.H. Heitman, A.P. IJzerman, Structure-kinetics relationships of Capadenoson derivatives as adenosine A 1 receptor agonists, European Journal of Medicinal Chemistry, 101 (2015) 681-691.
[92] M. Tendera, E. Gaszewska-Żurek, Z. Parma, P. Ponikowski, E. Jankowska, K. Kawecka-Jaszcz, D. Czarnecka, M. Krzemińska-Pakuła, Z. Bednarkiewicz, M. Sosnowski, The new oral adenosine A1 receptor agonist capadenoson in male patients with stable angina, Clinical Research in Cardiology, 101 (2012) 585-591.
[93] H.T. Lee, C.W. Emala, Protective effects of renal ischemic preconditioning and adenosine pretreatment: role of A1 and A3receptors, American Journal of Physiology-Renal Physiology, 278 (2000) F380-F387.
[94] C. Freiberg, I. Knezevic, T. Krahn, K. Ziegelbauer, M. Braun, N. Diedrichs, Use of adenosine A1 receptor agonists for the protection of renal cells against toxic effects caused by aminoglycosides during treatment of infectious diseases, WO2007073855, (2007).
[95] S. Hinz, S.K. Lacher, B.F. Seibt, C.E. Müller, BAY60-6583 acts as a partial agonist at adenosine A2B receptors, Journal of Pharmacology and Experimental Therapeutics, 349 (2014) 427-436.
[96] D. Anderson, N. Stehle, S. Kolodziej, E. Reinhard, Preparation of aminocyanopyridines as inhibitors of mitogen activated protein kinase-activated protein kinase-2 for treating TNFα mediated diseases, PCT Int. Appl. WO Patent, 55015 (2004) A1.
[97] M.A. Quraishi, 2-Amino-3, 5-dicarbonitrile-6-thio-pyridines: new and effective corrosion inhibitors for mild steel in 1 M HCl, Industrial & Engineering Chemistry Research, 53 (2014) 2851-2859.
[98] P.V. Shinde, S.S. Sonar, B.B. Shingate, M.S. Shingare, Boric acid catalyzed convenient synthesis of 2-amino-3, 5-dicarbonitrile-6-thio-pyridines in aqueous media, Tetrahedron Letters, 51 (2010) 1309-1312.
[99] R. Mamgain, R. Singh, D.S. Rawat, DBU-catalyzed three-component one-pot synthesis of highly functionalized pyridines in aqueous ethanol, Journal of Heterocyclic Chemistry, 46 (2009) 69.
[100] M. Kidwai, R. Chauhan, K_2CO_3 catalyzed green and rapid access to 2-amino-3, 5-dicarbonitrile-6-thio-pyridines, Journal of the Iranian Chemical Society, 11 (2014) 1005-1013.
[101] S.S. Kottawar, S.A. Siddiqui, S.R. Bhusare, Scandium triflate-catalyzed one-pot multi-component synthesis of 2-amino-6-thiopyridine-3, 5-dicarbonitriles, Heterocyclic Communications, 18 (2012) 249–252.
[102] M. Sridhar, B.C. Ramanaiah, C. Narsaiah, B. Mahesh, M. Kumaraswamy, K.K. Mallu, V.M. Ankathi, P.S. Rao, Novel ZnCl 2-catalyzed one-pot multicomponent synthesis of 2-amino-3, 5-dicarbonitrile-6-thio-pyridines, Tetrahedron Letters, 50 (2009) 3897-3900.
[103] A. Davoodnia, P. Attar, H. Eshghi, A. Morsali, N. Tavakoli-Hoseini, A. Tavakoli-Nishaburi, Ionic Liquid,[bmim] Br, as An Efficient Promoting Medium for Synthesis of 2-Amino-3, 5-dicarbonitrile-6-thiopyridines, Asian Journal of Chemistry, 23 (2011) 1273.
[104] B.C. Ranu, R. Jana, S. Sowmiah, An improved procedure for the three-component synthesis of highly substituted pyridines using ionic liquid, The Journal of Organic Chemistry, 72 (2007) 3152-3154.
[105] J. Safaei-Ghomi, H. Shahbazi-Alavi, E. Heidari-Baghbahadorani, SnO nanoparticles as an efficient catalyst for the one-pot synthesis of chromeno [2, 3-b] pyridines and 2-amino-3, 5-dicyano-6-sulfanyl pyridines, RSC Advances, 4 (2014) 50668-50677.

[106] B. Baghernejad, Nano-TiO 2 as a novel and efficient catalyst for the synthesis of pyridine dicarbonitriles, Bulletin of the Chemical Society of Ethiopia, 28 (2014) 149-153.
[107] J. Safaei-Ghomi, M. Ghasemzadeh, M. Mehrabi, Calcium oxide nanoparticles catalyzed one-step multicomponent synthesis of highly substituted pyridines in aqueous ethanol media, Scientia Iranica, 20 (2013) 549-554.
[108] S. Sobhani, M. Honarmand, Ionic liquid immobilized on γ-Fe 2 O 3 nanoparticles: A new magnetically recyclable heterogeneous catalyst for one-pot three-component synthesis of 2-amino-3, 5-dicarbonitrile-6-thio-pyridines, Applied Catalysis A: General, 467 (2013) 456-462.
[109] J. Safaei-Ghomi, M.A. Ghasemzadeh, ZnO Nanoparticles as New and Efficient Catalyst for the One-pot Synthesis of Polyfunctionalized Pyridines, Acta Chimica Slovenica, 59 (2012) 697-702.
[110] S. Banerjee, G. Sereda, One-step, three-component synthesis of highly substituted pyridines using silica nanoparticle as reusable catalyst, Tetrahedron Letters, 50 (2009) 6959-6962.
[111] K. Guo, M.J. Thompson, T.R. Reddy, R. Mutter, B. Chen, Mechanistic studies leading to a new procedure for rapid, microwave assisted generation of pyridine-3, 5-dicarbonitrile libraries, Tetrahedron, 63 (2007) 5300-5311.
[112] D.R. Boverhof, C.M. Bramante, J.H. Butala, S.F. Clancy, M. Lafranconi, J. West, S.C. Gordon, Comparative assessment of nanomaterial definitions and safety evaluation considerations, Regulatory Toxicology and Pharmacology, 73 (2015) 137-150.
[113] A. Schröfel, G. Kratošová, I. Šafařík, M. Šafaříková, I. Raška, L.M. Shor, Applications of biosynthesized metallic nanoparticles–A review, Acta Biomaterialia, 10 (2014) 4023-4042.
[114] F.J. Heiligtag, M. Niederberger, The fascinating world of nanoparticle research, Materials Today, 16 (2013) 262-271.
[115] R. Bhattacharya, P. Mukherjee, Biological properties of "naked" metal nanoparticles, Advanced Drug Delivery Reviews, 60 (2008) 1289-1306.
[116] S.W. Wijnhoven, W.J. Peijnenburg, C.A. Herberts, W.I. Hagens, A.G. Oomen, E.H. Heugens, B. Roszek, J. Bisschops, I. Gosens, D. Van De Meent, Nano-silver–a review of available data and knowledge gaps in human and environmental risk assessment, Nanotoxicology, 3 (2009) 109-138.
[117] A. Majdalawieh, M.C. Kanan, O. El-Kadri, S.M. Kanan, Recent advances in gold and silver nanoparticles: synthesis and applications, Journal of Nanoscience and Nanotechnology, 14 (2014) 4757-4780.
[118] M.F. Hochella, S.K. Lower, P.A. Maurice, R.L. Penn, N. Sahai, D.L. Sparks, B.S. Twining, Nanominerals, Mineral Nanoparticles, and Earth Systems, Science, 319 (2008) 1631-1635.
[119] K. Kobayashi, J. Wei, R. Iida, K. Ijiro, K. Niikura, Surface engineering of nanoparticles for therapeutic applications, Polymer Journal, 46 (2014) 460-468.
[120] V.V. Mody, R. Siwale, A. Singh, H.R. Mody, Introduction to metallic nanoparticles, Journal of Pharmacy and Bioallied Sciences, 2 (2010) 282.
[121] H. Liao, C.L. Nehl, J.H. Hafner, Biomedical applications of plasmon resonant metal nanoparticles, Future Medicine, 1 (2006) 201-208.
[122] Y. Zhang, R. Huang, X. Zhu, L. Wang, C. Wu, Synthesis, properties, and optical applications of noble metal nanoparticle-biomolecule conjugates, Chinese Science Bulletin, 57 (2012) 238-246.
[123] X. Huang, M.A. El-Sayed, Gold nanoparticles: optical properties and implementations in cancer diagnosis and photothermal therapy, Journal of Advanced Research, 1 (2010) 13-28.
[124] S.M. Dizaj, F. Lotfipour, M. Barzegar-Jalali, M.H. Zarrintan, K. Adibkia, Antimicrobial activity of the metals and metal oxide nanoparticles, Materials Science and Engineering: C, 44 (2014) 278-284.
[125] G. Franci, A. Falanga, S. Galdiero, L. Palomba, M. Rai, G. Morelli, M. Galdiero, Silver nanoparticles as potential antibacterial agents, Molecules, 20 (2015) 8856-8874.
[126] P. Dibrov, J. Dzioba, K.K. Gosink, C.C. Häse, Chemiosmotic mechanism of antimicrobial activity of Ag+ in Vibrio cholerae, Antimicrobial Agents and Chemotherapy, 46 (2002) 2668-2670.
[127] I. Sondi, B. Salopek-Sondi, Silver nanoparticles as antimicrobial agent: a case study on E. coli as a model for Gram-negative bacteria, Journal of Colloid and Interface Science, 275 (2004) 177-182.

[128] N.A. Amro, L.P. Kotra, K. Wadu-Mesthrige, A. Bulychev, S. Mobashery, G.-y. Liu, High-resolution atomic force microscopy studies of the Escherichia coli outer membrane: structural basis for permeability, Langmuir, 16 (2000) 2789-2796.
[129] J. Spadaro, T. Berger, S. Barranco, S. Chapin, R. Becker, Antibacterial effects of silver electrodes with weak direct current, Antimicrobial Agents and Chemotherapy, 6 (1974) 637-642.
[130] Q. Feng, J. Wu, G. Chen, F. Cui, T. Kim, J. Kim, A mechanistic study of the antibacterial effect of silver ions on Escherichia coli and Staphylococcus aureus, Journal of Biomedical Materials Research, 52 (2000) 662-668.
[131] J.S. Kim, E. Kuk, K.N. Yu, J.-H. Kim, S.J. Park, H.J. Lee, S.H. Kim, Y.K. Park, Y.H. Park, C.-Y. Hwang, Antimicrobial effects of silver nanoparticles, Nanomedicine: Nanotechnology, Biology and Medicine, 3 (2007) 95-101.
[132] A. Nagy, A. Harrison, S. Sabbani, R.S. Munson Jr, P.K. Dutta, W.J. Waldman, Silver nanoparticles embedded in zeolite membranes: release of silver ions and mechanism of antibacterial action, International Journal of Nanomedicine, 6 (2011) 1833.
[133] B. Nowack, H.F. Krug, M. Height, 120 years of nanosilver history: implications for policy makers, Environmental Science & Technology, 45 (2011) 1177-1183.
[134] B.S. Sekhon, S.R. Kamboj, Inorganic nanomedicine—part 2, Nanomedicine: Nanotechnology, Biology and Medicine, 6 (2010) 612-618.
[135] X. Li, S.M. Robinson, A. Gupta, K. Saha, Z. Jiang, D.F. Moyano, A. Sahar, M.A. Riley, V.M. Rotello, Functional gold nanoparticles as potent antimicrobial agents against multi-drug-resistant bacteria, ACS Nano, 8 (2014) 10682-10686.
[136] Y. Zhou, Y. Kong, S. Kundu, J.D. Cirillo, H. Liang, Antibacterial activities of gold and silver nanoparticles against Escherichia coli and bacillus Calmette-Guérin, Journal of Nanobiotechnology, 10 (2012) 1-9.
[137] V.P. Zharov, K.E. Mercer, E.N. Galitovskaya, M.S. Smeltzer, Photothermal nanotherapeutics and nanodiagnostics for selective killing of bacteria targeted with gold nanoparticles, Biophysical Journal, 90 (2006) 619-627.
[138] D. Bhattacharya, B. Saha, A. Mukherjee, C.R. Santra, P. Karmakar, Gold nanoparticles conjugated antibiotics: stability and functional evaluation, Nanoscience and Nanotechnology, 2 (2012) 14-21.
[139] R. Sinha, G.J. Kim, S. Nie, D.M. Shin, Nanotechnology in cancer therapeutics: bioconjugated nanoparticles for drug delivery, Molecular Cancer Therapeutics, 5 (2006) 1909-1917.
[140] P. Mukherjee, R. Bhattacharya, P. Wang, L. Wang, S. Basu, J.A. Nagy, A. Atala, D. Mukhopadhyay, S. Soker, Antiangiogenic properties of gold nanoparticles, Clinical Cancer Research, 11 (2005) 3530-3534.
[141] R.-A. Sperling, W. Parak, Surface modification, functionalization and bioconjugation of colloidal inorganic nanoparticles, Philosophical Transactions of the Royal Society of London A: Mathematical, Physical and Engineering Sciences, 368 (2010) 1333-1383.
[142] D. Guo, L. Zhu, Z. Huang, H. Zhou, Y. Ge, W. Ma, J. Wu, X. Zhang, X. Zhou, Y. Zhang, Anti-leukemia activity of PVP-coated silver nanoparticles via generation of reactive oxygen species and release of silver ions, Biomaterials, 34 (2013) 7884-7894.
[143] S. Gurunathan, J.W. Han, V. Eppakayala, M. Jeyaraj, J.-H. Kim, Cytotoxicity of biologically synthesized silver nanoparticles in MDA-MB-231 human breast cancer cells, BioMed Research International, 2013 (2013).
[144] S. Gurunathan, J.W. Han, A.A. Dayem, V. Eppakayala, J.H. Park, S.-G. Cho, K.J. Lee, J.-H. Kim, Green synthesis of anisotropic silver nanoparticles and its potential cytotoxicity in human breast cancer cells (MCF-7), Journal of Industrial and Engineering Chemistry, 19 (2013) 1600-1605.
[145] W. He, Y.-T. Zhou, W.G. Wamer, M.D. Boudreau, J.-J. Yin, Mechanisms of the pH dependent generation of hydroxyl radicals and oxygen induced by Ag nanoparticles, Biomaterials, 33 (2012) 7547-7555.
[146] V. Raji, J. Kumar, C. Rejiya, M. Vibin, V.N. Shenoi, A. Abraham, Selective photothermal efficiency of citrate capped gold nanoparticles for destruction of cancer cells, Experimental Cell Research, 317 (2011) 2052-2058.
[147] P. Mukherjee, R. Bhattacharya, N. Bone, Y.K. Lee, C.R. Patra, S. Wang, L. Lu, C. Secreto, P.C. Banerjee, M.J. Yaszemski, Potential therapeutic application of gold nanoparticles in B-chronic lymphocytic leukemia (BCLL): enhancing apoptosis, Journal of Nanobiotechnology, 5 (2007) 1-13.

[148] W. Lu, A.K. Singh, S.A. Khan, D. Senapati, H. Yu, P.C. Ray, Gold nano-popcorn-based targeted diagnosis, nanotherapy treatment, and in situ monitoring of photothermal therapy response of prostate cancer cells using surface-enhanced Raman spectroscopy, Journal of the American Chemical Society, 132 (2010) 18103-18114.
[149] E.S. Day, J.G. Morton, J.L. West, Nanoparticles for thermal cancer therapy, Journal of Biomechanical Engineering, 131 (2009) 074001.
[150] J. Chen, D. Wang, J. Xi, L. Au, A. Siekkinen, A. Warsen, Z.-Y. Li, H. Zhang, Y. Xia, X. Li, Immuno gold nanocages with tailored optical properties for targeted photothermal destruction of cancer cells, Nano Letters, 7 (2007) 1318-1322.
[151] J. Conde, G. Doria, P. Baptista, Noble metal nanoparticles applications in cancer, Journal of Drug Delivery, 2012 (2011).
[152] S. Dhar, W.L. Daniel, D.A. Giljohann, C.A. Mirkin, S.J. Lippard, Polyvalent oligonucleotide gold nanoparticle conjugates as delivery vehicles for platinum (IV) warheads, Journal of the American Chemical Society, 131 (2009) 14652-14653.
[153] J.D. Gibson, B.P. Khanal, E.R. Zubarev, Paclitaxel-functionalized gold nanoparticles, Journal of the American Chemical Society, 129 (2007) 11653-11661.
[154] N.L. Rosi, D.A. Giljohann, C.S. Thaxton, A.K. Lytton-Jean, M.S. Han, C.A. Mirkin, Oligonucleotide-modified gold nanoparticles for intracellular gene regulation, Science, 312 (2006) 1027-1030.
[155] J. Barar, Y. Omidi, Surface modified multifunctional nanomedicines for simultaneous imaging and therapy of cancer, BioImpacts: BI, 4 (2014) 3.
[156] K.L. Kelly, E. Coronado, L.L. Zhao, G.C. Schatz, The optical properties of metal nanoparticles: the influence of size, shape, and dielectric environment, The Journal of Physical Chemistry B, 107 (2003) 668-677.
[157] P.K. Jain, K.S. Lee, I.H. El-Sayed, M.A. El-Sayed, Calculated absorption and scattering properties of gold nanoparticles of different size, shape, and composition: applications in biological imaging and biomedicine, The Journal of Physical Chemistry B, 110 (2006) 7238-7248.
[158] D.J. Brenner, E.J. Hall, Computed tomography—an increasing source of radiation exposure, New England Journal of Medicine, 357 (2007) 2277-2284.
[159] E.C. Cho, C. Glaus, J. Chen, M.J. Welch, Y. Xia, Inorganic nanoparticle-based contrast agents for molecular imaging, Trends in Molecular Medicine, 16 (2010) 561-573.
[160] M.P. Melancon, W. Lu, C. Li, Gold-based magneto/optical nanostructures: challenges for in vivo applications in cancer diagnostics and therapy, MRS Bulletin, 34 (2009) 415-421.
[161] X. Shi, S. Wang, S. Meshinchi, M.E. Van Antwerp, X. Bi, I. Lee, J.R. Baker, Dendrimer-Entrapped Gold Nanoparticles as a Platform for Cancer-Cell Targeting and Imaging, Small, 3 (2007) 1245-1252.
[162] X. Huang, I.H. El-Sayed, W. Qian, M.A. El-Sayed, Cancer cell imaging and photothermal therapy in the near-infrared region by using gold nanorods, Journal of the American Chemical Society, 128 (2006) 2115-2120.
[163] J.C.Y. Kah, K.W. Kho, C.G.L. Lee, C.J. Richard, Early diagnosis of oral cancer based on the surface plasmon resonance of gold nanoparticles, International Journal of Nanomedicine, 2 (2007) 785.
[164] D. Kim, S. Park, J.H. Lee, Y.Y. Jeong, S. Jon, Antibiofouling Polymer-Coated Gold Nanoparticles as a Contrast Agent for in Vivo X-ray Computed Tomography Imaging [J. Am. Chem. Soc. 2007, 129, 7661-7665], Journal of the American Chemical Society, 129 (2007) 12585-12585.
[165] A.J. Haes, L. Chang, W.L. Klein, R.P. Van Duyne, Detection of a biomarker for Alzheimer's disease from synthetic and clinical samples using a nanoscale optical biosensor, Journal of the American Chemical Society, 127 (2005) 2264-2271.
[166] H. Uzawa, K. Ohga, Y. Shinozaki, I. Ohsawa, T. Nagatsuka, Y. Seto, Y. Nishida, A novel sugar-probe biosensor for the deadly plant proteinous toxin, ricin, Biosensors and Bioelectronics, 24 (2008) 923-927.
[167] S. Zhu, C. Du, Y. Fu, Localized surface plasmon resonance-based hybrid Au–Ag nanoparticles for detection of Staphylococcus aureus enterotoxin B, Optical Materials, 31 (2009) 1608-1613.

[168] P. Sistani, L. Sofimaryo, Z.R. Masoudi, A. Sayad, R. Rahimzadeh, B. Salehi, A Penicillin Biosensor by Using Silver Nanoparticles, International Journal of Electrochemical Science, 9 (2014) 6201-6212.
[169] H. Wei, C. Chen, B. Han, E. Wang, Enzyme colorimetric assay using unmodified silver nanoparticles, Analytical Chemistry, 80 (2008) 7051-7055.
[170] Y. Chen, J. Aveyard, R. Wilson, Gold and silver nanoparticles functionalized with known numbers of oligonucleotides per particle for DNA detection, Chemical Communications, (2004) 2804-2805.
[171] T. Ghodselahi, S. Arsalani, T. Neishaboorynejad, Synthesis and biosensor application of Ag-Au bimetallic nanoparticles based on localized surface plasmon resonance, Applied Surface Science, 301 (2014) 230-234.
[172] M. Ullmann, S.K. Friedlander, A. Schmidt-Ott, Nanoparticle formation by laser ablation, Journal of Nanoparticle Research, 4 (2002) 499-509.
[173] T.P. Yadav, R.M. Yadav, D.P. Singh, Mechanical milling: a top down approach for the synthesis of nanomaterials and nanocomposites, Nanoscience and Nanotechnology, 2 (2012) 22-48.
[174] E. Gaffet, M. Tachikart, O. El Kedim, R. Rahouadj, Nanostructural materials formation by mechanical alloying: morphologic analysis based on transmission and scanning electron microscopic observations, Materials Characterization, 36 (1996) 185-190.
[175] T. Tsuji, K. Iryo, N. Watanabe, M. Tsuji, Preparation of silver nanoparticles by laser ablation in solution: influence of laser wavelength on particle size, Applied Surface Science, 202 (2002) 80-85.
[176] F. Mafuné, J.-y. Kohno, Y. Takeda, T. Kondow, H. Sawabe, Formation of gold nanoparticles by laser ablation in aqueous solution of surfactant, The Journal of Physical Chemistry B, 105 (2001) 5114-5120.
[177] H.K. Iravani, S. Mirmohammadi, S. B Zolfaghari, Synthesis of silver nanoparticles: chemical, physical and biological methods, Research in Pharmaceutical Sciences, 9 (2014) 385-406.
[178] M. Cavicchioli, L.C. Varanda, A.C. Massabni, P. Melnikov, Silver nanoparticles synthesized by thermal reduction of a silver (I)–aspartame complex in inert atmosphere, Materials Letters, 59 (2005) 3585-3589.
[179] B. Aswathy, G. Avadhani, I. Sumithra, S. Suji, G. Sony, Microwave assisted synthesis and UV–Vis spectroscopic studies of silver nanoparticles synthesized using vanillin as a reducing agent, Journal of Molecular Liquids, 159 (2011) 165-169.
[180] L.-P. Jiang, S. Xu, J.-M. Zhu, J.-R. Zhang, J.-J. Zhu, H.-Y. Chen, Ultrasonic-assisted synthesis of monodisperse single-crystalline silver nanoplates and gold nanorings, Inorganic Chemistry, 43 (2004) 5877-5883.
[181] R.A. Khaydarov, R.R. Khaydarov, O. Gapurova, Y. Estrin, T. Scheper, Electrochemical method for the synthesis of silver nanoparticles, Journal of Nanoparticle Research, 11 (2009) 1193-1200.
[182] H. Jia, J. Zeng, W. Song, J. An, B. Zhao, Preparation of silver nanoparticles by photo-reduction for surface-enhanced Raman scattering, Thin Solid Films, 496 (2006) 281-287.
[183] R. Richards, H. Bönnemann, Synthetic approaches to metallic nanomaterials, Nanofabrication Towards Biomedical Applications: Techniques, Tools, Applications, and Impact, (2005) 2.
[184] K.M.A. El-Nour, A.a. Eftaiha, A. Al-Warthan, R.A. Ammar, Synthesis and applications of silver nanoparticles, Arabian Journal of Chemistry, 3 (2010) 135-140.
[185] K. Mavani, M. Shah, Synthesis of silver nanoparticles by using sodium borohydride as a reducing agent, in: International journal of engineering research and technology, ESRSA Publications, 2013.
[186] I. Ojea-Jiménez, F.M. Romero, N.G. Bastús, V. Puntes, Small gold nanoparticles synthesized with sodium citrate and heavy water: insights into the reaction mechanism, The Journal of Physical Chemistry C, 114 (2010) 1800-1804.
[187] Y. Qin, X. Ji, J. Jing, H. Liu, H. Wu, W. Yang, Size control over spherical silver nanoparticles by ascorbic acid reduction, Colloids and surfaces A: Physicochemical and Engineering Aspects, 372 (2010) 172-176.
[188] V.V. Tatarchuk, A.P. Sergievskaya, I.A. Druzhinina, V.I. Zaikovsky, Kinetics and mechanism of the growth of gold nanoparticles by reduction of tetrachloroauric acid by hydrazine in Triton N-42 reverse micelles, Journal of Nanoparticle Research, 13 (2011) 4997-5007.

[189] D. Hristozov, I. Malsch, Hazards and risks of engineered nanoparticles for the environment and human health, Sustainability, 1 (2009) 1161-1194.
[190] P.C. Ray, H. Yu, P.P. Fu, Toxicity and environmental risks of nanomaterials: challenges and future needs, Journal of Environmental Science and Health Part C, 27 (2009) 1-35.
[191] S. Ahmed, M. Ahmad, B.L. Swami, S. Ikram, A review on plants extract mediated synthesis of silver nanoparticles for antimicrobial applications: a green expertise, Journal of Advanced Research, 7 (2016) 17-28.
[192] R.M. Slawson, M.I. Van Dyke, H. Lee, J.T. Trevors, Germanium and silver resistance, accumulation, and toxicity in microorganisms, Plasmid, 27 (1992) 72-79.
[193] P. Mohanpuria, N.K. Rana, S.K. Yadav, Biosynthesis of nanoparticles: technological concepts and future applications, Journal of Nanoparticle Research, 10 (2008) 507-517.
[194] M.A. Faramarzi, A. Sadighi, Insights into biogenic and chemical production of inorganic nanomaterials and nanostructures, Advances in Colloid and Interface Science, 189 (2013) 1-20.
[195] J. Chen, Z. Lin, X. Ma, Evidence of the production of silver nanoparticles via pretreatment of Phoma sp. 3.2883 with silver nitrate, Letters in Applied Microbiology, 37 (2003) 105-108.
[196] N. Durán, P.D. Marcato, M. Durán, A. Yadav, A. Gade, M. Rai, Mechanistic aspects in the biogenic synthesis of extracellular metal nanoparticles by peptides, bacteria, fungi, and plants, Applied Microbiology and Biotechnology, 90 (2011) 1609-1624.
[197] P. Ramesh, T. Kokila, D. Geetha, Plant mediated green synthesis and antibacterial activity of silver nanoparticles using Emblica officinalis fruit extract, Spectrochimica acta part A: Molecular and Biomolecular Spectroscopy, 142 (2015) 339-343.
[198] J. Umashankari, D. Inbakandan, T.T. Ajithkumar, T. Balasubramanian, Mangrove plant, Rhizophora mucronata (Lamk, 1804) mediated one pot green synthesis of silver nanoparticles and its antibacterial activity against aquatic pathogens, Aquatic Biosystems, 8 (2012).
[199] S. Patra, S. Mukherjee, A.K. Barui, A. Ganguly, B. Sreedhar, C.R. Patra, Green synthesis, characterization of gold and silver nanoparticles and their potential application for cancer therapeutics, Materials Science and Engineering: C, 53 (2015) 298-309.
[200] S. Megarajan, K.B.A. Ahmed, G.R.K. Reddy, P.S. Kumar, V. Anbazhagan, Phytoproteins in green leaves as building blocks for photosynthesis of gold nanoparticles: An efficient electrocatalyst towards the oxidation of ascorbic acid and the reduction of hydrogen peroxide, Journal of Photochemistry and Photobiology B: Biology, 155 (2016) 7-12.
[201] N. Vigneshwaran, A.A. Kathe, P. Varadarajan, R.P. Nachane, R. Balasubramanya, Biomimetics of silver nanoparticles by white rot fungus, Phaenerochaete chrysosporium, Colloids and Surfaces B: Biointerfaces, 53 (2006) 55-59.
[202] P. Mukherjee, S. Senapati, D. Mandal, A. Ahmad, M.I. Khan, R. Kumar, M. Sastry, Extracellular synthesis of gold nanoparticles by the fungus Fusarium oxysporum, ChemBioChem, 3 (2002) 461-463.
[203] M.A. Faramarzi, H. Forootanfar, Biosynthesis and characterization of gold nanoparticles produced by laccase from Paraconiothyrium variabile, Colloids and Surfaces B: Biointerfaces, 87 (2011) 23-27.
[204] R.R. Bhattacharjee, A.K. Das, D. Haldar, S. Si, A. Banerjee, T.K. Mandal, Peptide-assisted synthesis of gold nanoparticles and their self-assembly, Journal of Nanoscience and Nanotechnology, 5 (2005) 1141-1147.
[205] B. Nair, T. Pradeep, Coalescence of nanoclusters and formation of submicron crystallites assisted by Lactobacillus strains, Crystal Growth & Design, 2 (2002) 293-298.
[206] M. Decker, Hybrid molecules incorporating natural products: applications in cancer therapy, neurodegenerative disorders and beyond, Current Medicinal Chemistry, 18 (2011) 1464-1475.
[207] L. Wang, W. Zhao, W. Tan, Bioconjugated silica nanoparticles: development and applications, Nano Research, 1 (2008) 99-115.

[208] R.P. Bagwe, C. Yang, L.R. Hilliard, W. Tan, Optimization of dye-doped silica nanoparticles prepared using a reverse microemulsion method, Langmuir, 20 (2004) 8336-8342.
[209] X. Wang, R. Zhang, C. Wu, Y. Dai, M. Song, S. Gutmann, F. Gao, G. Lv, J. Li, X. Li, The application of Fe3O4 nanoparticles in cancer research: a new strategy to inhibit drug resistance, Journal of Biomedical Materials Research Part A, 80 (2007) 852-860.
[210] M. Dickson, J.P. Gagnon, The cost of new drug discovery and development, Discovery Medicine, 4 (2009) 172-179.

Chapter 3

RESEARCH RESULTS I

Synthesis and antibacterial activity of silver and gold nanoparticles produced using aqueous seed extract of *Protorhus longifolia* as a reducing agent

This manuscript was published in

Digest Journal of Nanomaterials and Biostructures (2014)

Synthesis and antibacterial activity of silver and gold nanoparticles produced using aqueous seed extract of *Protorhus longifolia* as a reducing agent

Ramesh Gannimani[a], Amanda Perumal[a], Suresh Babu Naidu Krishna[a], Sershen[a], Karen Pillay[a], Ajay Mishra[b], Patrick Govender[a]

[a]Department of Biochemistry, School of Life Sciences, University of KwaZulu-Natal (UKZN), Westville, Durban 4000, South Africa

[b]Department of Applied Chemistry, Faculty of Science, University of Johannesburg, South Africa

3.1 Abstract

The aqueous seed extract of *Protorhus longifolia* was found to be an efficient reagent for simultaneous synthesis and functionalization of silver and gold nanoparticles from 1 mM silver nitrate and 1 mM chloroauric acid solution. The progress of the reaction was studied using UV-Visible spectroscopy. Scanning electron microscopy (SEM) and transmission electron microscopy (TEM) techniques were used to study surface morphology, size and crystalline nature of nanoparticles. Energy dispersive X-ray analysis confirmed the presence of silver and gold element in the nanoparticle samples. The presence of functional groups over the surface of nanoparticles was confirmed by Fourier transform infrared spectroscopy (FTIR) studies. Zeta potential contributing to the stability of silver and gold nanoparticles was recorded as -21.2 mv and -19.7 mv respectively. The modification of the composition and surface morphology of nanoparticles was a result of the capping of organic molecules from the seed extract yielding novel nanoparticles. These nanoparticles showed potential antibacterial activity against bacterial species *Escherichia coli* (ATCC 35218), *Klebsiella pneumoniae* (ATCC 700603), *Staphylococcus aureus* (ATCC 43300) and *Pseudomonas aeruginosa* (ATCC 27853).

3.2 Key words

Protorhus longifolia, Green synthesis, Silver nanoparticles (AgNPs), Gold nanoparticles (AuNPs), Antibacterial activity

3.3 Introduction

The use of plant extracts for the extracellular synthesis of AgNPs and AuNPs in a bottom-up reduction approach has recently been extensively researched [1]. The interest in these bottom-up methods is based on their ecofriendly nature and less cumbersome reaction procedures. Nanoparticles synthesized using chemical methods have limited application as the toxic chemicals used in the reaction become adsorbed onto the surface of nanoparticles [2] . Intracellular green methods using plants and microbes such as bacteria and fungi generates biocompatible nanoparticles, but at relatively slower rates [3]. On the other hand extracellular methods involving plant extracts are highly convenient due to short reaction times and easy availability of different plant materials as plant organs such as leaves can be harvested without removing the plant from the wild. Plant extracts are often a source of bioactive and medicinally useful compounds and can be generated using a range of plant tissues [4].

In the process of synthesizing nanoparticles from a metal ion solution, medicinally important phytochemicals in the plant extracts reduce the metal ions and also functionalize the surface of the nanoparticles. This functionalization may in this way increase the biocompatibility of green nanoparticles [5]. Steric repulsions between the functionalized molecules can also cause the nanoparticles to form stable colloidal solution and hence use of additional stabilizing chemicals can be avoided [6]. Silver and gold nanoparticles synthesized by using plant extracts very often have unique chemical and biological properties and are the subject of much interest in the field of catalysis, electronics and most importantly in the medical field as bactericidal and therapeutic agents [7-9]. The chemical composition of plant extract greatly influences on the size and shape of the nanoparticles, which in turn effects on the therapeutic and catalytic properties of nanoparticles [10]. Hence there is necessity to screen more plant extract for the green synthesis of AgNPs and AuNPs of desired size and shape.

There are at present many reports on the extracellular synthesis of silver and gold nanoparticles using various plant parts. Fruit peel of mango [11], lemon [12], Satsuma mandarin [13], were used for the synthesis of AgNPs and AuNPs. Root extract of *Zingiber officinale* [14] was used for the synthesis of AgNPs and AuNPS. Sea weed *Chaetomorpha linum* [15] for the synthesis of AgNPs and flower extracts of *Gnidia glauca* [16] , *Nyctanthes arbortristis* [17], *Carthamus tinctorius L* [18] were used for synthesis of AuNPs. Leaf extracts of *Gliricidia sepium* [19] for

the synthesis of AgNPs and even seed extracts of *Abelmoschus esculentus* [20] and *Acacia farnesiana* [21] have also been used for the synthesis of AuNPs and AgNPs.

In this present study we investigate the synthesis and antibacterial activity of silver and gold nanoparticles produced using aqueous seed extract of *Protorhus longifolia (Bernh.) Engl.* as a reducing agent. Nanoparticles synthesized using the seeds of other species have exhibited bioactivity [22, 23]. *Protorhus longifolia* belongs to the family Anacardiaceae, which is widely distributed throughout South Africa and its bark and leaves are used in traditional medicine to treat hemiplegic paralysis, heart burn and bleeding from stomach [24-27]. The seeds of the plant however, unexplored for their medicinal use. *Protorhus longifolia* produce recalcitrant seeds that are intolerant of desiccation and possibly sensitive to low temperatures, which effectively precludes their storage for any useful period of time [28]. Our interest in using the seeds of these species for the synthesis of nanoparticles is based on the fact that recalcitrant seeds have been shown to possess a number of antimicrobial agents (e.g. β-1,3-glucanase and chitinase) as part of their defense mechanisms against the range of microbes that plague them in the wild [29].

3.4 Experimental Section

3.4.1 Materials

Silver nitrate $AgNO_3$ and Chloroauric acid $HAuCl_4.3H_2O$ were analytical grade reagents purchased from Merck Germany. 1% JIK bleach was purchased from Reckitt Benckiser, South Africa. Seeds of *Protorhus longifolia* were collected from Westville campus, University of KwaZulu-Natal (GPS co-ordinates -29.817897, 30.942771).

3.4.2 Preparation of seed extract

Protorhus longifolia seeds were surface sterilized in 1% JIK bleach, washed with deionized water and then the seeds were air dried for 3 days at room temperature (28°C**) [28].** The dried seeds were ground to a fine powder using a commercial blender. Two grams of the fine seed powder was soaked in 25 ml of distilled water and shaken continuously for 24 h. The resulting leachate was filtered and stored at 4°C for further use.

3.4.3 Synthesis of silver and gold nanoparticles

For the synthesis of nanoparticles the method available in the literature was adopted [30]. 2 ml of plant extract was added to 25 ml of sterile 1 mM silver nitrate solution and 1 mM chloroauric acid solution and incubated with continuous stirring on the rotary shaker at 120 rpm, 30°C for 24h. Progress in the reaction was monitored by measuring the UV absorbance. The final reaction mixture was centrifuged and washed with distilled water to remove any unreacted materials. AgNPs were centrifuged (Eppendorf 5810R) at 4000 rpm (Rotor A-4-62) for 20 min, whereas AuNPs were centrifuged at 8000 rpm (Rotor F-34-6-38) for 20 min.

3.4.4 UV-Vis Spectrum analysis

The reduction reaction of silver and gold ions by aqueous seed extraction was followed by UV visible absorption measurements at room temperature as function of time using Specord 210, Analytikjena spectrometer. The broad absorbance peaks between 400-500 nm and 500-600 nm confirmed the formation silver and gold nanoparticles respectively. 1 mM $AgNO_3$ and 1 mM $HAuCl_4$ solution were used as the reference blank solution for these measurements [31].

3.4.5 Fourier Transform Infrared (FTIR-ATR) Spectroscopy Measurements

The nanoparticle pellet obtained after the washing was dried in a desiccator containing calcium chloride and the dry pellet obtained was thereafter used for the FTIR studies using Perkin Elmer Precisely Spectrometer 100 FTIR-ATR to identify the functional groups present on the surface of nanoparticles.

3.4.6 Scanning Electron Microscopy Measurements

Morphological studies of the synthesized AgNPs and AuNPs were carried out using scanning electron microscopy (FEGSEM ZEISS ULTRAPLUS). Samples prepared by adding a drop of sonicated nanoparticle solution over the carbon tape glued over copper grid. The samples thus obtained were coated with carbon and observed at 10000 X magnification. The energy dispersive X-ray analysis (EDX) was done at 20 kV using AZTEC software for the analysis.

3.4.7 Transmission Electron Microscopy (TEM) Measurements

Both silver and gold nanoparticle solution obtained after the purification were sonicated for 15 min to disrupt any possible aggregates [32]. A small amount of this sonicated solution was placed on carbon coated copper grid and dried under infrared light for solvent evaporation. High-resolution TEM images were obtained on JEOL TEM model no 2100 operating at accelerating voltage of 200 kV and 0.23 nm resolution.

3.4.8 Zeta potential measurements

The Zeta potential of green synthesized AgNPs and AuNPs was determined using Zetasizer Nano ZS90 (Malvern Instruments Ltd., UK). Water was used as dispersant and samples were sufficiently diluted to ensure that the light scattering intensity (between 6E+004 and 1E+006) was within the instrument sensitivity. Measurements were done at 25°C and medium refractive index was 1.330. Measurements were carried out in triplicates [33].

3.4.9 Antibacterial activity

Minimum Inhibitory Concentration

MIC, defined as the lowest concentration of an antimicrobial agent that inhibits the growth of a microorganism after overnight incubation, was determined by monitoring the growth of bacteria in a microplate reader (Synergy HT, BioTek Instruments) at 630 nm by micro dilution method as per NCCLS guidelines [34]. The bacterial test cultures used in this study were *Escherichia coli* (ATCC 35218), *Klebsiella pneumoniae* (ATCC 700603), *Staphylococcus aureus* (ATCC 43300), *Enterococcus faecalis* (ATCC 5129) and *Pseudomonas aeruginosa* (ATCC 27853). Serial twofold dilutions of AgNPs and AuNPs solution were prepared in sterile 96-well plates over the range of 200-1.25 µg/ml [32] . The wells were then inoculated with diluted overnight broth culture initially adjusted to 0.5 McFarland turbidity standards and incubated at 35°C for 24 hours. Neomycin (Sigma) served as a positive control; MIC was recorded as the lowest concentration at which no growth was observed. All the experiments were carried out in triplicates.

3.5 Results and Discussion

3.5.1 UV -Visible studies

Surface plasmon resonance a unique optical phenomenon of metal nanoparticles, in the UV region enables their easy detection. This property arises due to surface plasmon oscillation of free electrons [35]. Nanoparticles show strong absorbance in the UV region due to this phenomenon and the wavelength at which absorbance occurs is a characteristic property of particular metal nanoparticle and also depends on the size and shape of particles [36]. **Fig. 3.1** illustrates the UV-visible absorbance spectra of reaction mixture containing aqueous seed extract with silver nitrate (1 mM) and chloroauric acid (1 mM) at various time intervals. After the addition of the seed extract, the silver nitrate solution changed to brown and gold chloride solution changed to wine red. The intensity of the color and absorbance of both the solutions increased with the time as the reaction proceeded.

Both the AgNP and AuNP reaction mixtures showed a single broad surface plasmon resonance band between the wavelength 400-500 nm and 500-600 nm respectively. The change of color of reaction mixture within 15 min indicated that reduction of Ag^{+} and Au^{3+} is a rapid reaction. The reactions were carried out for 24 h to make sure they run to completion.

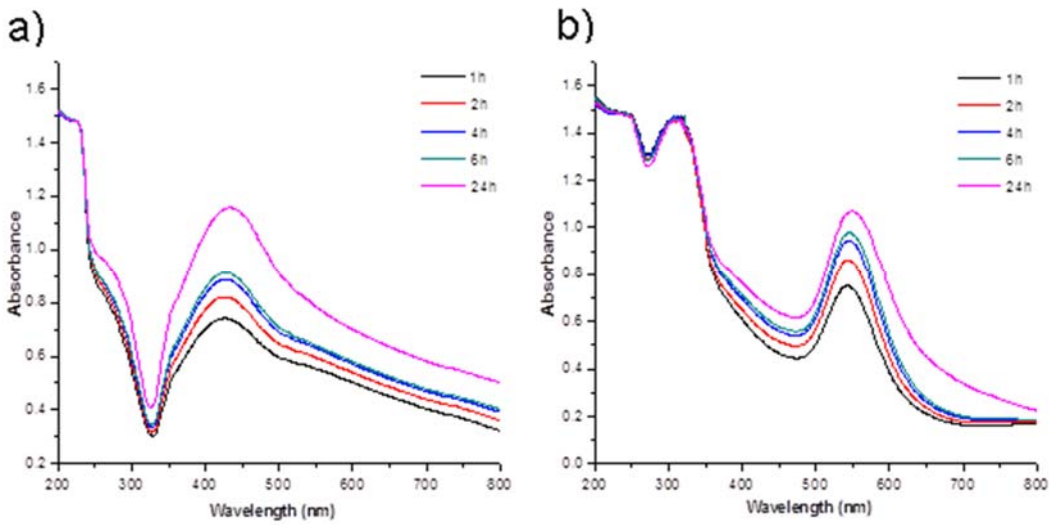

Figure 3.1 UV–Vis spectra recorded as a function of reaction time **a)** AgNPs and **b)** AuNPs.

3.5.2 FTIR-ATR studies

The IR spectrum results showed that some organic biomolecules from seed extract had become associated with the surface of silver and gold nanoparticles to form a capping agent. The steric repulsion between the capped molecules contributes to the stability of nanoparticles. The major IR bands at 3258, 1629, 1514, 1055 cm^{-1} for AgNPs (**Fig. 3.2a**) and the IR bands at 3263, 1739, 1635, 1530 and 1160 cm^{-1} for AuNPs (**Fig. 3.2b**) were observed. The broad spectrum of IR peak at 3260 cm^{-1} for both AgNPs and AuNPs referred to the strong stretching vibrations of -OH functional group. The band at 1160 cm^{-1} and 1055 cm^{-1} can be assigned to the ether linkages or –C-O- functional group. To a large extent, these bands might be the product of -C-O- groups of the polyols such as flavones, terpenoids and the polysaccharides of seed extract. The absorbance band centered at 1635 cm^{-1} and 1629 cm^{-1} is associated with the stretching vibrations of –C=C- or aromatic groups. The band around 1739 cm^{-1} for AuNPs can be assigned to C=O stretching vibrations of the carbonyl functional group in ketones, aldehydes, and carboxylic acids. The spectrum also exhibits two intense bands at 2851 cm^{-1} and 2919 cm^{-1}, for AuNPs which is assigned to the symmetric and asymmetric stretching vibration of sp^3 hybridized –CH groups.

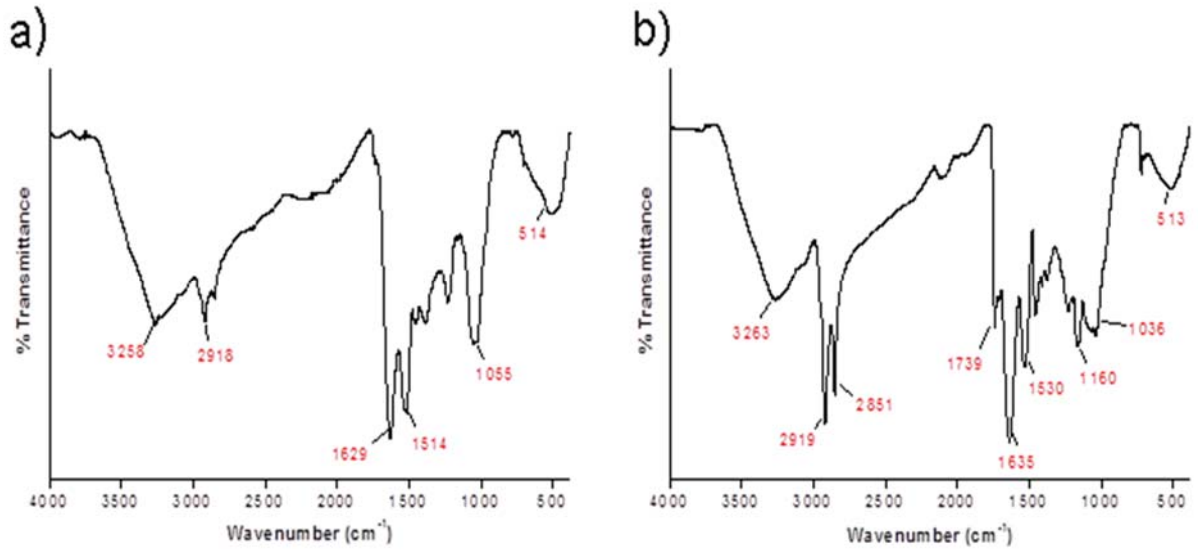

Figure 3.2 FTIR ATR spectra of **a)** AgNPs and **b)** AuNPs.

3.5.3 SEM and TEM Analysis

The AgNPs and AuNPs from the reaction mixture were repeatedly centrifuged and redispersed in sterile distilled water prior to SEM and TEM analysis to remove any unreacted plant material and metal ions. SEM analysis confirmed that particles are of a nano-size. The spherical shape of the nanoparticles is shown in the SEM images **(Fig. 3.3a** and **3.3b).** The EDX analysis confirmed that the particles were composed of elemental silver and gold **(Fig. 3.3c** and **3.3d)**.

TEM analysis showed that both silver and gold nanoparticles were poly-dispersed and predominantly spherical or polyhedral in shape. The majority of the silver nanoparticles were 20-30 nm in size whereas AuNPs were in the range of 10-20 nm. **Fig. 3.4A, a** and **Fig. 3.4B, a** shows clear morphology of silver and gold nanoparticles. The Selected area diffraction pattern clearly indicated that the AgNPs and AuNPs formed by the reduction of metal ions by the seed extract are polycrystalline in nature with clear lattice fringes (**Fig. 3.4A, b** and **Fig. 3.4B, b)** characteristic of crystalline nature of nanoparticles [37, 38].

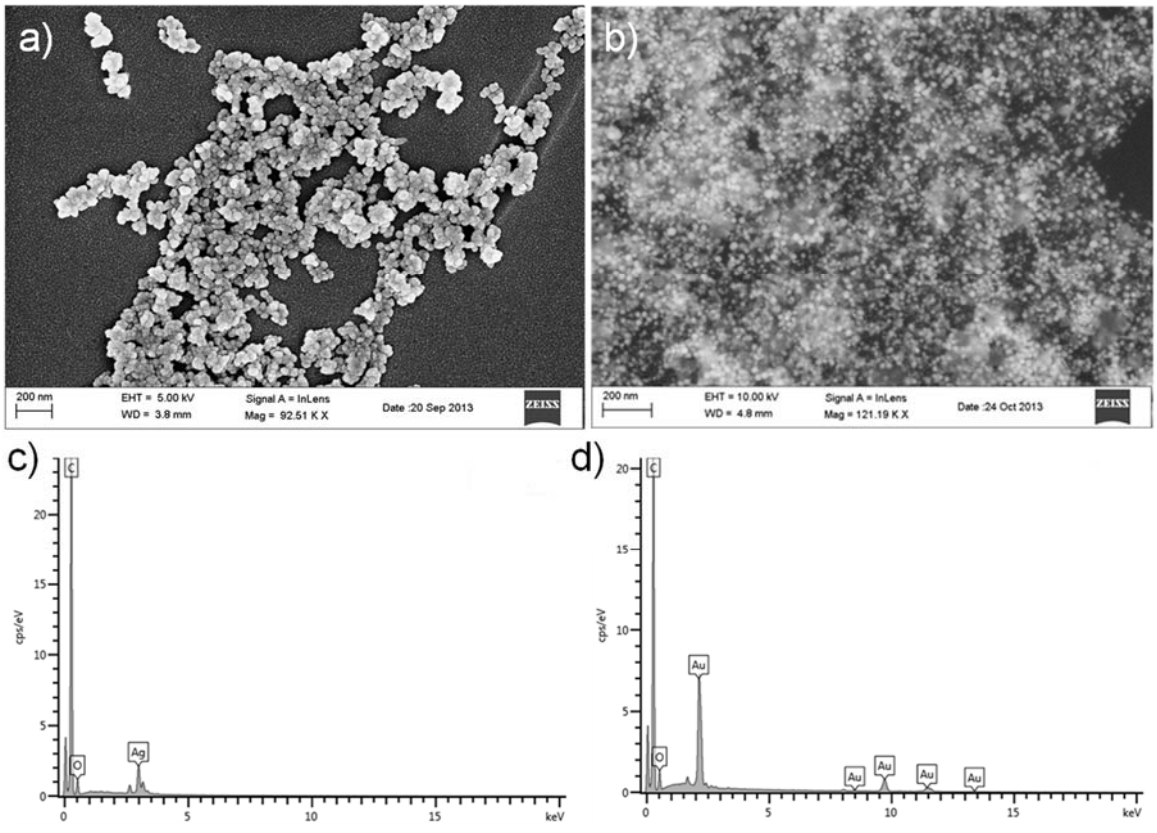

Figure 3.3 SEM morphology a and b, EDX pattern c and d of AgNPs and AuNPs respectively.

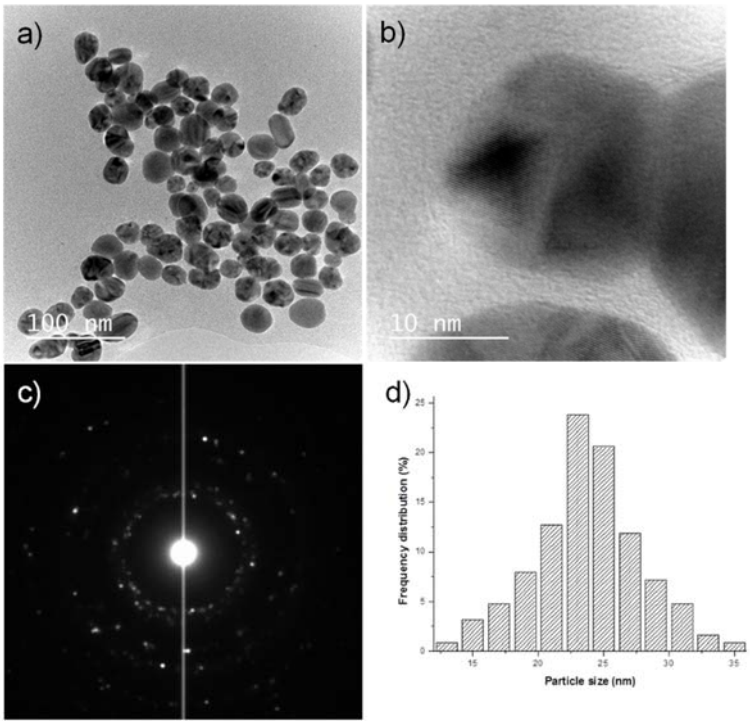

Figure 3.4A a) HRTEM micrograph **b)** Lattice fringes **c)** SAED pattern and **d)** Histogram of AgNPs.

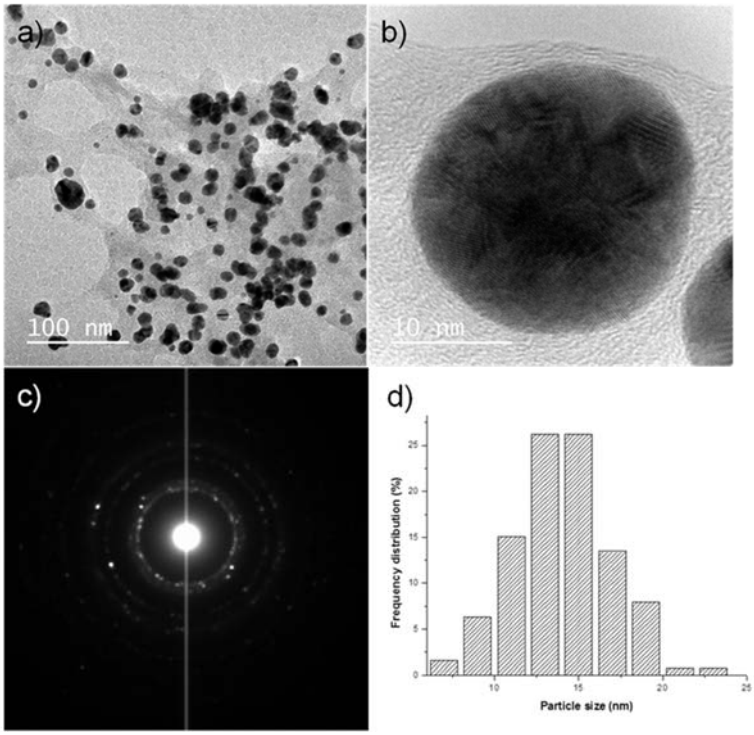

Figure 3.4B a) HRTEM micrograph **b)** Lattice fringes **c)** SAED pattern and **d)** Histogram of AuNPs.

3.5.4 Zeta potential measurements

The electric charge on the surface of nanoparticles can be measured in terms of Zeta potential. Zeta potential was found to be −21.2 mV for AgNPs and -19.5 mV for AuNPs **(Fig. 3.5)**. The negative zeta potential confirms the negative charge on the surface of colloidal nanoparticles. The coulombic repulsion forces induced by surface negative charge minimize the aggregation and thus contribute to the stability of the green synthesized nanoparticles [33].

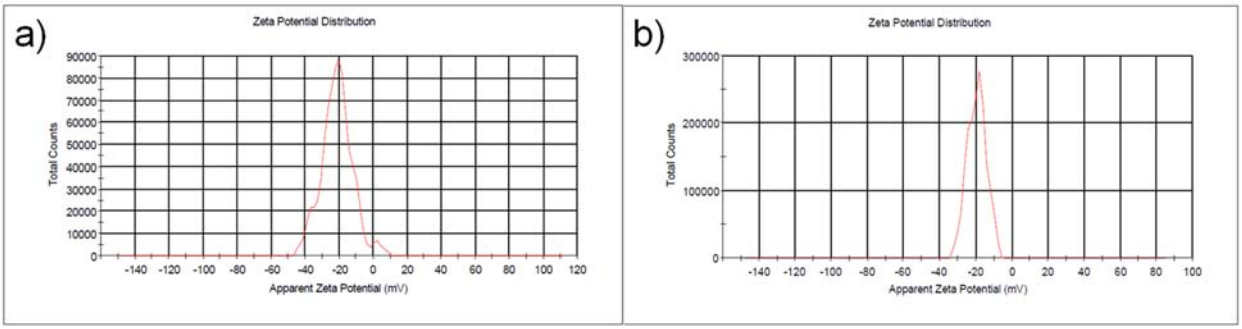

Figure 3.5 Zeta potential graphs of **a)** AgNPs and **b)** AuNPs.

3.5.5 Antibacterial Studies

The use of nanoparticles functionalized with antibacterial compounds is an interesting strategy to overcome the problem of multidrug resistance by bacteria [39]. Inorganic metal nanoparticles have been shown to target multiple components of the cell and hence, there is less scope for bacteria to develop resistance [40]. The antibacterial mechanisms of action of metal nanoparticles include cell wall disruption followed by leakage of cell content, binding of metal ions to DNA and proteins which results in inactivation or severe alteration of cellular metabolism [41]. Further properties of nanoparticles such as high surface area, slow and steady release of metal atoms compared to salt or bulk metal add to their antimicrobial properties.

In the present study silver and gold nanoparticles showed good antibacterial activity against tested pathogens (Table 1). These results also showed that AgNPs had higher antibacterial activity than AuNPs. This is in accord with other studies which have shown AgNPs to be more antibacterial than AuNPs, largely due to the relatively inert chemical nature of gold [40]. *E. coli* was the most sensitive to silver nanoparticles (MIC 3.12 µg/ml) followed by *P. aeruginosa* and

S. aureus (MIC 50 µg/mL). These results are in agreement with other studies [42]. *E. faecalis* was resistant to silver and gold nanoparticles. Similar results were observed in a previous study where silver nanoparticles were more active against gram negative bacteria than gram positive bacteria and this was attributed to change in the cell wall composition of bacteria [43]. Gold nanoparticles were effective at 200 µg/ml amongst the varied concentration range against the tested pathogens. The seed chemical content adsorbed onto the surface of nanoparticles could have added to their antibacterial activities and thus nanoparticles may have acted as carriers or drug delivery systems for the antibacterial content of plant material functionalized on their surface [32]. Recent reports also suggest similar mechanism where gold nanoparticles functionalized with small molecules have shown good antibacterial activity [44].

Table 3.1 Minimum inhibitory concentration of *Protorhus longifolia* seed extract derived silver and gold nanoparticles against bacteria.

Compound	**Minimum Inhibitory Concentration (µg/ml)**				
	Gram negative			**Gram positive**	
	E. coli	***K. pneumoniae***	***P. aeruginosa***	***S. aureus***	***E. faecalis***
AgNPs	3.12	100	50	50	NA
AuNPs	200	200	200	200	NA

3.6 Conclusion

In conclusion, we successfully synthesized silver and gold nanoparticles using aqueous seed extract of recalcitrant seeded *Protorhus longifolia* and confirmed the antibacterial activity of resultant nanoparticles. The reduction reaction for the synthesis of nanoparticles was moderately rapid under the ambient conditions and reaction handling was easy since it does not require boiling or subsequent treatment. The nanoparticles produced showed distinct poly-dispersity. The IR studies confirmed the capping of organic contents of seed extract of *Protorhus longifolia* onto the surface of nanoparticles. The capping of nanoparticles by organic molecules found in the seed extract and the negative charge of nanoparticles is suggested to have added to their stability. Further in yet to be reported research work we have also confirmed the antimicrobial activity of crude seed extract of *Protorhus longifolia*. Together these findings would significantly contribute to the advancement in the formulation of novel phytochemical based green material as antimicrobial agents.

3.7 Acknowledgement

This research was funded by National Research Foundation (NRF) of South Africa, the University of KwaZulu-Natal, South Africa.

3.8 References

[1] M.S. Akhtar, J. Panwar, Y.-S. Yun, Biogenic Synthesis of metallic nanoparticles by plant extracts, Acs Sustainable Chemistry & Engineering, 1 (2013) 591-602.
[2] R. Bhattacharya, P. Mukherjee, Biological properties of "naked" metal nanoparticles, Advanced Drug Delivery Reviews, 60 (2008) 1289-1306.
[3] D. Nath, P. Banerjee, Green nanotechnology - A new hope for medical biology, Environmental Toxicology and Pharmacology, 36 (2013) 997-1014.
[4] M.J. Balunas, A.D. Kinghorn, Drug discovery from medicinal plants, Life Sciences, 78 (2005) 431-441.
[5] O.V. Kharissova, H.V. Rasika Dias, B.I. Kharisov, B. Olvera Perez, V.M. Jimenez Perez, The greener synthesis of nanoparticles, Trends in Biotechnology, 31 (2013) 240-248.
[6] A.J. Kora, R.B. Sashidhar, J. Arunachalam, Gum kondagogu (Cochlospermum gossypium): A template for the green synthesis and stabilization of silver nanoparticles with antibacterial application, Carbohydrate Polymers, 82 (2010) 670-679.
[7] X. Chen, H.J. Schluesener, Nanosilver: A nanoproduct in medical application, Toxicology Letters, 176 (2008) 1-12.
[8] X.H. Huang, I.H. El-Sayed, W. Qian, M.A. El-Sayed, Cancer cell imaging and photothermal therapy in the near-infrared region by using gold nanorods, Journal of the American Chemical Society, 128 (2006) 2115-2120.
[9] B.R. Cuenya, Synthesis and catalytic properties of metal nanoparticles: Size, shape, support, composition, and oxidation state effects, Thin Solid Films, 518 (2010) 3127-3150.
[10] V. Kumar, S.K. Yadav, Plant-mediated synthesis of silver and gold nanoparticles and their applications, Journal of Chemical Technology and Biotechnology, 84 (2009) 151-157.
[11] N. Yang, W.-H. Li, Mango peel extract mediated novel route for synthesis of silver nanoparticles and antibacterial application of silver nanoparticles loaded onto non-woven fabrics, Industrial Crops and Products, 48 (2013) 81-88.
[12] S. Najimu Nishaa, O.S.A. , J.S.N.R. , P.V.K.a. , S.V.a. , P.N. , , A. Reen, Lemon peels mediated synthesis of silver nanoparticles and its antidermatophytic activity, Spectrochimica Acta Part A: Molecular and Biomolecular Spectroscopy, 124 (2014) 194-198.
[13] N. Basavegowda, Y.R. Lee, Synthesis of silver nanoparticles using Satsuma mandarin (Citrus unshiu) peel extract: A novel approach towards waste utilization, Materials Letters, 109 (2013) 31-33.
[14] P. Velmurugan, K. Anbalagan, M. Manosathyadevan, K.-J. Lee, M. Cho, S.-M. Lee, J.-H. Park, S.-G. Oh, K.-S. Bang, B.-T. Oh, Green synthesis of silver and gold nanoparticles using Zingiber officinale root extract and antibacterial activity of silver nanoparticles against food pathogens, Bioprocess and Biosystems Engineering, (2014) 1-9.
[15] R.R. Kannan, R. Arumugam, D. Ramya, K. Manivannan, P. Anantharaman, Green synthesis of silver nanoparticles using marine macroalga Chaetomorpha linum, Applied Nanoscience, 3 (2013) 229-233.
[16] S. Ghosh, S. Patil, M. Ahire, R. Kitture, D.D. Gurav, A.M. Jabgunde, S. Kale, K. Pardesi, V. Shinde, J. Bellare, D.D. Dhavale, B.A. Chopade, Gnidia glauca flower extract mediated synthesis of gold nanoparticles and evaluation of its chemocatalytic potential, Journal of Nanobiotechnology, 10 (2012).
[17] R.K. Das, N. Gogoi, U. Bora, Green synthesis of gold nanoparticles using *Nyctanthes arbortristis* flower extract, Bioprocess and Biosystems Engineering, 34 (2011) 615-619.

[18] B. Nagaraj, B. Malakar, T.K. Divya, N.B. Krishnamurthy, P. Liny, R. Dinesh, S.L. Iconaru, C.S. Ciobanu, Synthesis of plant mediated gold nanoparticles using flower extract of *Carthamus tinctorius* L.(Safflower) and evaluation of their biological activities, Digest Journal of Nanomaterials and Biostructures, 7 (2012) 1289-1296.
[19] R. Rajesh W, L. Jaya R, K. Niranjan S, M. Vijay D, K. Sahebrao B, Phytosynthesis of silver nanoparticle using gliricidia sepium (Jacq.), Current Nanoscience, 5 (2009) 117-122.
[20] C. Jayaseelan, R. Ramkumar, A.A. Rahuman, P. Perumal, Green synthesis of gold nanoparticles using seed aqueous extract of Abelmoschus esculentus and its antifungal activity, Industrial Crops and Products, 45 (2013) 423-429.
[21] S. Yallappa, J. Manjanna, S.K. Peethambar, A.N. Rajeshwara, N.D. Satyanarayan, Green synthesis of silver nanoparticles using *Acacia farnesiana* (Sweet Acacia) seed extract under microwave irradiation and their biological assessment, Journal of Cluster Science, 24 (2013) 1081-1092.
[22] U.B. Jagtap, V.A. Bapat, Green synthesis of silver nanoparticles using *Artocarpus heterophyllus Lam*. seed extract and its antibacterial activity, Industrial Crops and Products, 46 (2013) 132-137.
[23] A.I. Lukman, B. Gong, C.E. Marjo, U. Roessner, A.T. Harris, Facile synthesis, stabilization, and anti-bacterial performance of discrete Ag nanoparticles using *Medicago sativa* seed exudates, Journal of Colloid and Interface Science, 353 (2011) 433-444.
[24] J. Keirungi, C. Fabricius, Selecting medicinal plants for cultivation at Nqabara on the Eastern Cape Wild Coast, South Africa, South African Journal of Science, 101 (2005) 497-501.
[25] A.P. Dold, M.L. Cocks, The trade in medicinal plants in the Eastern Cape Province, South Africa, South African Journal of Science, 98 (2002) 589-597.
[26] R.A. Mosa, A.O. Oyedeji, F.O. Shode, M. Singh, A.R. Opoku, Triterpenes from the stem bark of Protorhus longifolia exhibit anti-platelet aggregation activity, African Journal of Pharmacy and Pharmacology, 5 (2011) 2698-2714.
[27] M.M. Suleiman, L.J. McGaw, V. Naidoo, J.N. Eloff, Detection of antimicrobial compounds by bioautography of different extracts of leaves of selected South African tree species, African Journal of Traditional Complementary and Alternative Medicines, 7 (2010) 64-78.
[28] C. Naidoo, E. Benson, P. Berjak, M. Goveia, N.W. Pammenter, Exploring the use of dmso and ascorbic acid to promote shoot development by excised embryonic axes of recalcitrant seeds, Cryoletters, 32 (2011) 166-174.
[29] V.S. Anguelova-Merhar, C. Calistru, P. Berjak, A study of some biochemical and histopathological responses of wet-stored recalcitrant seeds of *Avicennia marina* infected by *Fusarium moniliforme*, Annals of Botany, 92 (2003) 401-408.
[30] R.M. Gengan, K. Anand, A. Phulukdaree, A. Chuturgoon, A549 lung cell line activity of biosynthesized silver nanoparticles using *Albizia adianthifolia* leaf, Colloids and Surfaces B-Biointerfaces, 105 (2013) 87-91.
[31] R.W. Raut, N.S. Kolekar, J.R. Lakkakula, V.D. Mendhulkar, S.B. Kashid, Extracellular synthesis of silver nanoparticles using dried leaves of *pongamia pinnata (L) pierre*, Nano-Micro Letters, 2 (2010) 106-113.
[32] A. Annamalai, V.L.P. Christina, D. Sudha, M. Kalpana, P.T.V. Lakshmi, Green synthesis, characterization and antimicrobial activity of Au NPs using *Euphorbia hirta L*. leaf extract, Colloids and Surfaces B-Biointerfaces, 108 (2013) 60-65.
[33] Y.S. Rao, V.S. Kotakadi, T.N.V.K.V. Prasad, A.V. Reddy, D.V.R.S. Gopal, Green synthesis and spectral characterization of silver nanoparticles from Lakshmi tulasi (*Ocimum sanctum*) leaf extract, Spectrochimica Acta Part a-Molecular and Biomolecular Spectroscopy, 103 (2013) 156-159.
[34] P. Villanova, Methods for Dilution Antimicrobial Susceptibility Tests for Bacteria, which Grows Aerobically, NCCLS, (2000) 5th ed., Approved Standard M7-A5.
[35] T.R. Jensen, G.C. Schatz, R.P. Van Duyne, Nanosphere lithography: Surface plasmon resonance spectrum of a periodic array of silver nanoparticles by ultraviolet-visible extinction spectroscopy and electrodynamic modeling, Journal of Physical Chemistry B, 103 (1999) 2394-2401.
[36] S.J. Oldenburg, R.D. Averitt, S.L. Westcott, N.J. Halas, Nanoengineering of optical resonances, Chemical Physics Letters, 288 (1998) 243-247.

[37] H. Bar, D.K. Bhui, G.P. Sahoo, P. Sarkar, S. Pyne, A. Misra, Green synthesis of silver nanoparticles using seed extract of Jatropha curcas, Colloids and Surfaces a-Physicochemical and Engineering Aspects, 348 (2009) 212-216.
[38] A.J. Kora, S.R. Beedu, A. Jayaraman, Size-controlled green synthesis of silver nanoparticles mediated by gum ghatti (Anogeissus latifolia) and its biological activity, Organic and Medicinal Chemistry Letters, 2 (2012) 17-17.
[39] A.R. Shahverdi, A. Fakhimi, H.R. Shahverdi, S. Minaian, Synthesis and effect of silver nanoparticles on the antibacterial activity of different antibiotics against Staphylococcus aureus and *Escherichia coli*, Nanomedicine-Nanotechnology Biology and Medicine, 3 (2007) 168-171.
[40] Y. Zhou, Y. Kong, S. Kundu, J.D. Cirillo, H. Liang, Antibacterial activities of gold and silver nanoparticles against Escherichia coli and bacillus Calmette-Guerin, Journal of Nanobiotechnology, 10 (2012).
[41] Q.L. Feng, J. Wu, G.Q. Chen, F.Z. Cui, T.N. Kim, J.O. Kim, A mechanistic study of the antibacterial effect of silver ions on Escherichia coli and Staphylococcus aureus, Journal of Biomedical Materials Research, 52 (2000) 662-668.
[42] J.S. Kim, E. Kuk, K.N. Yu, J.-H. Kim, S.J. Park, H.J. Lee, S.H. Kim, Y.K. Park, Y.H. Park, C.-Y. Hwang, Y.-K. Kim, Y.-S. Lee, D.H. Jeong, M.-H. Cho, Antimicrobial effects of silver nanoparticles, Nanomedicine-Nanotechnology Biology and Medicine, 3 (2007) 95-101.
[43] S. Shrivastava, T. Bera, A. Roy, G. Singh, P. Ramachandrarao, D. Dash, Characterization of enhanced antibacterial effects of novel silver nanoparticles, Nanotechnology, 18 (2007).
[44] Y. Zhao, Y. Tian, Y. Cui, W. Liu, W. Ma, X. Jiang, Small molecule-capped gold nanoparticles as potent antibacterial agents that target gram-negative bacteria, Journal of the American Chemical Society, 132 (2010) 12349-12356.

Chapter 4

RESEARCH RESULTS II

Investigation of 3, 5-dicyanopyridine scaffolds as antidiabetic and antibacterial agents

This manuscript is being prepared for submission to the

Journal of *Medicinal Chemistry Research*

Investigation of 3, 5-dicyanopyridine scaffolds as antidiabetic and antibacterial agents

Ramesh Gannimani[a], Karen Pillay[a], Patrick Govender[a,*]

[a]Department of Biochemistry, School of Life Sciences, University of KwaZulu-Natal, Westville, Durban 4000, South Africa

4.1 Abstract

In this study, 3,5-dicyanopyridines have been evaluated as a small key organic molecule for their application as potential treatment of type-II diabetes mellitus and bacterial infections. Several molecules were synthesized with high yields in a single-step multicomponent approach, and then characterized by IR, NMR and HRMS. Inhibition of α-glucosidase and the antibacterial activities of the molecules were then evaluated. Five of the nine compounds tested showed good inhibition of α-glucosidase, which were similar to that of the standard drug acarbose. Molecular docking analysis was then conducted to further explain these results. However, no significant antibacterial activities were observed for these compounds.

4.2 Key words

3, 5-dicyanopyridine, α-glucosidase inhibition, antibacterial activity, molecular docking

4.3 Introduction

The increased world-wide prevalence of the metabolic disorder, diabetes mellitus, across all age groups is making a significant and growing contribution to morbidity and mortality rates [1]. Diabetes mellitus is mainly classified into two types; type I diabetes and type II diabetes [2]. Type I diabetes is insulin dependent and results from impaired functioning of pancreatic *beta* cells which cause cessation of insulin production [2]. Type II diabetes is non-insulin-dependent and results from the combination of insulin resistance and deficiency [3, 4]. Type II diabetes accounts for 85-95% of all modern diabetes cases [4]. Recent studies concluded that genetic predisposition, environmental factors, life style with wrong dietary habits, decreased physical activity, and stress all contribute to the occurrence of type II diabetes [4, 5]. The most common biochemical abnormality associated with diabetes mellitus is chronic hyperglycemia, a metabolic condition characterized by raised blood glucose levels and increased glucose intolerance [2]. The disruption of carbohydrate, fat and protein metabolism due to defects in insulin secretion or action can lead to hyperglycemia [2]. If untreated, the chronic high blood glucose levels can lead to complications including impaired vision or even blindness, nerve damage and kidney failure [6]. The long-term severe clinical manifestations of diabetes include; retinopathy, nephropathy and neuropathy [4]. Diabetic patients also face an increased risk of developing cardiac, peripheral arterial and cerebrovascular disease [6].

Complications associated with diabetes are prevented by administering therapeutic agents which manage blood glucose levels by targeting α-glucosidase; an enzyme which plays a pivotal role in the digestion of starch to glucose in the intestine, thereby elevating postprandial glucose concentrations [7]. This approach is particularly more effective in individuals with type II diabetes mellitus and the examples of drugs which inhibit α-glucosidase activity include acarbose, miglitol and voglibose **(Fig. 4.1)** [8, 9]. These compounds mainly suppress the absorption of carbohydrates in the small intestine and thus have a controlling effect on postprandial hyperglycemic events [10]. However their use is limited by unwanted side effects such as hypoglycemia, myocardial infarction, weight gain, increase in insulin resistance, flatulence and diarrhea [11]. There is therefore a need to discover novel α-glucosidase inhibitors which can be employed as safer anti-diabetic agents with minimal side effects. Several pyridine and pyrimidine derivatives have been recently reported to significantly inhibit α-glucosidase activity [12]. These findings have therefore prompted the need to investigate the structurally similar 3,5-dicyanopyridine frame-works for α-glucosidase inhibitory activity. 3,5-dicyanopyridines are important and medically useful heterocyclic scaffolds which have been

utilized in the generation of a library of compounds with diverse medicinal applications [13, 14]. Alterations of substituents at the pyridine core have produced structures with different biological activities such as; antimicrobial [15], anticancer [16], and cardiovascular agents [17]; inhibitors of prion replication [18], potassium channel openers with application in treating urinary incontinence [19], inhibitors of IKK2 with a potential for treating hepatitis B virus (HBV) infection [20], and also show agonistic activity for human adenosine A2B receptors with a potential for treating Parkinson's disease, hypoxia/ischemia, asthma, kidney disease, epilepsy and cancer [13, 21]. A preliminary evaluation of the molecular interactions of a series of 3,5-dicyanopyridine compounds with α-glucosidase was performed through molecular docking studies using Autodock Vina and it was concluded that these scaffolds are capable of binding in the α-glucosidase active site with good affinity. Hence, the synthesis of 3, 5-dicyanopyridines was conducted and their α-glucosidase inhibitory activities were evaluated *in vitro*. Since similar compounds have been reported as antibacterial agents, we also investigated the antibacterial activity of the molecules synthesized in this study [22]. Herein, we report the novel investigation of the anti-diabetic and antibacterial activities of some multicomponent derived 3,5-dicyanopyridine molecular frameworks.

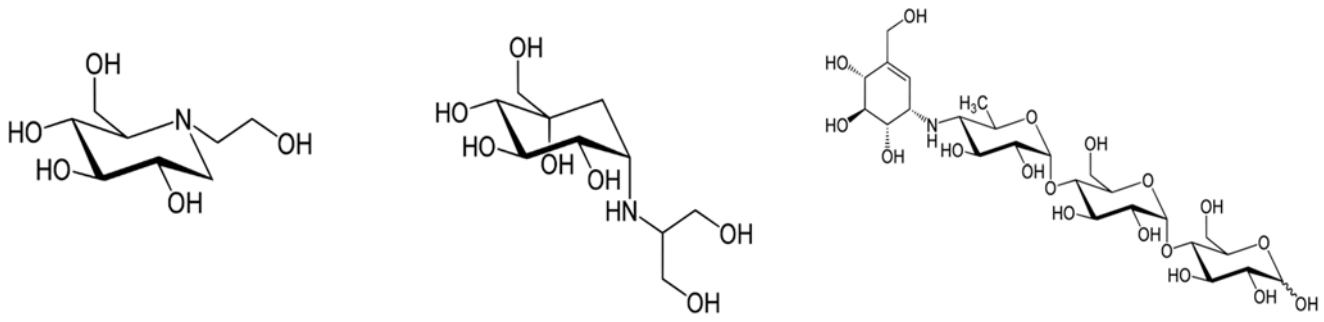

Miglitol **Voglibose** **Acarbose**

Figure 4.1 Structures of α-glucosidase inhibitors.

4.4 Materials and Methods

4.4.1 General procedures

Reagents and chemicals were purchased from Sigma Aldrich, Germany. Organic solvents were purified by re-distillation and dried according to standard procedures. Melting points were determined on a Thermonik Campbell melting point apparatus. Infrared spectra were recorded on a Bruker Infrared Spectrophotometer, Model 599-B. ^{1}H and ^{13}C NMR spectra were recorded in DMSO solution at room temperature using a Bruker Avance 400 MHz and Bruker Avance 600 MHz instruments. Chemical shifts are given in δ (ppm) against the internal standard tetramethylsilane. Mass spectroscopy (MS) was carried out on a Waters Micromass LCT Premier TOF-MS.

4.4.2 General procedure for the synthesis of 3, 5-dicyanopyridine

Synthesis of 1a-1h compounds: The procedure reported by Evdokimov et al. was adopted for the synthesis of these compounds [14]. To a solution of aryl or aryl alkyl aldehyde (2 mmol) in ethanol, a solution of malononitrile (4.2mmol) in 5 mL of ethanol was slowly added. To this reaction mixture triethylamine (Et_3N, 0.1 mmol) was added dropwise at ambient temperature and stirred at room temperature (RT) for half an hour. The resulting mixture was heated to 50°C and the desired thiol (2.1 mmol) was added. Thereafter the reaction mixture was refluxed for 4-5 h until the starting material was consumed. When no more starting material appeared on thin layer chromatography (TLC), the reaction mixture was allowed to cool to RT. Methanol was then added to the dark residue obtained after the removal of excess ethanol under reduced pressure, which resulted in the crystallization of the product. Further crystallization was conducted until no more side products were observed on the TLC plate.

Synthesis of compound 1i: A procedure reported by Evdokimov et al. was adopted for the synthesis of li [14]. To the solution of aldehyde (2 mmol) and malononitrile (3 mmol) in ethanol, 100 µL of Et_3N in 5 mL of ethanol was added drop wise. To this resulting mixture, ethanedithiol (0.55 mmol) was added slowly at RT. The reaction mixture was refluxed for 2h and then allowed to cool to RT. The product formed as a precipitate and after cooling, it was isolated by filtration. The filtrate was concentrated under reduced pressure to obtain a dark residue. The dark residue yielded further 5-10% of product after recrystalization using small amounts of methanol. The solids were combined and recrystallized from methanol to yield compound 1i.

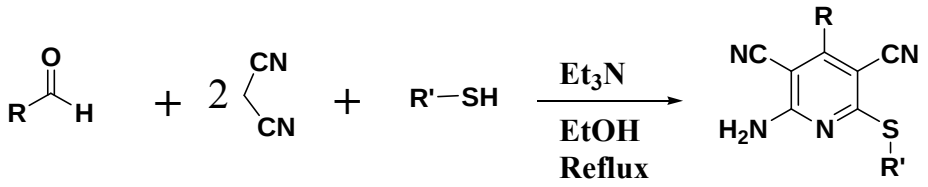

Figure 4.2 General scheme for the synthesis of 3, 5-Dicyanopyridines 1a-i via a multi-component reaction.

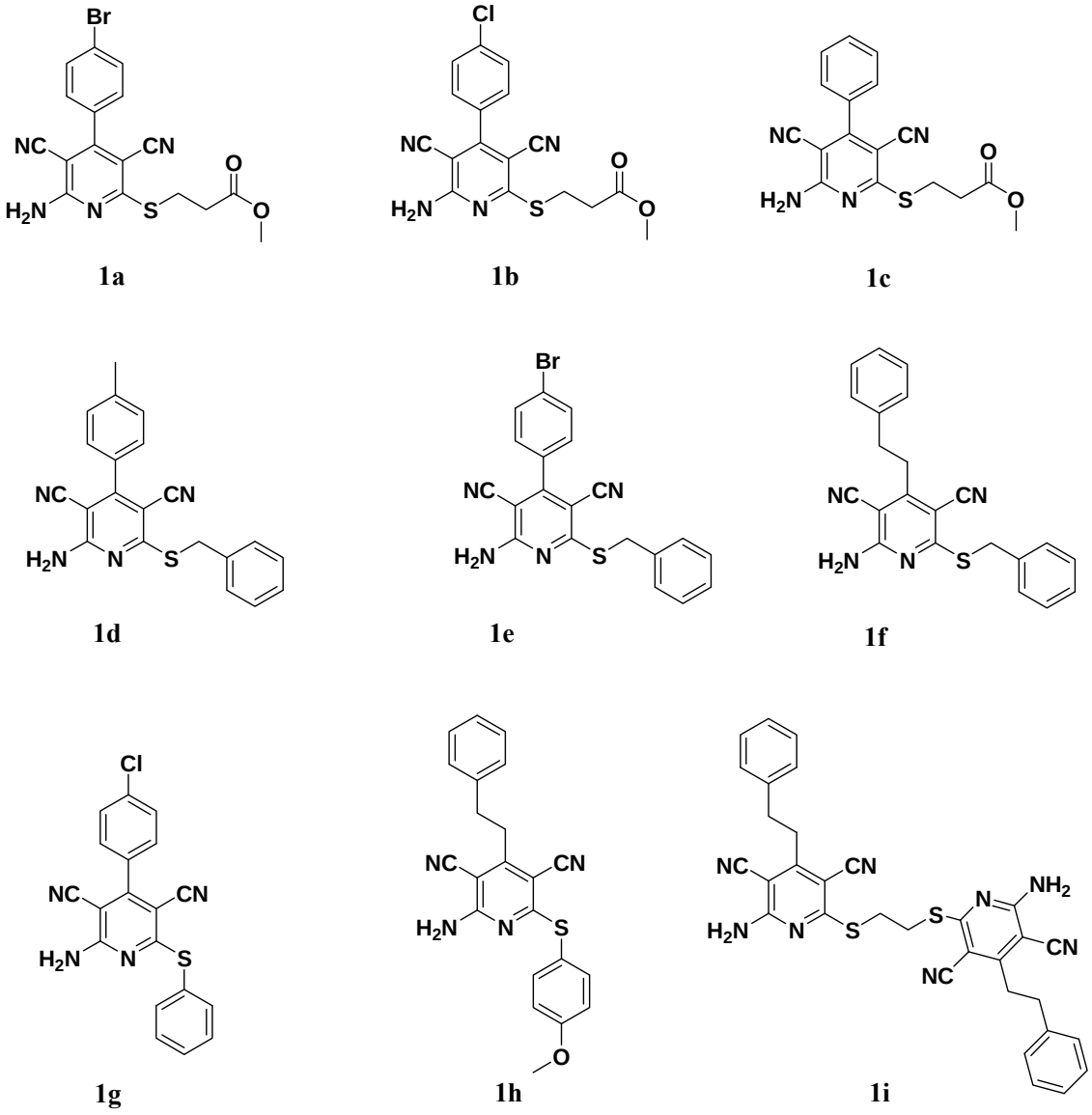

Figure 4.3 Compounds synthesized in this study.

4.4.3 Docking Study

The crystal structure of α-glucosidase (PDB ID: 3W37) complexed with acarbose was obtained from RCSB Protein Data Bank with the resolution of 1.70 Å [23]. This crystal structure was used to create separate protein and ligand pdb files using Discovery Studio 4.0 Client software. Protein was prepared for docking by removing water molecules and co-crystallized ligands, and by adding polar hydrogens. Similarly the pdbqt format of separated ligands was prepared for docking after adding polar hydrogens and setting torsions. The 3D structure of synthesized ligands were constructed in Chem3D Ultra 8.0 and were subjected to energy minimization and geometry optimization [24]. The pdbqt formats of obtained 3D structures were used for in silico protein-ligand docking calculations using AutoDock Vina [25]. The grid box with spacing 1 Å was constructed around the enzyme active site and the selected values for grid dimensions and the center were 16×24×28 and x = 0.11, y = -2.511, and z = -22.097, respectively. The validation of docking protocols was performed by re-docking of co-crystallized ligand acarbose with protein 3W37. After validation; the same parameters were used for the docking calculation of all other ligands. The predicted binding affinity (kcal/mol), which indicates how strongly a ligand binds to a receptor, was calculated on the basis of the scoring function used in AutoDock Vina. The best molecular interaction was identified using the binding affinity score. The best docking poses were visualized using Discovery Studio 4.0 Client software.

4.4.4 Determination of α-glucosidase inhibitory activity of compounds

The yeast (*Saccharomyces cerevisiae*) α-glucosidase inhibitory activity of compounds was determined according to the method described by Kim et al and Taha et al., with slight modifications [26, 27]. Initially, the effect of the DMSO solvent on enzyme activity was studied. From the results we concluded that 30% of DMSO in the total reaction mixture had no significant effect on enzyme activity. After standardization, the experiment was conducted in 24 well plates as follows; briefly, 100 µL of each dilution (1000-15.625 µg/ml) of compound in DMSO was added into 24 well plates and thereafter 200 µL of 100 mM phosphate buffer was added so that the final concentration of DMSO does not exceed 30%. Similarly, a control experiment with 100 µL of DMSO and acarbose at different concentrations (1000-15.625

µg/ml) was set. The resulting samples were incubated with 200 µl of 1.0 U/ml a-glucosidase solution in 100 mM phosphate buffer (pH 6.8) at 37°C for 15 min. Thereafter 150 µL of 5 mM pNPG (4-Nitrophenyl-beta-D-glucopyranoside) solution in 100 mM phosphate buffer (pH 6.8) was added and the mixture was further incubated at 37°C for 10 min. The absorbance of the reaction mixture was measured at 405 nm using an automated microplate reader (Synergy HT, BioTek Instruments) and the inhibitory activity was expressed as the percentage of the control sample (100 µL DMSO). All experiments were conducted in triplicate and the results were expressed as the mean ± S.E.M.

$$\% \text{ Inhibition activity} = \frac{(A_{control} - A_{sample})}{A_{Control}} \times 100$$

4.4.5 Antimicrobial assay

The bacterial test cultures used in this study were *Escherichia coli* (ATCC 35218), *Klebsiella pneumoniae* (ATCC 700603), *Staphylococcus aureus* (ATCC 43300), *Enterococcus faecalis* (ATCC 5129) and *Pseudomonas aeruginosa* (ATCC 27853). Initially, the microbial cultures were grown overnight and adjusted to a 0.5 McFarland standard using distilled water and lawn inoculated onto Mueller-Hinton agar (MHA) plates [28]. A stock solution of 10 mg/ml of each compound was prepared and a volume of 20 µL and 10 µL of each sample was inoculated onto antibiotic assay discs (6 mm diameter) and placed on the MHA plates. After overnight incubation at 37°C, zones of inhibition around the discs were measured using a transparent ruler. A control of dimethylsulphoxide (DMSO) only was also used to check its effect on the assay.

4.4.6 Statistical analysis

Statistical analysis was conducted using IBM SPSS statistics 22 software. The data sets were analyzed by one-way ANOVA and the Tukey's post-hoc test. A *p*-value of <0.05 was considered statistically significant.

4.5 Results and Discussion

4.5.1 Synthesis and characterization of compounds

The synthetic scheme for the preparation of compounds is shown in **Fig. 2**. The multicomponent reaction between malononitrile and various benzaldehydes and thiols resulted in the synthesis of 1a-1i compounds with good yields. The purification of these compounds was done by simple recrystallization in a methanol solvent. Thus the synthesis process was economical. The synthesized compounds were characterized using spectroscopic techniques such as IR NMR and were further confirmed by MS. The Scifinder search revealed that compounds 1d, 1e and 1g have been reported previously [29-31]. The remaining compounds are not reported elsewhere, and detailed characterization of the compounds is listed below.

1a. methyl-3-(6-amino-4-(4-Bromophenyl)-3,5-dicynopyridine-2-ylthio)propanoate : White solid; 70% yield; mp 228-230 °C ; C. IR (KBr, cm^{-1}): 3433, 3315, 3214, 2213, 1723, 1619; ^{1}H NMR (400 MHz, DMSO-d6) δ 7.79 (2H, d, *J* = 8.5 Hz, H-Ar), 7.50 (2H, d, *J* = 8.5 Hz, H-Ar), 3.63 (3H, s, H-CH_3), 3.40 (2H, t, *J* = 6.9 Hz, H-CH_2), 2.82 (2H, t, *J* = 6.9 Hz, H-CH_2), ^{13}C NMR (400 MHz, DMSO-d6) 171.7, 166.5, 159.6, 157.2, 133.1, 131.7, 130.6, 124.0, 115.2, 115.1, 93.3, 85.8, 51.6, 33.1, 24.9; HRMS (ESI m/z) $[M + H]^+$: calculated for $C_{17}H_{13}BrN_4O_2S$, 415.9943, found 415.9882.

1b methyl 3-(6-amino-4-(4-chlorophenyl)-3, 5-dicyanopyridin-2-ylthio)propanoate: brown solid; 74% yield; mp 218-220 °C ; C. IR (KBr, cm^{-1}): 3432, 3316, 3214, 2212, 1717, 1617, 1549; ^{1}H NMR (400 MHz, DMSO-d6) δ 7. 65 (2H, d, *J* = 8.6 Hz, H-Ar), 7.57 (2H, d, *J* = 8.6 Hz, H-Ar), 3.64 (3H, s, H-CH_3), 3.40 (2H, t, *J* = 6.9 Hz, H-CH_2), 2.82 (2H, t, *J* = 6.9 Hz, H-CH_2), ^{13}C NMR (400 MHz, DMSO-d6) 171.7, 166.5, 159.6, 157.2, 135.2, 132.7, 130.4, 128.8, 115.2, 115.1, 93.3, 85.8, 51.6, 33.1, 24.9; HRMS (ESI m/z) $[M + H]^+$: calculated for $C_{17}H_{13}ClN_4O_2S$, 372.0448, found 372.0389.

1c. methyl 3-(6-amino-3, 5-dicyano-4-phenylpyridin-2-ylthio)propanoate: yellow solid; 68% yield; mp 208-210 °C ; C. IR (KBr, cm^{-1}): 3395, 3324, 3230, 2210, 1712, 1647, 1550; ^{1}H NMR (400 MHz, DMSO-d6) δ 7. 56 (3H, m, H-Ar), 7.52 (2H, m, H-Ar), 3.64 (3H, s, H-CH_3), 3.40 (2H, t, *J* = 7.0 Hz, H-CH_2), 2.82 (2H, t, *J* = 7.0 Hz, H-CH_2), ^{13}C NMR (400 MHz, DMSO-d6) 171.7, 166.5, 159.7, 158.3, 133.9, 130.3, 128.7, 128.4, 115.3, 115.2, 93.4, 85.8, 51.5, 33.1, 24.9; HRMS (ESI m/z) $[M + H]^+$: calculated for $C_{17}H_{14}N_4O_2S$, 338.0837, found 338.0790.

1d. 2-amino-6-(benzylthio)-4-p-tolylpyridine-3,5-dicarbonitrile [29]: White solid; 80% yield; mp 210-212 °C ; C. IR (KBr, cm^{-1}): 3470, 3441, 3327, 3212, 2216,1614, 1525, 1495; ^{1}H NMR (400 MHz, DMSO-d6) δ 7. 51 (2H, d, *J* = 7.3 Hz, H-Ar), 7.40 (2H, d, *J* = 7.9 Hz, H-Ar), 7.33 (4H, m, H-Ar), 7.26 (1H, m, H-Ar), 4.50 (2H, s, H-CH_2), 2.38 (3H, s, H-CH_3), ^{13}C NMR (400 MHz, DMSO-d6) 166.2, 159.5, 158.4, 140.2, 137.5, 131.5, 130.9, 129.3, 129.1, 128.4, 128.3, 127.2 115.3, 115.2, 93.2, 85.9, 67.4, 33.1, 20.9; HRMS (ESI m/z) $[M + H]^+$: calculated for $C_{21}H_{16}N_4S$, 356.1096, found 356.1054.

1e. 2-amino-6-(benzylthio)-4-(4-bromophenyl)pyridine-3,5-dicarbonitrile [30]: White solid; 72% yield; mp 202-204 °C ; C. IR (KBr, cm^{-1}): 3435, 3324, 3219, 2211, 1628, 1492 ; ^{1}H NMR (400 MHz, DMSO-d6) δ 7. 77 (2H, d, *J* = 8.56 Hz, H-Ar), 7.50 (4H, m, H-Ar), 7.32 (2H, m, H-Ar), 7,25 (1H, m, H-Ar) 4.5 (2H, s, H-CH_2), ^{13}C NMR (400 MHz, DMSO-d6) 159.4, 157.3, 137.5, 133.1, 131.7, 130.5, 129.3, 128.4, 127.3, 124.0, 115.1, 115.0, 33.1; HRMS (ESI m/z) $[M + H]^+$: calculated for $C_{17}H_{13}BrN_4S$, 420.0044, found 420.0000.

1f. 2-amino-6-(benzylthio)-4-phenethylpyridine-3,5-dicarbonitrile: light yellow solid; 70% yield; mp 220-222 °C ; C. IR (KBr, cm^{-1}): 3443, 3331, 3213, 2208,1621, 1528; ^{1}H NMR (400 MHz, DMSO-d6) δ 7. 47 (2H, d, *J* = 7.6 Hz, H-Ar), 7.30 (4H, m, H-Ar), 7.24 (2H, m, H-Ar), 7.18 (2H, d, *J* = 7.34 Hz H-Ar) 4.46 (2H, s, H-CH_2), 2.94 (2H, m, H-CH_2), 2.85 (2H, m, H-CH_2) ^{13}C NMR (400 MHz, DMSO-d6) 165.9, 159.6, 159.4, 139.4, 137.4,129.2,128.5, 128.4, 128.1, 127.2, 126.5,114.8, 114.7, 93.2, 85.9, 35.5,34.6, 33.0 HRMS (ESI m/z) $[M + H]^+$: calculated for $C_{22}H_{18}ClN_4S$, 370.1252, found 370.1190.

1g. 2-amino-4-(4-chlorophenyl)-6-(phenylthio)pyridine-3,5-dicarbonitrile[31]: White solid; 78% yield; mp 222-224 °C ; C. IR (KBr, cm^{-1}): 3486, 3340, 3220, 2213, 1625, 1647, 1541, 1519; ^{1}H NMR (400 MHz, DMSO-d6) δ 7. 66 (2H, m, H-Ar), 7.60 (4H, m, H-Ar), 7.50 (3H, m, H-Ar), ^{13}C NMR (400 MHz, DMSO-d6) 166.1, 159.5, 157.5, 135.3, 134.8, 132.7, 130.4, 129.7, 129.4, 128.9, 127.0, 115.2, 114.8, 93.3, 87.1; HRMS (ESI m/z) $[M + H]^+$: calculated for $C_{19}H_{11}ClN_4S$, 362.0393, found 362.0349.

1h. 2-(4-methoxyphenylthio)-6-amino-4-phenethylpyridine-3,5-dicarbonitrile: light yellow solid; 70% yield; mp 206-208 °C ; C. IR (KBr, cm^{-1}): 3425, 3328, 3229, 2210, 1636, 1591, 1532; ^{1}H NMR (400 MHz, DMSO-d6) δ 7. 35 (3H, m, H-Ar), 7.23 (3H, m, H-Ar), 7.12 (2H, m, H-Ar), 7.04 (1H, m, H-Ar) 3.7 (3H, s, H-CH_3), 2.99 (2H, m, H-CH_2), 2.89 (2H, m, H-CH_2), ^{13}C NMR (400 MHz, DMSO-d6) 165.7, 159.9, 159.6, 139.4, 130.2, 128.5, 128.1, 126.6, 119.5,

115.8, 114.8, 114.5, 55.3, 35.6, 34.6; HRMS (ESI m/z) $[M + H]^+$: calculated for $C_{22}H_{18}N_4OS$, 386.1201, found 386.1155.

1i. 2-((2-(6-amino-3,5-dicyano-4-phenethylpyridin-2-ylthio)ethyl)sulfanyl)-6-amino-4-phenethyl pyridine-3,5-dicarbonitrile : White solid; 50% yield; mp 262 °C ; C. IR (KBr, cm^{-1}): 3462, 3429, 3331, 3223, 2209, 1627, 1555 ; ^1H NMR (600 MHz, DMSO-d6) δ 7. 32 (4H, t, *J* = 7.54Hz, H-Ar), 7.22 (6H, m, H-Ar), 3.51 (4H, bs, H-CH_2), 2.99 (4H, m, H-CH_2), 2.89 (4H, m, H-CH_2), ^{13}C NMR (600 MHz, DMSO-d6) 166.6, 160.2, 160.1, 140, 129, 128.6, 126.9, 115.3, 115.1, 94.5, 86.8, 35.9, 35.1, 29.7; HRMS (ESI m/z) $[M + H]^+$: calculated for $C_{22}H_{18}N_4OS$, 586.1722, found 586.1688.

4.5.2 Docking Results.

Molecular docking analysis for the compounds was carried out using a crystal structure of α-glucosidase (PDB ID: 3W37), and the binding affinity of the compounds to the enzyme active site was then explored. The initial molecular docking validation was performed by re-docking acarbose on the protein α-glucosidase (3W37). The confirmation that resulted was compared with the experimental co-crystalized structure of acarbose obtained from source pdb files. The finest overlapping was observed between the re-docked confirmation and crystal structure as shown in **Fig. 4.4** and the docking score for acarbose was found to be -8.9. With these satisfactory results, the molecular docking calculations for the energy minimized 3D structures of the desired ligands were preceded using the same coordinates obtained during the validation. The binding scores and observed amino acid interactions of compounds in the enzyme active site were reported in **Table 4.1**. The best binding poses obtained for each ligand-protein complex were shown in **Fig. 4.5**. The compound 1f showed the best affinity with a docking score of -8.6, which was similar to that of acarbose. Compounds 1d, 1e, 1f, 1g, 1h and 1i also displayed good affinity towards the enzyme active site, with docking scores of -8.1, -8.1, -8.6, -7.3, -8.4 and -7.9 respectively. These compounds had aryl or aryl alkyl substituents at position 6 of the pyridine ring (**Table 4.2**). The poor docking scores for the compounds; 1a, 1b, 1c, -6.4, -6.4, -6.2, respectively, indicated that when the aryl alkyl groups at position 6 of the pyridine ring were replaced by alkyl groups, affinity decreased drastically. Additionally, the docking studies revealed that the hydrophobic interaction such as π- π stacking between aromatic rings were the dominant forces involved in the interaction of compounds in the active pocket of enzymes, as fewer or no intermolecular hydrogen bonds were formed with the compounds

having best activity. Thus molecular docking identified the best affinity with the molecular framework of compound 1f out of all the synthesized compounds. Since the conversion of nitrile groups to other functional groups can easily be affected, docking with different functional groups such as amine, amide and acid at 3 and 5 positions of the pyridine ring was conducted. The change of this nitrile functionality with other functional group did not improve the affinity to a significant effect **(Table 4.2)**. Hence our synthesis was confined to nitrile derivatives and further conversion was not conducted.

Table 4.1 Binding energies calculated for the compounds using Autodock Vina software.

Compound	Affinity (kcal/mol)	Hydrogen bond interactions	Ligand binding site interactions
Acarbose	-8.9	ALA234, ASN237, ARG552, ARG552	ASP357, ILE358, TRP467, HIS626, TRP329, TRP432, ASP469, MET470, PHE601, ARG552, ASP232, SER497, PHE236, ASP568, ALA234, ASN237, SER 497
1a	-6.4	none	HIS626, MET470, PHE476, PHE601, TRP432, TRP467, TRP329
1b	-6.4	-	ALA234,ASP232, PHE476, MET470
1c	-6.2	ASP 232	ALA234,ASP232,ARG652, PHE476, TRP432, HIS626, PHE601
1d	-8.1	ASP 232	ASP357, HIS626, ALA234, ASP232, PHE476
1e	-8.1	ASP232	ASP357, ASP232, ASN237, HIS626, ALA234, PHE476
1f	-8.6	-	ARG552, PHE601, TRP329, TRP432, PHE476, LYS506
1g	-7.3	-	ARG662, ASP232, HIS 626, TRP467, TRP329,TRP432 PHE 601, PHE236, ASP568, MET470
1h	-8.4	-	PHE601, TRP329, ARG552,TRP432, PHE476
1i	-7.9	ARG552	ALA602, PHE601, PHE236, TRP329, ASP232, ARG552, TRP432

Table 4.2 Binding energies calculated for different derivatives of pyridine using Autodock Vina.

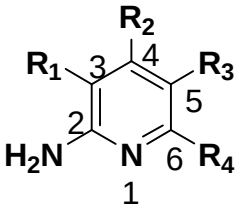

Compound	Docking scores			
	R_1=R_3=CN	R_1=R_3=COOH	R_1=R_3=$CONH_2$	R_1=R_3=CH_2NH_2
1a	-6.4	-6.2	-6.6	-6.7
1b	-6.4	-6.5	-6.2	-6.5
1c	-6.2	-6.2	-6.4	-6.5
1d	-8.1	-7.6	-7.9	-7.4
1e	-8.1	-7.4	-7.7	-7.3
1f	-8.6	-8.3	-8.4	-7.9
1g	-7.3	-6.7	-7.2	-6.8
1h	-8.4	-8.2	-8.1	-7.8
1i	-7.9	-8.5	-8.6	-7.9
Acarbose	-8.9	-	-	-

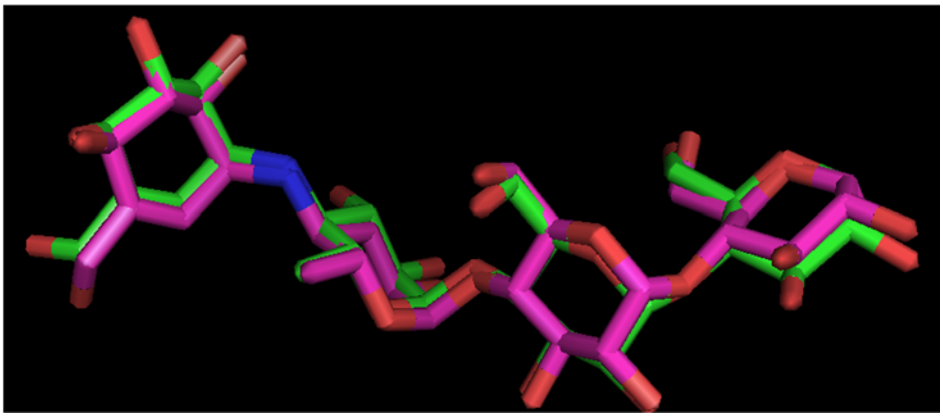

Figure 4.4 Best docked confirmation of acarbose overlapped with the X-ray binding mode of native ligand within the active site of α-glucosidase; hydrogen atoms are not shown for clarity.

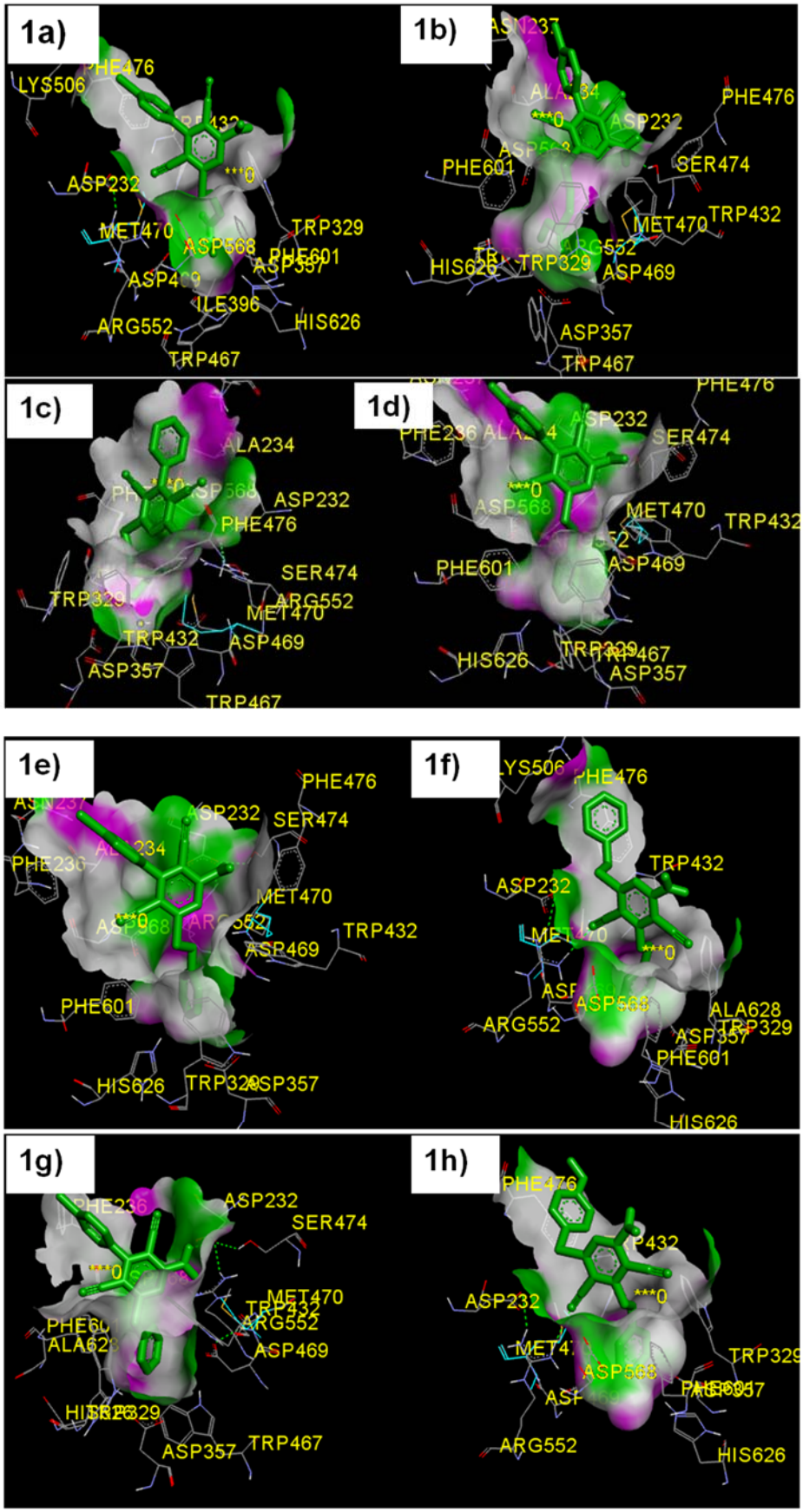
1a)
LYS506
PHE476
ASP232
MET470
TRP329
ASP568
PHE601
ASP357
ILE396
ARG552
HIS626
TRP467
1b)
PHE476
ASP232
SER474
PHE601
MET470
TRP432
HIS626
TRP329
ASP469
ASP357
TRP467
1c)
ALA234
ASP232
PHE476
SER474
ARG552
MET470
TRP432
ASP469
ASP357
TRP467
1d)
PHE476
ASP232
SER474
MET470
TRP432
ASP469
PHE601
HIS626
ASP357
1e)
PHE476
ASP232
SER474
MET470
TRP432
ASP469
PHE601
HIS626
ASP357
1f)
PHE476
TRP432
ASP232
ALA628
ARG552
ASP357
PHE601
HIS626
1g)
ASP232
SER474
MET470
ARG552
ASP469
ASP357
TRP467
1h)
PHE476
ASP232
TRP329
ARG552
HIS626

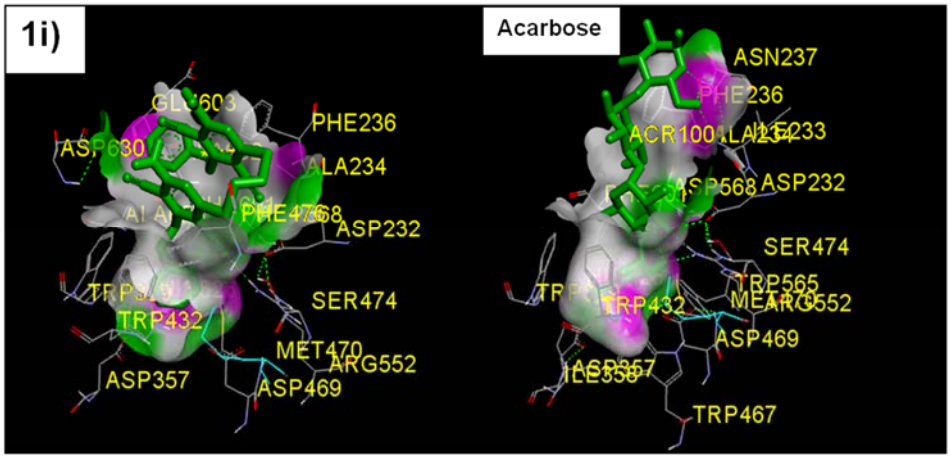

Figure 4.5 Binding mode of compounds 1a-1i and acarbose docked in their best conformation into the binding site of α-glucosidase (3W37); Hydrogen atoms are not shown for clarity.

4.5.3 α-Glucosidase inhibitory activity

The α-glucosidase inhibitory activities of 3, 5-dicyanopyridine scaffolds were evaluated and the results are shown in **Table 4.3**. The data in **Table 4.3** suggests that compounds 1a and 1b exhibited activities weaker than that of acarbose, whereas compound 1c did not show any activity at the tested concentration range. These compounds have alkyl side chains at the 6th position of the pyridine ring and the docking studies predicted that alkyl chains entered into the active pocket. Low binding scores indicated the loose fitting of alkyl chains inside the active pocket and as a consequence, weaker or no activities were observed for these compounds. However, when alkyl side chains were replaced by aryl or aryl alkyl groups at the 6th position, the activity of the compounds was drastically improved. The compounds 1d, 1e, 1f, 1g and 1h showed improved activity in comparison to 1a, 1b and 1c. At a concentration of 125 µg/ml, all these compounds exhibited approximately 90% inhibition and at 62.5 µg more than 50% inhibition was observed except for the compound 1f. The binding affinity of compound 1f was higher than that of compounds 1d, 1e and 1g, although relatively better activities were observed for the compounds 1d, 1e and 1g than 1f. Careful analysis of the best scored poses of these compounds showed that along with π-π interaction, compounds 1d and 1e also formed hydrogen bonds with the ASP 232 of the active site, while compound 1g had a different binding pose with aryl groups at 4 position entering the active site. These differences could have caused a better affinity between the protein and the compounds 1d, 1e and 1g than with compound 1f. The dimer 1i also exhibited good inhibitory activity with more than 50% inhibition at a concentration of 62.5 µg/ml. Interestingly, the amine group of the pyridine ring in all the

compounds displayed no apparent role in active site binding as no hydrogen bond interactions were observed between the amine group of the compound and active site amino acids of α-glucosidase. The trends observed in the biological activity were well correlated with the predictions made by docking studies and indicated that the presence of aryl groups at both the 4th and 6th positions of the pyridine ring **(Table 4.2)** is crucial for the best activity. Experimental results revealed that, although the π–π stacking interactions were found to be the major forces in the ligand -protein complex formation, hydrogen bond interactions also played an important role in the inhibitory activities. Introducing polar functional groups such as hydroxyl and nitro groups in the benzene ring at the 4th and 6th position of the pyridine ring could help in increasing the affinity of the compounds for binding to the active site by forming hydrogen bonds inside the active pocket. Thus both the theoretical and experimental results obtained in this study helped us to find a logical method for further improvement of compound activity.

Table 4.3 The percentage inhibition values for the inhibition of α-glucosidase by test compounds.

Compound	Concentration (µg/ml)						
	1000	500	250	125	62.5	31.25	15.625
1a	93.73±1.48^{a}	86.03±1.72^{a}	12.07±5.4^{b}	ND	ND	ND	ND
1b	89.47±2.67^{a}	76.50±1.39^{b}	ND	ND	ND	ND	ND
1c	ND	ND	ND	ND	ND	ND	ND
1d	90.47±1.29^{a}	93.37±0.68^{a}	92.90±0.44^{a}	92.82±0.41^{a}	71.57±2.48^{b}	11.9±3.08^{c}	ND
1e	94.67±0.19^{a}	94.73±0.14^{a}	94.52±0.10^{a}	93.82±0.92^{a}	64.65±0.59^{b}	10.96±0.50^{c}	5.89±0.38^{d}
1f	94.97±0.30^{a}	94.10±0.21^{a}	93.38±0.34^{a}	77.74±3.05^{b}	12.7±1.09^{c}	ND	ND
1g	94.57±0.6^{a}	94.68±0.17^{a}	94.78±0.1^{a}	92.72±0.97^{a}	78.69±1.6^{b}	23.25±1.90^{c}	6.57±4.24^{d}
1h	93.59±0.99^{a}	93.91±0.31^{a}	89.42±3.5^{a}	27.64±4.24^{b}	ND	ND	ND
1i	93.38±1.67^{a}	91.79±0.48^{a}	91.19±2.26^{a}	88.15±2.86^{a}	59.73±2.10^{b}	12.11±4.12^{c}	ND
Acarbose	95.87±1.98^{a}	93.82±2.12^{a}	92.89±0.71^{a}	85.15±1.65^{b}	65.63±0.64^{c}	39.67±3.80^{d}	14.50±1.65^{e}

ND, No inhibition detected

All values are expressed as mean ± standard deviation of experiments performed in triplicate. Statistical analysis showed that samples with different superscript letters were significantly different from each other ($p < 0.05$; one-way ANOVA, Tukey's post-hoc test).

4.5.4 Antibacterial activity

No significant zone of inhibition was observed for any of the compounds tested in this study. Hence we conclude that these compounds do not exhibit antibacterial properties.

4.6 Conclusion

In this study, α-glucosidase inhibitory and antibacterial activities of derivatives containing 3,5-dicyanopyridine were evaluated for the first time. These compounds were synthesized in a single step multi-component protocol with good yields from commercially available reagents. The binding affinities of the 3, 5-dicyanopyridine with α-glucosidase were calculated using Autodock Vina software. The *invitro* α-glucosidase inhibitory results demonstrated that, compounds of the type 1c, 1d, 1e, 1f and 1g showed significant α-glucosidase inhibition. However these compounds did not demonstrate any antibacterial activity. After carefully examining the theoretical and experimental inhibitory activities, a basic 3, 5-dicyanopyridine organic framework which could fit effectively in the enzyme's active site and inhibit its activity was discovered. This will enable us to design more active analogues of these compounds with the further introduction of polar groups such as hydroxyl and nitro groups and which are capable of forming hydrogen bonds with amino acids in the enzyme's active site. The findings reported in this study may thus help in the development of a new class of antidiabetic compounds.

4.7 Acknowledgement

This research work was funded by National Research Foundation (NRF) of South Africa and the University of KwaZulu-Natal, South Africa.

4.8 References

[1] D.W. Lam, D. LeRoith, The worldwide diabetes epidemic, Current Opinion in Endocrinology, Diabetes and Obesity, 19 (2012) 93-96.
[2] D. Mellitus, Diagnosis and classification of diabetes mellitus, Diabetes care, 28 (2005) S37.
[3] L. Eiselein, H.J. Schwartz, J.C. Rutledge, The challenge of type 1 diabetes mellitus, ILAR Journal, 45 (2004) 231-236.
[4] A.B. Olokoba, O.A. Obateru, L.B. Olokoba, Type 2 diabetes mellitus: a review of current trends, Oman Medical Journal, 27 (2012) 269-273.
[5] J.C. Lovejoy, The influence of dietary fat on insulin resistance, Current Diabetes Reports, 2 (2002) 435-440.

[6] K.G.M.M. Alberti, P.f. Zimmet, Definition, diagnosis and classification of diabetes mellitus and its complications. Part 1: diagnosis and classification of diabetes mellitus. Provisional report of a WHO consultation, Diabetic Medicine, 15 (1998) 539-553.
[7] A. Ceriello, Postprandial hyperglycemia and diabetes complications is it time to treat?, Diabetes, 54 (2005) 1-7.
[8] B. Gallwitz, Implications of postprandial glucose and weight control in people with type 2 diabetes understanding and implementing the international diabetes federation guidelines, Diabetes Care, 32 (2009) S322-S325.
[9] M. Toeller, α-Glucosidase inhibitors in diabetes: efficacy in NIDDM subjects, European Journal of Clinical Investigation, 24 (1994) 31-35.
[10] D.E. Kelley, P. Bidot, Z. Freedman, B. Haag, D. Podlecki, M. Rendell, D. Schimel, S. Weiss, T. Taylor, A. Krol, Efficacy and safety of acarbose in insulin-treated patients with type 2 diabetes, Diabetes Care, 21 (1998) 2056-2061.
[11] U. Ghani, Re-exploring promising α-glucosidase inhibitors for potential development into oral anti-diabetic drugs: Finding needle in the haystack, European Journal of Medicinal Chemistry, 103 (2015) 133-162.
[12] S. Riaz, I.U. Khan, M. Yar, M. Ashraf, T.U. Rehman, A. Shaukat, S.B. Jamal, V.C. Duarte, M.J. Alves, Novel pyridine-2, 4, 6-tricarbohydrazide derivatives: Design, synthesis, characterization and in vitro biological evaluation as α-and β-glucosidase inhibitors, Bioorganic Chemistry, 57 (2014) 148-154.
[13] U. Rosentreter, T. Kramer, M. Shimada, W. Hubsch, N. Diedrichs, T. Krahn, K. Henninger, J.-P. Stasch, Substituted 2-thio-3, 5-dicyano-4-phenyl-6-aminopyridines and their use as adenosine receptor-selective ligands, in, Google Patents, 2006.
[14] N.M. Evdokimov, A.S. Kireev, A.A. Yakovenko, M.Y. Antipin, I.V. Magedov, A. Kornienko, One-step synthesis of heterocyclic privileged medicinal scaffolds by a multicomponent reaction of malononitrile with aldehydes and thiols, The Journal of Organic Chemistry, 72 (2007) 3443-3453.
[15] M. Abdel-megid, M.A. Ibrahim, Y. Gabr, N.M. El-Gohary, E.-H.A. Mohamed, Synthesis and antimicrobial activity of some new nitrogen bridge-head pyrido [1, 2-b][1, 2, 4] triazepines incorporating 6-methylchromone moiety, 15th International. Electronic. Conference on. Synthetic. Organic. Chemistry., MDPI, 2011.
[16] H.-A.S. Abbas, W.A. El Sayed, N.M. Fathy, Synthesis and antitumor activity of new dihydropyridine thioglycosides and their corresponding dehydrogenated forms, European Journal of Medicinal Chemistry, 45 (2010) 973-982.
[17] U. Rosentreter, T. Krämer, A. Vaupel, W. Hübsch, N. Diedrichs, T. Krahn, K. Dembowsky, J.-P. Stasch, M. Shimada, Substituted 2-thio-3, 5-dicyano-4-phenyl-6-aminopyridines with adenosine receptor-binding activity and their use as cardiovascular preparations, in, Google Patents, 2006.
[18] B.C. May, J.A. Zorn, J. Witkop, J. Sherrill, A.C. Wallace, G. Legname, S.B. Prusiner, F.E. Cohen, Structure-activity relationship study of prion inhibition by 2-aminopyridine-3, 5-dicarbonitrile-based compounds: parallel synthesis, bioactivity, and in vitro pharmacokinetics, Journal of Medicinal Chemistry, 50 (2007) 65-73.
[19] H. Harada, S. Watanuk, T. Takuwa, K. Kawaguchi, T. Okazaki, Y. Hirano, C. Saitoh, Preparation of dicyanopyridine derivatives as high-conductance calcium-sensitive potassium channel openers, PCT Int. Appl. WO Patent, 2002006237 A1.
[20] H.Z. Chem, W.; Tam, R.; Raney, A. K., Preparation of 3-amino-5-cyanothieno[2,3-b]pyridine-2-carboxamides as IKK2 inhibitors for the treatment of HBV infectio, PCT Int. Appl. WO Patent 2005058315 A1 2005063, (2005).
[21] S. Hinz, S.K. Lacher, B.F. Seibt, C.E. Müller, BAY60-6583 acts as a partial agonist at adenosine A2B receptors, Journal of Pharmacology and Experimental Therapeutics, 349 (2014) 427-436.
[22] M.B. Kanani, M.P. Patel, Synthesis and in vitro antimicrobial evaluation of novel 2-amino-6-(phenylthio)-4-(2-(phenylthio) quinolin-3-yl) pyridine-3, 5-dicarbonitriles, Medicinal Chemistry Research, 22 (2013) 2912-2920.
[23] K. Han, Y. Li, Y. Zhang, Y. Teng, Y. Ma, M. Wang, R. Wang, W. Xu, Q. Yao, Y. Zhang, H. Qin, H. Sun, P. Yu, Design, synthesis and docking study of novel tetracyclic oxindole derivatives as α-glucosidase inhibitors, Bioorganic & Medicinal Chemistry Letters, 25 (2015) 1471-1475.

[24] X. Peng, G. Zhang, Y. Liao, D. Gong, Inhibitory kinetics and mechanism of kaempferol on α-glucosidase, Food Chemistry,190 (2015) 207-215.
[25] O. Trott, A.J. Olson, AutoDock Vina: improving the speed and accuracy of docking with a new scoring function, efficient optimization, and multithreading, Journal of Computational Chemistry, 31 (2010) 455-461.
[26] Y.-M. Kim, Y.-K. Jeong, M.-H. Wang, W.-Y. Lee, H.-I. Rhee, Inhibitory effect of pine extract on α-glucosidase activity and postprandial hyperglycemia, Nutrition, 21 (2005) 756-761.
[27] M. Taha, N.H. Ismail, S. Lalani, M.Q. Fatmi, S. Siddiqui, K.M. Khan, S. Imran, M.I. Choudhary, Synthesis of novel inhibitors of α-glucosidase based on the benzothiazole skeleton containing benzohydrazide moiety and their molecular docking studies, European Journal of Medicinal Chemistry, 92 (2015) 387-400.
[28] J.H. Jorgensen, J.D. Turnidge, Susceptibility Test Methods: Dilution and Disk Diffusion Methods*, (2015).
[29] M.N. Khan, S. Pal, T. Parvin, L.H. Choudhury, A simple and efficient method for the facile access of highly functionalized pyridines and their fluorescence property studies, RSC Advances, 2 (2012) 12305-12314.
[30] A. Molla, S. Hussain, Borax catalyzed domino reactions: synthesis of highly functionalised pyridines, dienes, anilines and dihydropyrano [3, 2-c] chromenes, RSC Advances, 4 (2014) 29750-29758.
[31] U.V. Desai, M.A. Kulkarni, K.S. Pandit, A.M. Kulkarni, P.P. Wadgaonkar, A simple, economical, and environmentally benign protocol for the synthesis of 2-amino-3, 5-dicarbonitrile-6-sulfanylpyridines at ambient temperature, Green Chemistry Letters and Reviews, 7 (2014) 228-235.

Chapter 5

RESEARCH RESULTS III

γ-cyclodextrin capped silver nanoparticles for molecular recognition and enhancement of antibacterial activity of Chloramphenicol

This manuscript was published in
Journal of Inorganic Biochemistry (2016)

γ-cyclodextrin capped silver nanoparticles for molecular recognition and enhancement of antibacterial activity of Chloramphenicol

Ramesh Gannimani[a], Muthusamy Ramesh[b], Sphamandla Mtambo[a], Karen Pillay[a], Mahmoud E. Soliman[b], Patrick Govender[a,*]

[a]Department of Biochemistry, School of Life Sciences, University of KwaZulu-Natal (UKZN), Westville, Durban 4000, South Africa

[b]Discipline of Pharmaceutical Sciences, School of Health Sciences, University of KwaZulu-Natal (UKZN), Westville, Durban 4000, South Africa

5.1 Abstract

Computational studies were conducted to identify the favourable formation of the inclusion complex of chloramphenicol with cyclodextrins. The results of molecular docking and molecular dynamics predicted the strongest interaction of chloramphenicol with γ-cyclodextrin. Further, the inclusion complex of chloramphenicol with γ-cyclodextrin was experimentally prepared and a phenomenon of inclusion was verified by using different characterization techniques such as thermogravimetric analysis, differential scanning calorimetry, ^{1}H nuclear magnetic resonance (NMR) and two dimensional nuclear overhauser effect spectroscopy (NOESY) experiments. From these results it was concluded that γ-cyclodextrins could be an appropriate cyclodextrin polymer which can be used to functionalize chloramphenicol on the surface of silver nanoparticles. In addition, γ-cyclodextrin capped silver nanoparticles were synthesized and characterized using UV-visible spectroscopy, scanning electron microscopy (SEM), transmission electron microscopy (TEM), energy dispersive X-ray analysis (EDX), Fourier transform infrared spectroscopy (FTIR) and zeta potential analysis. Molecular recognition of chloramphenicol by these cyclodextrin capped silver nanoparticles was confirmed by surface enhanced raman spectroscopy (SERS) experiments. Synergistic antibacterial effect of chloramphenicol with γ-cyclodextrin capped silver nanoparticles was evaluated against *Pseudomonas aeruginosa* (ATCC 27853), *Enterococcus faecalis* (ATCC 5129), *Klebsiella pneumoniae* (ATCC 700603) and *Staphylococcus aureus* (ATCC 43300). The results from the antibacterial experiment were favourable thus allowing us to conclude that the approach of modifying organic drug molecules with cyclodextrin capped inorganic silver nanoparticles could help to enhance thei antibacterial activity.

5.2 Key words

Chloramphenicol, inclusion complex, binding free energies, silver nanoparticles, synergistic antibacterial activity

5.3 Introduction

The necessity for the discovery of new therapeutic drug formulations to treat bacterial infection is increasing due to the emergence of drug resistance. However, the process of discovering, developing and clinically testing new antibiotics is time consuming and expensive [1]. In addition, the rapid development of resistance to newly introduced chemotherapeutic agents in bacteria makes the process of drug development more difficult. Hence, finding new strategies to make better use of existing medicine to overcome the problem of resistance has become an important area of research. This approach is economically sensible since the toxicological and pharmacological properties of the drugs are well known, which would also support rapid development of the new treatment [2].

Several approaches have been reported for overcoming the bacterial resistance for existing chemotherapeutic agents, one of which being combination therapy [2]. Combination therapy is a standard method in which two or more drugs with different modes of action are combined in a precisely controlled manner to maximize therapeutic efficacy and thus combating the problem of drug resistance. Recently, the application of inorganic material in association with organic drug molecules in combination therapy is drawing much attention [3]. For example, activity of amoxicillin, ampicillin, erythromycin, kanamycin and chloramphenicol was found to be enhanced in the presence of silver nanoparticles [4, 5]. Similarly, the coating of vancomycin, streptomycin, gentamycin, neomycin and acridine derivatives gold nanoparticles has improved their antibacterial efficacy [6-8]. Such strategies of combining antibiotics with inorganic materials can be very effective due to the ability of inorganic metal ions to target multiple sites of a biological system [3]. In this approach, drugs can be functionalized on the solid core surface of metal nanoparticles either by covalent or noncovalent interactions. Covalent linking requires additional chemical modification of drug molecules, which could result in the alteration of the properties of drug molecules [9]. However, non-covalent strategies to functionalize the drug molecules on the surface of nanoparticles involves only electrostatic and van der Waal's interactions, and thus drugs can be used in their native form [9].

Silver nanoparticles can be a preferred choice among other non-materials for such organic-inorganic combination antibacterial therapy, due to their innate antibacterial properties and their affinity to bind to organic molecules [10]. In addition, the large surface area of nanoparticles provides an opportunity for high drug loading and attachment of other surface constituents [10]. The antibacterial properties of silver nanoparticles together with the supramolecular chemistry

of cyclodextrins (CD) can provide an excellent platform as drug delivery systems with potential combination therapeutic applications. The supramolecular chemistry associated with cyclodextrins can result in noncovalent incorporation of organic molecules on the surface of nanoparticles, thus enhancing the molecular recognition properties of silver nanoparticles. The phenomenon of molecular functionalization of organic molecules on the surface of inorganic nanoparticle using cyclodextrins has recently been well demonstrated [9, 11, 12]. Since the cyclodextrins are available with various cavity sizes, fabrication of nanoparticles with them could generate nanomaterials for a variety of biomedical applications.

In this study, γ-cyclodextrin capped silver nanoparticles (CDAgNPs) were prepared and their application in improving the antibacterial efficacy of chloramphenicol (CMP) was investigated. Our interest in using the cyclodextrin capped nanoparticles for the enhancement of antibacterial efficacy of CMP is based on the fact that cyclodextrins can cause localized high concentration of drug on the surface of nanoparticles by encapsulating them into their hydrophobic cavity, thereby making the drug effective at lower dosages [13]. Another advantage of this approach is that it does not involve chemical modification of the drug thereby allowing the drug to be used in its native form.

5.4 Materials and Methods

5.4.1 Computational studies

5.4.1.1 Molecular docking analysis

To perform molecular docking, the 3D structure of CMP was built in Gauss view software and energetically minimized by Austin model 1 (AM1) in the Gaussian 09 software package [14]. The 3D structures of α-CD (PDB code: 2ZYM) [15], β-CD (PDB code: 3CGT) [16] and γ-CD (PDB code: 2ZYK) [17] were collated from protein data bank (PDB). Further, these structures were pre-processed for docking using Dock prep in the Chimera software package [18]. During this process, the missing hydrogen atoms and the atomic charges were added. The binding site was defined at the centroid of cyclodextrins. Molecular docking was carried out independently to generate the inclusion complex of CMP with three different cyclodextrins using AutoDock [19].

5.4.1.2 Molecular dynamics analysis

The inclusion complexes of CMP with three different cyclodextrins were subjected to molecular dynamics (MD) studies. The software package of AMBER 14 (Assisted Model Building with Energy Refinement) was used to conduct MD simulation (GPU version of PMEMD engine integrated with AMBER 14) [20]. The LEAP module was used to add hydrogen atoms, counter ions, charge, solvated water, and simulation box. The system of the inclusion complex was contained in solvated TIP3P water box [21, 22]. The atom types for the inclusion complexes were set using Antechamber module. Conjugate gradient energy minimization was run up to 1000 steps. During the simulation, all the residues in the inclusion complex were allowed to move. The simulations were set to 50 ps of heating from 0 to 300 K with the harmonic restraints of 5 kcal mol^{-1} $Å^{-2}$ for solute atoms and a Langevin thermostat with a 1ps random collision frequency. Further, the system was equilibrated for 500 ps at 300 K. MD runs were set for 10 ns in an isothermal isobaric (NPT) ensemble using a Berendsen barostat with a target pressure of 1 bar. After the MD simulation, the trajectories were visualized using graphical user interface of the UCSF Chimera package [18]. The binding free energies were then computed for all three inclusion complexes of chloramphenicol. Molecular Mechanics–Poisson–Boltzmann surface Area (MM–PBSA) was employed to calculate the binding free energies. The binding free energies were averaged over 200 snapshots taken from the post-equilibrated 10 ns MD trajectory [23-28].

5.4.2 Preparation of inclusion complexes and physical mixture

The inclusion complex of CMP was prepared by the freeze drying method described by *Lakkakula et al.* [29]. Chloramphenicol (Duchefa Biochemie; 0.1 g) and γ-CD (Wacker Chemie; 0.402 g) were dissolved in 25 ml of double distilled water in 1:1 molar ratios and stirred at room temperature for 24 h. The clear solution obtained was frozen at -72°C and lyophilized to yield a white amorphous solid. Physical mixture of CMP and γ-CD was obtained by mortaring a 1:1 mixture of each sample.

5.4.3 Synthesis of γ-CD capped silver nanoparticles

Methodology reported by *Premkumara et al.* was employed for the synthesis of nanoparticles [30]. Briefly, 50 ml of 5 mM γ-cyclodextrin and 100 ml of 20 mM sodium hydroxide solution were added to 50 ml of 2.5 mM silver nitrate (Merck). The resulting black solution was incubated at 30°C in an orbital shaker at 150 rpm for 24 h. The solution turned yellow after 24 h and the presence of nanoparticles in the solution was confirmed by UV absorbance. The reaction mixture was subsequently centrifuged at 12000 rpm (Eppendorf 5810R, Rotor F-34-6-38) for 10 minutes and the pellet obtained was washed three times with 50 ml deionized water to remove excess base. The resulting pellet of CDAgNPs was suspended in 10 ml deionized water and used as the stock solution for all the experiments.

5.4.4 Characterization of the inclusion complex and silver nanoparticles

Powder X-ray diffraction (XRD) patterns were obtained at ambient temperature by employing Bruker D8 Advance instrument equipped with an Anton-Paar XRK 900 reaction chamber and a Cu radiation source with a wavelength of 1.5406 Å. Infrared spectra of CMP, cyclodextrin and inclusion complex were recorded on a Perkin Elmer Spectrum 100 FT-IR spectrometer with universal ATR sampling accessory. Thermogravimetric analysis-differential scanning calorimetry (TGA-DSC) was performed on SDT Q600 TA instrument at a heating rate of 10°C min^{-1} over a wide temperature range (25-800°C) under nitrogen atmosphere. SEM morphological images of the samples were obtained using a scanning electron microscope (FEGSEM ZEISS ULTRAPLUS) with an excitation voltage of 20 kV and 10000 X magnification. Samples were placed on adhesive carbon tape glued over aluminium stub and made electrically conductive by thin gold coating in vacuum prior to the analysis. Nuclear magnetic resonance (NMR) experiments were conducted on a Bruker Avance^{III} 600 MHz spectrometer at 30°C. Samples were dissolved in deuterium oxide. Chemical shifts (δ) were recorded using tetramethylsilane (TMS) as an internal standard and the spectra obtained were referenced to the residual water signal of D_2O. The spectrometers were equipped with a BBOZ probe. In the ^1H-^1H NOESY experiment, the mixing time was 300 ms and relaxation time was 1s.

The reduction reaction of silver ions to silver nanoparticles was confirmed by UV visible absorption measurements at room temperature as a function of time using Specord 210,

Analytikjena spectrometer. The nanoparticle pellet obtained after washing was freeze dried and used for the FTIR studies (Perkin Elmer Precisely Spectrometer 100 FTIR-ATR). Morphological studies of the synthesized CDAgNPs were carried out using scanning electron microscopy (FEGSEM ZEISS ULTRAPLUS). Samples were prepared by adding a drop of sonicated nanoparticle solution over the carbon tape glued over an aluminium grid. The samples obtained were then coated with a gold layer and observed at 10000 X magnification. The energy dispersive X-ray analysis (EDX) was performed at 20 kV using AZTEC software for the analysis. The silver nanoparticle solutions obtained after the purification step were sonicated for 15 minutes to disrupt any possible aggregates and small amount of the resulting suspension was placed on carbon coated copper grids and dried by solvent evaporation. High-resolution TEM images were obtained on a JEOL TEM model no 2100 operating at an accelerating voltage of 200 kV and 0.23 nm resolution. The zeta potential and zeta size of the synthesized CDAgNPs was determined at 25°C using a Zetasizer Nano ZS90 (Malvern Instruments Ltd., UK). The ICP-OES instrument (PerkinElmer Precisely, optima 2100 DV) equipped with WinLab32 software was used to measure the concentration of silver nanoparticles. A 1 ml stock solution of CDAgNPs was digested with 8 ml of 65% nitric acid on a hot plate set at 90^0C and the resulting solution was diluted to 100 ml [31]. The Silver nitrate solution of concentration 1.625-50 ppm was used to generate a standard curve, which were then used for measurement of the unknown concentration. A nitric acid blank prepared similar to the unknown sample was used to compensate for the effect of nitric acid during analysis. The Raman and surface enhanced raman spectroscopy (SERS) experiments were conducted using a Raman spectrometer (Manufacturer: Delta Nu, Model: Advantage 532). The instrument was equipped with solid state 532 nm Nd:Yag crystal laser and charged couple device (CCD) detector.

5.4.5 Chloramphenicol γ-cyclodextrin capped CDAgNPs composite preparation and characterization

Briefly, to a 5 ml of 1 mg/ml stock solution of γ-cyclodextrin capped CDAgNPs, 5 ml solution of 1 mg/ml of CMP was added. The resulting solution was incubated at 30°C in an orbital shaker at 150 rpm for 24 h. The effect of CMP coating on size and stability of γ-cyclodextrin capped CDAgNPs was assessed by zeta potential and zeta size at 25°C using a Zetasizer Nano ZS90 (Malvern Instruments Ltd., UK).

5.4.6 Antibacterial activity

The synthesized γ-cyclodextrin capped CDAgNPs, CMP and CMP coated CDAgNPs were tested for their antibacterial activity against *Pseudomonas aeruginosa* (ATCC 27853), *Enterococcus faecalis* (ATCC 5129), *Klebsiella pneumoniae* (ATCC 700603) and *Staphylococcus aureus* (ATCC 43300) by micro broth dilution method in 96 well micro titre plates using Tryptic Soy (TS) broth [32]. Three day old single colonies of these organisms from the TS agar plates were inoculated into TS broth and sub-cultured at 37°C with shaking at 160 rpm for 24 h. 0.5 McFarland standards of each organism were prepared by adjusting the optical density of overnight cultures at 600 nm. The percentage inhibition of growth of the bacteria by the test samples was determined by monitoring the growth of bacteria in an automated microplate reader (Synergy HT, BioTek Instruments) at 600 nm [32, 33]. Serial two-fold dilutions (100 µl) of CDAgNPs, CMP and CMP coated CDAgNPs solutions were prepared in sterile 96 well plates using stock solutions of CDAgNPs (5 mg/10 ml), CMP (5 mg/10 ml) and CMP coated CDAgNPs solutions (5 mg of CDAgNPs + 5 mg of CMP in 10 ml). The wells were then inoculated with 100 µl of diluted broth culture (initially adjusted to 0.5 McFarland turbidity standards) and incubated at 37°C for 24 h. Control wells were prepared by adding 100 µl of sterile distilled water and 100 µl of bacterial suspension. All the experiments were carried out in triplicates. The percentage inhibition growth was calculated using the following equation [32].

$$I = \frac{(C_{24}-C_0)-(T_{24}-T_0)}{(C_{24}-C_0)}$$

Where, *I* is the percentage inhibition of growth, C_{24} and C_0 are the optical density at 600 nm of the control wells of the organism at 24 h and 0 h respectively, T_{24} and T_0 are the optical density at 600 nm of the sample wells at 24 h and 0 h respectively.

5.4.7 Statistical analysis

Statistical analysis was conducted using IBM SPSS statistics 22 software. The data sets were analysed by one-way ANOVA and the Tukey's post-hoc test. A *p*-value of <0.05 was considered statistically significant.

5.5 Results and discussion

5.5.1 Prediction of the binding mode of chloramphenicol inside cyclodextrins

The results of molecular docking were ranked based on docking scores and root mean square deviation (RMSD) (Table 1). The top ranked pose of CMP with its corresponding cyclodextrin was chosen as the best inclusion complex for further molecular dynamics analysis. The inclusion complex of CMP with γ-CD was found to be the strongest with a docking score of -5.3, when compared to α-CD and β-CD, which had scores of -4.7 and -5.2 respectively. Top three ranked docking scores of CMP varies from (-5.3 to -5.2) for γ-CD, (-5.2 to -5.2) for β-CD and (-4.7 to -4.6). The maximum docking score of (-5.3) and lowest RMSD values were obtained for the complex of CMP with γ-CD (**Table 5.1**). These results suggested the favourable formation of CMP inclusion complexes with γ-CD. This could be due to larger cavity volume of γ-CD to accommodate CMP inside the cavity. The lower cavity volume of α-CD did not help to sandwich the CMP inside the cavity leading to lower docking scores. In the binding pose of CMP -γ CD, chlorine atoms and aromatic nitro group of CMP were respectively oriented toward the primary and secondary hydroxyl rim of cyclodextrins. A similar binding mode was also obtained in the CMP - β-CD inclusion complex. The CPM formed three hydrogen bonds with γ-CD (2º OH, NH and nitro group of CPM) and one hydrogen bond with β-CD (NH of CPM) as well as α-CD (2º OH). In the inclusion complex of CPM-α-CD, the aromatic nitro group of CPM penetrated the cavity whereas the rest of the molecule remained out of the cavity (**Fig. 5.1a**). However, the entire molecule penetrated the cavity in β-CD (**Fig. 5.1b**) and in γ-CD (**Fig. 5.1c**). The formation of three hydrogen bonds in CPM- γ-CD suggests a strong stability as well as tight interaction of CPM with γ-CD and the favourable formation of inclusion complexes. 2º OH and NH group of CPM served as hydrogen bond donors whereas the nitro group of CPM served as a hydrogen bond acceptor.

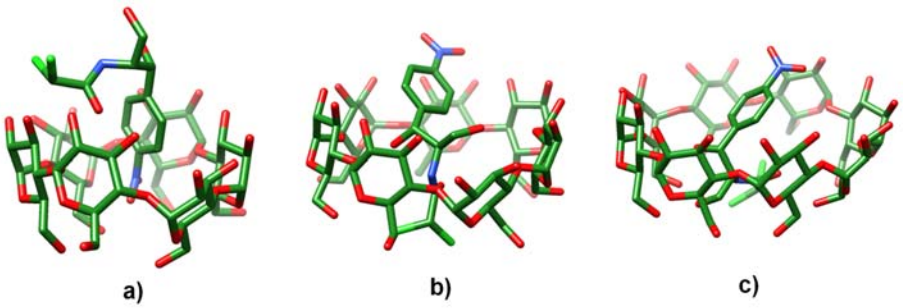

Figure 5.1 The binding mode of CMP inside the cavity of **a)** α-cyclodextrin **b)** β-cyclodextrin and **c)** γ-cyclodextrin.

Table 5.1 Docking scores of chloramphenicol with three different cyclodextrins.

Cyclodextrin	Ligand	Docking Scores			RMSD		
		1st Rank	2nd Rank	3rd Rank	1st Rank	2nd Rank	3rd Rank
α-CD	CMP	-4.7	-4.6	-4.6	0	3.6	1.3
β-CD	CMP	-5.2	-5.2	-5.2	0	3.8	3.9
γ-CD	CMP	-5.3	-5.3	-5.2	0	0.6	2.9

5.5.2 Host-guest interactions of chloramphenicol and cyclodextrins

Molecular dynamic simulation was performed to refine the stable conformation of the inclusion complex of chloramphenicol with cyclodextrins, and was followed to compute the binding free energies of the inclusion complexes. Further, this study helped to understand the guest-host interactions in the form of binding free energies. The estimated binding free energies were found to be -12.6103 kcal/mol, -24.0756 kcal/mol and -29.7697 kcal/mol for the inclusion complex of CMP-αCD, CMP-βCD, and CMP-γ CD respectively (Table 5.2). The results of MD suggested the favourable formation of inclusion complexes of CMP from γ-CD **(Fig. 5.2)**. The higher binding energy of the CMP-γ CD inclusion complex is attributed to larger cavity volume of γ-CD. The van der Waals interaction energy was found to be a crucial factor in determining the binding affinity as well as the formation CMP-γCD inclusion complexes.

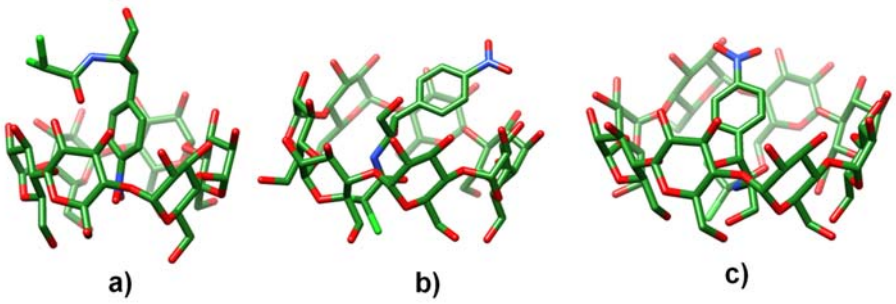

Figure 5.2 The minimum energy conformation of chloramphenicol with **a)** α-cyclodextrin **b)** β-cyclodextrin and **c)** γ-cyclodextrin obtained from molecular dynamic simulations.

Table 5.2 The computed binding free energies of the inclusion complexes.

Inclusion complexes	ΔG_{bind}	ΔG_{gas}	ΔG_{sol}
CMP/α-CD	-12.6103±11.3191	-16.1487±14.4924	3.5383±3.3728
CMP/β-CD	-24.0756±02.0881	-26.4006±02.3139	2.3250±0.8135
CMP/γ-CD	-29.7697±03.3833	-29.3537±03.6753	-0.4160±0.5021

5.5.3 X-ray powder diffractometry

The X-ray diffraction pattern of synthesized inclusion complexes were compared with pure CMP, γ-CD and their physical mixture**.** Inclusion complex formation is accompanied by changes in the crystalline properties of the guest and host molecules involved, which can be studied by observing disappearance, decreased intensity, broadening and appearance of new peaks in the diffractogram [34]. As shown in **Fig. 5.3**, the diffractogram of γ-CD has several sharp peaks at 2θ = 12, 16.5, 19 and 22 **(Fig. 5.3b)** whereas CMP has sharp peaks at 2θ = 13, 16, 18, 19.5, 21, 24.5 (**Fig. 5.3a)**, indicating that both the host and guest are crystalline in nature. The diffractogram of the physical mixture (**Fig. 5.3c)** of CMP and γ-CD was found to be different from that of native CMP and γ-CD. However, the presence of sharp peaks indicates only a partial inclusion, and thus it can be concluded that simple mixing did not result in the formation of complete inclusion complexes. Inclusion complexes produced a completely different diffractogram (**Fig. 5.3d)** to that of CMP and γ-CD, and contained broad peaks confirming the change in crystalline properties of guest CMP and host γ-CD. These significant changes in 2θ values and appearance of new crystalline phase confirms the encapsulation of guest CMP by host γ-CD [35, 36].

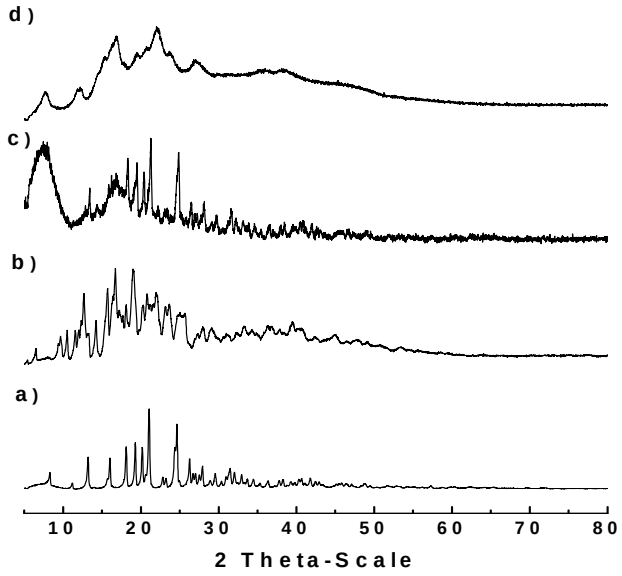

Figure 5.3 Diffractograms of **a)** CMP **b)** γ-CD **c)** Physical mixture and **d)** Inclusion complex (CMP/γ-CD).

5.5.4 FTIR-ATR spectroscopy measurements

FTIR spectra of CMP, γ-CD, physical mixtures and inclusion complexes are presented in **Fig. 5.4.** The major changes observed in FTIR is that the band at 3270 cm^{-1} corresponding to hydroxyl groups of γ-CD was broadened in the inclusion complex compared to free cyclodextrin. CMP was characterized by the presence of broad bands at 3257 cm^{-1}, 3079 cm^{-1}, 2961 cm^{-1}, and 2903 cm^{-1} for the primary and secondary OH groups and NH group. The peak at 1682 cm^{-1} is due to the carbonyl frequency. The peaks at 1516 cm^{-1} and 1343 cm^{-1} indicates the presence of nitro groups. The position of these bands is slightly shifted to a higher frequency of 1520 cm^{-1} and 1346 cm^{-1} in the inclusion complex. These changes in the FTIR spectroscopy suggests the existence of van der Waals interaction between CMP and γ-CD [37].

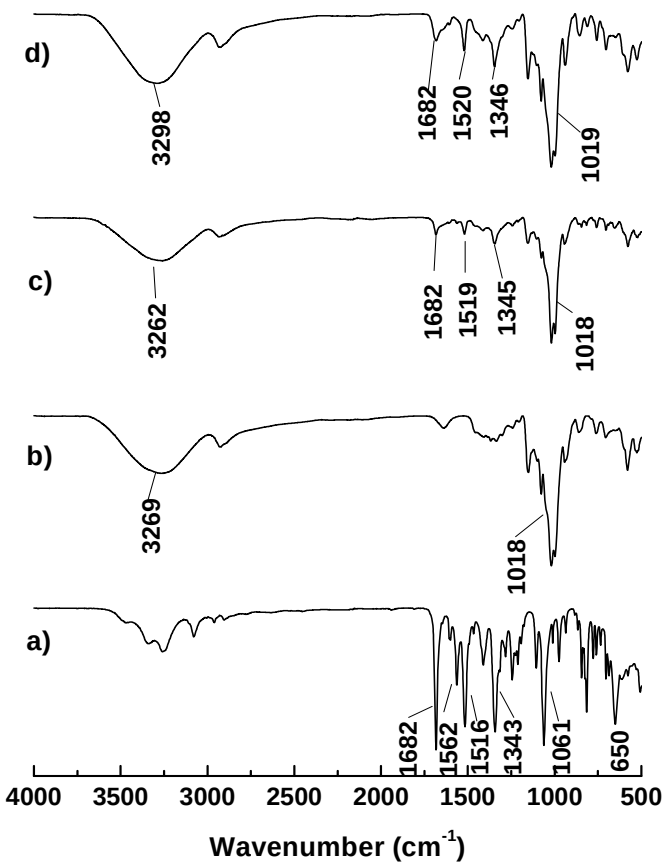

Figure 5.4 FTIR spectra of **a)** CMP **b)** γ-CD **c)** Physical mixture and **d)** Inclusion complex.

5.5.5 Scanning electron microscopy

The surface morphology of CMP appeared as irregularly shaped structures **(Fig. 5.5a)**, whereas pure γ-CD appeared as parallelogram shapes **(Fig.5.5b).** The physical mixture appeared as a mixture of both of the components described above **(Fig. 5.5c)**. However, inclusion complexes were seen as a single component with regular rectangular or cuboidal shapes unlike the physical mixture where individual components (CMP and γ-CD) could be identified. **(Fig. 5.5d)**. These drastic changes resulting in the single solid morphology confirms interaction between CMP and γ-CD, which is a consequence of inclusion complex formation [38].

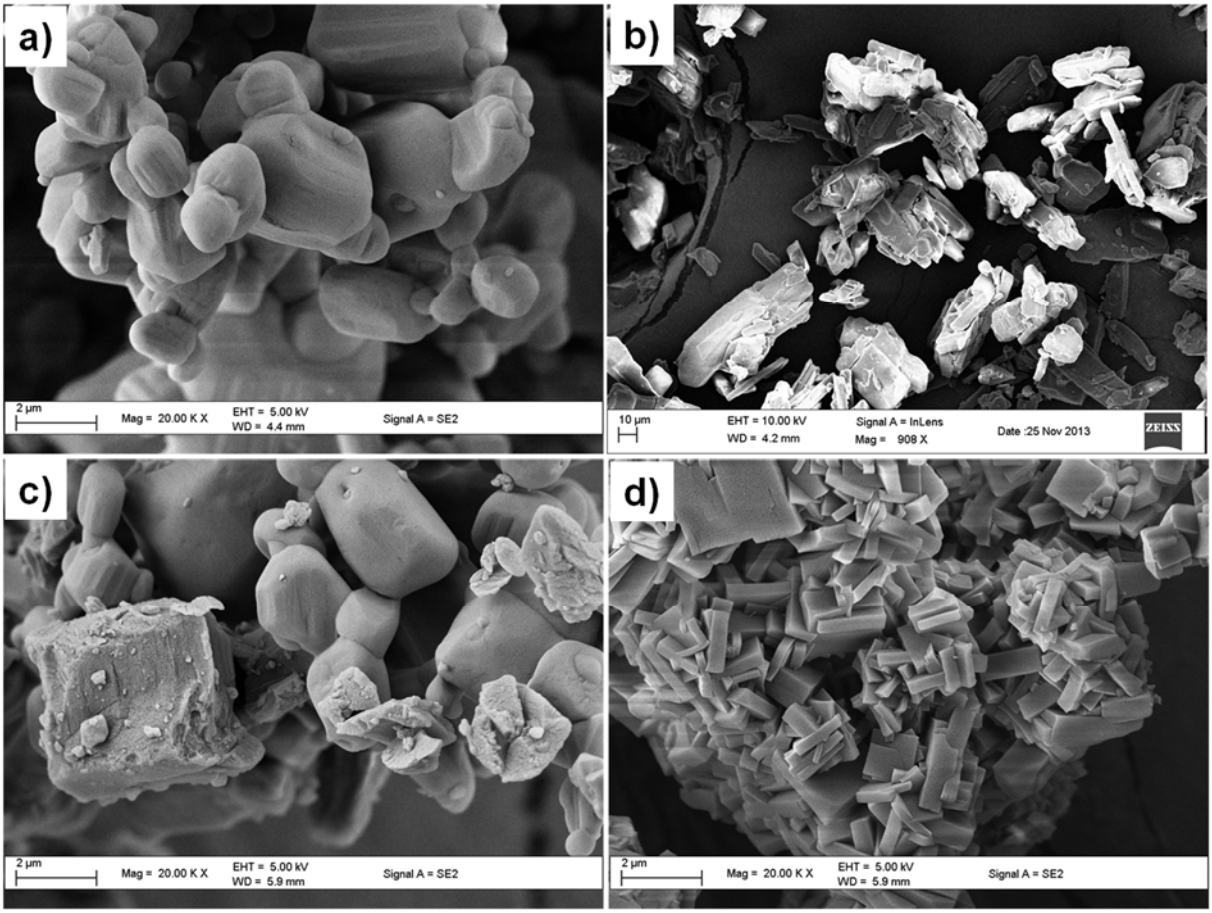

Figure 5.5 The morphological appearance of **a)** CMP **b)** γ-CD **c)** Physical mixture and **d)** Inclusion complex.

5.5.6 Thermogravimetric and differential scanning calorimetric analyses

Thermal degradation studies were conducted on CMP, γ-CD, and their physical mixture and inclusion complexes under nitrogen atmosphere. The percentage of weight loss as a function of temperature is plotted in **Fig. 5.6** in the temperature range of 25°C to 800°C. The CMP started to decompose at approximately 200°C and the maximum weight loss appeared at 280°C **(Fig. 5.6a)**. Two weight loss events were observed for host γ-CD **(Fig. 5.6b)**. The dehydration of cyclodextrin appeared first between 25°C and 125°C, followed by maximum weight loss at 325°C, due to decomposition of cyclodextrin macrocycles. Inclusion complexes underwent weight loss in three different stages **(Fig. 5.6d)**. The first weight loss was at 59°C which could be due to dehydration. The second weight loss begun at approximately 225°C with maximum weight loss at 255°C, whilst the third weight loss appeared at 290°C. The second weight loss could be due to the decomposition of cyclodextrin macrocycles indicating that cyclodextrin decomposes first, followed by decomposition of the encapsulated CMP at 290°C. In addition,

decomposition of free CMP started at 200°C and free cyclodextrin at 298°C, but for the inclusion complex the decomposition started at 225°C indicating that thermal stability increased for the guest CMP and decreased for the host cyclodextrin when they form inclusion complexes [39]. Furthermore, the DSC curve of CMP showed a sharp endothermic peak at 152°C with no weight loss, suggesting crystalline CMP melted at this temperature. This peak did not appear in the DSC thermogram of inclusion complexes, indicating that chloramphenicol is encapsulated by cyclodextrin which results in loss of its crystalline nature [40]. Thus DSC analysis further confirms the formation of inclusion complexes. The DSC curve of the physical mixture also contained the endothermic peak at 152°C **(Fig. 5.6c)** indicating that simple mixing did not result in the formation of inclusion complexes.

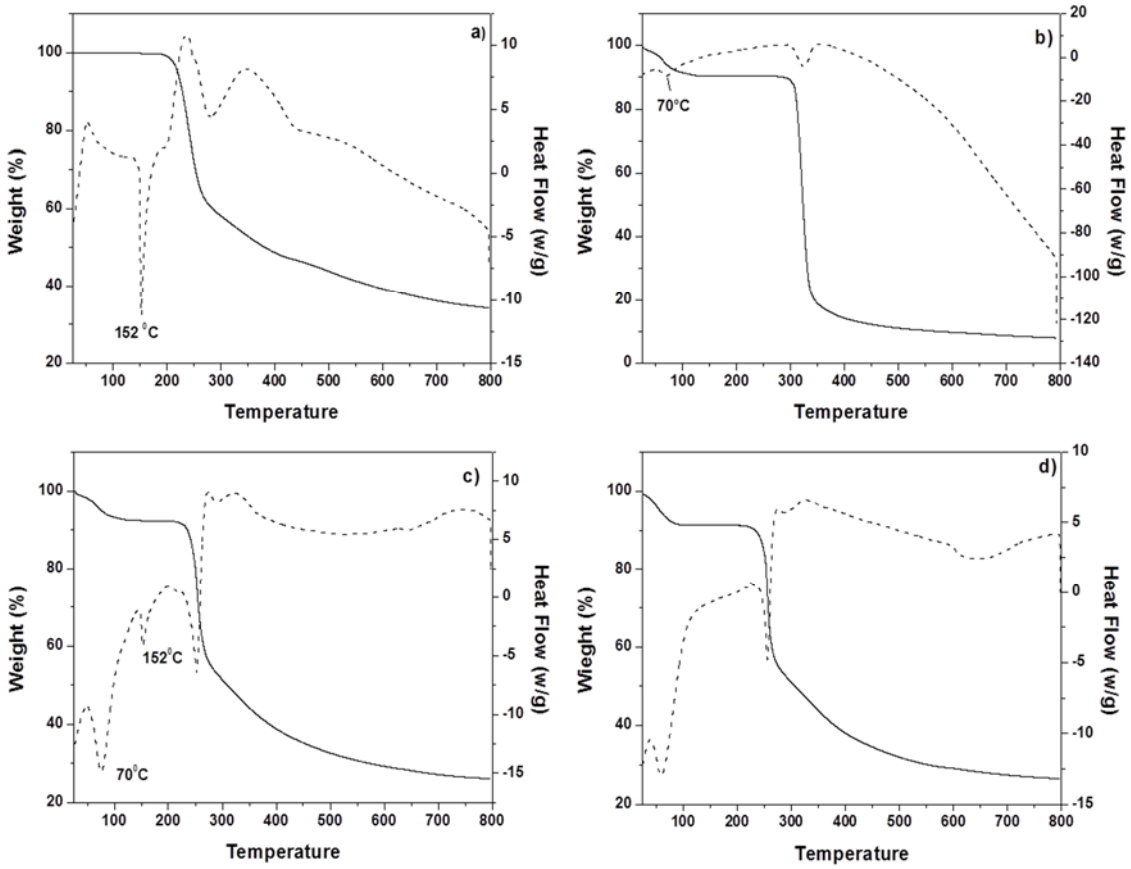

Figure 5.6 TGA (solid line) and DSC (dashed line) curves of **a)** CMP **b)** γ-CD **c)** Physical mixture and **d)** Inclusion complex.

5.5.7 NMR analysis

The formation of inclusion complexes was studied by ^{1}H NMR. **Fig. 5.7** shows the ^{1}H NMR spectra of CMP, CD and their inclusion complex. The values of chemical shift for different protons are listed in **Tables 5.3 and 5.4**. Since the chemical shift values of CMP and γ-CD were merging in the ^{1}H NMR spectrum of inclusion complex, the exact δ values were determined by correlating protons with corresponding carbons in HSQC spectrum **(Fig. 5.8a)**. It was found that the H3 and H5 protons of γ-CD are shifted the most, confirming the presence of guest CMP in the cavity of γ-CD [41]. The lipophilic microenvironment in the cyclodextrin cavity will be highly affected when non polar guests form inclusion complexes and hence protons lying inside the cyclodextrin cavity H3 and H5 will be the most shifted in ^{1}H NMR spectra [41]. Furthermore, all the protons of cyclodextrin shifted up-field, whilst the protons of CMP behaved differently. The protons named H1' and H6' shifted up-field, while all other protons of CMP shifted downfield. These changes in the shifts can be considered as direct evidence for the existence of noncovalent interaction between host γ-CD and guest CMP [42].

Table 5.3 ^{1}H NMR chemical shifts corresponding to γ-CD in the presence and absence of CMP

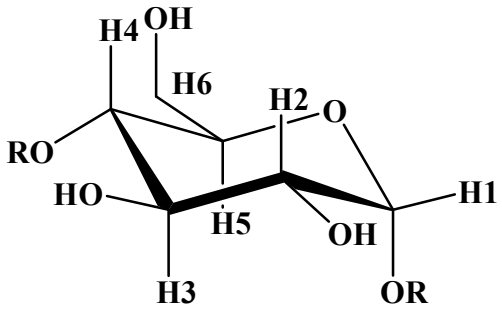

γ-CD proton	$\delta_{(free)}$	$\delta_{(complex)}$	$\Delta\delta = \delta_{(free)} - \delta_{(complex)}$
H1	5.0544	5.0388	0.0156
H2	3.5994	3.5918	0.0076
H3	3.8779	3.8481	0.0298
H4	3.5335	3.5223	0.0112
H5	3.7975	3.7610	0.0365
H6	3.8140	3.7987	0.0153

Table 5.4 ^{1}H NMR chemical shifts corresponding to CMP in the presence and absence of γ-CD

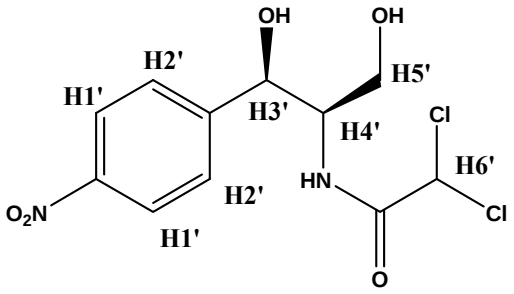

AP proton	$\delta_{(Complex)}$	$\delta_{(free)}$	$\Delta\delta = \delta_{(Complex)} - \delta_{(free)}$
H1'	8.1551 d	8.17895 d	-0.02385
H2'	7.58090 d	7.57070 d	0.01020
H3'	5.15315 d	5.13330 d	0.01985
H4'	4.17870 m	4.16540 m	0.01330
H5'	3.84100 m	3.82335 q	0.01765
	3.67210 q	3.65455 q	0.01755
H6'	6.14130 s	6.17540 s	-0.03410

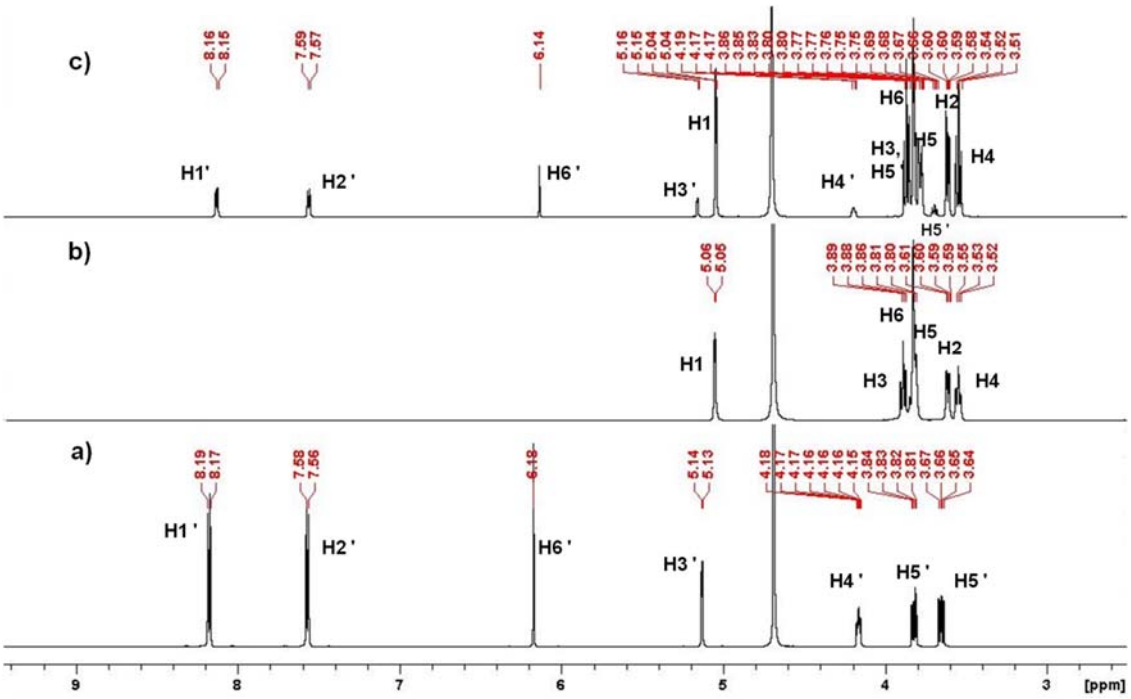

Figure 5.7 ^{1}H NMR spectra of **a)** CMP, **b)** γ-CD and **c)** Inclusion complex of CMP with γ-CD.

To obtain more details about the inclusion structure, a 2D NOESY experiment was conducted on the inclusion complex. In the rigid structure of cyclodextrin, H2 and H4 protons arranged

outside of the cavity of cyclodextrin [43]. The H4 proton lies towards the narrow end of the cavity or the primary face of cyclodextrin and the H2 proton lies towards the large cavity side or secondary face of cyclodextrin [43]. H3 and H5 protons are expected to fall inside the cavity [43]. In the 2D spectra, there was no NOESY correlation between H1' and H2' aromatic protons of CMP and H3 and H5 protons of cyclodextrin. However, there was a weak NOESY correlation between the H1' of CMP and H2 proton of cyclodextrin **(Fig. 5.8b)**.

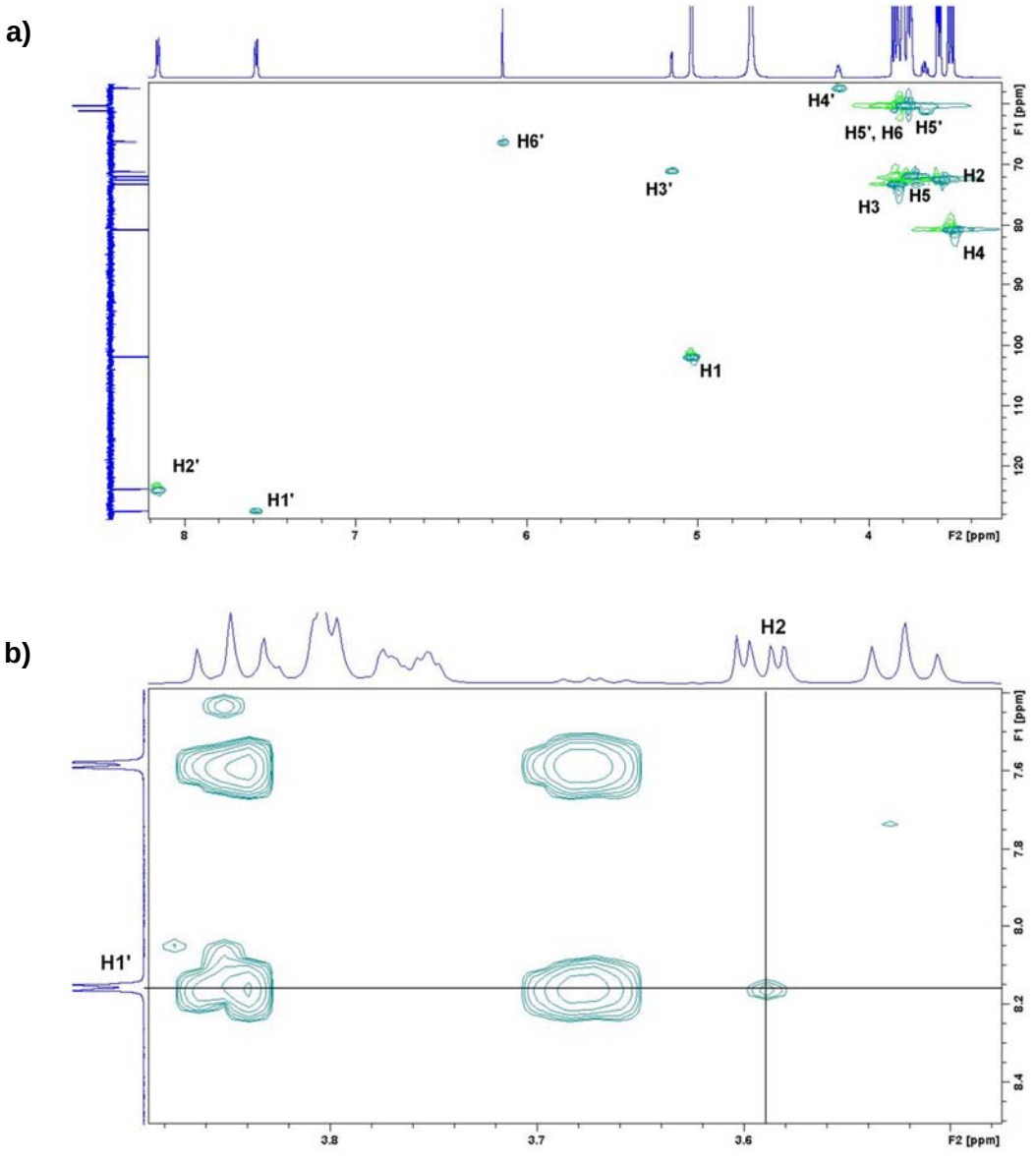

Figure 5.8 **A)** HSQC spectrum of inclusion complexes **B)** Expanded region of 2D NOESY spectrum showing ^{1}H-^{1}H NOE interaction between aromatic protons of CMP and γ-CD.

At the same time, there was no NOESY interaction with the H4 proton of cyclodextrin which is also outside the cavity. These observations collectively suggest that the benzene ring of CMP is close to the outer secondary face of the cavity whilst the aliphatic part of CMP lies inside the cavity of γ-CD. Molecular models generated in computational studies predicted a similar mode of inclusion.

5.5.8 Characterization of nanoparticles

The reaction mixture for the synthesis of nanoparticles turned yellowish brown after 24 h incubation. The formation of nanoparticles was confirmed by observing surface plasmon resonance at 412 nm in the UV visible spectroscopy studies **(Fig. 5.9a)**. The organic capping on the surface of nanoparticles was confirmed by IR studies. The steric repulsion between the capped molecules contributes to the stability of nanoparticles. The major IR bands at 3000, 1631, 1514, and 1055 cm^{-1} **(Fig. 5.9b)** were observed. The broad nature of the IR peak at 3000 cm^{-1} for CDAgNPs referred to the strong stretching vibrations of -OH functional groups of cyclodextrin. The bands at 1160 cm^{-1} and 1055 cm^{-1} can be assigned to the ether linkages or –C-O- functional group. The band around 1638 cm^{-1} for CDAgNPs can be assigned to $-COO^-$ stretching vibrations of the carbonyl functional group, which could be due to the oxidation of the primary hydroxyl groups to carboxylic acid during the synthesis of nanoparticles. SEM analysis displayed the particles or cluster-like structures with a size less than 200 nm **(Fig. 5.9c**), and the EDX analysis confirmed that the particles were composed of elemental silver **(Fig. 5.9d)**. The peaks of carbon and oxygen in the EDX pattern could be due to the presence of cyclodextrin capping on the surface of the nanoparticle. The other elemental peaks of gold and aluminium are due to the gold coated aluminium grid used for the analysis. TEM analysis showed that CDAgNPs were predominantly spherical or polyhedral in shape (**Fig. 5.9e**), and majority of the CDAgNPs were 20-30 nm in size (mean±SD = 23.99±4.36, n=200). The clear lattice fringes in the selected area diffraction pattern confirms the presence of polycrystalline CDAgNPs in the sample (**Fig. 5.9e inset)** [44]. The dynamic light scattering experiments provided more information about the size and stability of the nanoparticles. The electric charge on the surface of the nanoparticles measured in terms of Zeta potential was found to be −30.1 mV and the average hydrodynamic size was 54.87 nm **(Fig. 5.10a and 5.10c)**. When coated with CMP, the Zeta potential of CDAgNPs was slightly decreased to -27.6 mV and the average hydrodynamic size was 55.70 nm (**Fig. 5.10b and 5.10d**). Thus it confirms that the size and

stability of the nanoparticles was not altered to a significant extent after the coating with CMP. The lower PDI values suggests good mono-dispersity and high surface negative Zeta potential indicates good stability of the nanoparticle both in the presence and absence of CMP [45]. The concentration of the silver in the 10 ml stock solution of CDAgNPs prepared after purification was determined by ICP-OES analysis and found to be 11.71 mg/10 ml.

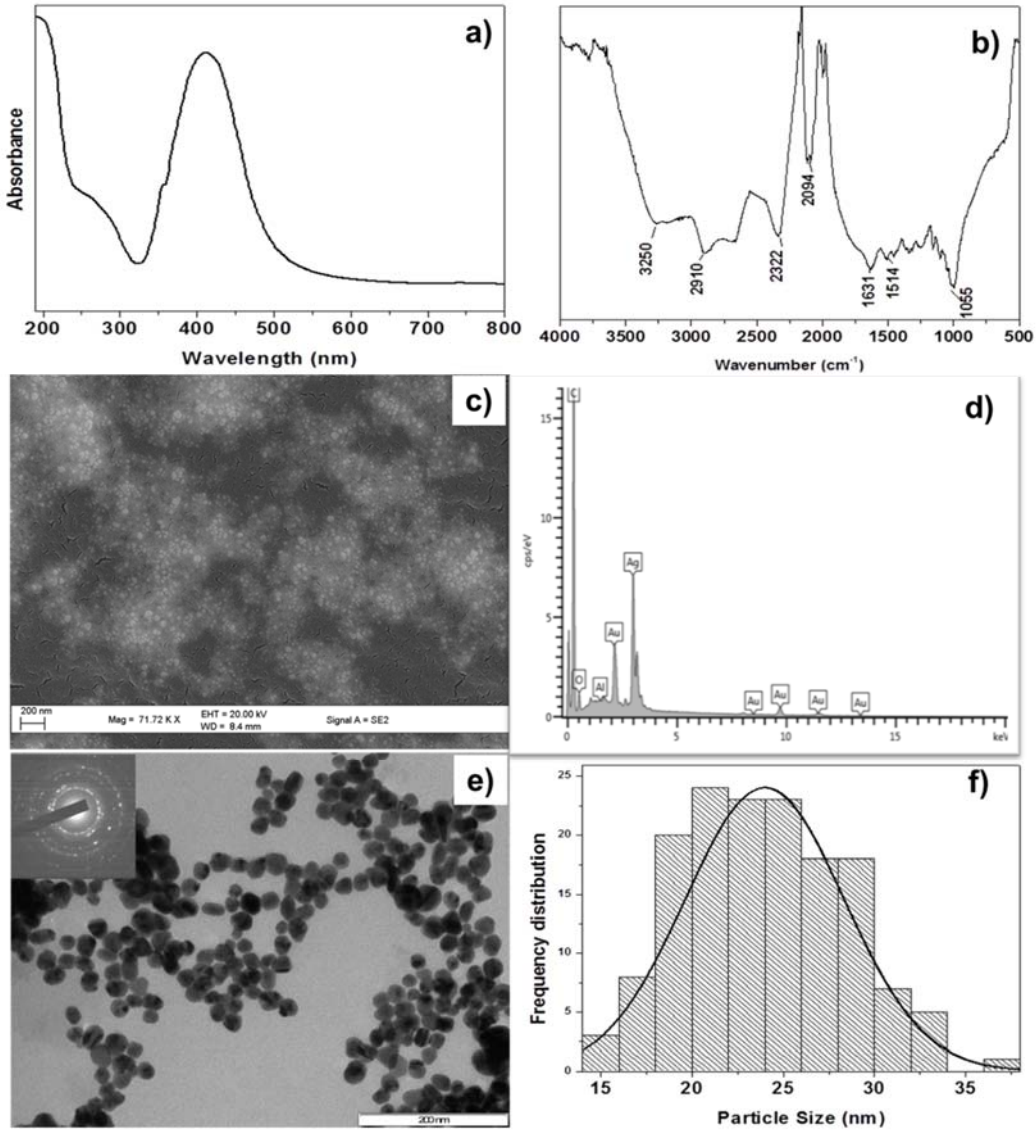

Figure 5.9 **a)** UV–Vis spectra, **b)** FTIR ATR spectra, **c)** SEM morphology analysis, **d)** EDX pattern, **e)** HRTEM micrograph (inset SAED pattern), **f)** Histogram.

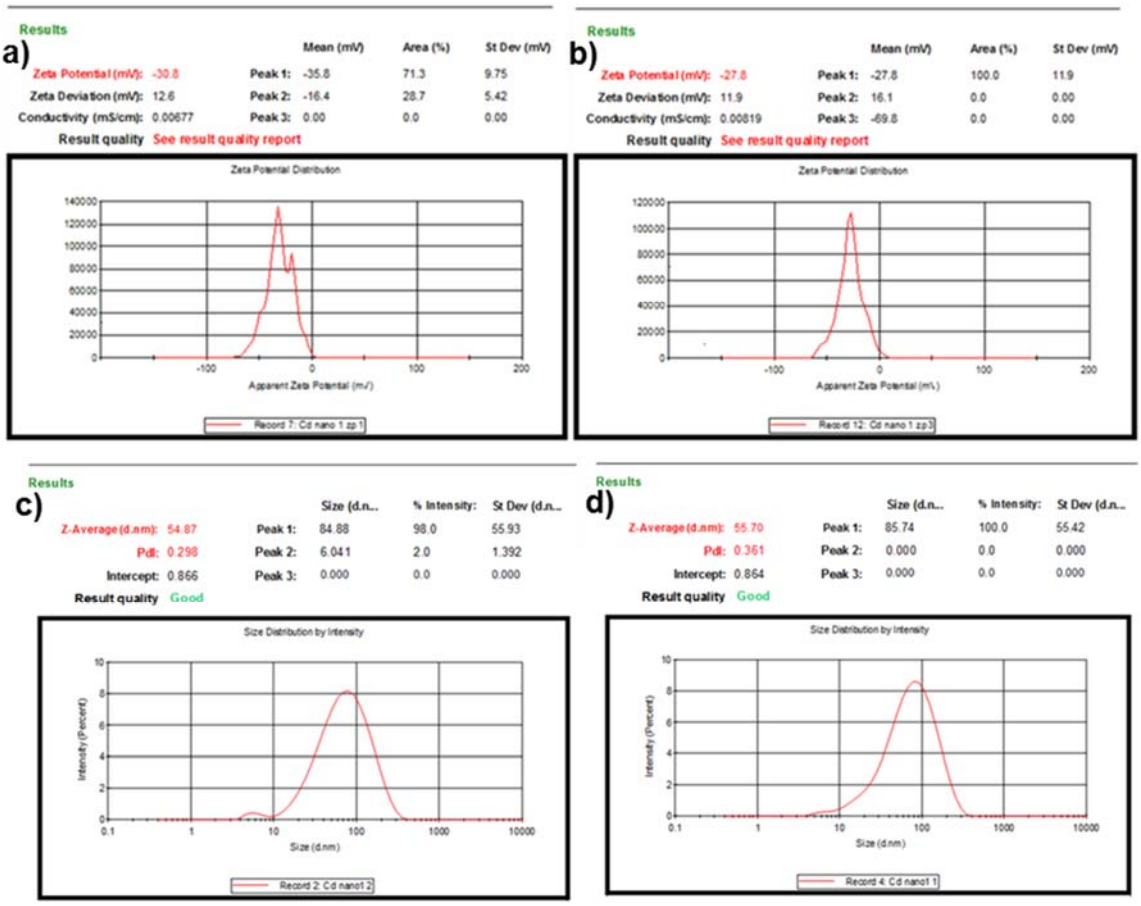

Figure 5.10 Zeta potential of **a)** AgNPs, **b)** CMP coated AgNPs and Zeta size of **c)** AgNPs, **d)** CMP coated AgNPs.

5.5.9 Raman spectroscopy studies

Surface enhanced Raman spectroscopy (SERS) is a powerful analytical method and was used to investigate CMP coating on the surface of cyclodextrin capped CDAgNPs in aqueous media [46]. Cyclodextrin can act as both a reducing and stabilizing agent, and can self-assemble on the surface of silver nanoparticles. Furthermore, the lipophilic cavity of cyclodextrin molecules provides a microenvironment into which appropriately sized non-polar drug moieties can enter to form drug-loaded nanoparticles. Thus, the functionalization of silver nanoparticles with appropriate cyclodextrins will introduce the molecular recognition properties to a metal surface and increase the ability of nanoparticles to absorb high concentrations of organic compounds [47]. The adsorption and sensing of CMP on colloidal γ-CD capped CDAgNPs was studied using SERS**.** Compared with the normal Raman spectrum of CMP in aqueous solution, a noticeable enhancement in the intensity and frequency shifts was observed in SERS of CMP

indicating that CMP is encapsulated into the cyclodextrin cavity on the surface of the nanoparticle. This encapsulation confirms the close contact of CMP to the metal surface because when the molecules are close to the metal surfaces, Raman signals appear at a higher magnitude. This could be due to the enhancement of polarizability of the molecule by chemical or electromagnetic interaction with the metal surface [48]. These interactions enhance the electric field of the laser beam, leading to an increase in resonance enhancement of molecules.

The Raman spectra of CMP solid and CMP solution state in the presence and absence of nanoparticles are also presented (**Fig. 5.11)**. Sample preparation for SERS was done according to a previous report [49]. Briefly, 1 ml of 3 mM CMP solution was mixed with 1 ml of γ-CD capped silver nanoparticles. All of the reported spectra represent an average of three scans with 20 s integration time at medium laser power. An assignment of SERS bands was performed by the comparison of the Raman spectra of both compounds in the solid state and in solutions.

In the Raman spectra of cyclodextrin capped CDAgNPs, the dominant peak was observed at 1414 cm^{-1} and can be assigned to symmetric stretching vibration of the carboxylate functional group [50]. The presence of this peak supports the concept that primary hydroxyl groups of cyclodextrin were oxidized to carboxylic acid while silver ions were reduced to silver metals [30]. Further, the strong intensity of this peak suggests that carboxylate ion binds to silver metal, acts as an anchor, and holds cyclodextrin on the surface of the nanoparticle [50]. The peaks at 949 cm^{-1} and 806 cm^{-1} could be due to the ring breathing vibrations of glucose rings [51].

The Raman spectra of solid chloramphenicol contained peaks for carbonyl stretching (1692 cm^{-1}), aromatic ring stretching (1609 cm^{-1}), -NO_2 symmetric stretching (1361 cm^{-1}), CH_2 twisting (1251 cm^{-1}), NH in plane bending (1114 cm^{-1}), C-H out of plane bending (983 cm^{-1}), C-C stretching (940 cm^{-1}), -NO_2 scissoring (854 cm^{-1}), ring breathing (767 cm^{-1}), and C-Cl symmetric stretching (632 cm^{-1}) [49, 52, 53]. An aqueous solution of CMP at a concentration of 1.5 mM did not show any of these Raman peaks. However, in the presence of cyclodextrin capped CDAgNPs, the intensity of some of the peaks of CMP was significantly enhanced and were shifted to lower frequency as compared to pure CMP. The intensity of C=C stretching frequency of the benzene ring was most enhanced and appeared at the lower frequency region of 1605 cm^{-1} (SERS experiment) as compared to 1609 cm^{-1} of pure CMP (Raman

spectroscopy). The peaks at 1361, 1297 and 1251 cm^{-1} were also enhanced and shifted to lower frequency at 1350, 1288 and 1244 cm^{-1}, respectively. However the carbonyl frequency of CMP did not show up in the SERS spectra. Certain peaks which are strong in conventional Raman spectra analysis may not appear in SERS. This could be attributed to the orientation or mode of adsorption of respective functional groups on the surface of nanoparticles [53, 54]. Similarly for CDAgNPs, the peak observed at 1414 cm^{-1} can be assigned to -COO^- stretching of cyclodextrin and this peak shifted slightly to a lower frequency of 1410 cm^{-1}. These major changes in the Raman signals confirms that cyclodextrins adsorbed on the surface of CDAgNPs acted as a molecular host and expressed their inclusion formation characteristics with CMP on the surface of nanoparticles [54]. In a previous study, based on surface plasmon resonance, calixarene capped CDAgNPs were found to be ineffective for molecular recognition of CMP [55]. Our studies prove thus that cyclodextrins can be more suitable supra-molecules for CMP inclusion when compared to caliaxrene.

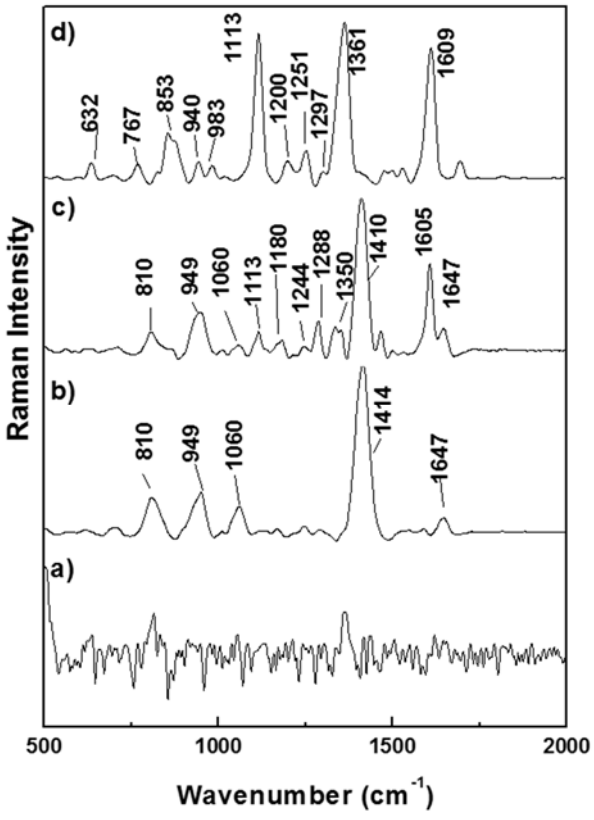

Figure 5.11 Raman Spectrum of **a)** 1.5 mM CMP solution and **b)** AgNPs. **c)** SERS spectrum of CMP, **d)** Raman spectrum of solid CMP.

5.5.10 Antibacterial Results

The antibacterial activity of CDAgNPs, CMP and CMP functionalized CDAgNPs were determined by measuring the percentage inhibition of bacterial growth using the quantitative micro-titre well dilution method (**Table 5.5)**. Chloramphenicol was found to be active at high concentrations against all the bacteria tested. The activity of CMP was found to gradually increase with an increase in concentration, with more than 90% inhibition being observed at a concentration of 150 μg/ml. CDAgNPs were found to be relatively less active when compared to the CMP. *P. aerugonisa* was the most sensitive to the CDAgNPs, with the highest concentration of nanoparticles resulting in 70% inhibition, whereas only 30-40% inhibition was observed for the other bacterial species. No significant activity was observed for the CMP/CDAgNPs below the concentration of 25 μg/ml. However, when CMP was coated on CDAgNPs, the antibacterial activity of CMP was significantly enhanced. The enhanced antibacterial activity by synergistic effect of CDAgNPs and CMP were clearly observed at lower concentrations. CMP alone exhibited 78% inhibition against *P. aeruginosa* at a concentration of 62.5 μg/ml and in the presence of CDAgNPs at the same concentration, CMP completely inhibited ($p < 0.05$) growth of *P. aerugonisa*. Similarly, CMP presented 76%, 64% and 74.27% activity against *E. faecalis*, *K. pneumoniae*, and *S. aureus* respectively at a concentration of 125 μg/ml. In the presence of CDAgNPs at the same concentration, more than 90% inhibition ($p < 0.05$) was observed. Similar trends were observed at other lower concentrations. The enhanced antibacterial effects can be explained by two mechanisms. The CMP can cease the growth of bacteria by affecting the protein synthesis, while silver ions exert their bactericidal properties by targeting multiple sites [10, 56]. Thus two different mechanisms can cause synergistic activity resulting in the enhanced antibacterial activity. Moreover, the inclusion formation ability of cyclodextrins could immobilize the CMP molecules on the surface of metal nanoparticles and thus resulting in localized high doses of drug concentration. When bacteria are exposed to such localized concentrations of drugs, higher level of interaction between the drug and the bacterial cell surface can occur resulting in higher antibacterial activity [5]. This phenomenon of localization also makes the nanoparticles an effective drug delivery system. Although CMP is classified as a broad spectrum antibiotic, its usage is limited by neurotoxicity and bone marrow toxicity in chemotherapy [57]. The antibacterial effects of silver combined with molecular recognition properties can be exploited to generate a combination therapy in which CMP can be used at lower doses and thus its side effects can be minimized.

Table 5.5 Percentage inhibition of different bacterial species in the presence of CDAgNPs, CMP and CMP coated CDAgNPs at different concentrations

Microorganism	Sample	Concentrations (µg/ml)*					
		250	125	62.5	31.25	15.625	7.81
Pseudomonas aeruginosa	CDAgNPs	70.87±2.09^{c}	49.72±2.67^{d}	31.55±0.36^{f}	20.52±1.50^{h}	13.72±0.82^{i}	ND
	CMP	101.8±0.83 ^{a}	101.7±0.59^{a}	77.96±2.40^{b}	41.67±1.43^{e}	23.45±1.95^{gh}	12.84±1.40^{i}
	CDAgNPs / CMP	104.1±2.09^{a}	100.0±0.94^{a}	99.95±0.43^{a}	68.23±0.69^{c}	40.99±2.03^{e}	24.67±0.31^{g}
Enterococcus faecalis	CDAgNPs	45.89±2.47^{e}	29.19±2.59^{f}	9.09±1.19^{h}	ND	ND	ND
	CMP	98.14±1.51^{b}	76.47±3.03^{d}	11.52±0.71^{g}	6.7±0.34^{gh}	ND	ND
	CDAgNPs / CMP	99.98±2.00^{a}	93.33±3.29^{c}	40.25±3.34^{e}	26.52±1.02^{fg}	9.80±1.04^{gh}	ND
Klebsiella pneumoniae	CDAgNPs	40.58±0.59^{d}	16.93±1.12^{e}	5.28±0.89^{f}	ND	ND	ND
	CMP	98.63±0.14^{b}	64.17±3.60^{c}	4.09±0.63^{f}	ND	ND	ND
	CDAgNPs / CMP	101.0±2.18^{a}	98.39±4.11^{b}	43.66±1.36^{d}	19.88±0.85^{e}	ND	ND
Staphylococcus aureus	CDAgNPs	34.54± 2.55^{d}	17.86±2.37^{e}	13.12±0.89^{f}	ND	ND	ND
	CMP	97.26±3.28^{a}	74.27±1.68^{b}	5.78±1.43^{g}	ND	ND	ND
	CDAgNPs / CMP	107.0±4.55^{a}	102.0±2.16^{a}	44.18±2.19^{c}	12.75±1.22^{f}	ND	ND

ND, No growth inhibition detected

*All values are expressed as mean ± standard deviation of experiments performed in triplicate. Different superscript letters presented in each column are significantly different from each other ($p < 0.05$; one-way ANOVA, Tukey's post-hoc test)

5.6 Conclusions

In this study, three different cyclodextrin supramolecules have been studied for their complexing ability with chloramphenicol using molecular modelling techniques. The computed binding free energies indicated the strong interaction between γ-cyclodextrin and chloramphenicol. To further confirm the results observed in theoretical calculation, the inclusion complex of chloramphenicol with γ-cyclodextrin was synthesized and thoroughly characterized. The results of computational studies were found to be well correlated with the experimental results to explain the favourable formation of inclusion complex. Thereafter γ-

cyclodextrin capped silver nanoparticles were prepared, characterized and confirmed for their ability to molecular recognition of chloramphenicol using surface enhanced Raman spectroscopy studies. Also the chloramphenicol γ-cyclodextrin capped silver nanoparticles composite was prepared and evaluated for their synergistic antibacterial effects. The enhancement in the antibacterial activity of chloramphenicol was observed when applied together with cyclodextrin capped silver nanoparticles. Thus it was concluded that cyclodextrin capped silver nanoparticles are the attractive supramolecular hosts and can complex a wide variety of organic drug molecules on the surface of silver nanoparticles. This property of complexing ability of cyclodextrin capped silver nanoparticles can be exploited to generate biosensors, drug delivery systems or new and effective pharmaceutical formulations for combination therapy.

5.7 Acknowledgement

This research work was funded by National Research Foundation (NRF) of South Africa and the University of KwaZulu-Natal, South Africa.

5.8 References

[1] P. Csermely, T. Korcsmáros, H.J. Kiss, G. London, R. Nussinov, Structure and dynamics of molecular networks: a novel paradigm of drug discovery: a comprehensive review, Pharmacology & Therapeutics, 138 (2013) 333-408.
[2] B.D. Brooks, A.E. Brooks, Therapeutic strategies to combat antibiotic resistance, Advanced Drug Delivery Reviews, 78 (2014) 14-27.
[3] R.Y. Pelgrift, A.J. Friedman, Nanotechnology as a therapeutic tool to combat microbial resistance, Advanced Drug Delivery Reviews, 65 (2013) 1803-1815.
[4] A.M. Fayaz, K. Balaji, M. Girilal, R. Yadav, P.T. Kalaichelvan, R. Venketesan, Biogenic synthesis of silver nanoparticles and their synergistic effect with antibiotics: a study against gram-positive and gram-negative bacteria, Nanomedicine: Nanotechnology, Biology and Medicine, 6 (2010) 103-109.
[5] P. Li, J. Li, C. Wu, Q. Wu, J. Li, Synergistic antibacterial effects of β-lactam antibiotic combined with silver nanoparticles, Nanotechnology, 16 (2005) 1912.
[6] P. Mitra, P.K. Chakraborty, P. Saha, P. Ray, S. Basu, Antibacterial efficacy of acridine derivatives conjugated with gold nanoparticles, International Journal of Pharmaceutics, 473 (2014) 636-643.
[7] H. Gu, P. Ho, E. Tong, L. Wang, B. Xu, Presenting vancomycin on nanoparticles to enhance antimicrobial activities, Nano Letters, 3 (2003) 1261-1263.
[8] A.N. Grace, K. Pandian, Antibacterial efficacy of aminoglycosidic antibiotics protected gold nanoparticles—A brief study, Colloids and Surfaces A: Physicochemical and Engineering Aspects, 297 (2007) 63-70.
[9] Y. HeeáKook, E. TaxáOh, H. JooáPark, Cyclodextrin-covered gold nanoparticles for targeted delivery of an anti-cancer drug, Journal of Materials Chemistry, 19 (2009) 2310-2315.
[10] K.M. Hindi, A.J. Ditto, M.J. Panzner, D.A. Medvetz, D.S. Han, C.E. Hovis, J.K. Hilliard, J.B. Taylor, Y.H. Yun, C.L. Cannon, The antimicrobial efficacy of sustained release silver–carbene complex-loaded L-tyrosine polyphosphate nanoparticles: Characterization, in vitro and in vivo studies, Biomaterials, 30 (2009) 3771-3779.

[11] Y. Xie, X. Wang, X. Han, X. Xue, W. Ji, Z. Qi, J. Liu, B. Zhao, Y. Ozaki, Sensing of polycyclic aromatic hydrocarbons with cyclodextrin inclusion complexes on silver nanoparticles by surface-enhanced Raman scattering, Analyst, 135 (2010) 1389-1394.
[12] X. Chen, S.G. Parker, G. Zou, W. Su, Q. Zhang, β-Cyclodextrin-functionalized silver nanoparticles for the naked eye detection of aromatic isomers, ACS nano, 4 (2010) 6387-6394.
[13] I. Ojea-Jimenez, J. Comenge, L. Garcia-Fernandez, Z.A. Megson, E. Casals, V.F. Puntes, Engineered inorganic nanoparticles for drug delivery applications, Current Drug Metabolism, 14 (2013) 518-530.
[14] G.W.T. M.J. Frisch, H.B. Schlegel, G.E. Scuseria, M.A. Robb, J.R. Cheeseman, J.A. Montgomery Jr., T. Vreven, K.N. Kudin, J.C. Burant, J.M. Millam, S.S. Iyengar, J. Tomasi, V. Barone, B. Mennucci, M. Cossi, G. Scalmani, N. Rega, G.A. Petersson, H. Nakatsuji, M. Hada, M. Ehara, K. Toyota, R. Fukuda, J. Hasegawa, M. Ishida, T. Nakajima, Y. Honda, O. Kitao, H. Nakai, M. Klene, X. Li, J.E. Knox, H.P. Hratchian, J.B. Cross, V. Bakken, C. Adamo, J. Jaramillo, R. Gomperts, R.E. Stratmann, O. Yazyev, A.J. Austin, R. Cammi, C. Pomelli, J.W. Ochterski, P.Y. Ayala, K. Morokuma, G.A. Voth, P. Salvador, J.J. Dannenberg, V.G. Zakrzewski, S. Dapprich, A.D. Daniels, M.C. Strain, O. Farkas, D.K. Malick, A.D. Rabuck, K. Raghavachari, J.B. Foresman, J.V. Ortiz, Q. Cui, A.G. Baboul, S. Clifford, J. Cioslowski, B.B. Stefanov, G. Liu, A. Liashenko, P. Piskorz, I. Komaromi, R.L. Martin, D.J. Fox, T. Keith, M.A. Al-Laham, C.Y. Peng, A. Nanayakkara, M. Challacombe, P.M.W. Gill, B. Johnson, W. Chen, M.W. Wong, C. Gonzalez, J.A. Pople, Gaussian 03, Revision E.01, Gaussian Inc., Wallingford, CT, (2004).
[15] N. Matsumoto, M. Yamada, Y. Kurakata, H. Yoshida, S. Kamitori, A. Nishikawa, T. Tonozuka, Crystal structures of open and closed forms of cyclo/maltodextrin-binding protein, FEBS Journal, 276 (2009) 3008-3019.
[16] A.K. Schmidt, S. Cottaz, H. Driguez, G.E. Schulz, Structure of cyclodextrin glycosyltransferase complexed with a derivative of its main product β-cyclodextrin, Biochemistry, 37 (1998) 5909-5915.
[17] T. Tonozuka, A. Sogawa, M. Yamada, N. Matsumoto, H. Yoshida, S. Kamitori, K. Ichikawa, M. Mizuno, A. Nishikawa, Y. Sakano, Structural basis for cyclodextrin recognition by Thermoactinomyces vulgaris cyclo/maltodextrin-binding protein, FEBS Journal, 274 (2007) 2109-2120.
[18] E.F. Pettersen, T.D. Goddard, C.C. Huang, G.S. Couch, D.M. Greenblatt, E.C. Meng, T.E. Ferrin, UCSF Chimera—a visualization system for exploratory research and analysis, Journal of Computational Chemistry, 25 (2004) 1605-1612.
[19] O. Trott, A.J. Olson, AutoDock Vina: improving the speed and accuracy of docking with a new scoring function, efficient optimization, and multithreading, Journal of Computational Chemistry, 31 (2010) 455-461.
[20] V.B. D. A. Case, J. T. Berryman, R. M. Betz, Q. Cai, D. S. Cerutti, T. E. Cheatham, III, T. A. Darden, R. E. Duke, H. Gohlke, A. W. Goetz, S. Gusarov, N. Homeyer, P. Janowski, J. Kaus, I. Kolossva´ry, A. Kovalenko, T. S. Lee, S. LeGrand, T. Luchko, R. Luo, B. Madej, K. M. Merz, F. Paesani, D. R. Roe, A. Roitberg, C. Sagui, R. Salomon-Ferrer, G. Seabra, C. L. Simmerling, W. Smith, J. Swails, R. C. Walker, J. Wang, R. M. Wolf, X. Wu and P. A. Kollman, AMBER 14, 2014, University of California, San Francisco.
[21] K. Kholmurodov, W. Smith, K. Yasuoka, T. Darden, T. Ebisuzaki, A smooth-particle mesh Ewald method for DL_POLY molecular dynamics simulation package on the Fujitsu VPP700, Journal of Computational Chemistry, 21 (2000) 1187-1191.
[22] W.L. Jorgensen, J. Chandrasekhar, J.D. Madura, R.W. Impey, M.L. Klein, Comparison of simple potential functions for simulating liquid water, The Journal of Chemical Physics, 79 (1983) 926-935.
[23] P.A. Kollman, I. Massova, C. Reyes, B. Kuhn, S. Huo, L. Chong, M. Lee, T. Lee, Y. Duan, W. Wang, Calculating structures and free energies of complex molecules: combining molecular mechanics and continuum models, Accounts of Chemical Research, 33 (2000) 889-897.
[24] I. Massova, P.A. Kollman, Combined molecular mechanical and continuum solvent approach (MM-PBSA/GBSA) to predict ligand binding, Perspectives in Drug Discovery and Design, 18 (2000) 113-135.

[25] V. Tsui, D.A. Case, Theory and applications of the generalized Born solvation model in macromolecular simulations, Biopolymers, 56 (2000) 275-291.
[26] A. Onufriev, D. Bashford, D.A. Case, Modification of the generalized Born model suitable for macromolecules, The Journal of Physical Chemistry B, 104 (2000) 3712-3720.
[27] T. Hou, J. Wang, Y. Li, W. Wang, Assessing the performance of the MM/PBSA and MM/GBSA methods. 1. The accuracy of binding free energy calculations based on molecular dynamics simulations, Journal of Chemical Information and Modeling, 51 (2010) 69-82.
[28] L. Xu, H. Sun, Y. Li, J. Wang, T. Hou, Assessing the performance of MM/PBSA and MM/GBSA methods. 3. The impact of force fields and ligand charge models, The Journal of Physical Chemistry B, 117 (2013) 8408-8421.
[29] J. Lakkakula, R.W.M. Krause, D.T. Ndinteh, S.P. Vijaylakshmi, A.M. Raichur, Detailed investigation of a gamma-cyclodextrin inclusion complex with L-thyroxine for improved pharmaceutical formulations, Journal of Inclusion Phenomena and Macrocyclic Chemistry, 74 (2012) 397-405.
[30] T. Premkumar, K.E. Geckeler, Facile synthesis of silver nanoparticles using unmodified cyclodextrin and their surface-enhanced Raman scattering activity, New Journal of Chemistry, 38 (2014) 2847-2855.
[31] Z.-Y. Hseu, Evaluating heavy metal contents in nine composts using four digestion methods, Bioresource Technology, 95 (2004) 53-59.
[32] J. Casey, C. O'Cleirigh, P. Walsh, D. O'Shea, Development of a robust microtiter plate-based assay method for assessment of bioactivity, Journal of Microbiological Methods, 58 (2004) 327-334.
[33] S. Jaiswal, B. Duffy, A.K. Jaiswal, N. Stobie, P. McHale, Enhancement of the antibacterial properties of silver nanoparticles using beta-cyclodextrin as a capping agent, International Journal of Antimicrobial Agents, 36 (2010) 280-283.
[34] R. Periasamy, S. Kothainayaki, R. Rajamohan, K. Sivakumar, Spectral investigation and characterization of host–guest inclusion complex of 4, 4′-methylene-bis (2-chloroaniline) with beta-cyclodextrin, Carbohydrate Polymers, 114 (2014) 558-566.
[35] R. Gannimani, A. Perumal, M. Ramesh, K. Pillay, M.E. Soliman, P. Govender, Antipyrine–gamma cyclodextrin inclusion complex: Molecular modeling, preparation, characterization and cytotoxicity studies, Journal of Molecular Structure, 1089 (2015) 38-47.
[36] B. Liu, W. Li, J. Zhao, Y. Liu, X. Zhu, G. Liang, Physicochemical characterisation of the supramolecular structure of luteolin/cyclodextrin inclusion complex, Food Chemistry, 141 (2013) 900-906.
[37] D. Bonenfant, P. Niquette, M. Mimeault, A. Furtos-Matei, R. Hausler, UV-VIS and FTIR spectroscopic analyses of inclusion complexes of nonylphenol and nonylphenol ethoxylate with β-cyclodextrin, Water Research, 43 (2009) 3575-3581.
[38] D.-W. Wang, C.-B. Ouyang, Q. Liu, H.-L. Yuan, X.-H. Liu, Inclusion of quinestrol and 2, 6-di-O-methyl-β-cyclodextrin: Preparation, characterization, and inclusion mode, Carbohydrate Polymers, 93 (2013) 753-760.
[39] C. Yuan, Z. Jin, X. Xu, H. Zhuang, W. Shen, Preparation and stability of the inclusion complex of astaxanthin with hydroxypropyl-β-cyclodextrin, Food Chemistry, 109 (2008) 264-268.
[40] R.O. Williams III, V. Mahaguna, M. Sriwongjanya, Characterization of an inclusion complex of cholesterol and hydroxypropyl-β-cyclodextrin, European Journal of Pharmaceutics and Biopharmaceutics, 46 (1998) 355-360.
[41] C. Yujuan, L. Runhua, 1 H NMR titration and quantum calculation for the inclusion complexes of cis-cyclooctene, cis, cis-1, 3-cyclooctadiene and cis, cis-1, 5-cyclooctadiene with β-cyclodextrin, Spectrochimica acta part A: Molecular and Biomolecular Spectroscopy, 73 (2009) 713-718.
[42] L.-J. Yang, S.-X. Ma, S.-Y. Zhou, W. Chen, M.-W. Yuan, Y.-Q. Yin, X.-D. Yang, Preparation and characterization of inclusion complexes of naringenin with β-cyclodextrin or its derivative, Carbohydrate Polymers, 98 (2013) 861-869.
[43] U. Kemelbekov, Y. Luo, Z. Orynbekova, Z. Rustembekov, R. Haag, W. Saenger, K. Praliyev, IR, UV and NMR studies of β-cyclodextrin inclusion complexes of kazcaine and prosidol bases, Journal of Inclusion Phenomena and Macrocyclic Chemistry, 69 (2011) 181-190.

[44] L.S. Devi, S. Joshi, Ultrastructures of silver nanoparticles biosynthesized using endophytic fungi, Journal of Microscopy and Ultrastructure, (2014).
[45] A.K. Mittal, D. Tripathy, A. Choudhary, P.K. Aili, A. Chatterjee, I.P. Singh, U.C. Banerjee, Bio-synthesis of silver nanoparticles using Potentilla fulgens Wall. ex Hook. and its therapeutic evaluation as anticancer and antimicrobial agent, Materials Science and Engineering: C, 53 (2015) 120-127.
[46] M. Kühn, N.P. Ivleva, S. Klitzke, R. Niessner, T. Baumann, Investigation of coatings of natural organic matter on silver nanoparticles under environmentally relevant conditions by surface-enhanced Raman scattering, Science of the Total Environment, (2014).
[47] Y. Tauran, A. Brioude, A.W. Coleman, M. Rhimi, B. Kim, Molecular recognition by gold, silver and copper nanoparticles, World Journal of Biological Chemistry, 4 (2013) 35.
[48] D.V. Chulhai, L. Jensen, Determining molecular orientation with surface-enhanced Raman scattering using inhomogenous electric fields, The Journal of Physical Chemistry C, 117 (2013) 19622-19631.
[49] M. Si, Y. Kang, Z. Zhang, Surface-enhanced Raman scattering (SERS) spectra of chloramphenicol in Ag colloids prepared by microwave heating method, Journal of Raman Spectroscopy, 40 (2009) 1319-1323.
[50] M. Moskovits, J. Suh, Conformation of mono-and dicarboxylic acids adsorbed on silver surfaces, Journal of the American Chemical Society, 107 (1985) 6826-6829.
[51] W. Li, B. Lu, A. Sheng, F. Yang, Z. Wang, Spectroscopic and theoretical study on inclusion complexation of beta-cyclodextrin with permethrin, Journal of Molecular Structure, 981 (2010) 194-203.
[52] D. Sajan, G. Sockalingum, M. Manfait, I. Hubert Joe, V. Jayakumar, NIR-FT Raman, FT-IR and surface-enhanced Raman scattering spectra, with theoretical simulations on chloramphenicol, Journal of Raman Spectroscopy, 39 (2008) 1772-1783.
[53] K. Lai, Y. Zhang, R. Du, F. Zhai, B.A. Rasco, Y. Huang, Determination of chloramphenicol and crystal violet with surface enhanced Raman spectroscopy, Sensing and Instrumentation for Food Quality and Safety, 5 (2011) 19-24.
[54] P. Leyton, C. Domingo, S. Sanchez-Cortes, M. Campos-Vallette, J. Garcia-Ramos, Surface enhanced vibrational (IR and Raman) spectroscopy in the design of chemosensors based on ester functionalized p-tert-butylcalix [4] arene hosts, Langmuir, 21 (2005) 11814-11820.
[55] F. Perret, Y. Tauran, K. Suwinska, B. Kim, C. Chassain-Nely, M. Boulet, A.W. Coleman, Molecular recognition and transport of active pharmaceutical ingredients on anionic calix [4] arene-capped silver nanoparticles, Journal of Chemistry, 2013 (2012) 1-9.
[56] G.E. Magoulas, O.N. Kostopoulou, T. Garnelis, C.M. Athanassopoulos, G.G. Kournoutou, M. Leotsinidis, G.P. Dinos, D. Papaioannou, D.L. Kalpaxis, Synthesis and antimicrobial activity of chloramphenicol-polyamine conjugates, Bioorganic & Medicinal chemistry, 23 (2015) 3163-3174.
[57] A. Yunis, Chloramphenicol toxicity: 25 years of research, The American Journal of Medicine, 87 (1989) 44N-48N.

Chapter 6

RESEARCH RESULTS IV

Pharmaceutical salts of fluoroquinolones with quinic acid

This manuscript is being prepared for submission to

Journal of Pharmaceutical and Biomedical Analysis

Pharmaceutical salts of fluoroquinolones with quinic acid

Ramesh Gannimani[a], Karen Pillay[a], Patrick Govender[a,*]

[a]Department of Biochemistry, School of Life Sciences, University of KwaZulu-Natal, Westville, Durban 4000, South Africa

6.1 Abstract

Novel organic salts of fluoroquinolones (ciprofloxacin and norfloxacin) were prepared using biocompatible quinic acid in a direct protonation reaction in which water served as the solvent followed by the freeze-drying approach. The salts were characterized by spectroscopic techniques that included FTIR-ATR, NMR and MS. Additionally salts were also evaluated by thermal analysis (DSC and TGA) and X-ray diffraction. The water solubility of the newly-formed salts was analyzed, followed by determination of their octanol-water partition coefficients. The cytotoxicity of newly synthesized salts was evaluated in comparison to their commercially available fluoroquinolone-hydrochloride salts *in vitro* using the mammalian VERO cell line. The results of this study indicate that salts were amorphous and highly water soluble when compared to their respective parent pharmaceutical compounds. Interestingly the fluoroquinolone-quinic acid salts were similarly biocompatible to their currently available fluoroquinolone-hydrochloride salt forms. This study demonstrates that rational design and development of innovative salt forms of commercially available drug candidates provides a resourceful cost-effective avenue to overcome solubility issues while limiting their toxic side effects.

6.2 Key words

Quinic acid, fluoroquinolones, solubility enhancement, cytotoxicity

6.3 Introduction

Presently based on economic and market demand, pharmaceutical drug design and development generally follows two main processing streams. Firstly, the drive of large pharmaceutical corporations to unravel novel therapeutic agents is associated with high risk and enormous expense. In the second approach smaller pharmaceutical entrepreneurs reformulate drug candidates that are out of patent protection to make them safer, more effective or more cost-effective to produce. Many pharmaceutical research strategies to design novel pharmaceutically active compounds fail at clinical trials due to limited solubility of the proposed novel bioactive agent [1]. A diverse range of physiochemical factors including crystallinity (amorphous, crystalline), polymorphism, temperature, pH and particle size can negatively affect the solubility of otherwise promising bioactive candidates. The solubility or dissolution of the drug substances can be improved through material engineering of the drug substance or through formulation approaches [2, 3]. Several different strategies to enhance the solubility of poorly soluble drug substances include techniques like particle size reduction, solid state engineering, solid dispersions, salt formation, microemulsions, liposomes, complexation with cyclodextrins, lyophilization, co-solvent systems, micellar/surfactant systems etc. [2, 4]. Salt formation is the most commonly used method to enhance the solubility of the drug substances which are either weak bases or weak acids and most of the marketable formulation today are in the form of salts [5, 6]. When converted into salts, many drugs were found to be more stable, less hygroscopic and thus easy to handle than their corresponding free bases or acids which qualify them as the preferred forms to be used as the therapeutic agents [6].

Together with the solubility, the permeability behavior of the salt is a key determinant of its bioavailability [7]. Ion pairing is an effective chemical approach to increase the lipophilicity of ionized drugs and to enhance their permeability across the membranes [7, 8]. Several organic counter ions have been demonstrated to form ion pairs with pharmaceutically active compounds [9-12]. Ion pairing gives rise to a neutralized complex, which partitions into the membrane and may dissociate to liberate the charged species [13]. Salts of pharmaceuticals with inorganic counter ions are highly ionic in nature and have difficulty crossing the membrane in order to reach their site of action [14]. The existence of salt in the form of ionic pair is critical for its transport across the absorbing membrane [7]. Thus organic counter ions merits over inorganic

counter ions in salt formation technique. However, choosing an appropriate organic counter ion is important and at the same time very challenging since many of the existing ones like trichloroacetate, cholate, alkylsulfates, etc. can be too irritative and impart toxic side effects limiting their application [7].

Quinic acid is a cyclic polyol present in many plant products like coffee beans, cinchona bark, tobacco leaves, apples and peaches [15, 16]. Recently, quinic acid has been identified as an essential bioactive dietary component which initiates the synthesis of potential antioxidants *viz.* tryptophan and nicotinamide in humans which play a role in DNA repair [17, 18]. Quinic acid is endowed with favorable pharmacokinetics properties like greater value of drug score (0.48), drug likeness (0.51), less toxicity and was recently shown as a potential drug candidate against prostate cancer [19]. The significant biological activities and biocompatibility associated with quinic acid has propelled this study to evaluate its application as salt forming active pharmaceutical ingredient in combination with fluoroquinolones (ciprofloxacin and norfloxacin). Ideally there should be a difference of at least two units between the pKa value of acid and base to form a stable salt in water [20, 21]. The pKa of the carboxylic acid group of quinic acid is 3.66 [22] and the pKa for basic -NH group of ciprofloxacin and norfloxacin were shown to be 8.62 and 8.75 respectively [23]. Hence, quinic acid was strategically selected in this study to generate salts of these fluoroquinolones.

To date, quinic acid and quinic acid derived amphoteric compositions are therapeutically useful in the treatment of common dry skin ailments [24, 25]. It is envisaged that antibacterial fluoroquinolones may be incorporated into similar quinic acid derived amphoteric pharmaceutical compositions to promote simultaneous treatment of dry skin and bacterial infections of skin. Fluoroquinolones are classified as amino acid type amphoterics since they contain both amino basic group and carboxylic acidic group. Incorporating them in quinic acid formulation will help in raising the overall pH of the composition, so that the composition becomes less or non-irritating to the skin and also quadruple ionic salt complex formed acts as buffering system to control the release of quinic acid into the skin [25]. Thus, fluoroquinolones when coupled to quinic acid could neutralize its undesirable side effects, whilst at the same instance quinic acid as counter ion could increase solubility and introduce a secondary activity to fluoroquinolone formulations. A symbiotic enhancement in the therapeutic efficacy of both

quinic acid and fluoroquinolones may be achieved by administering them together as a salt. Hence the study of quinic acid salts of fluoroquinolone drugs is rational and interesting which would pave way for new directions in pharmaceutical sectors.

6.4 Materials and methods

Ciprofloxacin, norfloxacin and octanol were analytical grade reagents purchased from Sigma Aldrich, Germany and quinic acid was purchased from Merck, Germany. Infrared spectra of samples were recorded on a Perkin Elmer Spectrum 100 FT-IR spectrometer with universal ATR sampling accessory. ^{1}H and ^{13}C NMR spectra were recorded using a Bruker Avance 400 MHz instrument equipped with BBOZ probe. Chemical shifts are given in δ (ppm) against the internal standard tetramethylsilane. Samples for NMR were prepared in deuterium oxide. The chemical shifts were referenced to the residual water signal of D_2O. MS was carried out on a Waters Micromass LCT Premier TOF-MS. Powder X-ray diffraction (XRD) patterns were recorded on a Bruker D8 Advance instrument equipped with an Anton-Paar XRK 900 reaction chamber and a Cu radiation source with a wavelength of 1.5406 Å at ambient temperature. Thermogravimetric analysis-differential scanning calorimetry (TGA-DSC) was conducted on SDT Q600 TA instrument. The temperature of samples was increased from 25-800°C at a heating rate of 10°C min^{-1} under nitrogen atmosphere.

6.5 Experimental

6.5.1 Synthesis of quinic acid salts of ciprofloxacin and norfloxacin

6.5.1.1 Ciprofloxacin quinate [Cip] [Qui]:

Ciprofloxacin (1.00 g; 3.19 mmol) was first added into a flask containing 25 mL of water. A 5 mL water solution of quinic acid (0.58 g; 3.19 mmol) was slowly added to the ciprofloxacin suspension. The reaction mixture was stirred at room temperature for 24 h and the solvent was removed by freeze drying. The [Cip] [Qui] product **(Fig. 6.1)** was obtained as a white amorphous solid (1.42 g).

6.5.1.2 Norfloxacin quinate [Nor] [Qui]:

Norfloxacin (1.00 g; 3.13 mmol) was first added into a flask containing 25 mL of water. A 5 mL water solution of quinic acid (0.601g; 3.13 mmol) was slowly added to the norfloxacin suspension. The reaction mixture was stirred at room temperature for 24 h and the solvent was removed by freeze drying. The desired [Nor] [Qui] product was obtained as a pale yellow solid (1.47 g).

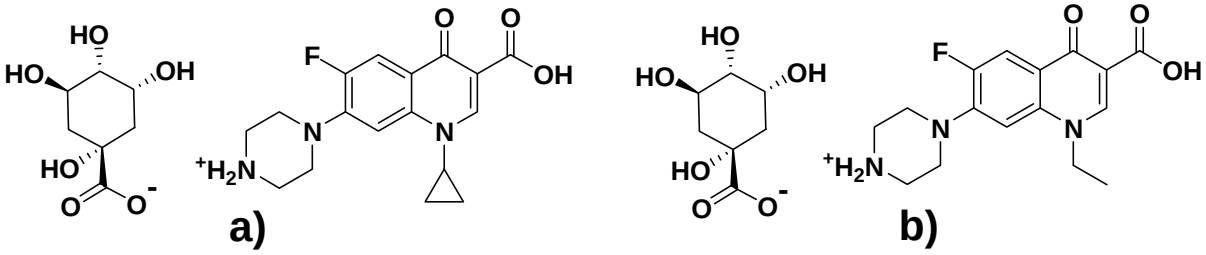

Figure 6.1 Molecular structure of fluoroquinolone salts with quinate counter ion **a)** [Cip] [Qui] **b)** [Nor] [Qui] synthesized in this study.

6.5.2 Water Solubility

Water solubility of the compounds was determined by adding excess compounds to 5 mL of water in a sample vial. The vials were maintained at 25°C and agitated vigorously for 24 h. Afterwards the vials were centrifuged for 1 h at 3000 rpm and the supernatant was further filter sterilized with a 0.45 micron filter. Aliquots of the sterile solution in quart cuvettes were analyzed by UV spectroscopy at wavelength 276 nm. The standard curves were established for each compound in water using five different concentrations prior to their analysis. The experiment was performed in triplicate and the standard deviation was determined.

6.5.3 Determination of octanol-water partition coefficients

The partition coefficient (Log P) of both quinate and hydrochloride derived salts of ciprofloxacin and norfloxacin between n-octanol and water was determined by a slight modification of the method described by Ross et al. [26, 27]. A mixture of 1.9 mL of water and

2 mL of octanol were shaken for 24 h. To this pre-equilibrated octanol and water mixture was added 100 µl of fluoroquinolone salt solutions (1 mg/mL). The resulting mixtures contained in vials were vigorously stirred for 24 h at 25°C. The vials were centrifuged at 3000 rpm for 30 minutes to ensure distinct phase separation of octanol and water. Thereafter the concentration of the solute present in both phases was determined by UV spectrophotometry. The partition coefficient of salts between the two phases was determined using the following equation.

$$\text{Log } P = (C_o/C_w) \text{ X } (W_w/W_o)$$

Where C_o and C_w refer to the octan-1-ol phase and water phase concentrations, respectively, and W_w and W_o the weight of the aqueous and octanol phases in the samples.

6.5.4 Cytotoxicity studies

The VERO cell line was obtained from the European Culture Collection of Cell lines (Sigma-Aldrich) were cultured in RPMI 1640 (without phenol red) growth medium containing 10% heat-inactivated foetal bovine serum, 25 mM 4-(2-hydroxyethyl)-1-piperazineethanesulfonic acid (HEPES), 1 mM sodium pyruvate and 0.1 mg/mL penicillin / streptomycin). Cells ($5x10^4$ cells per well) were plated in 96 well plates (Greiner Bio-One GmbH, Germany) and incubated at 37˚C (5 % CO_2 incubator) for 24 hours. Subsequently, the spent medium was removed from all wells and replaced with fresh fully constituted medium along with quinic acid, ciprofloxacin hydrochloride, [Cip] [qui], norfloxacin hydrochloride, and [Nor][qui] at different concentrations (62.5 to 250 µM). Plates were further incubated under the same conditions for 24 h before the addition of 3-(4,5-dimethylthiazol-2-yl)-5-(3-carboxymethoxyphenyl) 2-(4-sulphenyl)-2H- tetrazolium (MTS) into each wells to perform CellTiter 96 AQueous One Solution Assay (Promega, Madison, WI). Upon incubation for additional 2 h, plates were spun down at 3000 rpm for 3 minutes and transferred to new 96 well plates and immediately read using Bio-Tek Synergy HT Automated Microplate Reader. Cadmium was used as the control and all assays were carried out in quintuplicate (n=5).

6.6 Results and discussion

6.6.1 Characterization of the compounds

Ciprofloxacin quinate: White solid; 92 % yield; C. IR (KBr, cm^{-1}): 3257, 2919, 2535, 1724, 1628, 1585; ^{1}H NMR (400 MHz, D_2O): δ 8.35 (1H, bs), 7.28 (1H, d, *J* = 7.30 Hz), 7.10 (1H, m), 4.04(1H, q, *J* = 3.5Hz) , 3.92 (1H, m), 3.51 (5H, m), 3.44 (5H, m), 1.96 (2H, m), 1.86 (1H, m) 1.78 (1H, m), 1.32 (2H, d, J = 7.23 Hz) 1.05 (2H, s); ^{13}C NMR (400 MHz, D_2O): 181.1, 175.4, 168.5, 154.3, 151.8, 147.9, 144.5, 144.4, 138.7, 118.3, 118.2 110.5, 110.3, 106.3, 105.5, 76.8, 75.1, 70.3, 66.9, 46.2, 43.1, 40.5, 37.3, 36, 7.4; HRMS (ESI m/z) $[M + H]^+$ calculated for $C_{17}H_{19}FN_3O_3^+$: 332.1405, found 332.1408; (ESI m/z) $[M + H]^+$ calculated for $C_7H_{11}O_6^-$: 191.0561, found 191.0560.

Norfloxacin quinate: Pale yellow solid; 90% yield; C. IR (KBr, cm^{-1}): 3277, 3046, 2918, 1705, 1626; ^{1}H NMR (400 MHz, D_2O): δ 8.21 (1H, m, H-Ar), 7.08 (1H, m, H-Ar), 6.77 (1H, m, H-Ar), 4.21(2H, m, H-CH_2) , 4.04 (1H, d, *J* = 2.97 Hz, H-CH_2), 3.92 (1H, m, H-CH_2), 3.44 (9H, m, H-CH_2, and H-CH), 1.96 (1H, m, H-CH_2), 1.86 (1H, m, H-CH_2) 1.78 (1H, m, H-CH_2), 1.36 (1H, m, H-CH_3): ^{13}C NMR (400 MHz, D_2O): 181.2, 174.9, 168.6, 154, 151.5, 147.3, 144.6, 136.7, 118.8, 110.7, 110.5, 105.9, 105.3, 76.9, 75.1, 70.3, 66, 50.1, 46.2, 43.1, 40.6, 37.3, 13.6; HRMS (ESI m/z) $[M + H]^+$ calculated for $C_{16}H_{19}FN_3O_3^+$: 320.1400, found 320.1406; (ESI m/z) $[M + H]^+$ calculated for $C_7H_{11}O_6^-$: 191.0561, found 191.0560.

6.6.2 Thermogravimetric and differential scanning calorimetric analyses

The free base fluoroquinolones and their respective quinate organic salts were characterized for their thermal properties using SDT Q600 TA instrument. The solid TGA weight loss and dashed DSC thermal curve are displayed in **Fig. 6.2**. The DSC curve of free bases of ciprofloxacin and norfloxacin exhibited sharp endothermal crystal melt event at 278°C and 232°C indicating their crystalline nature. After the melt transition the free bases underwent a rapid pyrolysis and decomposition which is indicated by irregular changes in the TGA weight loss curves. On the contrary, quinate salts of both ciprofloxacin and norfloxacin did not exhibit any sharp crystal melting event and they undergo gradual weight loss after the temperature point 230°C. These changes in the thermal events confirm salt formation and their amorphous nature. The method

used for the synthesis of salts in this study i.e., direct protonation followed by isolation of salt from the aqueous phase by freeze drying resulted in amorphous solid formation. In pharmaceutical industries amorphous solids are of especially attractive due to their fast dissolving nature and improved bioavailability [28].

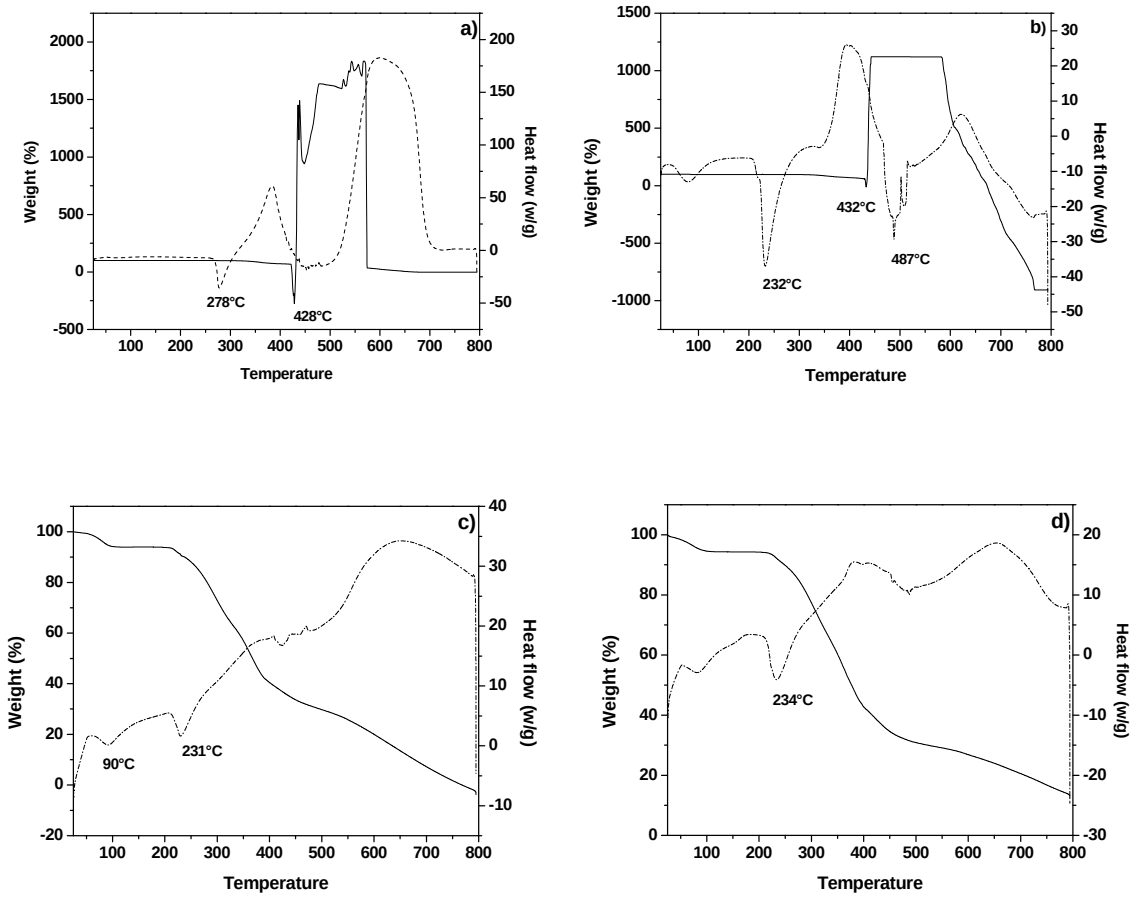

Figure 6.2 TGA and DSC curves of **a)** Ciprofloxacin, **b)** Norfloxacin, **c)** [Cip] [Qui] and **d)** [Nor] [Qui].

6.6.3 X-ray powder diffractometry

The X-ray diffraction pattern of quinic acid, free base and quinate salt forms of fluoroquinolones were studied using powder XRD. The powder XRD patterns of quinic acid, ciprofloxacin and norfloxacin contained several sharp characteristic peaks due to their crystalline nature. The major sharp and intense peaks were observed for quinic acid at 2θ = 19.23, 21.37, 23.58, for ciprofloxacin at 2θ = 16.81, 21.02, 25.55 and for norfloxacin at 2θ = 16.86, 18.23, 19.34, 21.44, 22.82, 23.71 **(Fig. 6.3)**. The XRD patterns of salts were distinctive

when compared to the parent compounds. The formation of salt resulted in the broadening, disappearance or appearance of new peaks. The powder XRD patterns of [Cip] [Qui] showed broad peaks at 2θ = 16.76, 20.18, 23.50, 25.92, whilst that of [Nor] [Qui] showed broad peaks corresponding to 2θ = 15.60, 19.60, 25.87. These changes in the diffractogram confirm the salt formation of fluoroquinolones. Also the broad peaks observed in the diffractogram indicate that freeze drying method synthesized salts were amorphous in nature. The amorphous solids which lack long range molecular arrangement fail to scatter X-ray and hence produce broad peaks. The crystallography studies were well aligned to the results observed for thermogravimetric analysis.

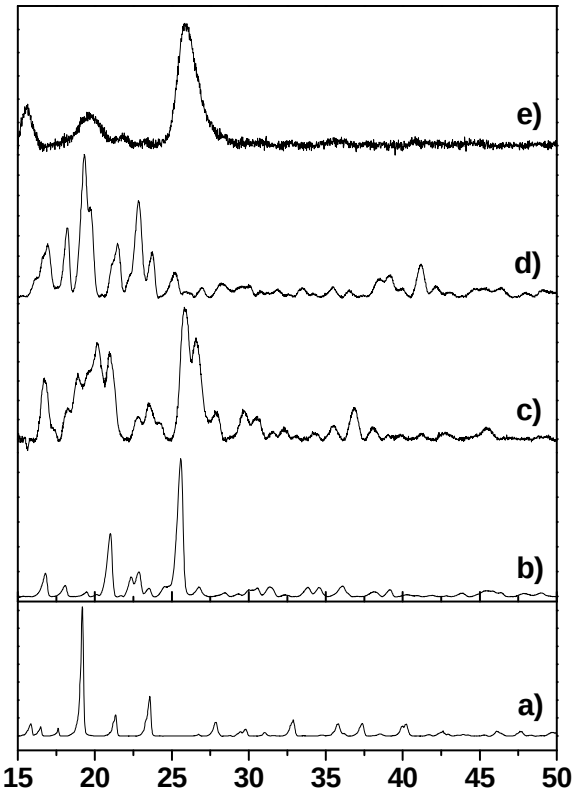

Figure 6.3 Diffractograms of **a)** Quinic acid, **b)** Ciprofloxacin, **c)** [Cip] [qui], **d)** Norfloxacin and **e)** [Nor] [Qui].

6.6.4 Solubility in water

Solubility values determined at 25°C for unionized fluoroquinolones and their respective quinate salts are listed in the **Table 6.1.** The results indicate that solubility of both ciprofloxacin and norfloxacin increased significantly. The solubility's of ciprofloxacin and norfloxacin were found to be 0.14 mg and 0.54 mg/ml respectively [29]. The solubility increased to 409 mg and 355 mg when converted to quinate salt. This can be explained in that the acid-base reaction between quinic acid and fluoroquinolone base resulted in the protonation of secondary amine present in the piperazine ring thereby generating ionic species. The interaction of ions with water molecules will be higher than compared to their neutral species and thus water solubility of salts will be increased [5].

Table 6.1 Water solubility at 25°C

Compound	Solubility (mg/mL)	Reference
Ciprofloxacin	0.14 ± 0.01	[29]
[Cip] [Qui]	409 ± 4.8	This study
Norfloxacin	0.54 ± 0.02	[29]
[Nor] [Qui]	355 ± 3.7	This study

6.6.5 Determination of octanol-water partition coefficients

Octanol-water partition coefficient of quinate and hydrochloride salts of fluoroquinolones were determined by a modified shake flask method and are presented in **Table 6.2.** The experiments were performed in triplicate and the results obtained are presented with their standard deviations. Quinate salts have higher Log P values than their corresponding hydrochloride salt counterparts indicating that organic acid derived salts have higher lipophilicity than inorganic acid derived salts. Also the [Nor] [Qui] derivative has a higher Log P value than the [Cip] [Qui] salt. Research studies to date reveal that higher lipophilicities indicate an increased capacity of pharmaceutical salts to pass thorough cell membranes [30, 31]. As such the quinate counter ion employed in this study can facilitate greater permeability of fluoroquinolones than the chloride ion across the biological membranes. However, it should be noted that permeability of drugs cannot be decided solely based on Log P values [30]. The hydrochloride salts probably were highly ionic and thus will have less affinity towards hydrophobic octanol [32]. On the other hand, the quinate counter ion might have formed an ion pair with the fluoroquinolone base and thus favoring higher Log P values [33].

Table 6.2 Octanol water partition coefficient

Compound	Log P	Std Curve Equation	R^2
[Cip] [Qui]	0.544 ± 0.01123	y=0.0894x+0.1109	0.9939
[Nor] [Qui]	0.773 ± 0.00222	y=0.0921x+0.0011	0.9990
[Cip] [H]	0.411±0.016731	y=0.0659x+0.0689	0.9998
[Nor] [H^+]	0.499±0.016182	y=0.0691x+0.0867	1

6.6.6 Cytotoxicity studies

The *in vitro* cytotoxicity of quinic acid, quinate and hydrochloride salt forms of fluoroquinolones were evaluated at three different concentrations against the VERO mammalian cell line to assess the impact of quinate salt modification on cellular toxicity when compared to their hydrochloride counterparts. Percentage cell viabilities are tabulated in **Table 6.3.** Quinic acid was not found to be toxic at all the concentrations tested. A near 100% viabilities were observed even at high concentration (250 μM) tested indicating their biocompatibility. Both hydrochloride and quinate salts of fluoroquinolones were nontoxic at lower concentrations. However, at a higher concentration of 250 μM, they displayed low grade toxicity. From the table it can be observed that quinate counter ion did not increase the toxicity when compared to hydrochloride salts of fluoroquinolones. Hence, fluoroquinolone salts using quinate counter ion can be used in pharmaceutical formulations.

Table 6.3 Percentage cell viabilities of VERO cells in the presence of quinic acid, fluoroquinolones and their salts at different concentrations

Compound	Concentrations (µM)		
	62.5	125	250
Quinic acid	110.62±6.49[a]	101.47±5.23[a]	99.88±7.36[a]
[Cip][H]	102.83±7.22[a]	102.32±8.7[a]	78.69±5.79[b]
[Cip] [Qui]	97.60±8.06[a]	96.68± 7.66[a]	72.01±7.54[b]
[Nor] [H]	110.23±6.09[a]	106.77±7.57[a]	75.68±6.09[b]
[Nor] [Qui]	108.02±7.70[a]	108.91±5.36[a]	77.70±6.03[b]

All values are expressed as mean ± standard deviation of experiments performed in five replicates. Different superscript letters (a and b) presented in each column are significantly different from each other ($p < 0.05$; one-way ANOVA, Tukey's post-hoc test)

6.7 Conclusion

In short, the present study discusses the salt formation of fluoroquinolones using quinate counter ion exchange. Solubility of both ciprofloxacin and norfloxacin was significantly increased by converting them into the quinate salt forms. As compared to the hydrochloride salts, quinate salts of fluoroquinolones have higher octanol-water partition coefficient indicating their lipophilic character. This could help in simultaneous increase of solubility and permeability of fluoroquinolones. XRD data analysis confirms that the method of direct protonation followed by freeze drying yielded amorphous salt forms. Conversion of free bases to amorphous may increase the solubility, stability and bioavailability of drugs. The cytotoxicity studies indicated that quinic acid is biocompatible and did not increase the toxicity of fluoroquinolones when applied as a counter ion. The data from the present study tentatively suggests that the novel fluoroquinolone-quinic acid salts are likely potential drug candidates for economic development.

In this regard the following parameters of the novel pharmaceutical salts synthesized in this study will be the subject of future research; thermodynamic stability of salt forms, evaluation of their membrane absorption and permeability using *in vitro* tools like parallel artificial membrane permeability assay (PAMPA) [34, 35] and profiling salts for their solubility in bio-relevant dissolution media with differing pH [36].

6.8 Acknowledgement

This research work was funded by National Research Foundation (NRF) of South Africa and the University of KwaZulu-Natal, South Africa.

6.9 References

[1] S. Basavaraj, G.V. Betageri, Can formulation and drug delivery reduce attrition during drug discovery and development—review of feasibility, benefits and challenges, Acta Pharmaceutica Sinica B, 4 (2014) 3-17.
[2] Y. Kawabata, K. Wada, M. Nakatani, S. Yamada, S. Onoue, Formulation design for poorly water-soluble drugs based on biopharmaceutics classification system: basic approaches and practical applications, International Journal of Pharmaceutics, 420 (2011) 1-10.
[3] M. Kakran, L. Li, R.H. Müller, Overcoming the challenge of poor drug solubility, Pharmaceutical Engineering, 32 (2012) 1-7.
[4] K.T. Savjani, A.K. Gajjar, J.K. Savjani, Drug solubility: importance and enhancement techniques, ISRN Pharmaceutics, 2012 (2012).
[5] A.T. Serajuddin, Salt formation to improve drug solubility, Advanced Drug Delivery Reviews, 59 (2007) 603-616.
[6] P.H. Stahl, C.G. Wermuth, Handbook of Pharmaceutical Salts Properties, Selection, and Use, John Wiley & Sons, 2008.
[7] R. Neubert, Ion pair transport across membranes, Pharmaceutical Research, 6 (1989) 743-747.
[8] Z.S. Teksin, K. Hom, A. Balakrishnan, J.E. Polli, Ion pair-mediated transport of metoprolol across a three lipid-component PAMPA system, Journal of Controlled Release, 116 (2006) 50-57.
[9] J.M. Miller, A. Dahan, D. Gupta, S. Varghese, G.L. Amidon, Quasi-equilibrium analysis of the ion-pair mediated membrane transport of low-permeability drugs, Journal of Controlled Release, 137 (2009) 31-37.
[10] H.-W. Chae, I.-W. Kim, H.-E. Jin, D.-D. Kim, S.-J. Chung, C.-K. Shim, Effect of ion-pair formation with bile salts on the in vitro cellular transport of berberine, Archives of Pharmacal Research, 31 (2008) 103-110.
[11] C. Shim, R. Nishigaki, T. Iga, M. Hanano, Determination of extraction constant, true partition coefficient and formation constant of ion-pair complexes of quaternary ammonium salts, tetrabutylammonium bromide and isopropamide iodide. with some organic anions by a solvent extraction technique, International Journal of Pharmaceutics, 8 (1981) 143-151.
[12] J. Van Gelder, M. Witvrouw, C. Pannecouque, G. Henson, G. Bridger, L. Naesens, E. De Clercq, P. Annaert, M. Shafiee, G. Van den Mooter, Evaluation of the potential of ion pair formation to improve the oral absorption of two potent antiviral compounds, AMD3100 and PMPA, International Journal of Pharmaceutics, 186 (1999) 127-136.
[13] S.J. Lee, S.W. Kim, Hydrophobization of ionic drugs for transport through membranes, Journal of Controlled Release, 6 (1987) 3-13.
[14] J.D. Meyer, M.C. Manning, Hydrophobic ion pairing: altering the solubility properties of biomolecules, Pharmaceutical Research, 15 (1998) 188-193.
[15] A. Kumar, I. Kannan, M. Jayalakshmi, S. Shantha, An insilico study of quinic acid derivatives as inhibitors of com a, the quorum sensing protein of streptococcus mutans responsible for the pathogenesis in dental caries, International Journal of Biotechnology and Allied Fields, 1 (2013) 76-84.
[16] A.C.B. da Silva, D.R. da Silva, S.A. de Macêdo Ferreira, G.G. Agripino, A.R. Albuquerque, T.G. do Rêgo, In Silico Approach for the Identification of Potential Targets and Specific Antimicrobials for Streptococcus mutans, Advances in Bioscience and Biotechnology, 2014 (2014).
[17] R.W. Pero, H. Lund, T. Leanderson, Antioxidant metabolism induced by quinic acid. Increased urinary excretion of tryptophan and nicotinamide, Phytotherapy Research, 23 (2009) 335-346.

[18] R.W. Pero, H. Lund, Dietary quinic acid supplied as the nutritional supplement AIO+ AC-11® leads to induction of micromolar levels of nicotinamide and tryptophan in the urine, Phytotherapy Research, 25 (2011) 851-857.
[19] E. Padmini, L. Inbathamizh, Quinic acid as a potent drug candidate for prostate cancer–a comparative pharmacokinetic approach, Asian Journal of Pharmaceutical and Clinical Research, 1 (2013).
[20] A. Serajuddin, M. Pudipeddi, P. Stahl, C. Wermuth, Handbook of pharmaceutical salts, Verlag Helvetica Chimica Acta: Zurich and Wiley-VCH: Weinheim, (2002) 138-139.
[21] A. Yadav, A. Shete, A. Dabke, P. Kulkarni, S. Sakhare, Co-crystals: a novel approach to modify physicochemical properties of active pharmaceutical ingredients, Indian Journal of Pharmaceutical Sciences, 71 (2009) 359.
[22] M. Sadaka, A. Garcia, Extraction of shikimic and quinic acids, Chemical Engineering Communications, 173 (1999) 91-102.
[23] S. Basavoju, D. Boström, S.P. Velaga, Pharmaceutical Salts of Fluoroquinolone Antibacterial Drugs with Acesulfame Sweetener, Molecular Crystals and Liquid Crystals, 562 (2012) 254-264.
[24] J.Y. Ruey, E.J. Van Scott, Alpha hydroxyacids, alpha ketoacids and their use in treating skin conditions, in, Google Patents, 1982.
[25] J.Y. Ruey, E.J. Van Scott, Amphoteric compositions and polymeric forms of alpha hydroxyacids, and their therapeutic use, in, Google Patents, 1992.
[26] D.L. Ross, S.K. Elkinton, C.M. Riley, Physicochemical properties of the fluoroquinolone antimicrobials. III. 1-Octanol/water partition coefficients and their relationships to structure, International Journal of Pharmaceutics, 88 (1992) 379-389.
[27] J. Vazquez, S. Merino, Ò. Doměnech, M. Berlanga, M. Vinas, M. Montero, J. Hernández-Borrell, Determination of the partition coefficients of a homologous series of ciprofloxacin: influence of the N-4 piperazinyl alkylation on the antimicrobial activity, International Journal of Pharmaceutics, 220 (2001) 53-62.
[28] L. Yu, Amorphous pharmaceutical solids: preparation, characterization and stabilization, Advanced Drug Delivery Reviews, 48 (2001) 27-42.
[29] C. Florindo, A. Costa, C. Matos, S.L. Nunes, A.N. Matias, C.M. Duarte, L.P.N. Rebelo, L.C. Branco, I.M. Marrucho, Novel organic salts based on fluoroquinolone drugs: Synthesis, bioavailability and toxicological profiles, International Journal of Pharmaceutics, 469 (2014) 179-189.
[30] F. Alves, F.S. Oliveira, B. Schröder, C. Matos, I.M. Marrucho, Synthesis, characterization, and liposome partition of a novel tetracycline derivative using the ionic liquids framework, Journal of Pharmaceutical Sciences, 102 (2013) 1504-1512.
[31] C. Hansch, W.J. Dunn, Linear relationships between lipophilic character and biological activity of drugs, Journal of Pharmaceutical Sciences, 61 (1972) 1-19.
[32] A. Leo, C. Hansch, D. Elkins, Partition coefficients and their uses, Chemical Reviews, 71 (1971) 525-616.
[33] W.C. Stahl PH, Handbook of pharmaceuticalsalts: Properties, selection, and use. , VHCA, Verlag Helvetica Chimica Acta, Zurich, Switzerland, and Wiley-VCH, Verlag GmbH & Co. KGaA, Weinheim, F. R. Germany, (2008).
[34] S. Stegemann, F. Leveiller, D. Franchi, H. De Jong, H. Lindén, When poor solubility becomes an issue: from early stage to proof of concept, European Journal of Pharmaceutical Sciences, 31 (2007) 249-261.
[35] M. Bermejo, A. Avdeef, A. Ruiz, R. Nalda, J.A. Ruell, O. Tsinman, I. González, C. Fernández, G. Sánchez, T.M. Garrigues, PAMPA—a drug absorption in vitro model: 7. Comparing rat in situ, Caco-2, and PAMPA permeability of fluoroquinolones, European Journal of Pharmaceutical Sciences, 21 (2004) 429-441.
[36] K. Sugano, A. Okazaki, S. Sugimoto, S. Tavornvipas, A. Omura, T. Mano, Solubility and dissolution profile assessment in drug discovery, Drug Metabolism and Pharmacokinetics, 22 (2007) 225-254.

Chapter 7

GENERAL DISCUSSION AND CONCLUSION

7.1 General Discussion and Conclusion

Traditional methods to develop new medicines involve identifying and compiling a large number of promising compounds, which could become a potential therapeutic agent. The medicinal compounds are either identified from the natural resources or created in the laboratory in large number after strategic designing and thereafter will be subjected to high-throughput screening to find out a few potential candidates from the large library [1, 2]. Recently nanotechnology is making a significant contribution in the field of drug discovery and the number of medicinally useful inorganic nanomaterial generated, providing more options in the drug discovery [3]. However the process of researching and developing new medication is long, expensive and complex [4]. It is thus very hard to source new medicines with fewer side effects. On average, it takes at least ten years for a new therapeutic agent to complete clinical trials and go into the market [4]. The average cost to research and develop each successful drug is estimated to be $2.6 billion [5]. From thousands of compounds screened and assessed in the early research and development process, only a few substances pass all of the tests, trials and receive approval [6]. The overall probability of clinical success is estimated to be less than 12% [5]. Clinical trials also involve the risk of exposing human volunteers to potentially harmful substances or possibly ineffective treatments. The increasing number of high profile drug withdrawals from the market due to later detection of associated adverse reactions is another issue [7, 8]. Hence conversion of well-designed compounds to an approved medical drug is an uphill task.

Alternatively, methods to further improve the existing medicinal compounds is of value, since safety and efficacy of those compounds is already characterized and quick development of new treatments can be expected [9]. Thus investigation and improvement of existing medicine has become an important aspect of the modern pharmaceutical sector. Better management of existing medication as well as cost reduction and harm of drug discovery on human health care is global priority.

This thesis is focused on both identifying likely targets as new therapeutic agents and strategies to improve the existing medication. Chapters 3 and 4 focused on finding new antibacterial and

anti- diabetic compounds, while chapters 5 and 6 were concerned with different strategies to improve existing medication. Although, this PhD research study initially focused on designing new and/or improving currently available antibacterial agents. The antidiabetic evaluation was only initiated since similar compounds were previously shown to have antidiabetic activity [10].

In Chapter 3, we described that biomolecules present in aqueous seed extract of *Protorhus longifolia* could be used to reduce silver and gold ions to their respective metal nanoparticles in a green synthesis protocol. This environmentally benign reaction for the synthesis of nanoparticle was rapid and readily conducted at room temperature. Surface plasmon resonance in the UV visible region for AgNPs at 400-500 nm and for AuNPs at around 500-600 nm confirmed their formation. The IR spectrum confirmed the presence of organic functional groups on the surface of nanoparticle. The poly-dispersed nanoparticles were 10 nm-30 nm in size. Zeta potential of -21.2 mv for AgNPs and -19.7 mv for AuNPs was contributing to the stability of nanoparticles. Green synthesized AgNPs and AuNPs showed potential antibacterial activity against bacterial species *Escherichia coli* (ATCC 35218), *Klebsiella pneumoniae* (ATCC 700603), *Staphylococcus aureus* (ATCC 43300) and *Pseudomonas aeruginosa* (ATCC 27853). Our results showed that AgNPs were comparatively more potent than AuNPs as antibacterial agents. In this study we demonstrated that phytochemical based formulations constituting inorganic nanoparticle capped with medicinal compounds from the plant extract form novel potent antimicrobial agents.

In Chapter 4, by using traditional approaches we attempted to find out a new class of possible antidiabetic heterocyclic molecules. Chapter 4 interrogates the potential of heterocyclic compounds as antibacterial agents. Since this class of compounds was also found to be good anti-diabetic agents [10], anti-diabetic testing was also performed. As such this chapter provides a brief discussion on the synthesis, characterization and evaluation of α-glucosidase inhibitory and antibacterial activities of 2-amino-3, 5-dicyano-6-sulfanyl pyridines scaffolds. The 2-amino-3, 5-dicyano-6-sulfanyl pyridines core structures are known to possess various biological activities. In this study along with antibacterial activity, for the first time we have evaluated the α-glucosidase inhibitory activity of these compounds. Compounds were

synthesized in a single step multi-component protocol with good yields from commercially available reagents. Our results show that 2-amino-3, 5-dicyano-6-sulfanyl pyridine derivatives have poor antibacterial activity. However they possess good α-glucosidase inhibitory activity. Five of the nine compounds tested showed good inhibition of α-glucosidase enzyme, which was similar to the standard drug acarbose. The prediction of binding affinities of the compounds towards the enzyme model by molecular docking analysis helped us to explain the experimental results observed. We were able to show that aromatic substitution at position 4 and 6 of the pyridine ring increased the α-glucosidase inhibitory activity. Thus both the theoretical and experimental inhibitory activities, helped us to find a novel 3, 5-dicyanopyridine organic framework with potential anti-diabetic activity.

Thus the study highlights the importance of pyridine compounds as anti-diabetic agents. The bioactivity can be improved upon by taking the most active molecules from this study and building new molecules by introducing different functional groups capable of forming hydrogen bonds with amino acids in the enzyme's active site. The easy one pot multi-component method involving benzaldehyde, thiol and malononitrile can yield compounds with broader substitutions of interesting bioactivities. Also metal complexes can be synthesized using these molecules and thus more bioactivities like anticancer can be introduced into these molecules.

Since the aim of this project is to make a significant contribution to the pharmaceutical industry; once two new classes of potential antibacterial and antidiabetic agents were generated, attention then turned to improving the currently available medication. Some of the identified shortcomings of the commercially available treatment are resistance, toxicity, and low solubility, with the last factor having a huge impact on permeability and thus efficacy.

In Chapter 5, we demonstrated a novel hybrid material constituting cyclodextrin capped AgNPs and antibacterial drug chloramphenicol for the application in combination therapy to overcome resistance and toxicity problems. Cyclodextrins attached to the surface of silver nanoparticles acted as both stabilizing and drug encapsulating agents. Initially α-, β- and γ-cyclodextrin supramolecules have been studied for their complexing ability with chloramphenicol, using

molecular modeling techniques. The computed binding free energies indicated the strong interaction between γ-cyclodextrin and chloramphenicol. To further confirm the results observed in theoretical calculation, the inclusion complex of chloramphenicol with γ-cyclodextrin was synthesized and thoroughly characterized. Thereafter γ-cyclodextrin capped silver nanoparticles were prepared, characterized and confirmed for their ability of molecular recognition of chloramphenicol using surface enhanced Raman spectroscopy studies. The chloramphenicol γ-cyclodextrin capped silver nanoparticles composite showed enhanced antibacterial activities against different bacterial species and clearly demonstrated that the organic-inorganic hybrid materials or nanocomposites can be an ideal platform for combination therapy. Thus this study has opened a new perspective of a novel combination therapy. Further studies can be considered for loading of other antimicrobial and anticancer drugs and multiple drug substances within the similar system but with a variety of inorganic material such as AgNPs, AuNPs and other metal nanoparticles to generate new treatments.

In Chapter 6, we demonstrated the salt formation of fluoroquinolones using quinate counter ion exchange. In a bid to further improve currently available antibacterial agents, solubility of both ciprofloxacin and norfloxacin was significantly increased by converting them into the quinate salt forms. As compared to the hydrochloride salts, quinate salts of fluoroquinolone's have higher octanol-water partition coefficient indicating their lipophilic character. This could help in simultaneous increase of solubility and permeability of fluoroquinolones. XRD data analysis confirms that the method of direct protonation followed by freeze drying yielded amorphous salt forms. Conversion of free bases to amorphous may increase the solubility, stability and bioavailability of drugs. The cytotoxicity studies indicated that quinic acid is biocompatible and did not increase the toxicity of fluoroquinolones when applied as a counter ion. The utility of the present work may be further improved by studying thermodynamic stability of salt forms, assessing drug absorption and permeability using *in vitro* tools like parallel artificial membrane permeability assay (PAMPA) and profiling salts for their solubility in bio-relevant dissolution media with different pH [11].

7.2 References

[1] A.G. Atanasov, B. Waltenberger, E.-M. Pferschy-Wenzig, T. Linder, C. Wawrosch, P. Uhrin, V. Temml, L. Wang, S. Schwaiger, E.H. Heiss, Discovery and resupply of pharmacologically active plant-derived natural products: A review, Biotechnology Advances, 33 (2015) 1582-1614.

[2] S. Dandapani, G. Rosse, N. Southall, J.M. Salvino, C.J. Thomas, Selecting, acquiring, and using small molecule libraries for high-throughput screening, Current Protocols in Chemical Biology, (2011) 177-191.

[3] J.J. Giner-Casares, M. Henriksen-Lacey, M. Coronado-Puchau, L.M. Liz-Marzán, Inorganic nanoparticles for biomedicine: where materials scientists meet medical research, Materials Today, (2015).

[4] J. Hughes, S. Rees, S. Kalindjian, K. Philpott, Principles of early drug discovery, British Journal of Pharmacology, 162 (2011) 1239-1249.

[5] R. Mullin, Cost to develop new pharmaceutical drug now exceeds $2.5 B, Scientific American, 24 (2014).

[6] L. Hutchinson, R. Kirk, High drug attrition rates—where are we going wrong?, Nature Reviews Clinical Oncology, 8 (2011) 189-190.

[7] Z.P. Qureshi, E. Seoane-Vazquez, R. Rodriguez-Monguio, K.B. Stevenson, S.L. Szeinbach, Market withdrawal of new molecular entities approved in the United States from 1980 to 2009, Pharmacoepidemiology and Drug Safety, 20 (2011) 772-777.

[8] R. McNaughton, G. Huet, S. Shakir, An investigation into drug products withdrawn from the EU market between 2002 and 2011 for safety reasons and the evidence used to support the decision-making, Biomedical Journal open, 4 (2014) e004221.

[9] A. Fabbretti, C.O. Gualerzi, L. Brandi, How to cope with the quest for new antibiotics, FEBS Letters, 585 (2011) 1673-1681.

[10] S. Riaz, I.U. Khan, M. Yar, M. Ashraf, T.U. Rehman, A. Shaukat, S.B. Jamal, V.C. Duarte, M.J. Alves, Novel pyridine-2, 4, 6-tricarbohydrazide derivatives: Design, synthesis, characterization and in vitro biological evaluation as α-and β-glucosidase inhibitors, Bioorganic Chemistry, 57 (2014) 148-154.

[11] C. Florindo, A. Costa, C. Matos, S.L. Nunes, A.N. Matias, C.M. Duarte, L.P.N. Rebelo, L.C. Branco, I.M. Marrucho, Novel organic salts based on fluoroquinolone drugs: Synthesis, bioavailability and toxicological profiles, International Journal of Pharmaceutics, 469 (2014) 179-189.

APPENDIX 1

RESEARCH RESULTS

Antipyrine-gamma cyclodextrin inclusion complex: Molecular modelling, preparation, characterization and cytotoxic studies

This manuscript was published in
Journal of Molecular Structure (2015)

Antipyrine-gamma cyclodextrin inclusion complex: Molecular modelling, preparation, characterization and cytotoxic studies

Ramesh Gannimani[a], Amanda Perumal[a], Muthusamy Ramesh[b], Karen Pillay[a], Mahmoud E. Soliman[b], Patrick Govender[a,*]

[a]Department of Biochemistry, School of Life Sciences, University of KwaZulu-Natal, Westville, Durban 4000, South Africa

[b]Discipline of Pharmaceutical Sciences, School of Health Sciences, University of KwaZulu-Natal, Westville, Durban 4000, South Africa

A 1.1 Abstract

Molecular docking, semi-empirical and molecular dynamics studies were conducted for α, β and γ- cyclodextrin-associated inclusion complexes of antipyrine. The results of molecular modeling were systematically analyzed to determine the stability of inclusion complexes. In preliminary computational screening, β and γ-cyclodextrin inclusion complexes of antipyrine were found to be more stable as compared to α-cyclodextrin based on docking score and binding free energies. Further, inclusion complex of antipyrine with γ-cyclodextrin was prepared by freeze drying method. Formation of the inclusion complex was investigated by solid state characterization techniques such as thermogravimetric analysis, differential scanning calorimetry, X-ray diffraction, Fourier transform infrared spectroscopy and scanning electron microscopy. The changes observed in decomposition temperature, diffractogram, vibrational frequencies and morphological appearance confirmed the formation of inclusion complex. In addition, results from ^{1}H NMR and 2D NOESY studies supported the inclusion phenomenon. The results obtained from computational studies were found to be in consistent with experimental data to ascertain the encapsulation of antipyrine into γ-cyclodextrin. The inclusion complex was found to be non-toxic towards MDCK-1 cell lines. Thus, this approach may be helpful in the formulation of drug molecules using cyclodextrins.

A 1.2 Key words

Molecular modeling, binding free energies, antipyrine, γ-cyclodextrin, inclusion complex

A 1.3 Introduction

Cyclodextrins (CDs) are truncated, cone-shaped cyclic host materials made up of α-D-glucopyranose units linked by α-1,4 glycosidic bonds [1]. They are commercially available in the form of α, β and γ with varying number of glucose units (6-8) and cavity size (5-9 Å) [2]. The α-D-glucopyranose of cyclodextrin exists in stable $^4C_1$ chair conformation, with hydrophobic ether linkages and carbon skeletons of glucose units inside and hydrophilic hydroxyl groups outside the cavity of CD [3]. This structural arrangement makes the CDs amphiphilic in nature. Cyclodextrins have the ability to form supramolecular host-guest assemblies with a variety of organic and inorganic molecules. The driving forces for this phenomena include weak van der Waals forces, hydrogen bonding and charge transfer interactions between the host and guest molecule [4]. The process is also influenced by thermodynamic factors such as enthalpy and entropy changes associated with replacement of water molecules from the CD cavity by hydrophobic molecules [4]. There is a huge interest in the cyclodextrin-based pharmaceutical formulation due to their ability to improve water solubility, stability and bioavailability of a variety of potential drugs [5]. Furthermore, CDs are biodegradable and do not require additional treatment to remove them after application [6]. The cyclodextrin derived materials can also effectively remove the organic and inorganic pollutants present in water [3, 7, 8]. CDs and their chemical modifications thus provide novel applications in both pharmaceutical and environmental related fields.

Antipyrine (AP; 2,3-dimethyl-1-phenyl-5-pyrazolone) is an inhibitor of cyclooxygenase and is known for anti-inflammatory, analgesic and antipyretic activity in clinical therapy [9]. Antipyrine and their derivatives have also been reported for a variety of pharmacological activities [10, 11]. AP is a commonly used non-steroidal anti-inflammatory drug (NSAID) and is also one of the pharmaceutical products that contaminate water sources [12]. The most common side effects of NSAIDs include ulcer perforation and upper gastrointestinal bleeding. These side effects can be minimized by complexion with CDs, as they release the drug in a controlled manner thereby making drugs effective at lower dosages [13].

The long term exposure of AP through water contamination exerts toxic effects causing damage to lungs and mucosa [14]. Recently, chlorination of water, use of activated persulfate and hydroxide radicals were discussed for the degradation of AP or phenazone-like compounds in the water [15-17]. However, the use of cyclodextrin-derived polymers and materials could be an interesting strategy for the treatment of AP contamination as they are harmless to nature.

Hence, understanding the host-guest relationship between AP and CDs will help in designing suitable CD-based material for water treatment. The study of AP inclusion complexes is thus significant in view of both pharmaceutical and environmental interests.

The inclusion complex of AP with β-CD in the solid state has previously been studied and it was suggested that the existence of AP in a betainic state which forms a weak inclusion with β-CD in the solution state [18]. Furthermore the formation of inclusion complex was characterized by thermal analysis [18]. However, to the best of our knowledge the role of γ-CD in the formation of inclusion complex with AP has not been described. In this study, we detail the molecular modeling of inclusion complexes of AP with α, β and γ cyclodextrins, using semi-empirical AM1 calculation methods. In addition, the synthesis, characterization and cytotoxicity of AP/γ-CD inclusion complex has been discussed in detail.

A 1.4 Materials and Methods

A 1.4.1 Computational Studies

A 1.4.1.1 Preparation of 3D structures of α-, β- & γ-cyclodextrins and antipyrine

The crystal structures of α-CD (PDB code: 2ZYM) [19], β-CD (PDB code: 3CGT) [20] and γ-CD (PDB code: 2ZYK) [21] were extracted from protein data bank (PDB). The structure of AP was obtained from Pubchem (CID: 2206). The missing hydrogen atoms to CDs and atomic charges to CDs as well as AP were added using CHIMERA software package [22]. These structures were used as a starting point to perform the computational studies.

A 1.4.1.2 Molecular docking

The complexes of AP with α-, β- and γ-CD were generated from molecular docking approaches. Molecular docking was carried out using AutoDock software which employs Lamarckian genetic algorithm [23]. The Lamarckian aspect is an added feature that allows individual conformations to search their local conformations. AutoDock uses a grid based method to allow rapid evaluation of the binding free energy. The solution of AutoDock is based on the energy scores of final docking energy (FDE) and the estimated final energy of binding (EFEB). The energies comprise van der Waals, electrostatic interactions, the loss of entropy and the number of hydrogen bonds. To perform molecular docking, CDs were defined as a receptor and AP was defined as a ligand. The binding site was located using GRID and the GRID was defined from the centroid of the cavity of CDs. The top ranked complex of AP with α-CD, β-CD and γ-CD were separately stored for AM1 and AMBER studies.

A 1.4.1.3 Semi-empirical calculation

The complexes of AP with three different CDs were optimized by AM1 method using Gaussian03 software packages [24]. Analytical frequencies were also computed at the same level to characterize the optimized structures as minima or transition states (one negative frequency) on the potential energy surface. Partial atomic charges were estimated by performing Mulliken population analysis.

A 1.4.1.4 Molecular dynamics simulations

Molecular dynamics (MD) simulations were carried out using AMBER 12 software packages running under GPU version of PMED engine [25]. The atom types were modeled using ANTECHAMBER module of AMBER software packages [26]. The FF99SB force field was used to describe the solvent system [27]. The hydrogen atoms were added to the α-CD, β-CD and γ-CD using LEAP module incorporated in AMBER. The system was neutralized by the addition counter ions either Na^+ or Cl^-. The system was embedded within an orthorhombic box (8 Å) composed of TIP3P water molecules [28]. Periodic boundary conditions were maintained. The long range electrostatic interactions were treated based on particle mesh Ewald method [29]. A restraint potential of 500 kcal/mol A^2 was applied to the solute. Initial energy minimization was performed for 2500 steps using steepest descent algorithm. Further, 2500 steps of unrestrained conjugate gradient minimization were carried out. Canonical ensemble (NVT) MD simulations were then carried out for 50 ps, with gradual heating from 0 to 300K with harmonic restraints of 5 kcal/mol A^2 was applied to all solute atoms and a Langevin thermostat with a random collision frequency of 1/ps. The systems were subsequently equilibrated at 300 K in the NPT ensemble for 500 ps, during which no restraints were imposed and a Berendsen barostat was used to maintain the pressure at 1 bar. The bonds of all hydrogen atoms were constrained using SHAKE algorithm [30]. For MD runs, SPFP precision model was used [31]. Production MD runs were performed for 10 ns in an isothermal isobaric (NPT) ensemble using a Berendsen barostat with a target pressure of 1 bar. The trajectories were saved and analysed in every 1ps using CPPTRAJ module integrated with amber 12.

A 1.4.1.5 Binding free energy calculation

The binding free energies for the α-CD, β-CD and γ-CD associated inclusion complex of AP was carried out using Molecular Mechanics- Poisson-Boltzmann surface Area (MM-PBSA) [32, 33]. The binding free energies were averaged over 200 snapshots taken from the post equilibrated 10ns MD trajectory at 10 ps intervals. To determine the individual energy contribution towards total binding free energy between AP and cyclodextrin, a decomposition analysis of the interaction energy was computed by MM/PBSA binding free energy decomposition protocol in Amber 12. The following equation (**Eq.1**) was employed to compute the binding free energies.

$$\Delta G_{bind} = G_{complex} - G_{receptor} - G_{ligand} \quad \textbf{(Eq.1)}$$

A 1.4.2 Preparation of inclusion complex and physical mixture

The inclusion complex of AP was prepared by freeze drying method [34]. A solution of γ-CD (Wacker Chemie; 1.38 g) and AP (Fluka; 0.2 g) prepared in 25 ml of double distilled water in 1:1 molar ratio and stirred at room temperature for 48 hrs The resulting clear solution was frozen at -72 °C for 4 hrs and freeze-dried to yield a white amorphous solid. On the other hand, sample of physical mixture was obtained by mortaring 1:1 mixture of each reactant.

A 1.4.3 Characterization of the inclusion complex

Powder X-ray diffraction (XRD) patterns were recorded on a Bruker D8 Advance instrument equipped with an Anton-Paar XRK 900 reaction chamber and a Cu radiation source with a wavelength of 1.5406 Å at ambient temperature. Infrared spectra of AP, CD and inclusion complex were recorded on a Perkin Elmer Spectrum 100 FT-IR spectrometer with universal ATR sampling accessory. Thermogravimetric analysis-differential scanning calorimetry (TGA-DSC) was conducted on SDT Q600 TA instrument. The temperature of samples was increased from 25-800°C at a heating rate of 10°C min^{-1} under nitrogen atmosphere. Morphological studies of the samples were performed using scanning electron microscope (FEGSEM ZEISS

ULTRAPLUS). Samples for SEM analysis were prepared by fixing powdered sample on adhesive carbon tape glued over metal stub and thin gold coating was added to make samples more electrically conductive. The samples were observed at 10000X magnification with an excitation voltage of 20 kV. ^{1}H nuclear magnetic resonance (NMR) spectra were recorded on a Bruker Avance^{III} 400 MHz spectrometer. ^{13}C APT, COSY, HSQC and NOESY spectra were recorded on a Bruker Avance^{III} 600 MHz spectrometer at 30°C. Chemical shifts (δ) were recorded using tetramethylsilane (TMS) as the internal standard. The spectrometers were equipped with a BBOZ probe. In the ^{1}H-^{1}H NOESY experiment, the mixing time was 300 ms and relaxation time was 1s. Samples were prepared in deuterium oxide. The chemical shifts were referenced to the residual water signal of D_2O.

A 1.4.4 Cytotoxicity studies

The MDCK-1 cell line (European Collection of Cell Cultures, Sigma-Aldrich) was cultured in RPMI 1640 growth medium containing 10% heat-inactivated fetal bovine serum, 2 mM glutamine, 1 mM sodium pyruvate, 25 mM 2-[4-(2-hydroxyethyl)-1-piperazinyl] ethanesulfonic acid (HEPES), and 0.1 mg/mL penicillin/streptomycin. Cells were plated at a density of 1×10^4 cells/mL (100 µL/well) 96 well plates (Sigma-Aldrich) and incubated at 37 °C for 24 hours. Thereafter, spent media were removed from all wells and fresh fully constituted media containing AP, free CD or inclusion complexes at varying concentrations (7.8-500 µM) were added. Plates were incubated at 37 °C for a further 24 hours before the CellTiter 96 AQueous One Solution Assay (Promega, Madison, WI) was performed. This assay was carried out as per manufacturer's instructions to assess cell viability by measuring the cellular reduction of 3-(4,5-dimethylthiazol-2-yl)-5-(3-carboxymethoxyphenyl)-2-(4-sulphenyl)-2H- tetrazolium (MTS). Absorbance readings for the MTS assay were performed using an Automated Microplate Reader (Synergy HT) from Bio-Tek Instruments. Untreated cells were used as the control. All samples were assayed on two separate occasions and in triplicate.

A 1.5 Results and discussion

A 1.5.1 Prediction of the binding mode of antipyrine inside cyclodextrins

The possible binding mode of the inclusion complex of AP with α-, β- and γ-CD was identified from molecular docking approaches. The top ranked pose of AP inside CD was considered as a favorable binding mode. In docking pose, the phenyl ring of AP was slightly penetrated inside the cavity of α-CD and the pyrazole ring was found to be positioned away from the cavity (**Fig. A 1.1 a**). This could be attributed towards lower cavity volume of α-CD. In the inclusion complex of AP-β-CD, the phenyl ring was deeply penetrated toward the primary hydroxyl rim of β-CD whereas the pyrazolone ring oriented toward secondary hydroxyl rim **(Fig. A 1.1 b)**. In case of AP-γ-CD inclusion complex, the entire skeleton of AP was completely sequestered due to larger cavity volume **(Fig. A 1.1 c)**. The docking scores of the inclusion complex suggested the favorable formation of inclusion complex of AP with β-CD (-4.7) and γ-CD (-4.5) **(Table A 1.1).**

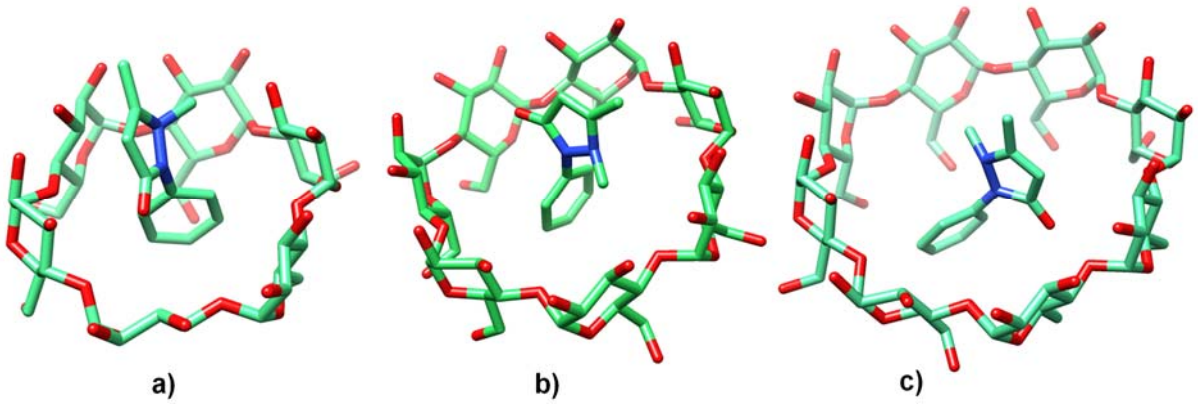

Figure A 1.1 The binding mode of AP inside the cavity of **a)** α-cyclodextrin **b)** β-cyclodextrin and **c)** γ-cyclodextrin.

Table A 1.1 Docking scores of antipyrine with three different cyclodextrins

Cyclodextrins	Ligand	Docking Scores
α-CD	AP	-0.7
β-CD	AP	-4.7
γ-CD	AP	-4.5

A 1.5.2 Conformational analysis of antipyrine inside cyclodextrins

The top ranked pose of AP obtained molecular docking using three different CDs was subjected for geometry optimization in order to determine the stable conformation and interactions. The geometry optimization was carried out using semi-empirical method since the inclusion system constitutes larger number of atoms (AP-α-CD: 152 atoms; AP-β-CD: 173 atoms and AP-γ-CD: 194 atoms). The approach reduces the computational cost as compared to *ab initio* studies. AM1 is one of the most accurate semi-empirical computational methods. The method ignores or approximates the some of the integrals employed in *ab initio* methods. In this study, the geometry optimization was carried out based on AM1 method. In the optimized geometry of AP-γ-CD inclusion complex, antipyirine achieved twisted conformation with a bond angle of (θ_1=117.25°) across C-N-N bond and (θ_2=116.32°) across C-N-C bond. This angle was found to be diminished as compared to the optimized geometry of AP alone (θ_1=123.41°; θ_2=126.65°). In the optimized geometry of AP -γ-CD inclusion complex, AP enters into the γ-CD cavity from its phenyl ring and deeply penetrated into the cavity towards the edge of primary hydroxyl group of sugar unit **(Fig. A 1.2)**. This can be related to appearance of NOESY peaks between H6 of γ-CD and aromatic protons of AP. The distance between the hydrogens of AP and γ-CD were found to be in the range of 2.3-5 Å, suggests the transfer of spin polarization between the protons of AP and γ-CD possible. This was further confirmed by the appearance of several NOESY interactions in 2D NMR studies. The carbonyl IR frequency was also shifted to low indicating a strong hydrogen bond with cyclodextrin protons, which can be possible when pyrazolone ring of the AP is inside the cavity. Thus FTIR spectra also correlate with molecular models obtained.

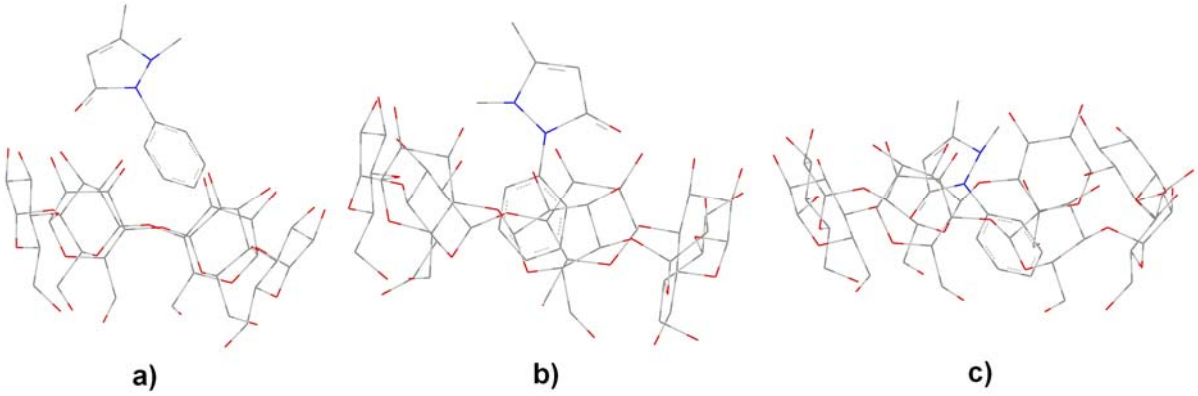

Figure A 1.2 The optimized geometry of antipyrine with **a)** α-cyclodextrin **b)** β-cyclodextrin and **c)** γ-cyclodextrin.

A 1.5.3 Host-guest interactions of antipyrine and cyclodextrins

To analyze the guest-host interactions of AP with CD, the binding affinity of AP with three different CDs were computed based on MD simulation **(Table A 1.2) (Fig. A 1.3)**. The binding free energies were calculated using MM-PBSA method. The binding free energy for the complexes of AP with α, β and γ-CD was found to be 13.82 kcal/mol, 21.13 kcal/mol and 19.52 kcal/mol respectively. The results indicate the favorable formation of inclusion complex of AP with β-CD and γ-CD over α-CD. A similar trend was also observed in molecular docking analysis.

The van der Waals and electrostatic interactions were found to be main forces contributing for ligand binding. The van der Waals interaction was higher in both AP-β-CD (-28.1691±0.1321 kcal/mol) and AP- γ-CD (-24.9421±0.0997 kcal/mol) complexes due to closer contacts of guest and host moiety , whereas it was found to be -13.8241±0.1547 kcal/mol in case of AP-α-CD inclusion complex due to lack of encapsulation. The electrostatic interaction between AP and γ-CD is highly favorable (-7.1133±0.2069 kcal/mol) as compare to β-CD (-7.0764±0.1501 kcal/mol) and α-CD (-5.1102±0.2311 kcal/mol) suggesting β-CD and γ-CD as the suitable encapsulating material for AP. The quantitative information of van der Waals interaction, electrostatic interaction, binding free energy can be useful to understand the guest-host interactions of AP-CD inclusion complexes and to determine its favorable formation.

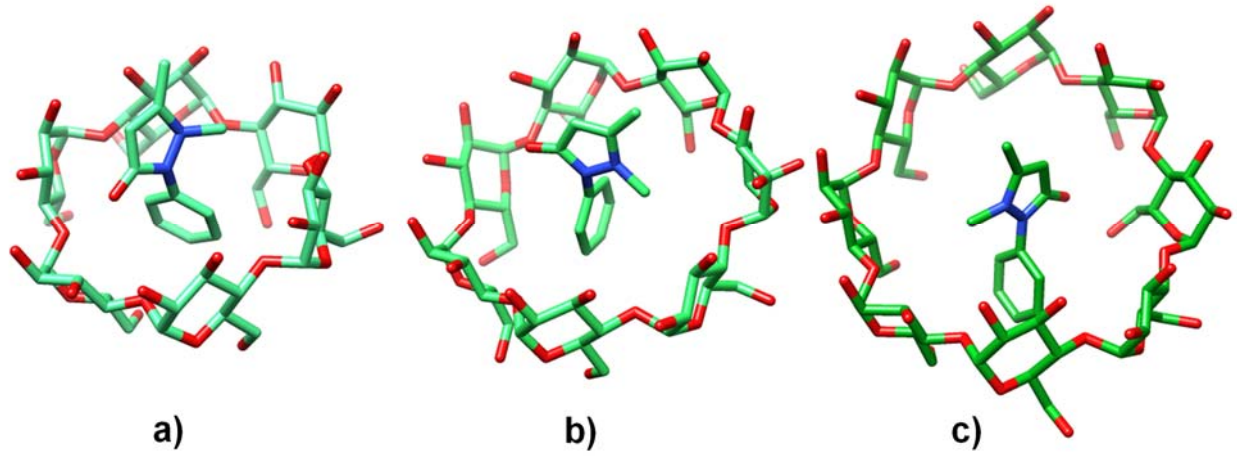

Figure A 1.3 The energy minimum conformation of antipyrine with **a)** α-cyclodextrin **b)** β-cyclodextrin and **c)** γ-cyclodextrin obtained from molecular dynamics simulations.

Table A 1.2 The computed binding free energies of the inclusion complexes

Inclusion complexes	ΔG_{bind}	ΔE_{ele}	ΔE_{vdW}	ΔG_{gas}	ΔG_{sol}
AP-α-CD	13.8241±0.1547	5.1102±0.2311	17.5783±0.1600	22.6886±0.2683	8.8645±0.1654
AP-β-CD	21.1339±0.1296	7.0764±0.1501	28.1691±0.1321	35.2455±0.2041	14.1117±0.1239
AP-γ-CD	19.5201±0.1244	7.1133±0.2069	24.9421±0.0997	32.0554±0.2246	12.5353±0.1329

A 1.5.4 X-ray powder diffractometry

The X-ray diffraction pattern of AP, γ-CD, physical mixture and inclusion complex were studied using powdered XRD. The formation of inclusion complex causes major changes in the diffraction pattern of both guest (AP) and host (CD). The changes were observed in the form of disappearance, decreased intensity, broadening and appearance of new peaks. The powder XRD patterns of AP and γ-CD showed strong sharp peaks due to their crystalline nature. Sharp and intense peaks were observed for AP at 2θ = 10.2 (d = 7.38), 24 (d = 3.72) and for γ-CD at 2θ = 12 (d = 6.92), 16.5 (d = 4.47), 19 (d = 4.18) and 22 (d=3.85) **(Fig. A 1.4)**. These peaks were not found in the diffractogram of inclusion complex, instead broad peaks were observed confirming the amorphous nature of inclusion complex. Thus by converting guest molecule to amorphous, the solubility of AP may increase [35]. However intense sharp peaks found in the physical mixture at 2θ = 12.5 (d = 7.31) and 20.5 (d = 4.37) which indicates simple mixing did not result in the formation of inclusion complex. The changes in diffractogram confirms the formation of inclusion complex and similar results have been observed in other cases [36, 37].

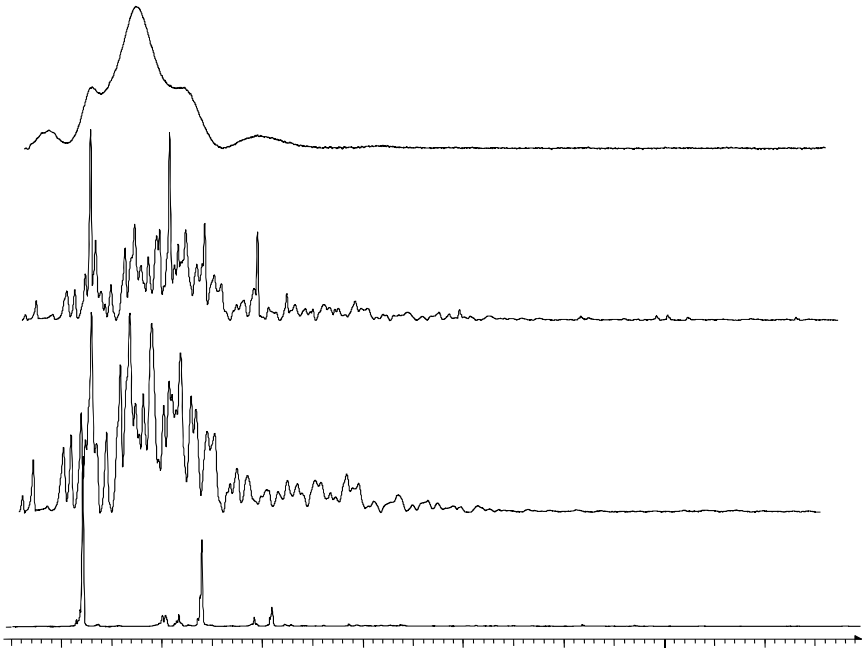

Figure A 1.4 Diffractograms of **a)** AP, **b)** γ-CD, **c)** Physical mixture and **d)** Inclusion complex (AP-γ-CD).

A 1.5.5 FTIR-ATR spectroscopy measurements

The formation of inclusion complex was studied from the changes in the infrared vibrational frequencies of chemical bonds resulting from the inclusion phenomenon. The formation of inclusion complex alters the molecular interactions such as hydrogen bonding, dipole-dipole interaction [38], which results in the IR frequency shift of functional groups [39]. The FTIR spectrum of γ-CD **(Fig. A 1.5)** was characterized by a broad band at 3260 cm^{-1} for the primary and secondary OH groups. The position of this band is shifted to higher frequency 3295 cm^{-1} and is broadened after the formation of inclusion complex. The bands at 1615, 1588 and 1496

cm^{-1} confirm the presence of AP in the complex. In inclusion complex the carbonyl frequency of AP was shifted from 1659 to 1615 cm^{-1}. The lowering of carbonyl group frequency of AP could be due to its reduced double bond character resulted from its involvement in the hydrogen bonding interaction with hydroxyl groups of γ-CD. The close proximity of carbonyl groups to hydroxyl groups of γ-CD (2 Å) was found in the optimized geometry of inclusion complex. The intensity of peaks at both functional group and finger print region for AP was also significantly reduced in the inclusion complex. These variations in the IR spectrum of the inclusion complex can be attributed to intermolecular interactions between the AP and γ-CD [40].

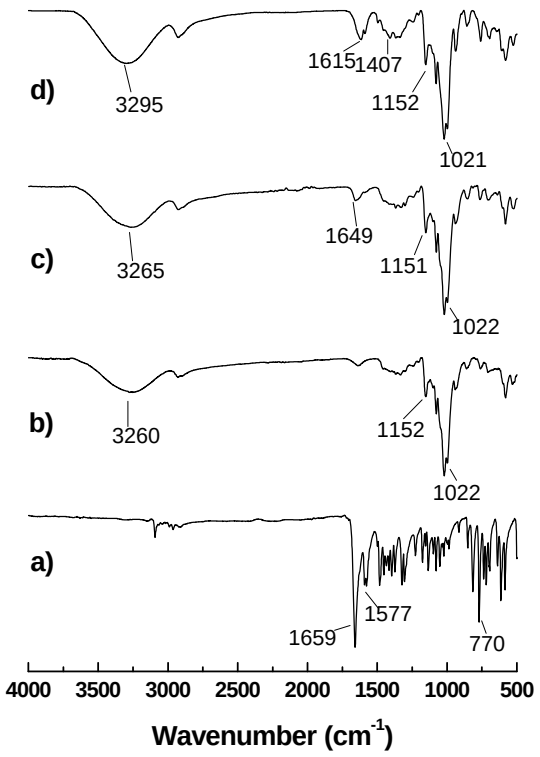

Figure A 1.5 FTIR spectra of **a)** AP, **b)** γ-CD, **c)** Physical mixture and **d)** Inclusion complex.

A 1.5.6 Thermogravimetric and differential scanning calorimetric analyses

Thermal degradation properties of the samples were studied by thermogravimetric analysis where the weight loss of the sample was studied as a function of temperature under nitrogen atmosphere. The change in the thermal stability of AP and γ-CD on formation of inclusion complex was studied by comparing TGA and DSC curves **(Fig. A 1.6)**. The AP exhibited single weight loss between the temperature 210-335°C. On the other hand, the encapsulating γ-CD exhibited weight loss at two different points. The first weight loss at 25-125°C was due to dehydration and another weight loss at 290°C was due to decomposition of γ-CD. In inclusion complex the corresponding weight loss for AP was observed at 255°C suggesting the increased thermal stability of AP **(Fig. A 1.6 d).**

The DSC analysis of samples provided further evidence for the formation of inclusion complex. The DSC thermogram of AP showed a sharp endothermic peak at about 110°C (**Fig. A 1.6 a)** which was consistent with its melting point. Similar peak was also observed in the DSC curve of physical mixture (**Fig. A 1.6 c)**. However, DSC of inclusion complex did not show up this endothermic peak (**Fig. A 1.6 d)**. The loss of endothermal melting peak of crystalline AP confirms the formation of inclusion complex [41]. These findings were found in agreement with the XRD analysis results. The change in intermolecular interaction caused by the formation of inclusion complex results in the loss of crystallinity of antipyrine and thus no endothermic peak was observed for the inclusion complex. The DSC of γ-CD and physical mixture also exhibited broad endothermic peak between 310°C to 330°C respectively.

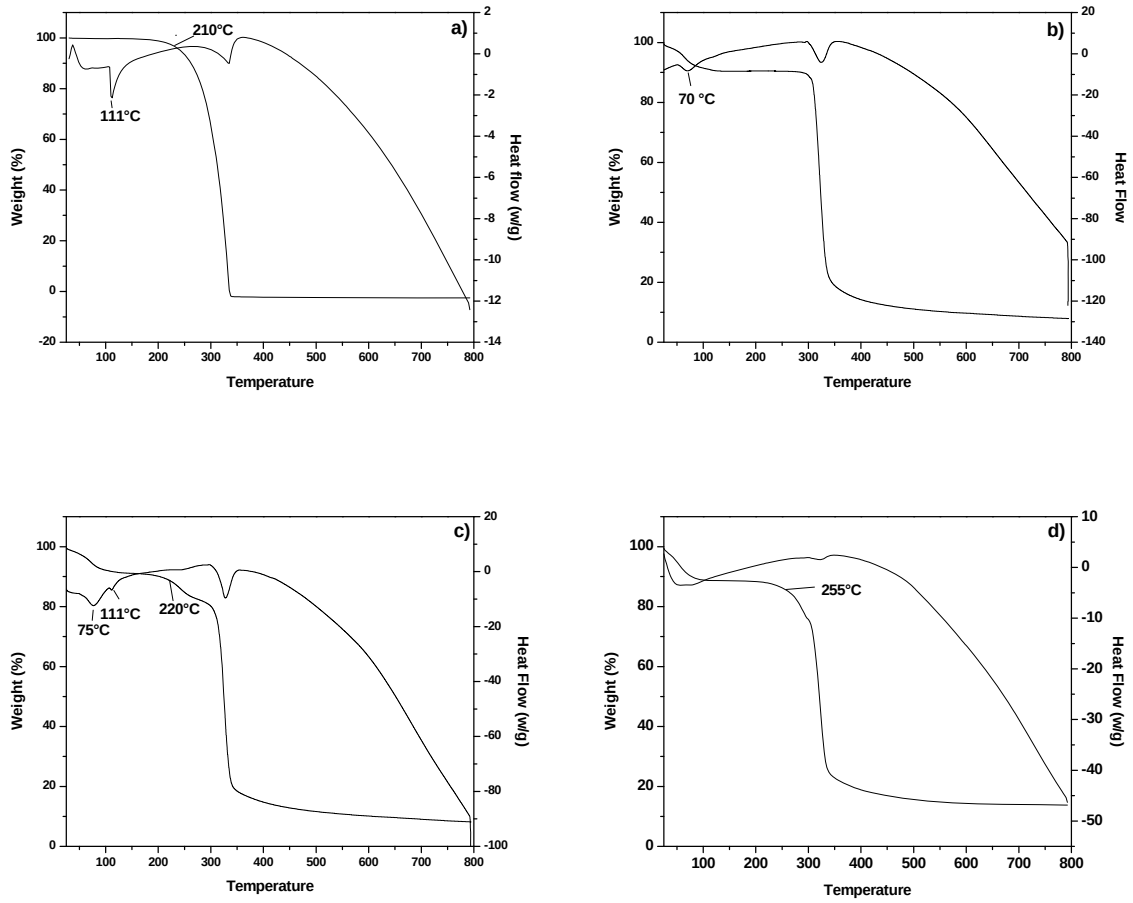

Figure A 1.6 TGA and DSC curves of **a)** AP, **b)** γ-CD **c)** Physical mixture and **d)** Inclusion complex.

A 1.5.7 Scanning electron microscopy

The change in the structure and physical appearance of substances on the formation of inclusion complex was studied by SEM technology. The AP appeared as irregular plate like structures **(Fig. A 1.7 a)** whereas γ-CD appeared as parallelogram shapes **(Fig. A 1.7 b).** Physical mixture contained morphology of both the components **(Fig. A 1.7 c)**. In the inclusion complex, a single component with completely different and irregular amorphous morphology was observed **(Fig. A 1.7 d)**. The morphological changes which appeared in SEM images confirm the existence of interaction between AP and γ-CD [42].

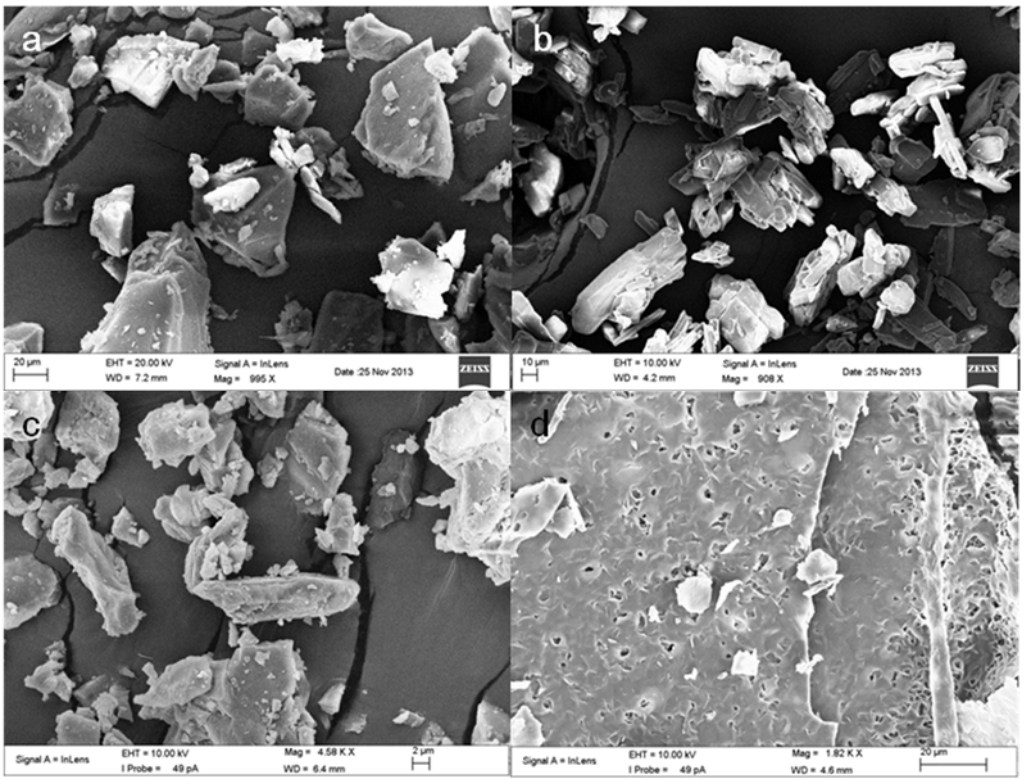

Figure A 1.7 The morphological appearance of **a)** AP, **b)** γ-CD and **c)** Physical mixture **d)** Inclusion complex.

A 1.5.8 NMR analysis

^{1}H NMR and two dimensional NOESY spectroscopy provides detailed information about inclusion mode [43, 44]. The significant chemical shift variations of host γ-CD and guest AP protons that occurred in the ^{1}H spectrum provided preliminary evidence for the formation of inclusion complexes in solution. The magnetic anisotropy of the aromatic ring of AP in the hydrophobic cavity of γ-CD results in these chemical shift changes [45]. **Fig. A 1.8** represents ^{1}H NMR spectra of γ-CD, AP and their inclusion complex. Peak assignments for the protons of γ-CD in ^{1}H NMR was performed according to the previous report [46]. From the ^{1}H NMR spectrum of the inclusion complex, it is evident that all the cyclodextrin protons, namely, H1-H6 chemical shifts were slightly shifted up-field and protons of AP shifted downfield, resulting from inclusion of the guest molecule into the hydrophobic cavity of γ-CD . The ^{1}H chemical shifts of γ-CD in the presence and absence of AP are shown in **Table A 1.3** and **A 1.4**. It is observed that the protons named H3 and H5 of γ-CD shifted the most. Since these protons lie inside the cavity, they are the ones most affected, and this thus confirms the formation of inclusion complex.

Table A 1.3 ^{1}H NMR chemical shifts corresponding to γ-CD in the presence and absence of AP

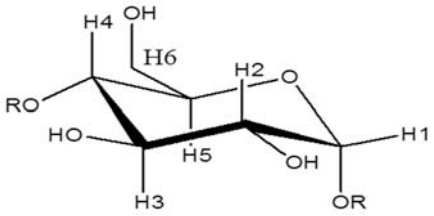

γ-CD proton	$\delta_{(free)}$	$\delta_{(complex)}$	$\Delta\delta = \delta_{(free)} - \delta_{(complex)}$
H1	5.0428	5.0322	0.0106
H2	3.5871	3.5786	0.0085
H3	3.8672	3.8399	0.0273
H4	3.5217	3.5121	0.0096
H5	3.7817	3.7582	0.0235
H6	3.8046	3.7883	0.0163

Table A 1.4 ^{1}H NMR chemical shifts corresponding to AP in the presence and absence of γ-CD

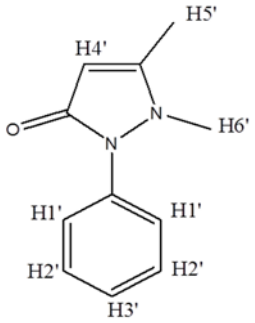

AP proton	$\delta_{(Complex)}$	$\delta_{(free)}$	$\Delta\delta = \delta_{(Complex)} - \delta_{(free)}$
H1'	7.2996 d	7.2216 d	0.078
H2', H3'	7.521 (m, 7.4844-7.5575)	7.467 (m, 7.4474-7.4871)	0.054
H4'	5.344	5.306	0.038
H5'	2.23	2.175	0.055
H6'	3.177	3.089	0.088

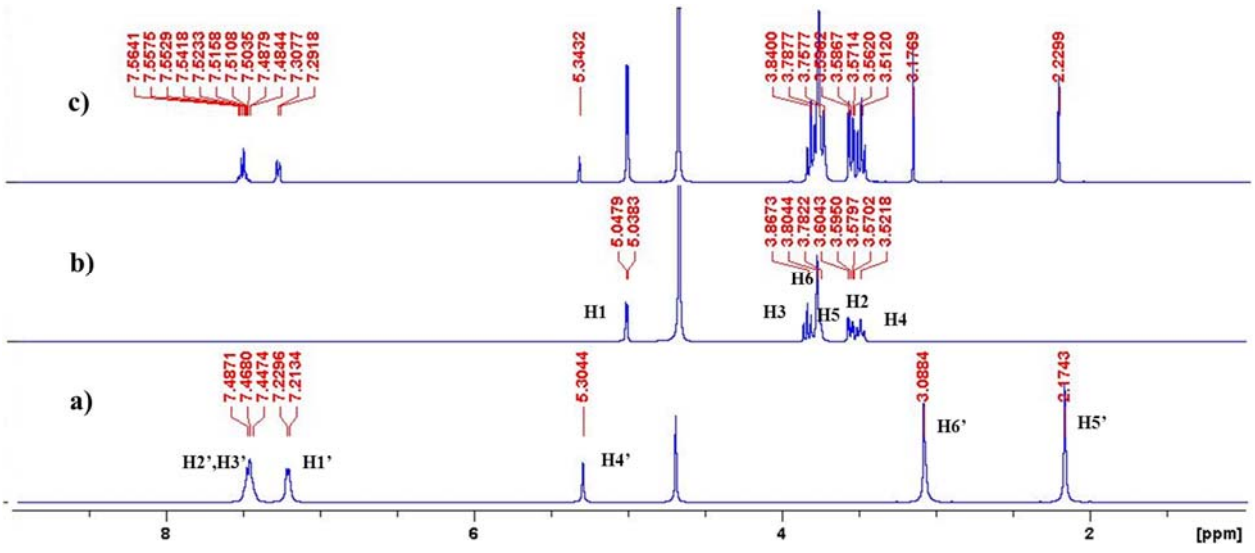

Figure A 1.8 ^{1}H NMR spectra of **a)** AP, **b)** γ-CD and **c)** Inclusion complex of AP with γ-CD.

The NOESY spectrum of the inclusion complex exhibited interesting NOE interactions between the AP and γ-CD protons. NOE interactions are highlighted in **Fig. A 1.9 a**. Protons in the vicinity of 2-5 Å shows NOE correlations in 2D NMR [47]. The protons H1'-H4' of AP exhibited prominent NOE interactions with protons of γ-CD i.e. H2, H3, H5 and H6 **(Fig. A 1.9 b)**. These NOE peaks were further confirmed by studying sequential COSY **(Fig. A 1.10)** coupling in HSQC **(Fig. A 1.11)** spectrum. The characteristic well separated anomeric protons (H-1) of the glucose unit of γ-CD and the methyl and methylene protons of AP were the most convenient points for the elucidation of 2D NMR spectra of the inclusion complex. Using these protons as a reference, chemical shifts and correlations of all other protons of γ-CD were confirmed. After the assignment of protons, the corresponding carbon atoms were identified using the HSQC spectrum. To further confirm our observation in the NOESY spectrum, we studied the molecular models. It was observed that the aromatic ring of AP was close to the edge of primary hydroxyl groups of γ-CD and distance between the H1'-H4' of AP and H3, H5 and H6 protons of γ-CD was found to be in the range of 2.4-5Å. It seems that NOESY interactions are possible. Interestingly there were also NOESY interaction between aromatic protons of AP (H1', H2' and H3') with H2 of γ-CD and methyl (H5' and H6') and methylene (H4') protons of AP **Fig. A 1.9 a**. Thus the major changes in the δ values of H3 and H5 protons lying inside the cavity of γ-CD and NOE interaction between the AP and γ-CD confirms the formation of inclusion complex.

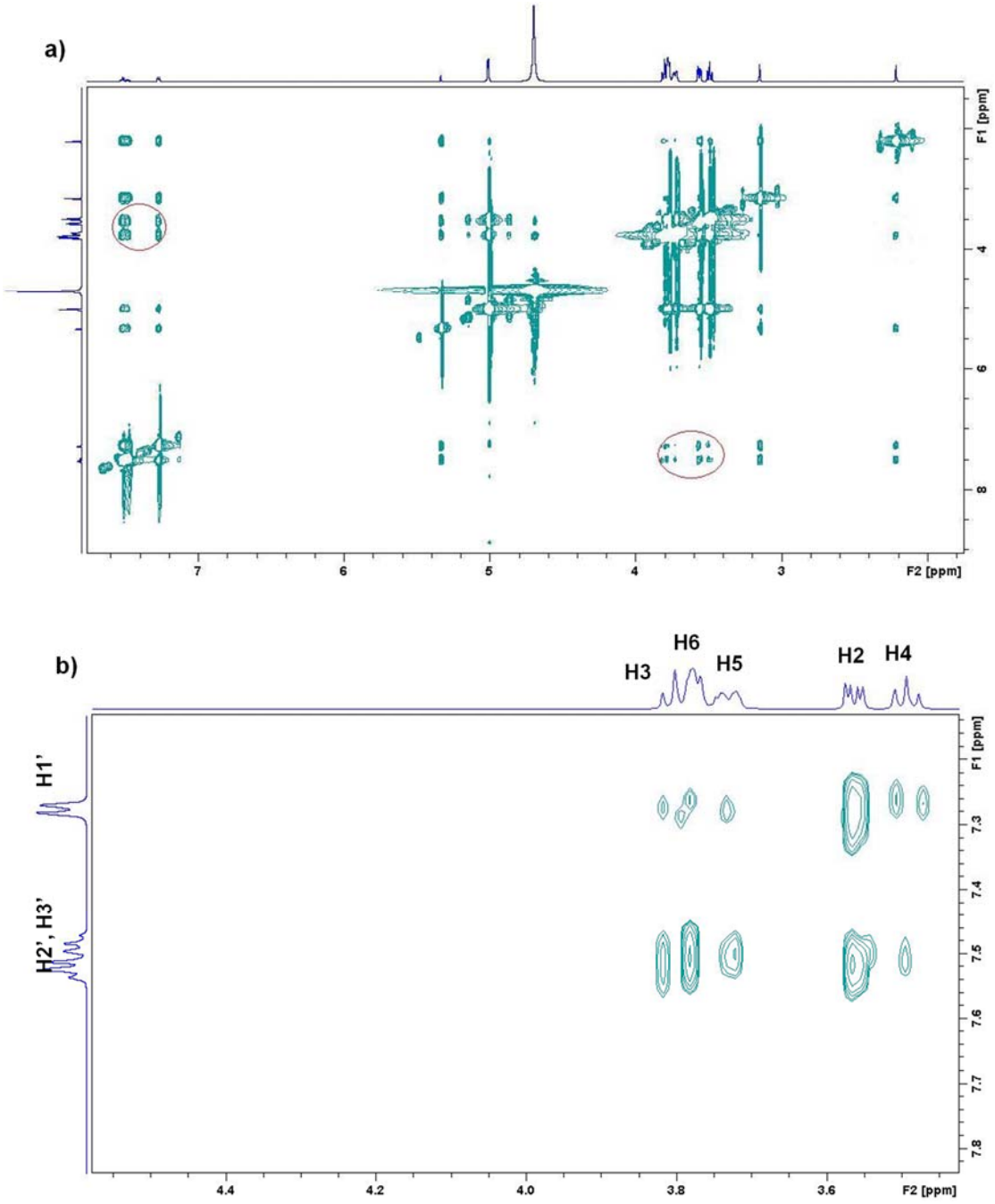

Figure A 1.9 **a)** 2D NOESY spectrum of inclusion complex **b)** Expanded region of 2D NOESY spectrum showing ^{1}H-^{1}H NOE interaction between aromatic protons of AP and γ-CD.

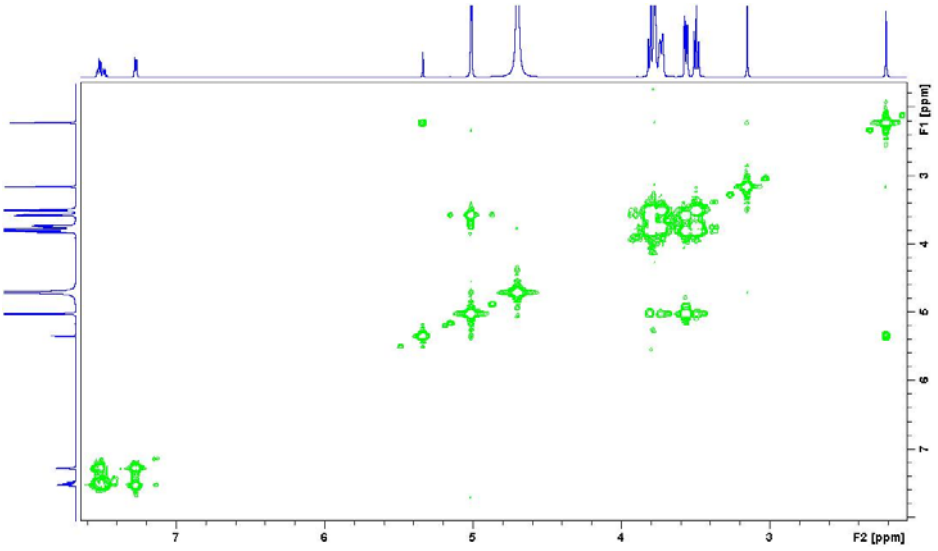

Figure A 1.10 COSY spectrum of inclusion complex.

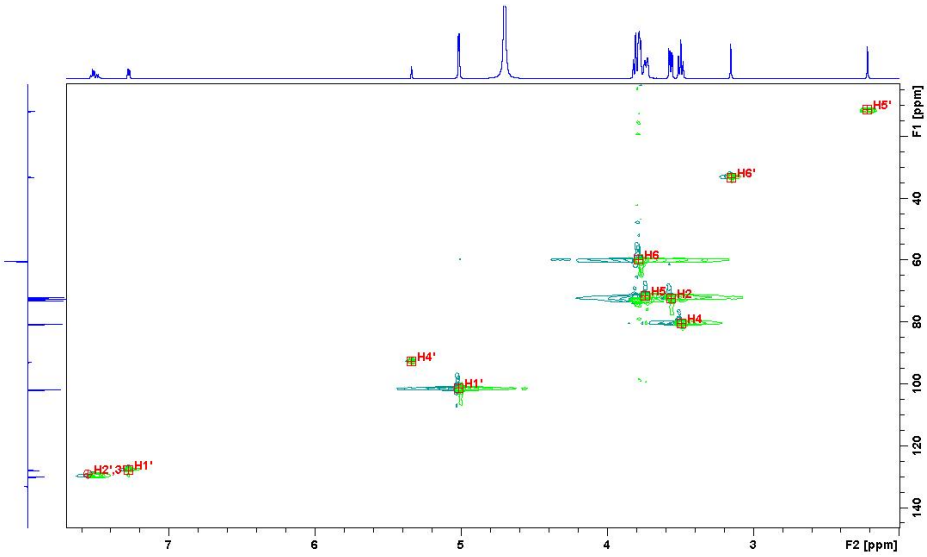

Figure A 1.11 HSQC spectrum of inclusion complex.

A 1.5.9 Cytotoxicity

The *in vitro* comparison of cytotoxicity of free AP, γ-CD and inclusion complex was assessed to verify its safe application in pharmaceutical formulations. For all the tested concentrations (7.8-500 µM) of AP, γ-CD and inclusion complex, cell viabilities greater than 85% were observed indicating that γ-CD inclusion did not induce or increase the toxicity of AP. Hence, cyclodextrin based approach for the design of new formulations of AP would be an interesting strategy.

A 1.6 Conclusion

In this study, molecular modeling techniques were employed to identify the possible conformation of inclusion complexes of AP. Based on the computed binding free energies β-CD and γ-CD were found to be a suitable polymers for encapsulation. The encapsulation of AP inside the cavity of γ-CD was thoroughly characterized by calorimetric and spectroscopic techniques. In addition, the toxicity profile of the inclusion complex (AP-γ-CD) was also investigated. The inclusion complex of AP-γ-CD was found to be non-toxic against MDCK-1 cells even at high concentration. The approach of making use of inclusion complexes may help in the design and development of γ-CD associated pharmaceutical formulations. In addition, the knowledge gained in this study may be applied for the treatment of AP contaminated water using γ-CD derived polymers and materials.

A 1.7 Acknowledgement

This research was funded by National Research Foundation (NRF) of South Africa and the University of KwaZulu-Natal, South Africa.

A 1.8 References

[1] L. Szente, J. Szeman, Cyclodextrins in Analytical Chemistry: Host-Guest Type Molecular Recognition, Analytical Chemistry, 85 (2013) 8024-8030.
[2] E.M.M. Del Valle, Cyclodextrins and their uses: a review, Process Biochemistry, 39 (2004) 1033-1046.
[3] N. Morin-Crini, G. Crini, Environmental applications of water-insoluble β-cyclodextrin–epichlorohydrin polymers, Progress in Polymer Science, 38 (2013) 344-368.
[4] R.L. Carrier, L.A. Miller, M. Ahmed, The utility of cyclodextrins for enhancing oral bioavailability, Journal of Controlled Release, 123 (2007) 78-99.
[5] T. Loftsson, D. Duchêne, Cyclodextrins and their pharmaceutical applications, International Journal of Pharmaceutics, 329 (2007) 1-11.
[6] Y. Fu, W.J. Kao, Drug release kinetics and transport mechanisms of non-degradable and degradable polymeric delivery systems, Expert Opinion on Drug Delivery, 7 (2010) 429-444.
[7] B.B. Mamba, R.W. Krause, T.J. Malefetse, G. Gericke, S.P. Sithole, Cyclodextrin nanosponges in the removal of organic matter to produce water for power generation, Water SA, 34 (2008) 657-660.
[8] A.Z.M. Badruddoza, Z.B.Z. Shawon, W.J.D. Tay, K. Hidajat, M.S. Uddin, Fe3O4/cyclodextrin polymer nanocomposites for selective heavy metals removal from industrial wastewater, Carbohydrate Polymers, 91 (2013) 322-332.
[9] N. Chandrasekharan, H. Dai, K.L.T. Roos, N.K. Evanson, J. Tomsik, T.S. Elton, D.L. Simmons, COX-3, a cyclooxygenase-1 variant inhibited by acetaminophen and other analgesic/antipyretic drugs: cloning, structure, and expression, Proceedings of the National Academy of Sciences, 99 (2002) 13926-13931.

[10] F. Mahle, T.d.R. Guimaraes, A.V. Meira, R. Correa, R.C. Bella Cruz, A.B. Cruz, R.J. Nunes, V. Cechinel-Filho, F. de Campos-Buzzi, Synthesis and biological evaluation of N-antipyrine-4-substituted amino-3-chloromaleimide derivatives, European Journal of Medicinal Chemistry, 45 (2010) 4761-4768.
[11] H.M. Aly, N.M. Saleh, H.A. Elhady, Design and synthesis of some new thiophene, thienopyrimidine and thienothiadiazine derivatives of antipyrine as potential antimicrobial agents, European Journal of Medicinal Chemistry, 46 (2011) 4566-4572.
[12] S. Zuehlke, U. Duennbier, B. Lesjean, R. Gnirss, H. Buisson, Long-term comparison of trace organics removal performances between conventional and membrane activated sludge processes, Water Environment Research, 78 (2006) 2480-2486.
[13] A. Rasheed, A. Kumar, V. Sravanthi, Cyclodextrins as drug carrier molecule: a review, Scientia Pharmaceutica, 76 (2008) 567-598.
[14] M. Cai, L. Zhang, F. Qi, L. Feng, Influencing factors and degradation products of antipyrine chlorination in water with free chlorine, Journal of Environmental Sciences-China, 25 (2013) 77-84.
[15] C. Tan, N. Gao, Y. Deng, W. Rong, S. Zhou, N. Lu, Degradation of antipyrine by heat activated persulfate, Separation and Purification Technology, 109 (2013) 122-128.
[16] R. Rodil, J.B. Quintana, R. Cela, Transformation of phenazone-type drugs during chlorination, Water Research, 46 (2012) 2457-2468.
[17] C. Tan, N. Gao, Y. Deng, Y. Zhang, M. Sui, J. Deng, S. Zhou, Degradation of antipyrine by UV, UV/H2O2 and UV/PS, Journal of Hazardous Materials, 260 (2013) 1008-1016.
[18] V. Meltzer, E. Pincu, A. Rogozea, G. Ionita, Inclusion complexes of some antipyrine derivatives with cyclodextrins: influence of guest configuration, Journal of Inclusion Phenomena and Macrocyclic Chemistry, 65 (2009) 385-390.
[19] N. Matsumoto, M. Yamada, Y. Kurakata, H. Yoshida, S. Kamitori, A. Nishikawa, T. Tonozuka, Crystal structures of open and closed forms of cyclo/maltodextrin-binding protein, FEBS journal, 276 (2009) 3008-3019.
[20] A.K. Schmidt, S. Cottaz, H. Driguez, G.E. Schulz, Structure of cyclodextrin glycosyltransferase complexed with a derivative of its main product beta-cyclodextrin, Biochemistry, 37 (1998) 5909-5915.
[21] T. Tonozuka, A. Sogawa, M. Yamada, N. Matsumoto, H. Yoshida, S. Kamitori, K. Ichikawa, M. Mizuno, A. Nishikawa, Y. Sakano, Structural basis for cyclodextrin recognition by Thermoactinomyces vulgaris cyclo/maltodextrin-binding protein, FEBS Journal, 274 (2007) 2109-2120.
[22] E.F. Pettersen, T.D. Goddard, C.C. Huang, G.S. Couch, D.M. Greenblatt, E.C. Meng, T.E. Ferrin, UCSF Chimera—a visualization system for exploratory research and analysis, Journal of Computational Chemistry, 25 (2004) 1605-1612.
[23] O. Trott, A.J. Olson, AutoDock Vina: improving the speed and accuracy of docking with a new scoring function, efficient optimization, and multithreading, Journal of Computational Chemistry, 31 (2010) 455-461.
[24] Frisch, M. J.; Trucks, G. W.; Schlegel, H. B.; Scuseria, G. E.; Robb, M. A.; Cheeseman, J. R.; Montgomery, Jr., J. A.; Vreven, T.; Kudin, K. N.; Burant, J. C.; Millam, J. M.; Iyengar, S. S.; Tomasi, J.; Barone, V.; Mennucci, B.; Cossi, M.; Scalmani, G.; Rega, N.; Petersson, G. A.; Nakatsuji, H.; Hada, M.; Ehara, M.; Toyota, K.; Fukuda, R.; Hasegawa, J.; Ishida, M.; Nakajima, T.; Honda, Y.; Kitao, O.; Nakai, H.; Klene, M.; Li, X.; Knox, J. E.; Hratchian, H. P.; Cross, J. B.; Bakken, V.; Adamo, C.; Jaramillo, J.; Gomperts, R.; Stratmann, R. E.; Yazyev, O.; Austin, A. J.; Cammi, R.; Pomelli, C.; Ochterski, J. W.; Ayala, P. Y.; Morokuma, K.; Voth, G. A.; Salvador, P.; Dannenberg, J. J.; Zakrzewski, V. G.; Dapprich, S.; Daniels, A. D.; Strain, M. C.; Farkas, O.; Malick, D. K.; Rabuck, A. D.; Raghavachari, K.; Foresman, J. B.; Ortiz, J. V.; Cui, Q.; Baboul, A. G.; Clifford, S.; Cioslowski, J.; Stefanov, B. B.; Liu, G.; Liashenko, A.; Piskorz, P.; Komaromi, I.; Martin, R. L.; Fox, D. J.; Keith, T.; Al-Laham, M. A.; Peng, C. Y.; Nanayakkara, A.; Challacombe, M.; Gill, P. M. W.; Johnson, B.; Chen, W.; Wong, M. W.; Gonzalez, C.; Pople, J. A. Gaussian 03, Revision E.01; Gaussian, Inc.: Wallingford, CT, 2004.

[25] A.W. Götz, M.J. Williamson, D. Xu, D. Poole, S. Le Grand, R.C. Walker, Routine microsecond molecular dynamics simulations with AMBER on GPUs. 1. Generalized Born, Journal of Chemical Theory and Computation, 8 (2012) 1542-1555.
[26] P. Cieplak, W.D. Cornell, C. Bayly, P.A. Kollman, Application of the multimolecule and multiconformational RESP methodology to biopolymers: charge derivation for DNA, RNA, and proteins, Journal of Computational Chemistry, 16 (1995) 1357-1377.
[27] K. Lindorff-Larsen, S. Piana, K. Palmo, P. Maragakis, J.L. Klepeis, R.O. Dror, D.E. Shaw, Improved side-chain torsion potentials for the Amber ff99SB protein force field, Proteins: Structure, Function, and Bioinformatics, 78 (2010) 1950-1958.
[28] W.L. Jorgensen, J. Chandrasekhar, J.D. Madura, R.W. Impey, M.L. Klein, Comparison of simple potential functions for simulating liquid water, The Journal of Chemical Physics, 79 (1983) 926-935.
[29] M. Harvey, G. De Fabritiis, An implementation of the smooth particle mesh Ewald method on GPU hardware, Journal of Chemical Theory and Computation, 5 (2009) 2371-2377.
[30] J.-P. Ryckaert, G. Ciccotti, H.J. Berendsen, Numerical integration of the cartesian equations of motion of a system with constraints: molecular dynamics of -alkanes, Journal of Computational Physics, 23 (1977) 327-341.
[31] S. Le Grand, A.W. Götz, R.C. Walker, SPFP: Speed without compromise. A mixed precision model for GPU accelerated molecular dynamics simulations, Computer Physics Communications, 184 (2013) 374-380.
[32] H. Tzoupis, G. Leonis, A. Avramopoulos, T. Mavromoustakos, M.G. Papadopoulos, Systematic Molecular Dynamics, MM–PBSA, and Ab Initio Approaches to the Saquinavir Resistance Mechanism in HIV-1 PR Due to 11 Double and Multiple Mutations, The Journal of Physical Chemistry B, (2014).
[33] P.A. Kollman, I. Massova, C. Reyes, B. Kuhn, S. Huo, L. Chong, M. Lee, T. Lee, Y. Duan, W. Wang, O. Donini, P. Cieplak, J. Srinivasan, D.A. Case, T.E. Cheatham, Calculating Structures and Free Energies of Complex Molecules: Combining Molecular Mechanics and Continuum Models, Accounts of Chemical Research, 33 (2000) 889-897.
[34] L.M.A. Pinto, L.F. Fraceto, M.H.A. Santana, T.A. Pertinhez, S.O. Junior, E. de Paula, Physico-chemical characterization of benzocaine-β-cyclodextrin inclusion complexes, Journal of Pharmaceutical and Biomedical Analysis, 39 (2005) 956-963.
[35] R. Periasamy, R. Rajamohan, S. Kothainayaki, K. Sivakumar, Spectral investigation and structural characterization of Dibenzalacetone: β-Cyclodextrin inclusion complex, Journal of Molecular Structure, 1068 (2014) 155-163.
[36] B. Liu, W. Li, J. Zhao, Y. Liu, X. Zhu, G. Liang, Physicochemical characterisation of the supramolecular structure of luteolin/cyclodextrin inclusion complex, Food Chemistry, 141 (2013) 900-906.
[37] R. Yang, J.-B. Chen, C.-F. Xiao, Z.-C. Liu, Z.-Y. Gao, S.-J. Yan, J.-H. Zhang, H.-B. Zhang, J. Lin, Inclusion complex of GA-13316 with β-cyclodextrin: Preparation, characterization, molecular modeling, and in vitro evaluation, Carbohydrate Polymers, 111 (2014) 655-662.
[38] G. Venkatesh, T. Sivasankar, M. Karthick, N. Rajendiran, Inclusion complexes of sulphanilamide drugs and beta-cyclodextrin: a theoretical approach, Journal of Inclusion Phenomena and Macrocyclic Chemistry, 77 (2013) 309-318.
[39] K. Srinivasan, K. Kayalvizhi, K. Sivakumar, T. Stalin, Study of inclusion complex of β-cyclodextrin and diphenylamine: Photophysical and electrochemical behaviors, Spectrochimica Acta Part A: Molecular and Biomolecular Spectroscopy, 79 (2011) 169-178.
[40] J.S. Negi, S. Singh, Spectroscopic investigation on the inclusion complex formation between amisulpride and γ-cyclodextrin, Carbohydrate Polymers, 92 (2013) 1835-1843.
[41] D.H.A. Corrêa, P.S. Melo, C.A.A. de Carvalho, M.B.M. de Azevedo, N. Durán, M. Haun, Dehydrocrotonin and its β-cyclodextrin complex: Cytotoxicity in V79 fibroblasts and rat cultured hepatocytes, European Journal of Pharmacology, 510 (2005) 17-24.
[42] P. Dandawate, K. Vemuri, E.M. Khan, M. Sritharan, S. Padhye, Synthesis, characterization and anti-tubercular activity of ferrocenyl hydrazones and their β-cyclodextrin conjugates, Carbohydrate Polymers, 108 (2014) 135-144.

[43] H. Jiang, H. Sun, S. Zhang, R. Hua, Y. Xu, S. Jin, H. Gong, L. Li, NMR investigations of inclusion complexes between beta-cyclodextrin and naphthalene/anthraquinone derivatives, Journal of Inclusion Phenomena and Macrocyclic Chemistry, 58 (2007) 133-138.
[44] G. Tárkányi, K. Németh, R. Mizsei, O. Tőke, J. Visy, M. Simonyi, L. Jicsinszky, J. Szemán, L. Szente, Structure and stability of warfarin-sodium inclusion complexes formed with permethylated monoamino-β-cyclodextrin, Journal of Pharmaceutical and Biomedical Analysis, 72 (2013) 292-298.
[45] W.H. Chen, M. Fukudome, D.Q. Yuan, T. Fujioka, K. Mihashi, K. Fujita, Restriction of guest rotation based on the distortion of a cyclodextrin cavity, Chemical Communications, (2000) 541-542.
[46] H.J. Schneider, F. Hacket, V. Rudiger, H. Ikeda, NMR studies of cyclodextrins and cyclodextrin complexes, Chemical Reviews, 98 (1998) 1755-1785.
[47] E. Leyva, E. Moctezuma, J. Strouse, M.A. Garcia-Garibay, Spectrometric and 2D NMR studies on the complexation of chlorophenols with cyclodextrins, Journal of Inclusion Phenomena and Macrocyclic Chemistry, 39 (2001) 41-46.

Supplementary information for Chapter 4

FTIR, NMR and HRMS spectra of compounds synthesized in this study

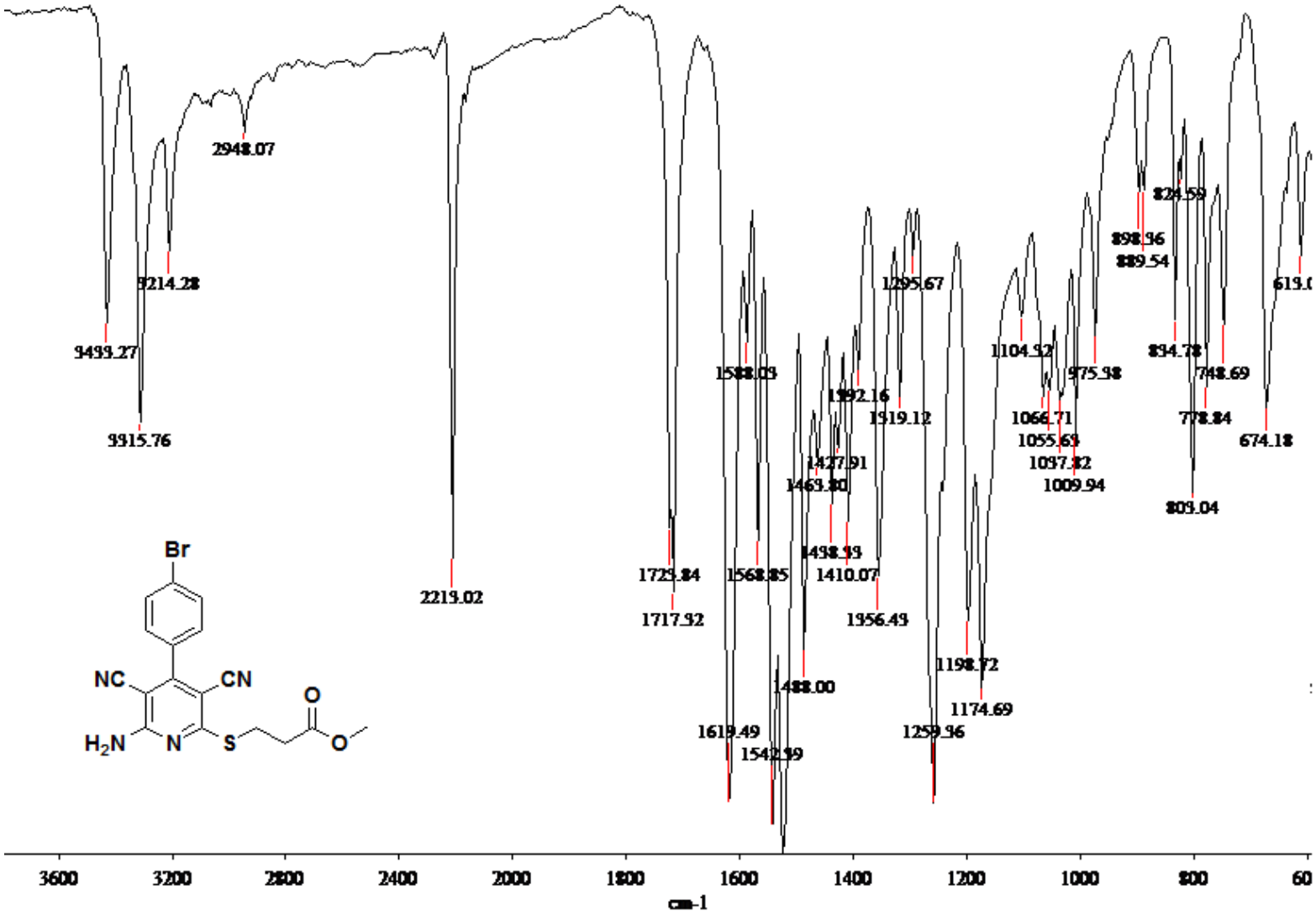

1a. methyl 3-(6-amino-4-(4-bromophenyl)-3,5-dicyanopyridin-2-ylthio)propanoate

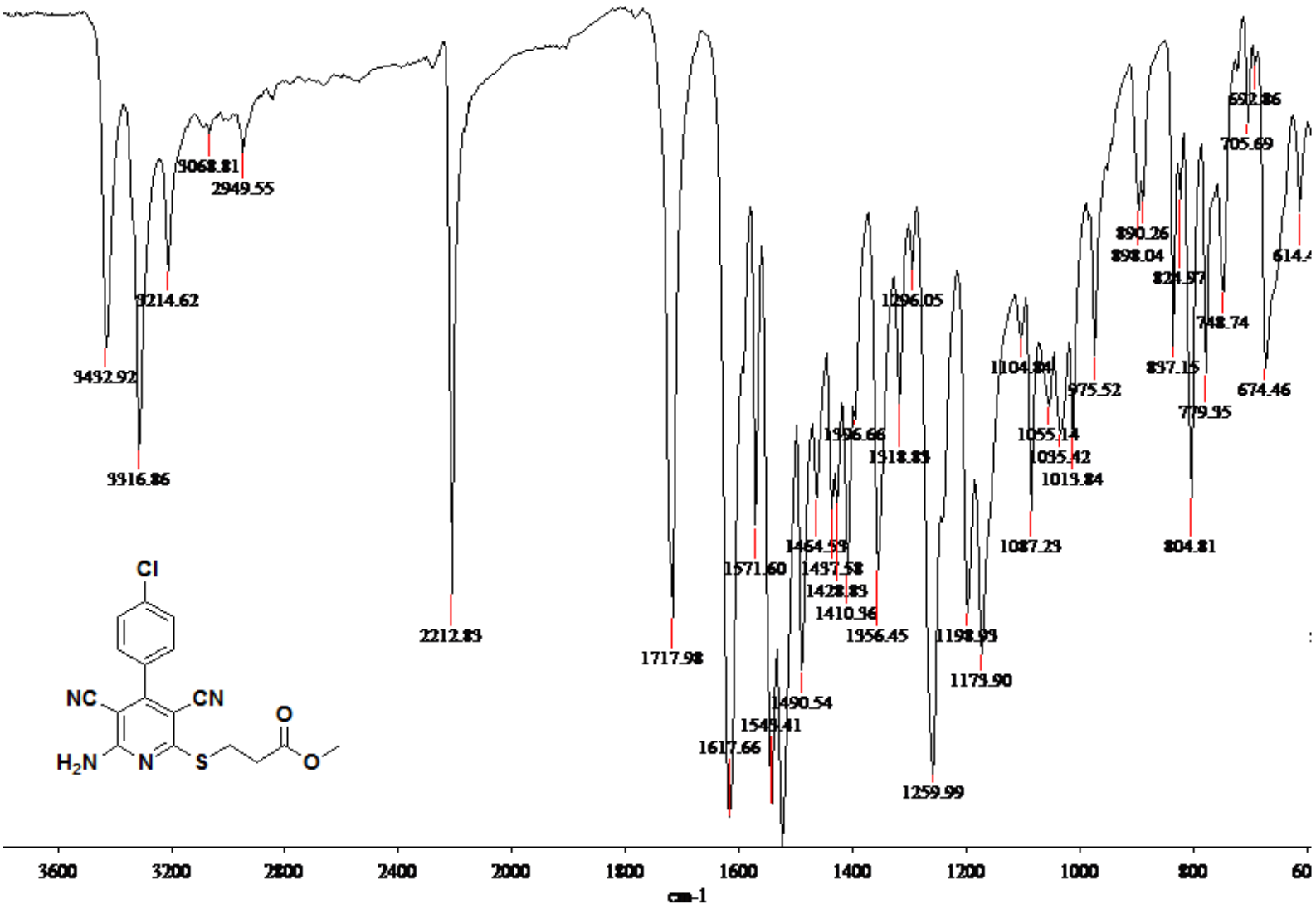

1b. methyl 3-(6-amino-4-(4-chlorophenyl)-3,5-dicyanopyridin-2-ylthio)propanoate

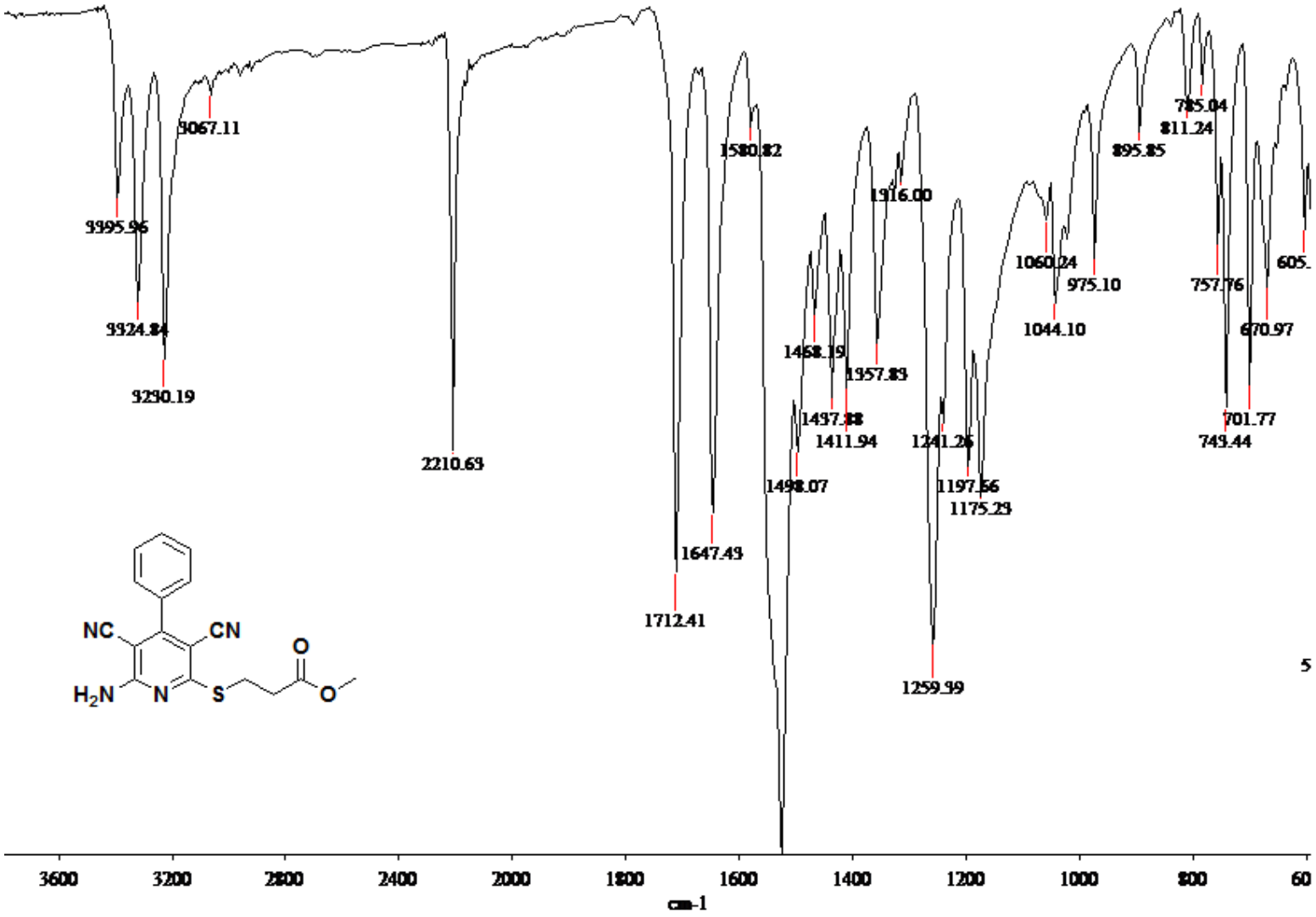

1c. methyl 3-(6-amino-3,5-dicyano-4-phenylpyridin-2-ylthio)propanoate

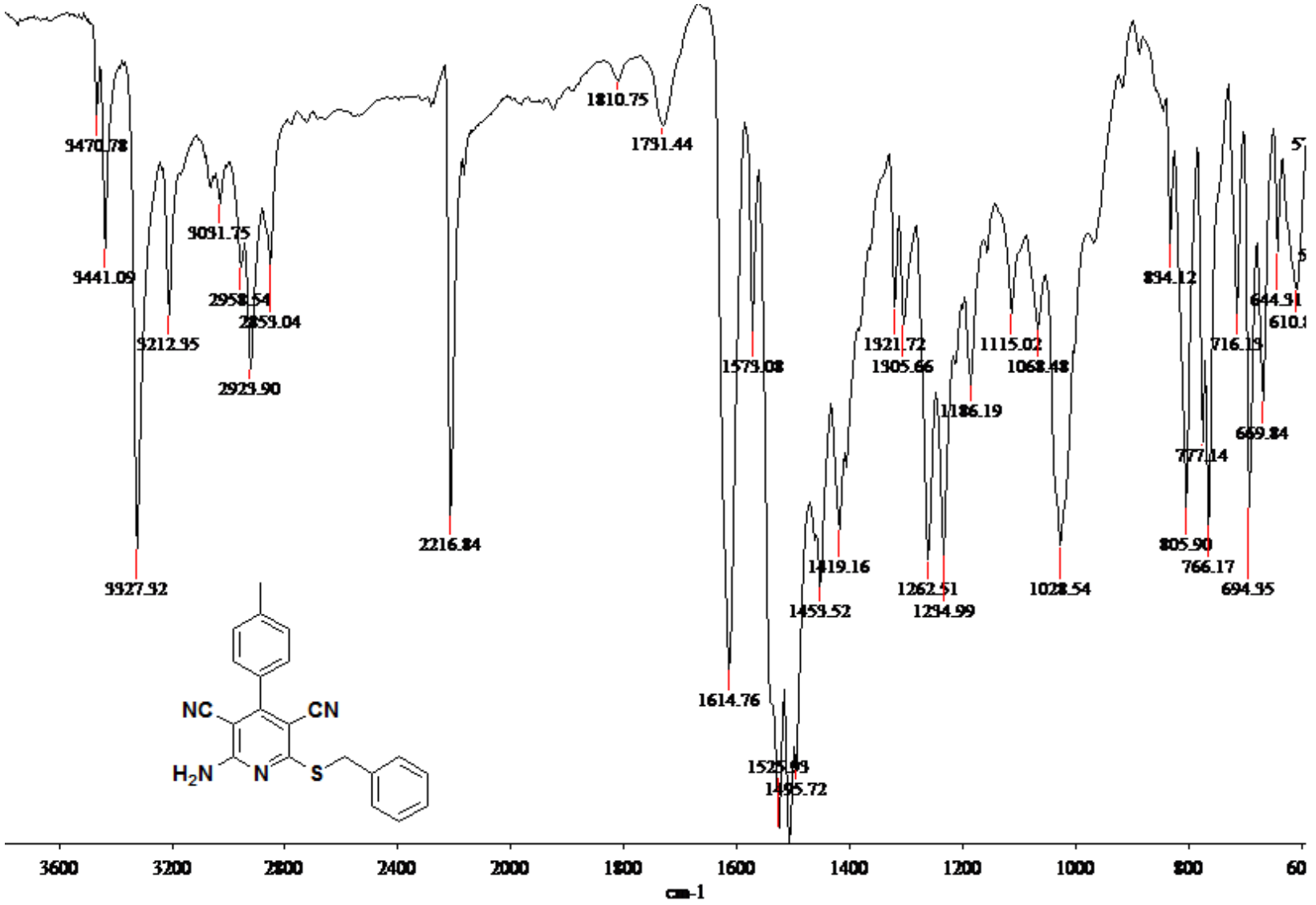

1d. 2-amino-6-(benzylthio)-4-p-tolylpyridine-3,5-dicarbonitrile

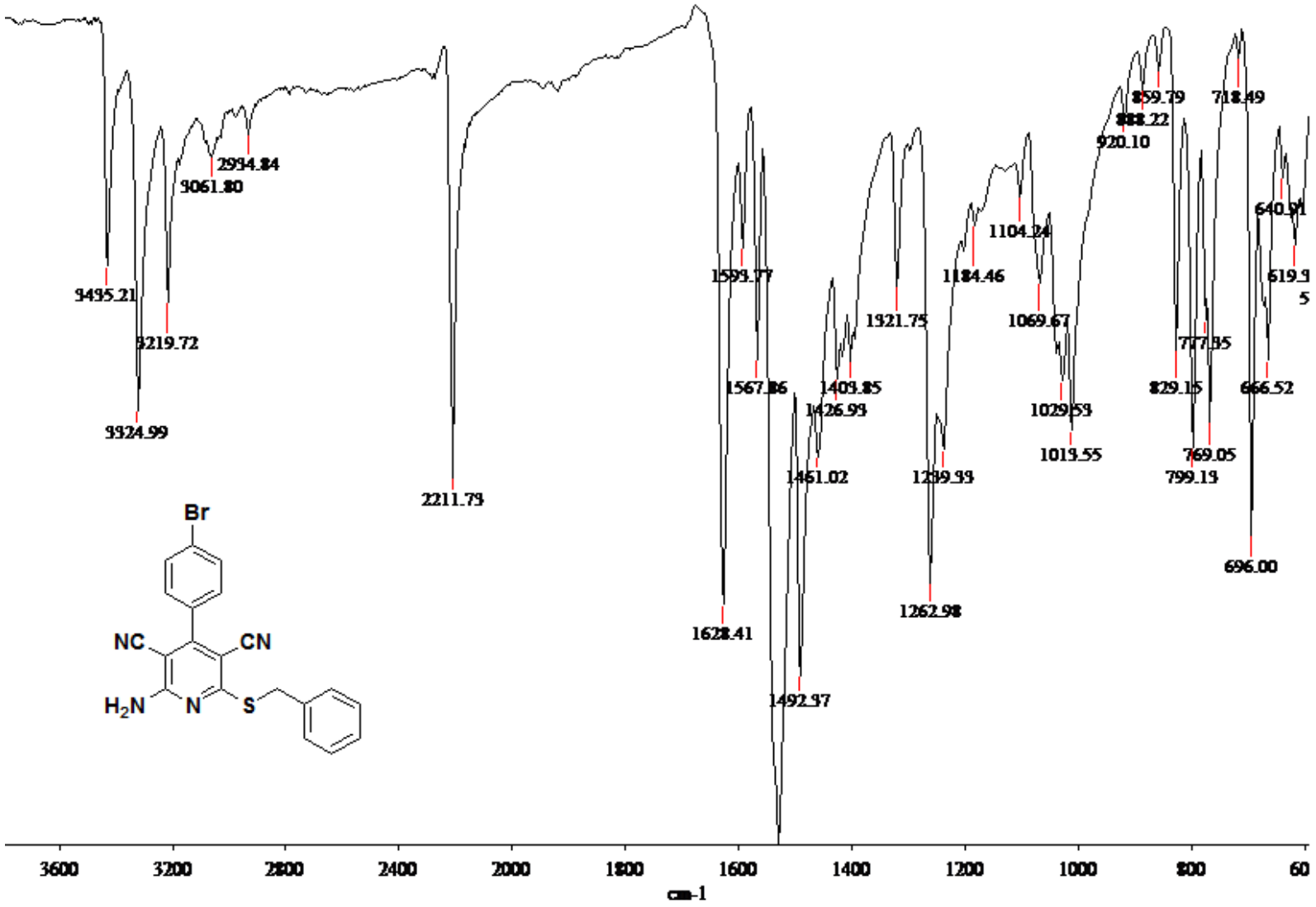

1e. 2-amino-6-(benzylthio)-4-(4-bromophenyl)pyridine-3,5-dicarbonitrile

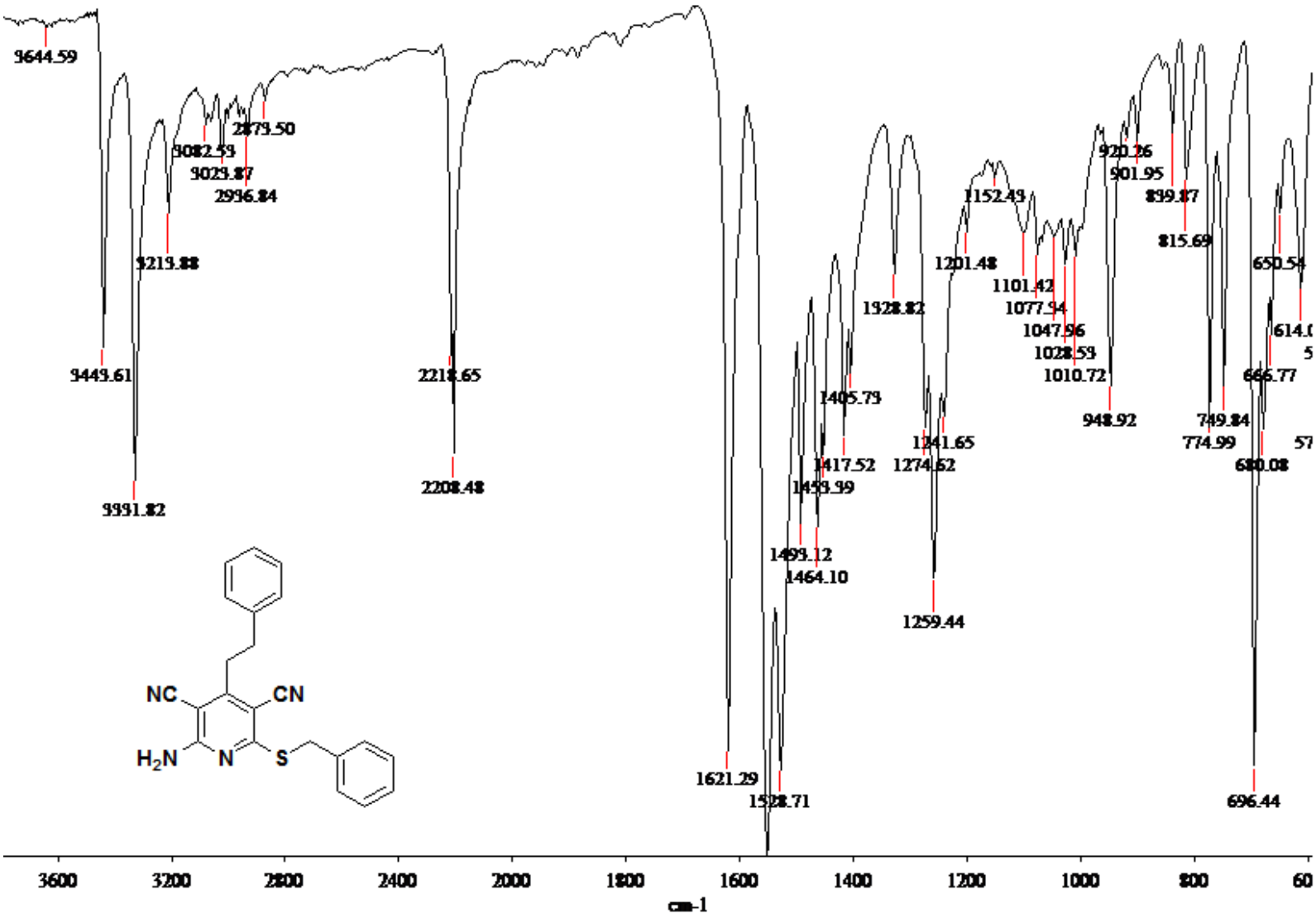

1f. 2-amino-6-(benzylthio)-4-phenethylpyridine-3, 5-dicarbonitrile

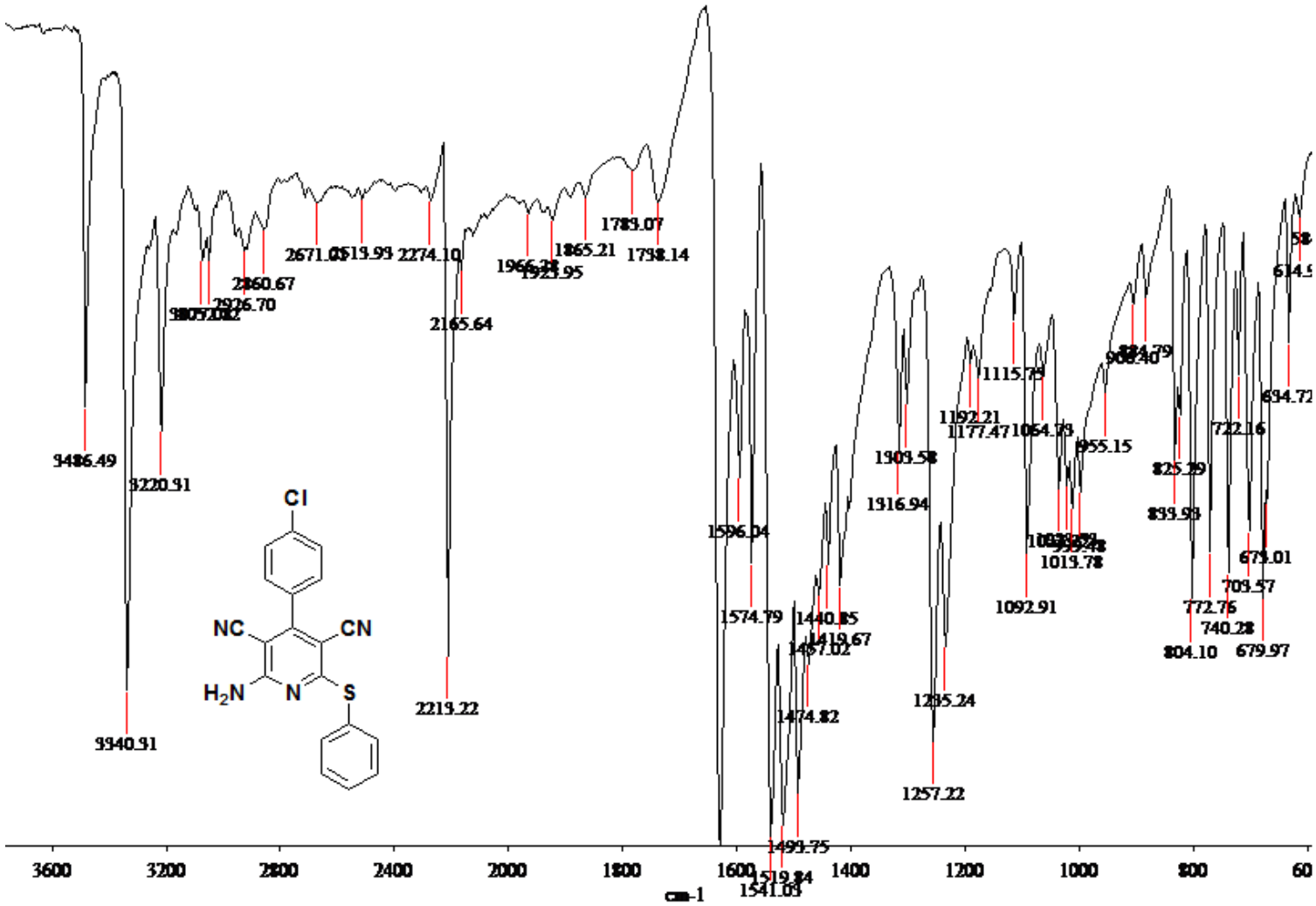

1g. 2-amino-4-(4-chlorophenyl)-6-(phenylthio)pyridine-3,5-dicarbonitrile

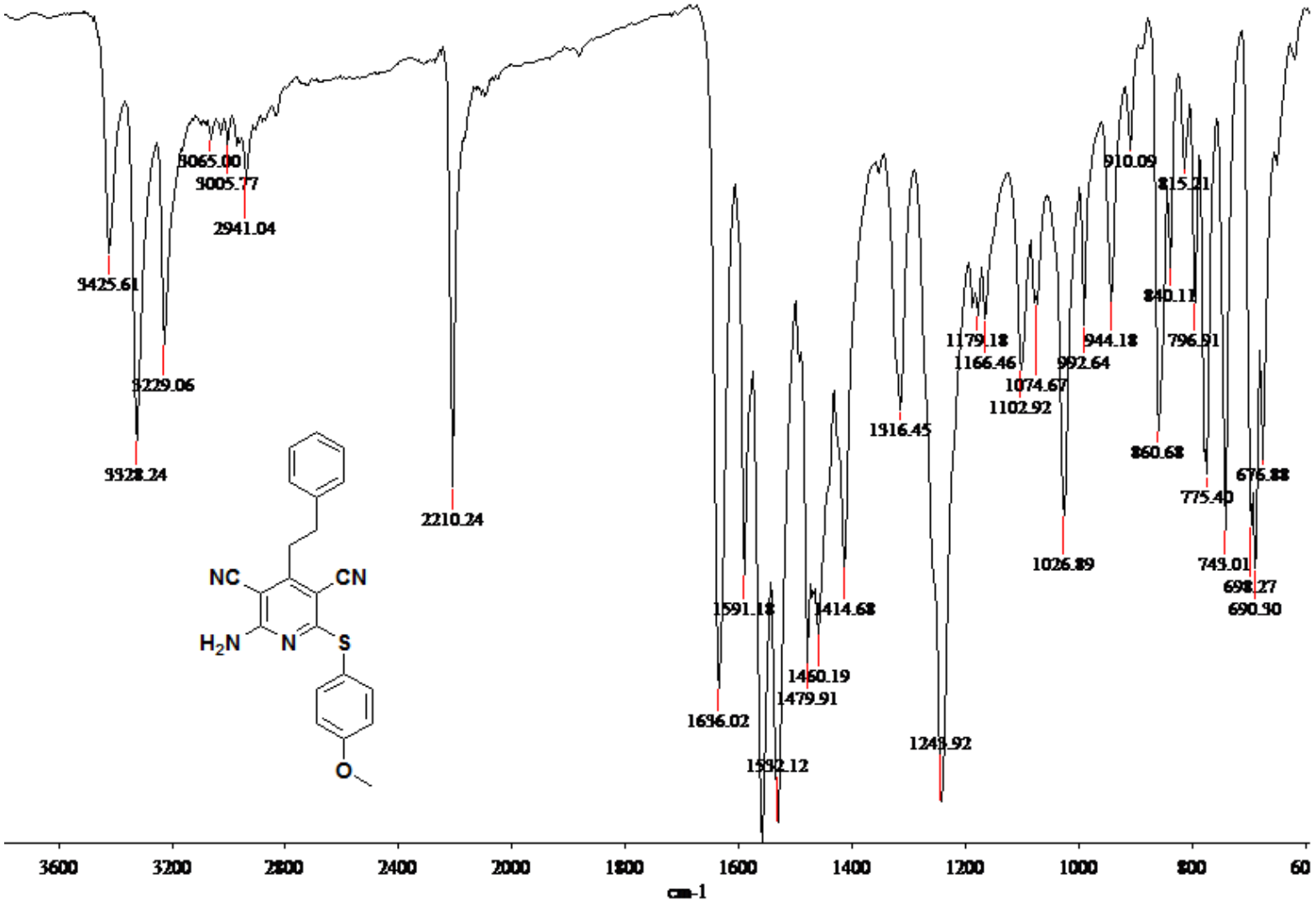

1h. 2-(4-methoxyphenylthio)-6-amino-4-phenethylpyridine-3,5-dicarbonitrile

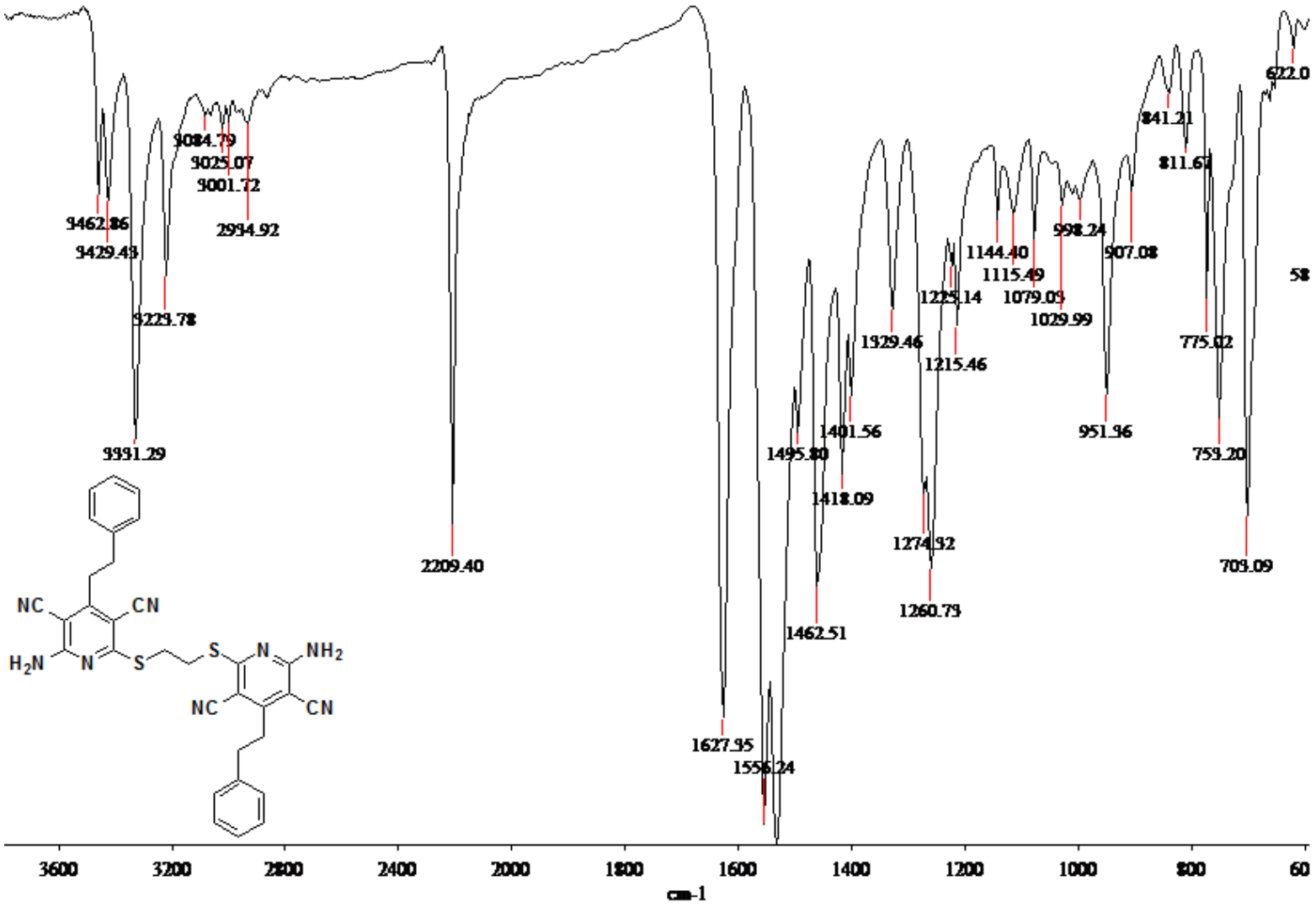

1i. 2-((2-(6-amino-3,5-dicyano-4-phenethylpyridin-2-ylthio)ethyl)sulfanyl)-6-amino-4-phenethylpyridine-3,5-dicarbonitrile

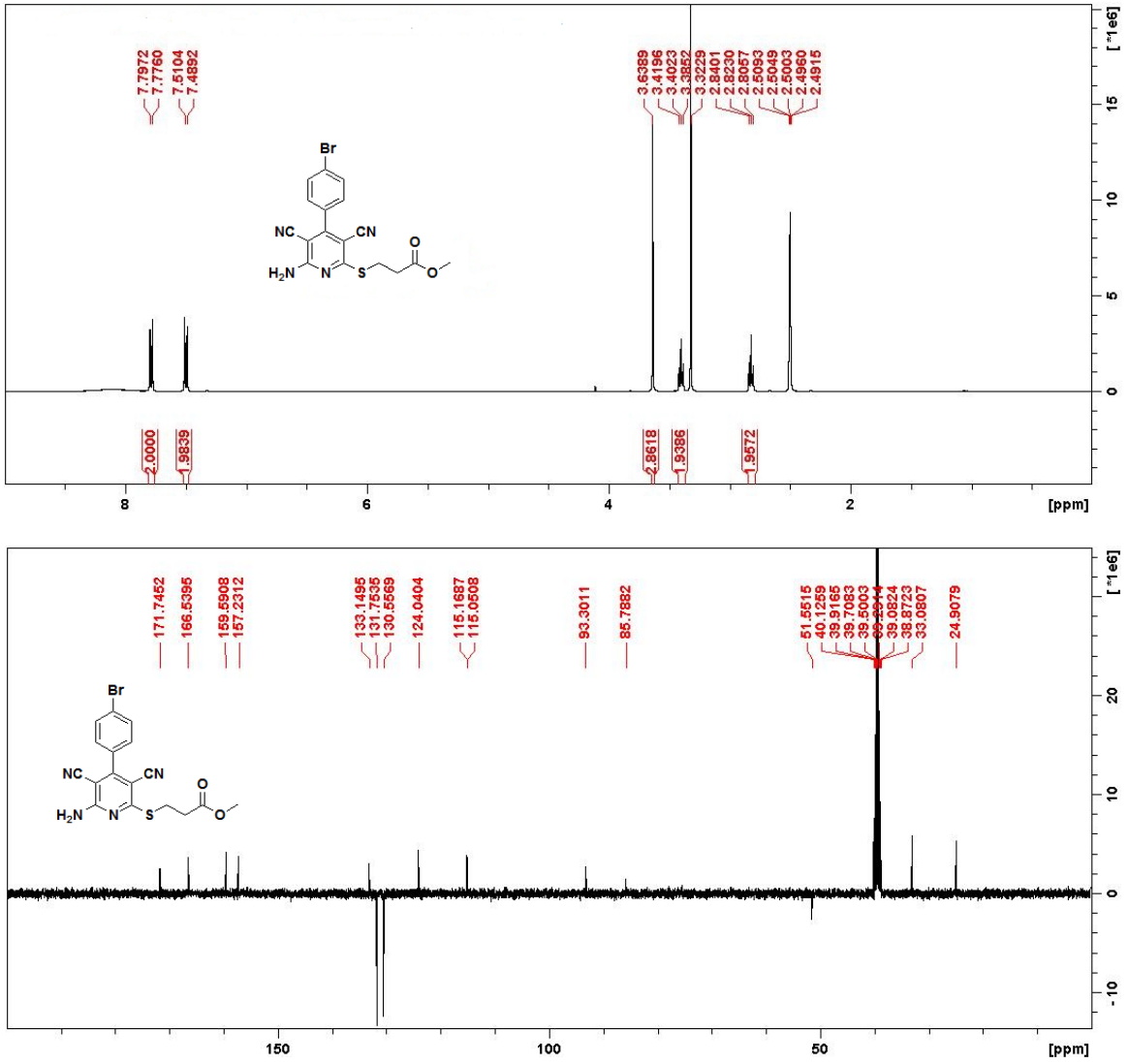

1a. methyl 3-(6-amino-4-(4-bromophenyl)-3,5-dicyanopyridin-2-ylthio)propanoate

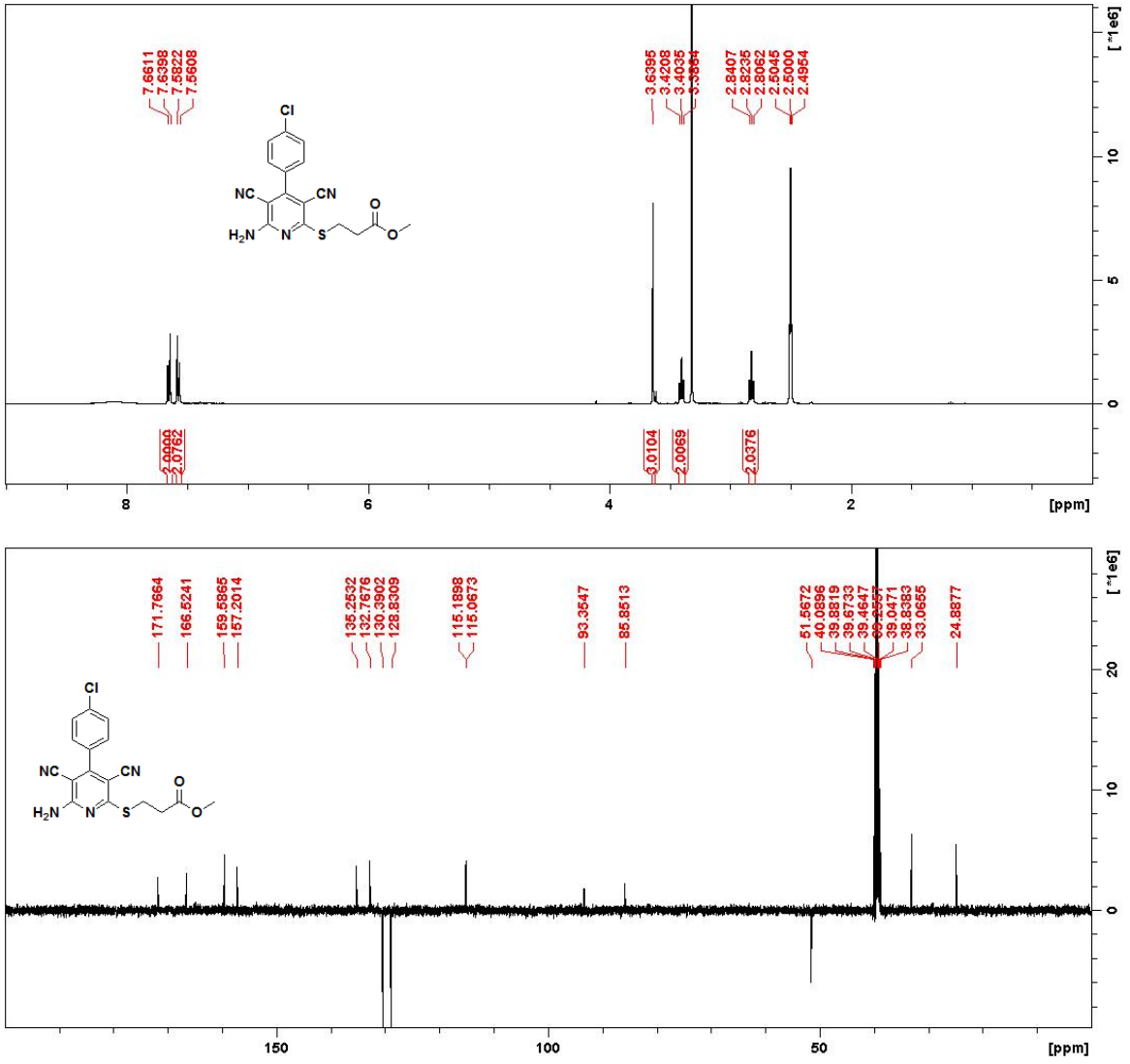

1b. methyl 3-(6-amino-4-(4-chlorophenyl)-3,5-dicyanopyridin-2-ylthio)propanoate

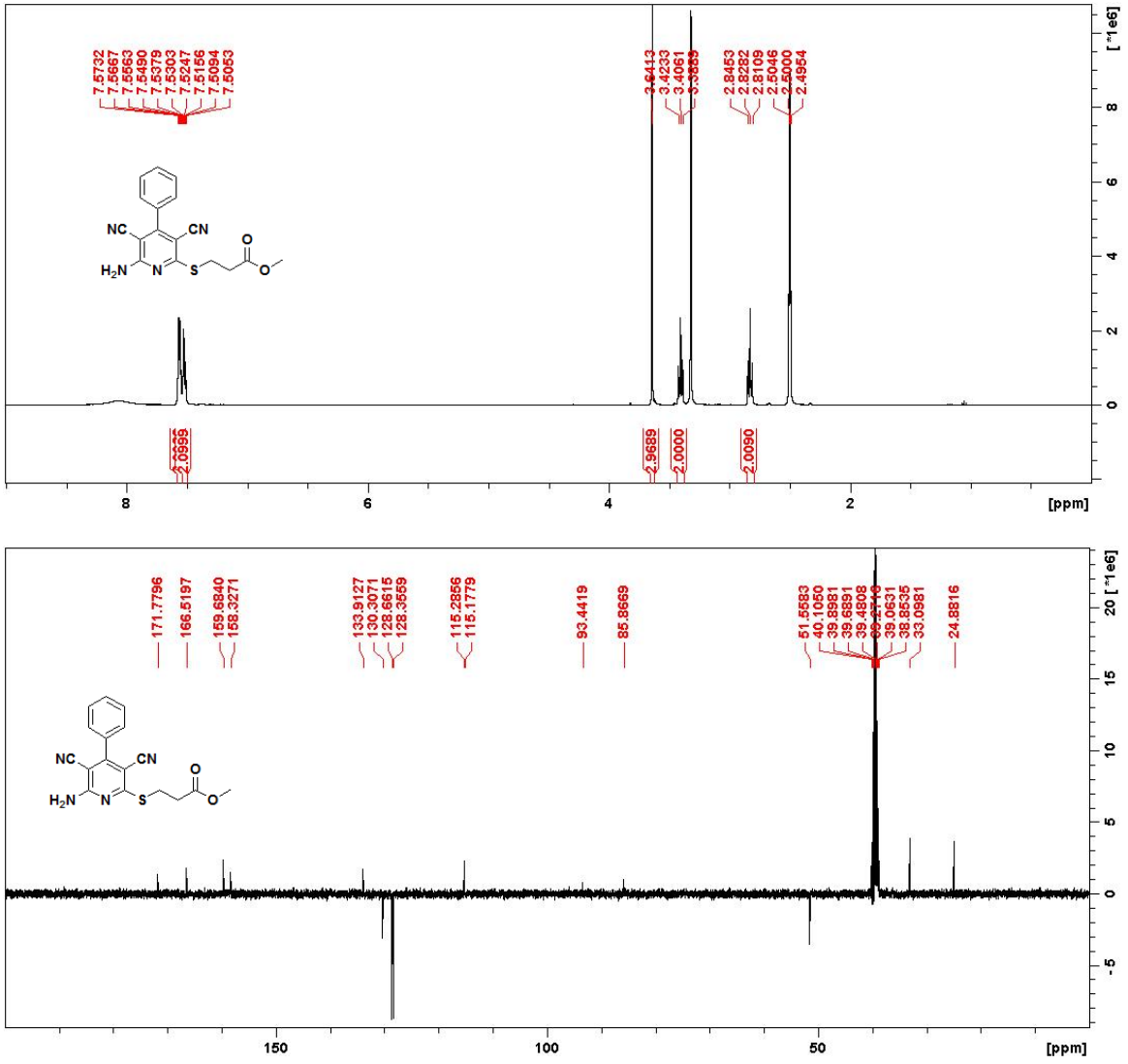

1c. methyl 3-(6-amino-3,5-dicyano-4-phenylpyridin-2-ylthio)propanoate

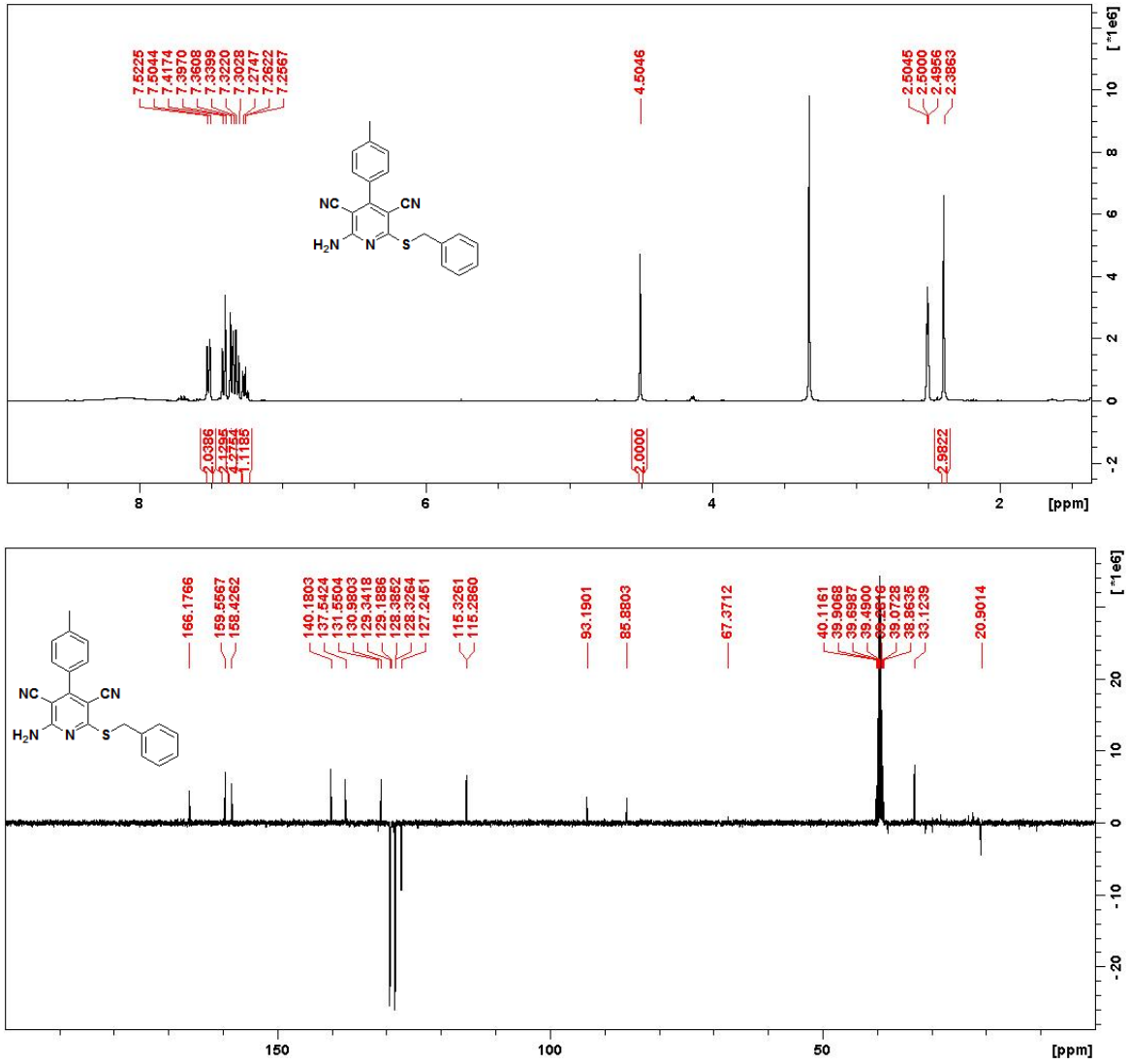

1d. 2-amino-6-(benzylthio)-4-p-tolylpyridine-3,5-dicarbonitrile

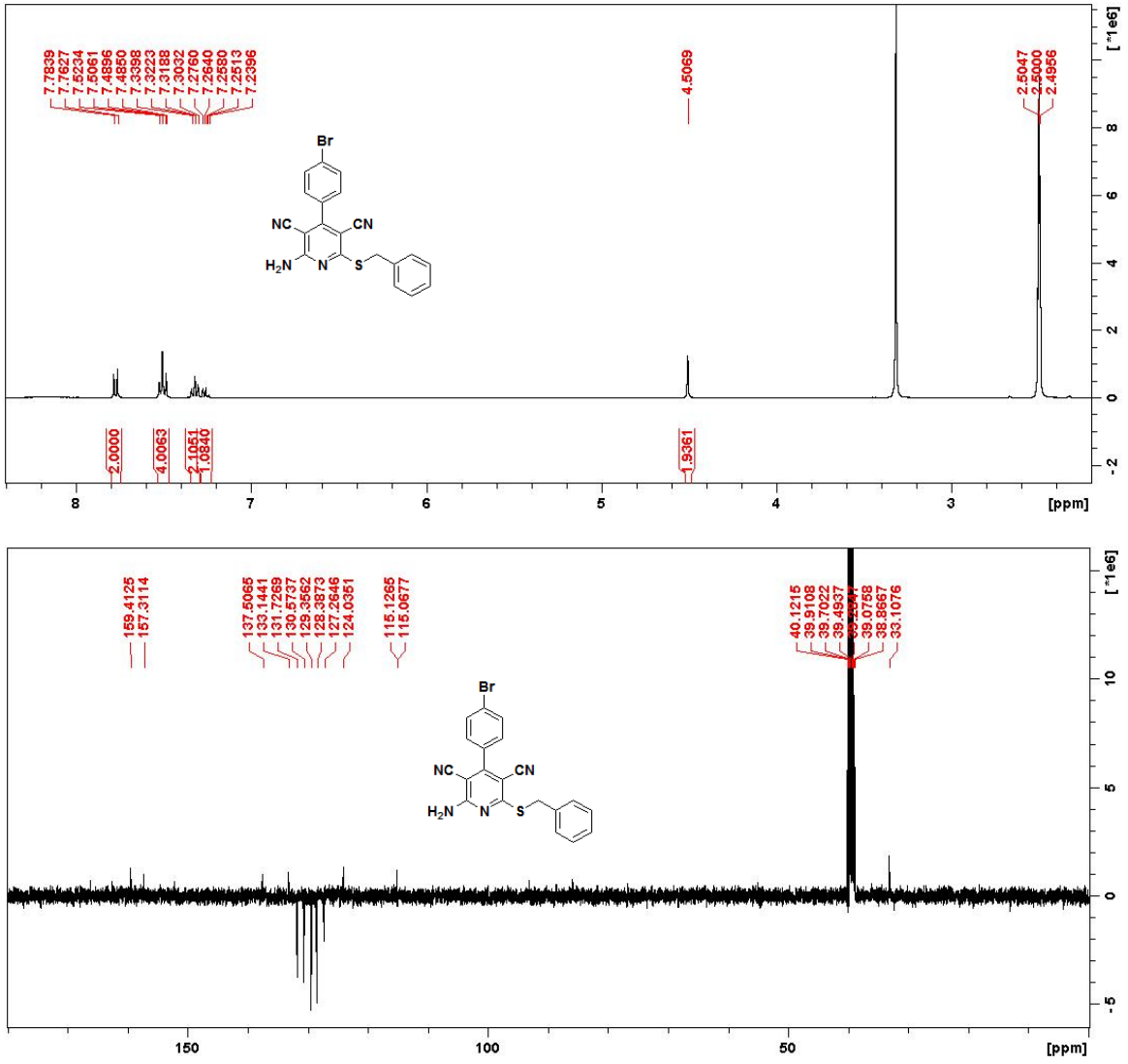

1e. 2-amino-6-(benzylthio)-4-(4-bromophenyl)pyridine-3,5-dicarbonitrile

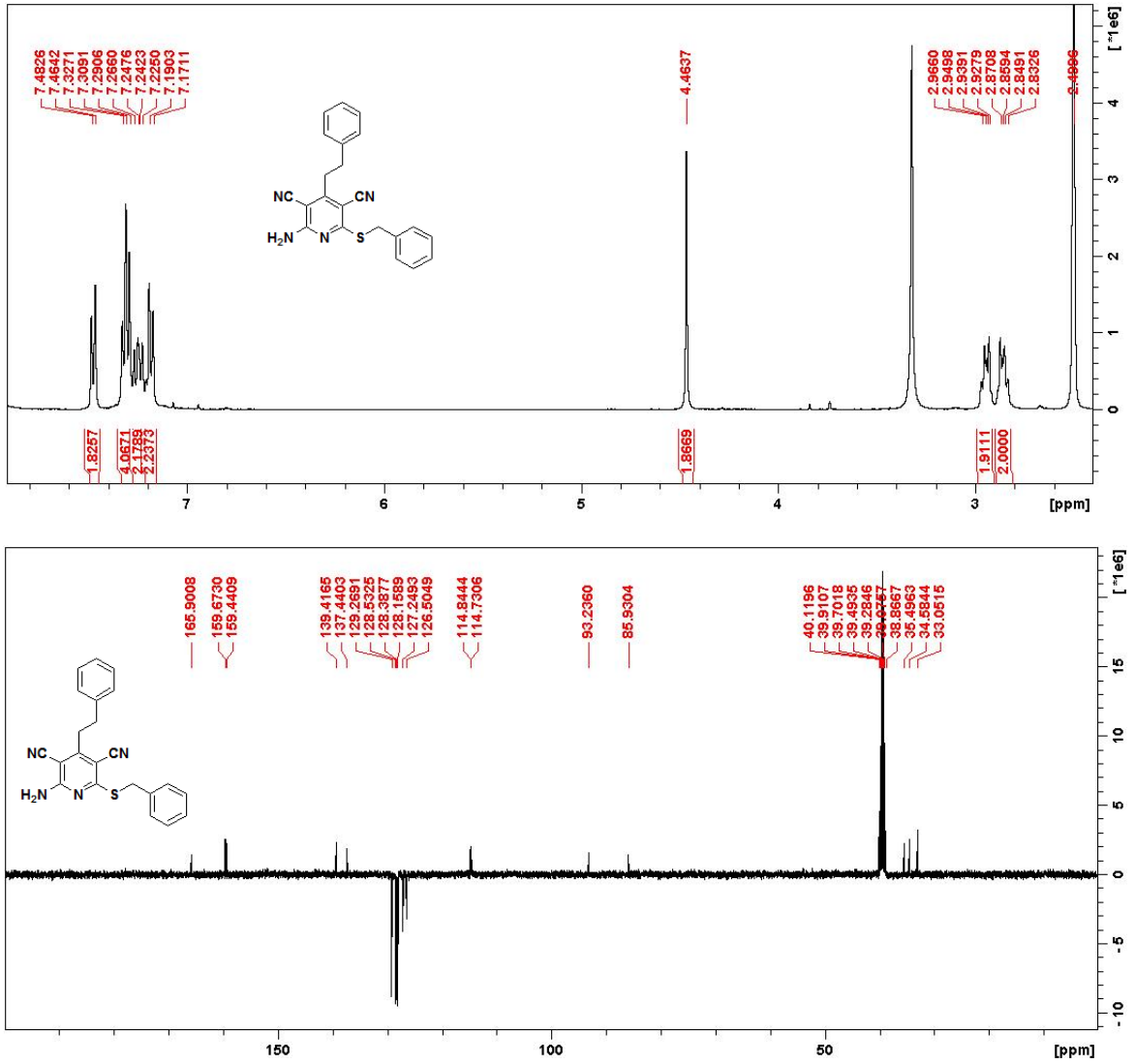

1f. 2-amino-6-(benzylthio)-4-phenethylpyridine-3,5-dicarbonitrile

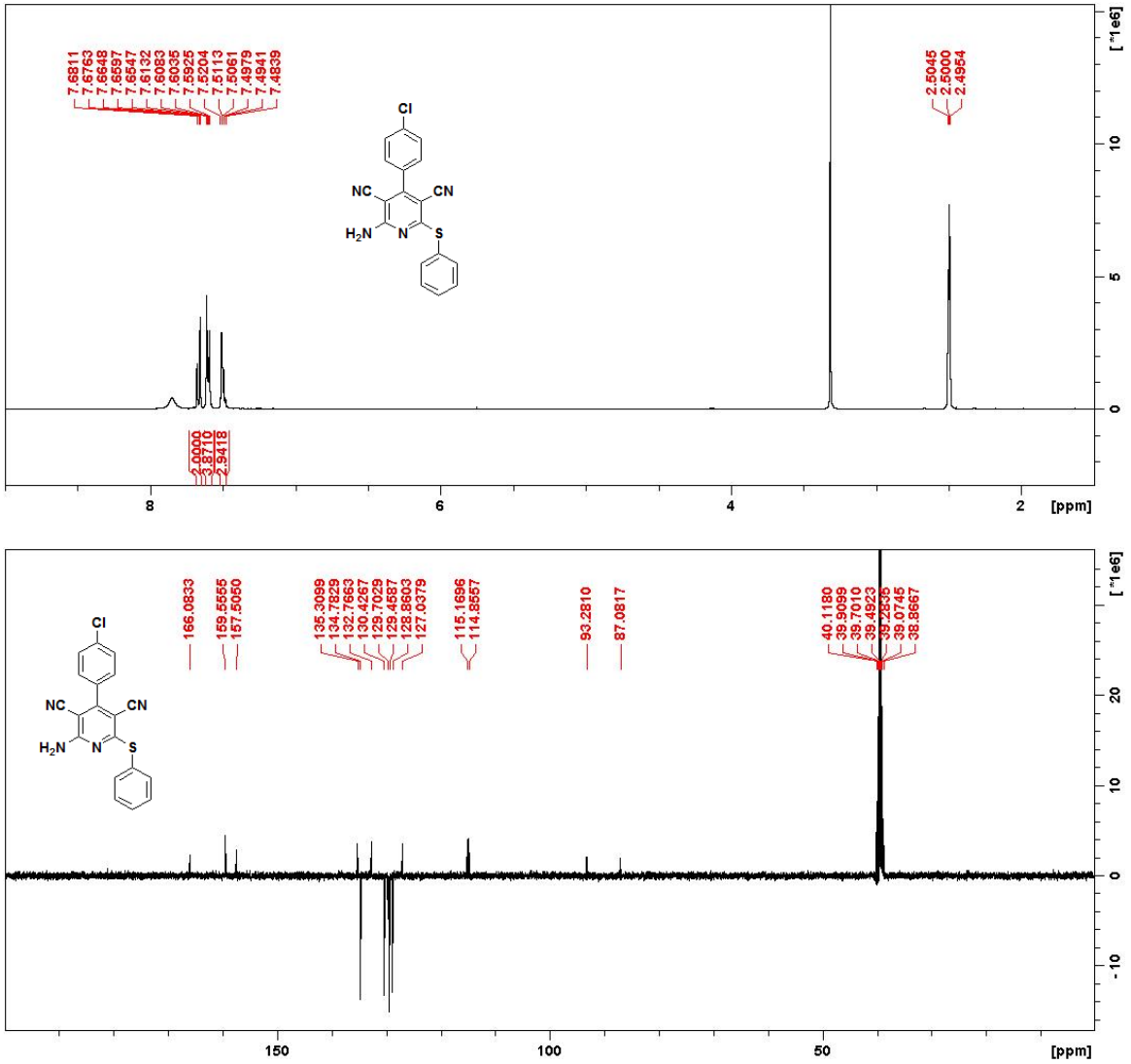

1g. 2-amino-4-(4-chlorophenyl)-6-(phenylthio)pyridine-3,5-dicarbonitrile

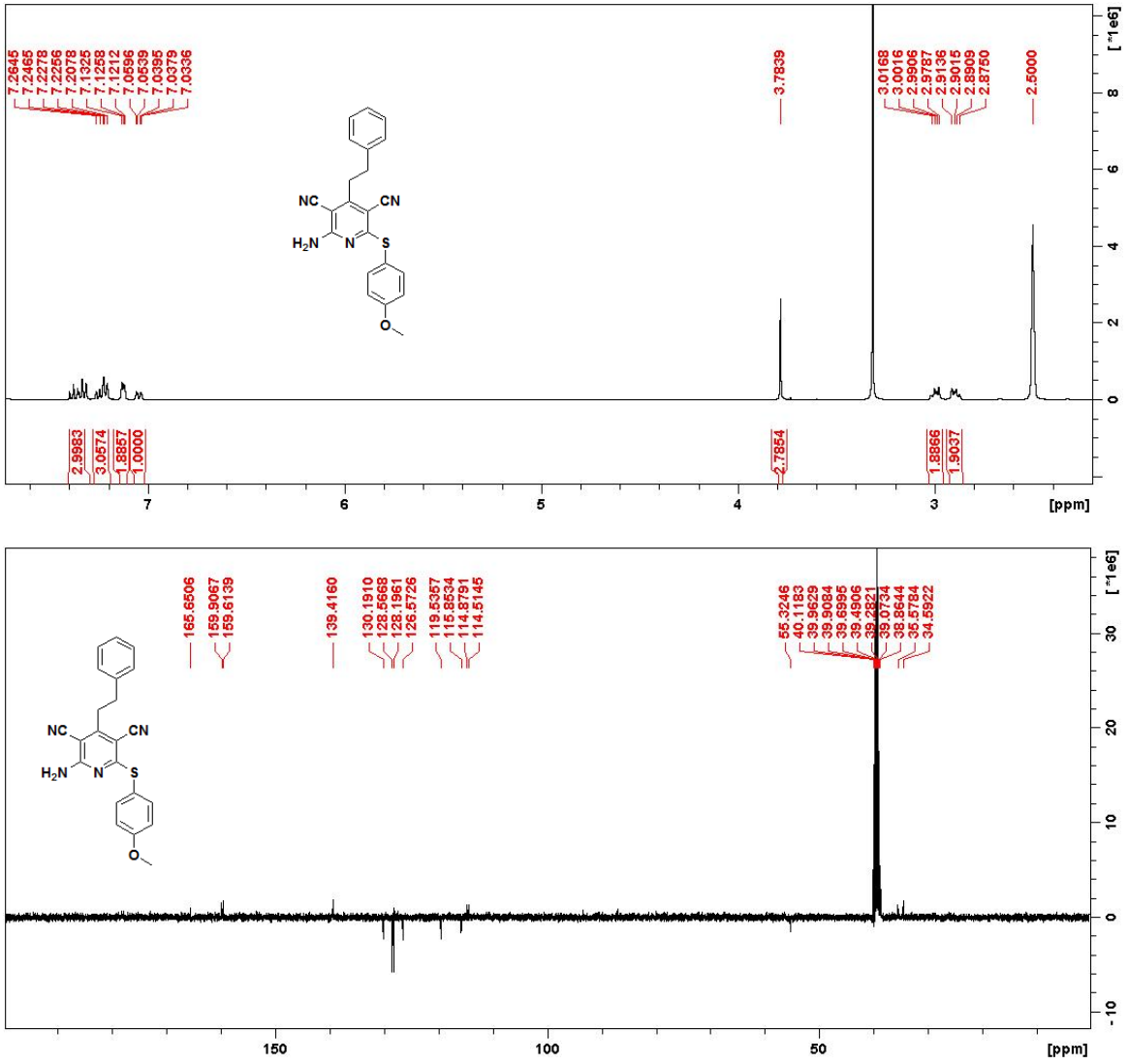

1h. 2-(4-methoxyphenylthio)-6-amino-4-phenethylpyridine-3,5-dicarbonitrile

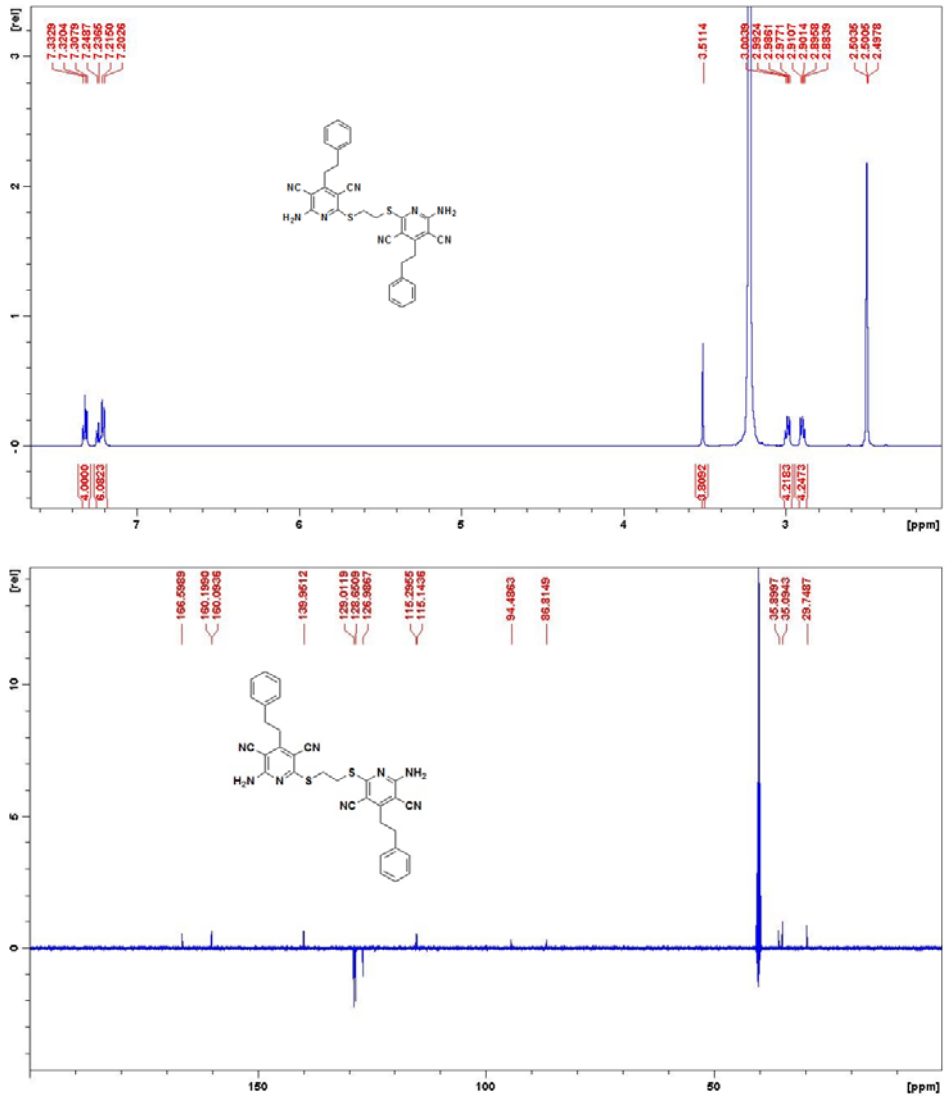

1i. 2-((2-(6-amino-3, 5-dicyano-4-phenethylpyridin-2-ylthio)ethyl)sulfanyl)-6-amino-4-phenethylpyridine-3,5-dicarbonitrile

Elemental Composition Report

Single Mass Analysis

Tolerance = 5.0 PPM / DBE: min = -1.5, max = 100.0
Element prediction: Off
Number of isotope peaks used for i-FIT = 3

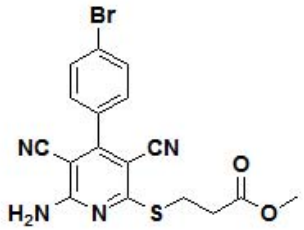

Monoisotopic Mass, Even Electron Ions
78 formula(e) evaluated with 1 results within limits (up to 20 closest results for each mass)
Elements Used:
C: 15-20 H: 10-15 N: 0-5 O: 0-5 S: 0-1 Br: 0-1

Rnc-1 5 (0.135) Cm (1:61)
TOF MS ES-

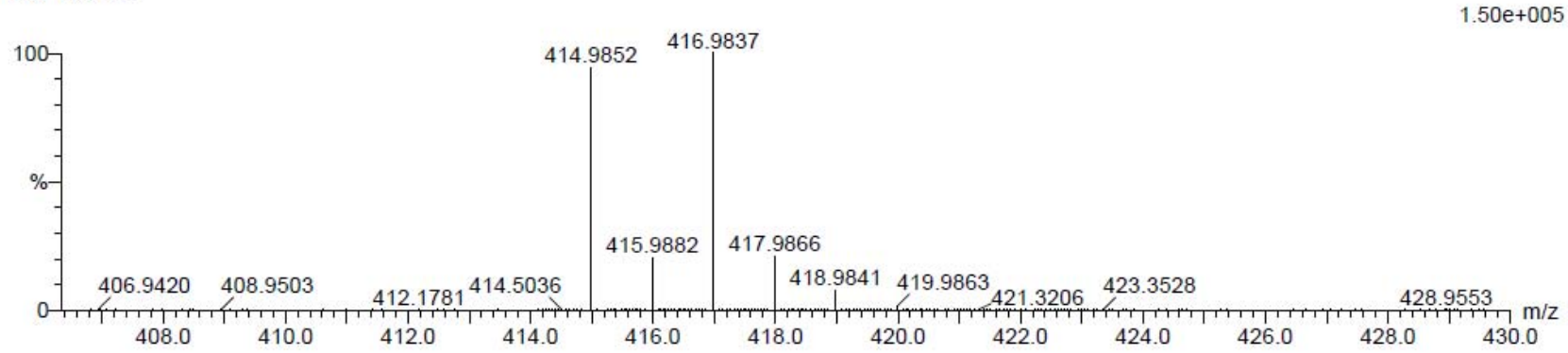

Minimum:				-1.5			
Maximum:		5.0	5.0	100.0			
Mass	Calc. Mass	mDa	PPM	DBE	i-FIT	i-FIT (Norm)	Formula
414.9852	414.9864	-1.2	-2.9	13.5	543.0	0.0	C17 H12 N4 O2 S Br

1a.

methyl 3-(6-amino-4-(4-bromophenyl)-3,5-dicyanopyridin-2-ylthio)propanoate

Elemental Composition Report

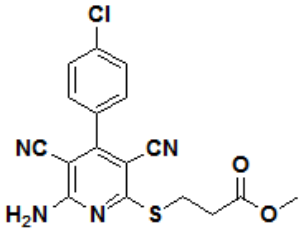

Single Mass Analysis

Tolerance = 5.0 PPM / DBE: min = -1.5, max = 100.0
Element prediction: Off
Number of isotope peaks used for i-FIT = 3

Monoisotopic Mass, Even Electron Ions
59 formula(e) evaluated with 1 results within limits (up to 20 closest results for each mass)
Elements Used:
C: 15-20 H: 10-15 N: 0-5 O: 0-5 S: 0-1 Cl: 0-1

Rnc-2 61 (2.025) Cm (1:61)
TOF MS ES-

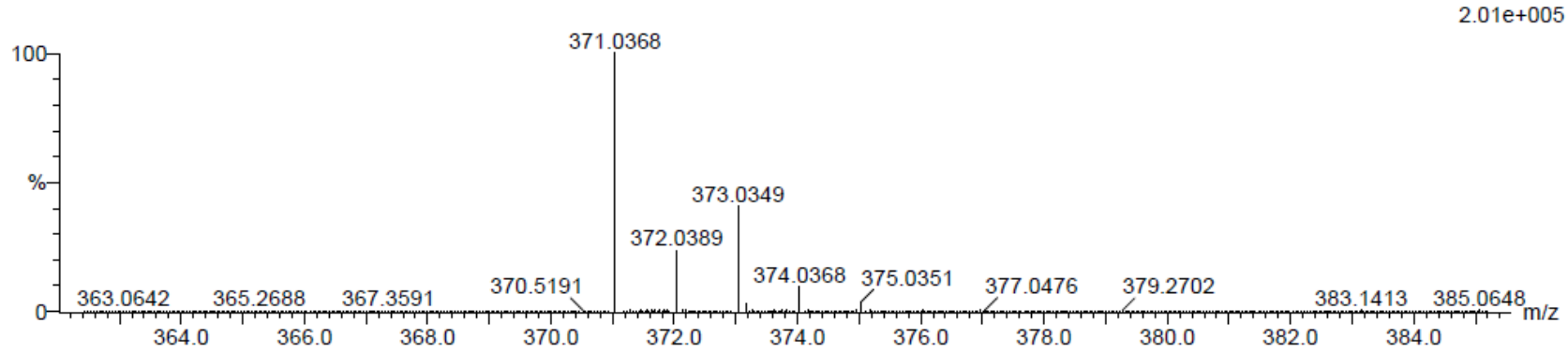

Minimum:				-1.5			
Maximum:		5.0	5.0	100.0			
Mass	Calc. Mass	mDa	PPM	DBE	i-FIT	i-FIT (Norm)	Formula
371.0368	371.0370	-0.2	-0.5	13.5	566.7	0.0	C17 H12 N4 O2 S Cl

1b. methyl 3-(6-amino-4-(4-chlorophenyl)-3,5-dicyanopyridin-2-ylthio)propanoate

Elemental Composition Report **Page 1**

Single Mass Analysis
Tolerance = 5.0 PPM / DBE: min = -1.5, max = 100.0
Element prediction: Off
Number of isotope peaks used for i-FIT = 3

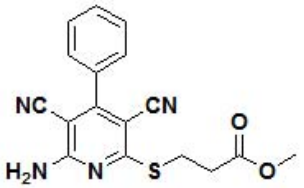

Monoisotopic Mass, Even Electron Ions
27 formula(e) evaluated with 1 results within limits (up to 20 closest results for each mass)
Elements Used:
C: 15-20 H: 10-15 N: 0-5 O: 0-5 S: 0-1
Rnc-3 18 (0.574) Cm (1:61)
TOF MS ES-

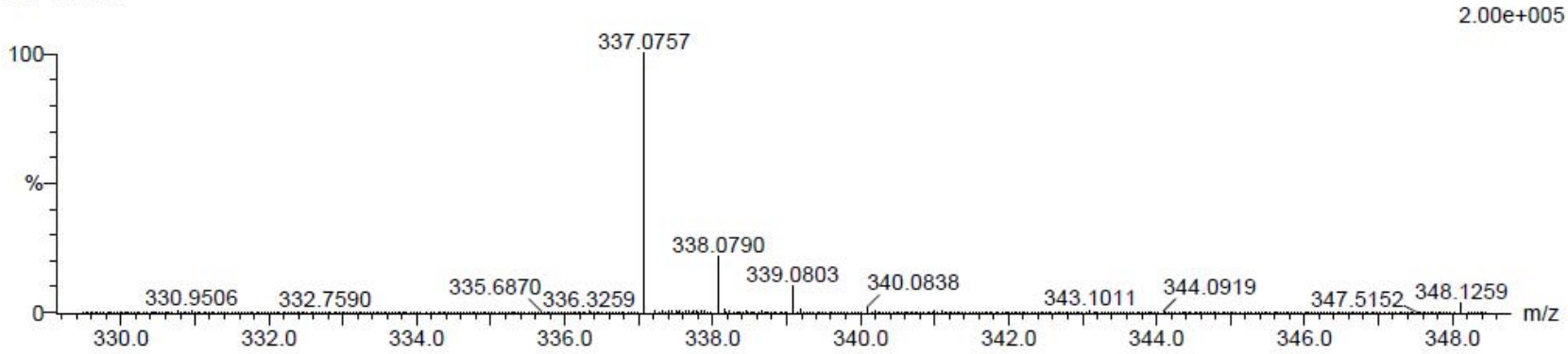

Minimum:				-1.5			
Maximum:		5.0	5.0	100.0			
Mass	Calc. Mass	mDa	PPM	DBE	i-FIT	i-FIT (Norm)	Formula
337.0757	337.0759	-0.2	-0.6	13.5	607.4	0.0	C17 H13 N4 O2 S

1c. methyl 3-(6-amino-3,5-dicyano-4-phenylpyridin-2-ylthio)propanoate

Elemental Composition Report **Page 1**

Single Mass Analysis
Tolerance = 5.0 PPM / DBE: min = -1.5, max = 100.0
Element prediction: Off
Number of isotope peaks used for i-FIT = 3

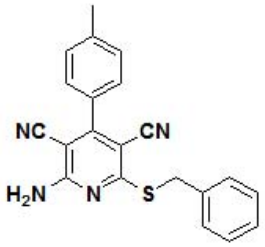

Monoisotopic Mass, Even Electron Ions
6 formula(e) evaluated with 1 results within limits (up to 20 closest results for each mass)
Elements Used:
C: 15-25 H: 10-20 N: 0-5 S: 0-1
Rnc-5 31 (1.013) Cm (1:61)
TOF MS ES-

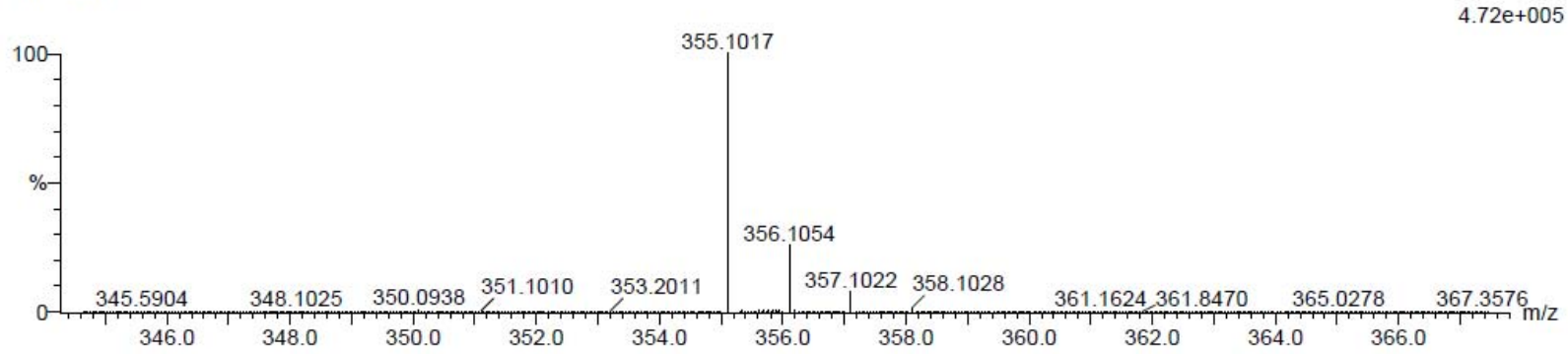

Minimum:				-1.5			
Maximum:		5.0	5.0	100.0			
Mass	Calc. Mass	mDa	PPM	DBE	i-FIT	i-FIT (Norm)	Formula
355.1017	355.1017	0.0	0.0	16.5	604.7	0.0	C21 H15 N4 S

1d. 2-amino-6-(benzylthio)-4-p-tolylpyridine-3,5-dicarbonitrile

Elemental Composition Report

Single Mass Analysis

Tolerance = 5.0 PPM / DBE: min = -1.5, max = 100.0
Element prediction: Off
Number of isotope peaks used for i-FIT = 3

Monoisotopic Mass, Even Electron Ions
17 formula(e) evaluated with 1 results within limits (up to 20 closest results for each mass)
Elements Used:
C: 15-25 H: 10-20 N: 0-5 S: 0-1 Br: 0-1

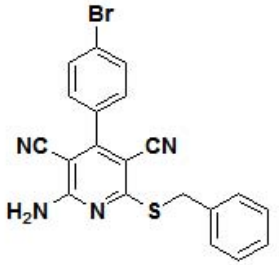

Rnc-6 18 (0.574) Cm (1:61)
TOF MS ES-

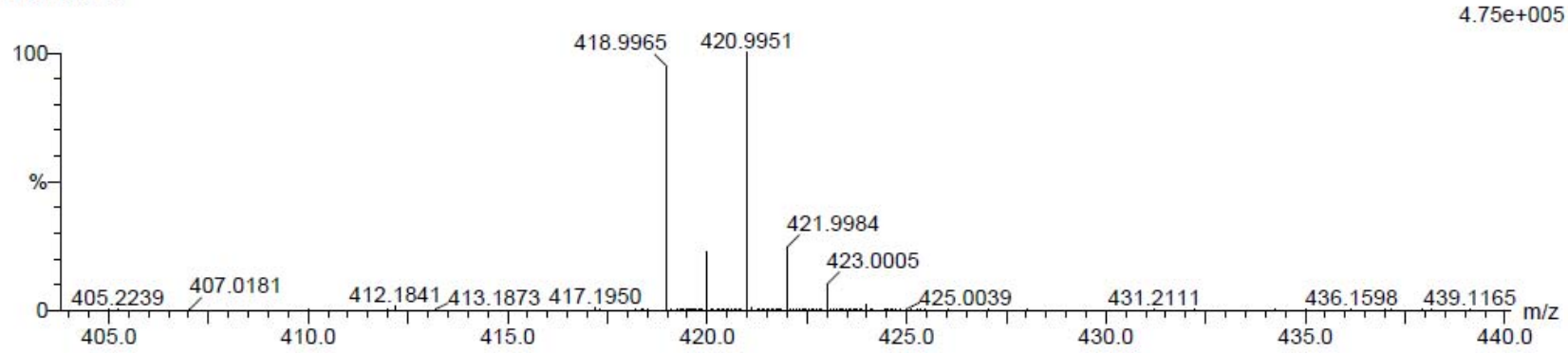

Minimum:				-1.5			
Maximum:		5.0	5.0	100.0			
Mass	Calc. Mass	mDa	PPM	DBE	i-FIT	i-FIT (Norm)	Formula
418.9965	418.9966	-0.1	-0.2	16.5	571.1	0.0	C20 H12 N4 S Br

1e. 2-amino-6-(benzylthio)-4-(4-bromophenyl)pyridine-3,5-dicarbonitrile

Elemental Composition Report

Single Mass Analysis

Tolerance = 5.0 PPM / DBE: min = -1.5, max = 100.0
Element prediction: Off
Number of isotope peaks used for i-FIT = 3

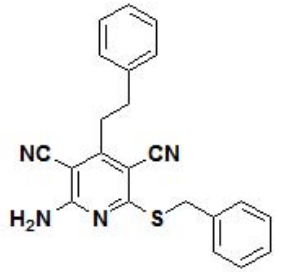

Monoisotopic Mass, Even Electron Ions
6 formula(e) evaluated with 1 results within limits (up to 20 closest results for each mass)
Elements Used:
C: 15-25 H: 10-20 N: 0-5 S: 0-1

Rnc-7 3 (0.068) Cm (1:61)
TOF MS ES-

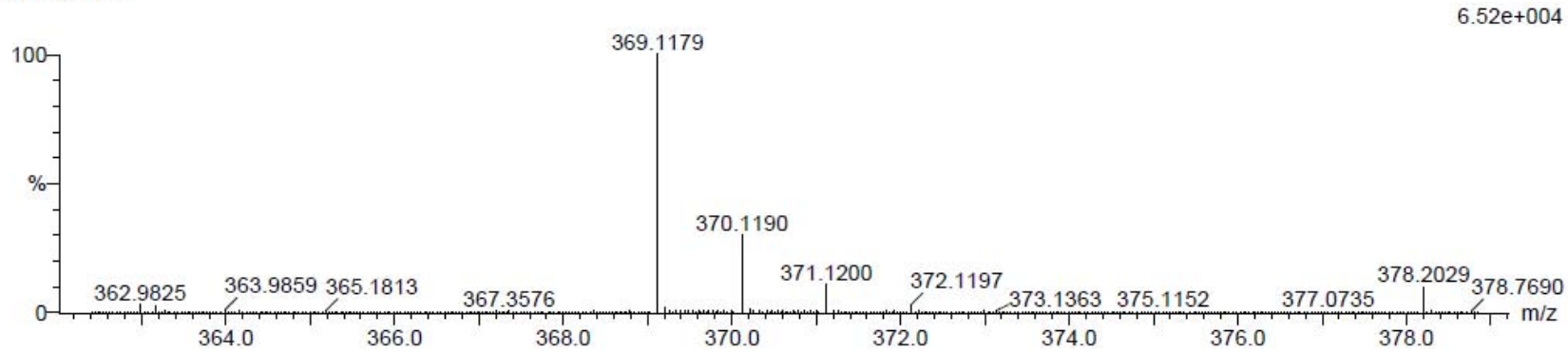

Minimum:				-1.5			
Maximum:		5.0	5.0	100.0			
Mass	Calc. Mass	mDa	PPM	DBE	i-FIT	i-FIT (Norm)	Formula
369.1179	369.1174	0.5	1.4	16.5	539.9	0.0	C22 H17 N4 S

1f. 2-amino-6-(benzylthio)-4-phenethylpyridine-3,5-dicarbonitrile

Elemental Composition Report

Single Mass Analysis

Tolerance = 5.0 PPM / DBE: min = -1.5, max = 100.0
Element prediction: Off
Number of isotope peaks used for i-FIT = 3

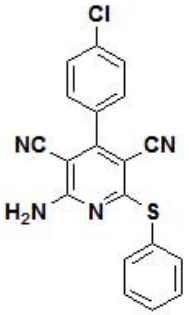

Monoisotopic Mass, Even Electron Ions
18 formula(e) evaluated with 1 results within limits (up to 20 closest results for each mass)
Elements Used:
C: 15-25 H: 10-20 N: 0-5 S: 0-1 Cl: 0-1

Rnc-8 2 (0.034) Cm (1:61)
TOF MS ES-

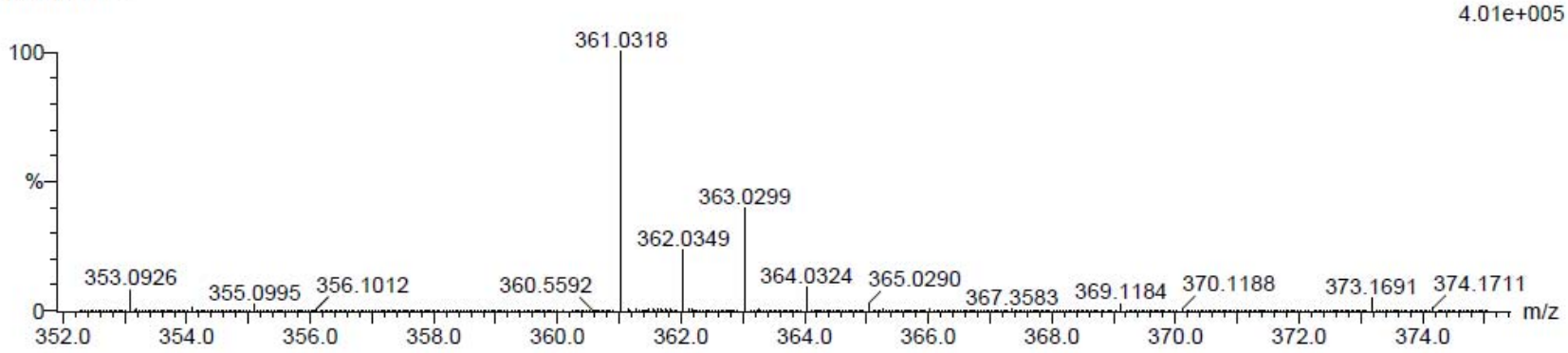

Minimum:				-1.5			
Maximum:		5.0	5.0	100.0			
Mass	Calc. Mass	mDa	PPM	DBE	i-FIT	i-FIT (Norm)	Formula
361.0318	361.0315	0.3	0.8	16.5	615.2	0.0	C19 H10 N4 S Cl

1g. 2-amino-4-(4-chlorophenyl)-6-(phenylthio)pyridine-3,5-dicarbonitrile

Elemental Composition Report

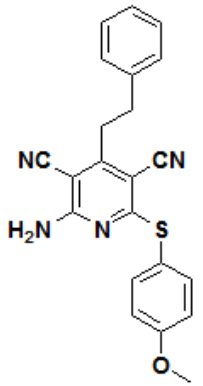

Single Mass Analysis

Tolerance = 5.0 PPM / DBE: min = -1.5, max = 100.0
Element prediction: Off
Number of isotope peaks used for i-FIT = 3

Monoisotopic Mass, Even Electron Ions
145 formula(e) evaluated with 1 results within limits (up to 20 closest results for each mass)
Elements Used:
C: 20-25 H: 15-20 N: 0-5 O: 0-5 S: 0-5

Rnc-14 61 (2.024) Cm (1:61)
TOF MS ES-

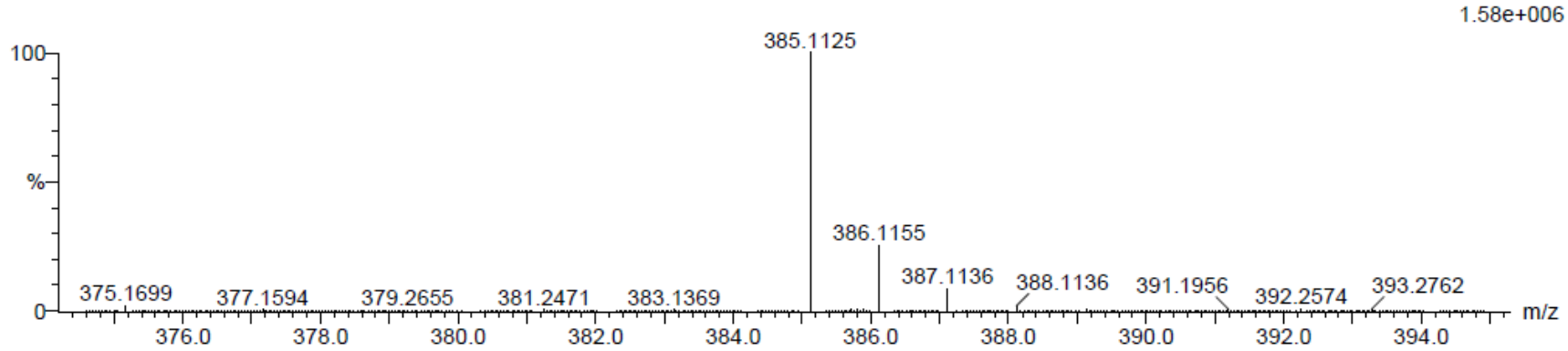

Minimum:				-1.5			
Maximum:		5.0	5.0	100.0			
Mass	Calc. Mass	mDa	PPM	DBE	i-FIT	i-FIT (Norm)	Formula
385.1125	385.1123	0.2	0.5	16.5	571.4	0.0	C22 H17 N4 O S

1h. 2-(4-methoxyphenylthio)-6-amino-4-phenethylpyridine-3,5-dicarbonitrile

Elemental Composition Report

Single Mass Analysis

Tolerance = 5.0 PPM / DBE: min = -1.5, max = 100.0
Element prediction: Off
Number of isotope peaks used for i-FIT = 3

Monoisotopic Mass, Even Electron Ions
15 formula(e) evaluated with 1 results within limits (up to 20 closest results for each mass)
Elements Used:
C: 30-35 H: 25-30 N: 5-10 S: 0-5

Rnc-9 15 (0.473) Cm (1:61)
TOF MS ES-

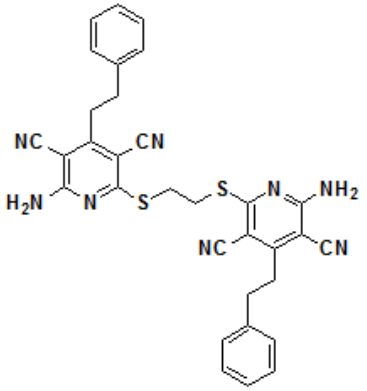

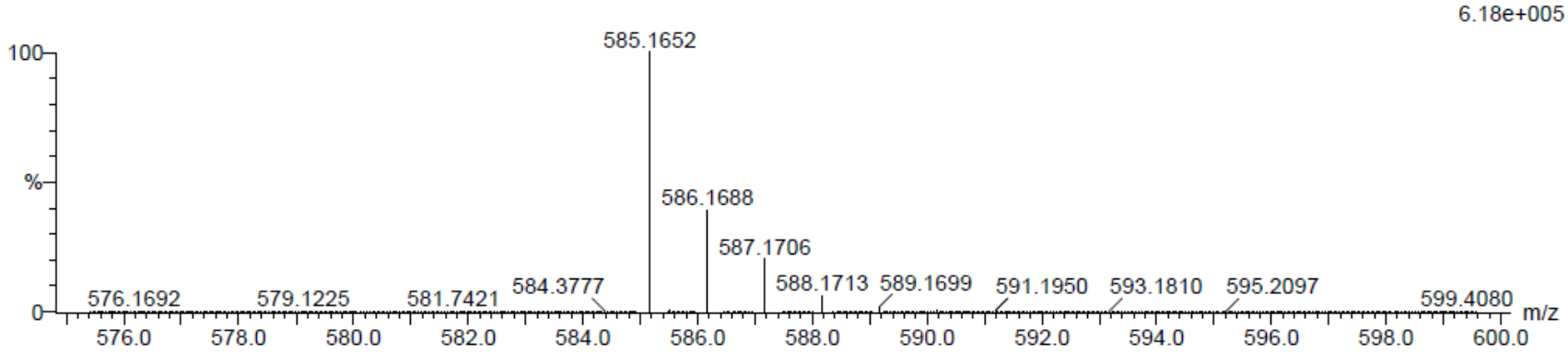

Minimum:				-1.5			
Maximum:		5.0	5.0	100.0			
Mass	Calc. Mass	mDa	PPM	DBE	i-FIT	i-FIT (Norm)	Formula
585.1652	585.1644	0.8	1.4	24.5	376.7	0.0	C32 H25 N8 S2

1i. 2-((2-(6-amino-3,5-dicyano-4-phenethylpyridin-2-ylthio)ethyl)sulfanyl)-6-amino-4-phenethylpyridine-3,5-dicarbonitrile

Supplementary information for Chapter 6
FTIR, NMR and HRMS spectra of quinate salts of ciprofloxacin and norfloxacin

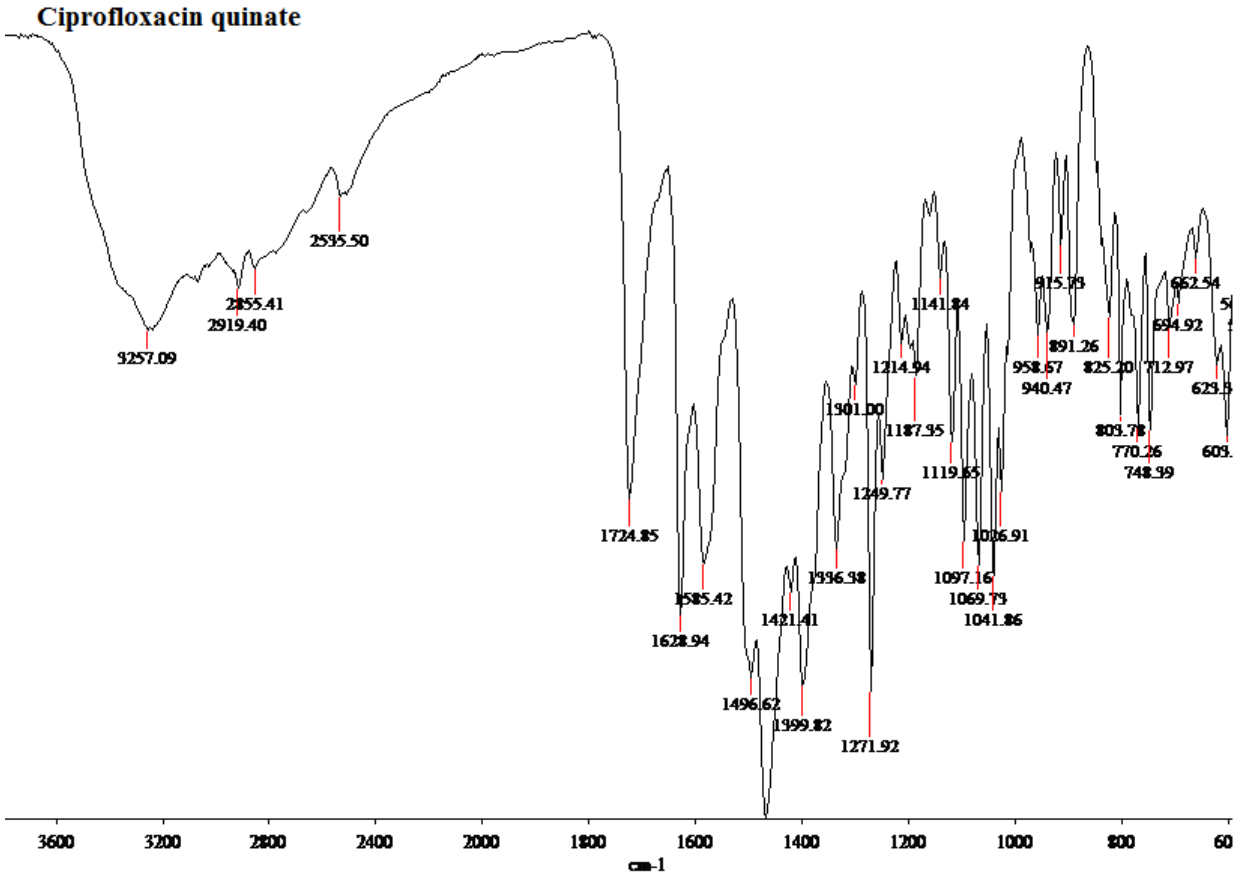
Ciprofloxacin quinate
3257.09
2919.40
2855.41
2595.50
1724.85
1628.94
1585.42
1496.62
1421.41
1399.82
1336.98
1271.92
1249.77
1214.94
1187.95
1141.84
1119.65
1097.16
1069.73
1041.86
1026.91
958.67
940.47
915.73
891.26
825.20
803.73
770.26
748.99
712.97
694.92
652.54
609.
3600
3200
2800
2400
2000
1800
1600
1400
1200
1000
800
cm-1

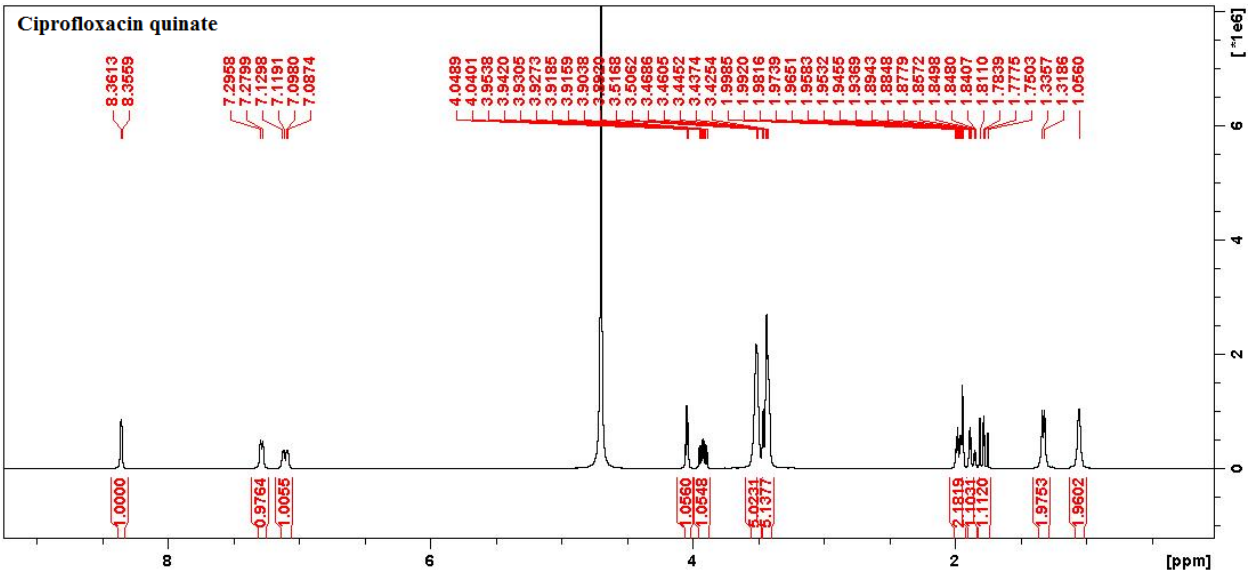
Ciprofloxacin quinate
8.3613
8.3559
7.2958
7.2799
7.1298
7.1191
7.0980
7.0874
4.0489
4.0401
3.9538
3.9420
3.9305
3.9273
3.9185
3.9159
3.9038
3.8820
3.5168
3.5062
3.4686
3.4605
3.4452
3.4374
3.4254
1.9985
1.9920
1.9816
1.9739
1.9651
1.9583
1.9532
1.9455
1.9369
1.8943
1.8848
1.8779
1.8572
1.8498
1.8480
1.8407
1.8110
1.7839
1.7715
1.7503
1.3357
1.3186
1.0560
1.0000
0.9764
1.0055
1.0560
1.0548
5.0231
5.1377
2.1819
2.1701
1.1120
1.9753
1.9602
[*1e6]
[ppm]

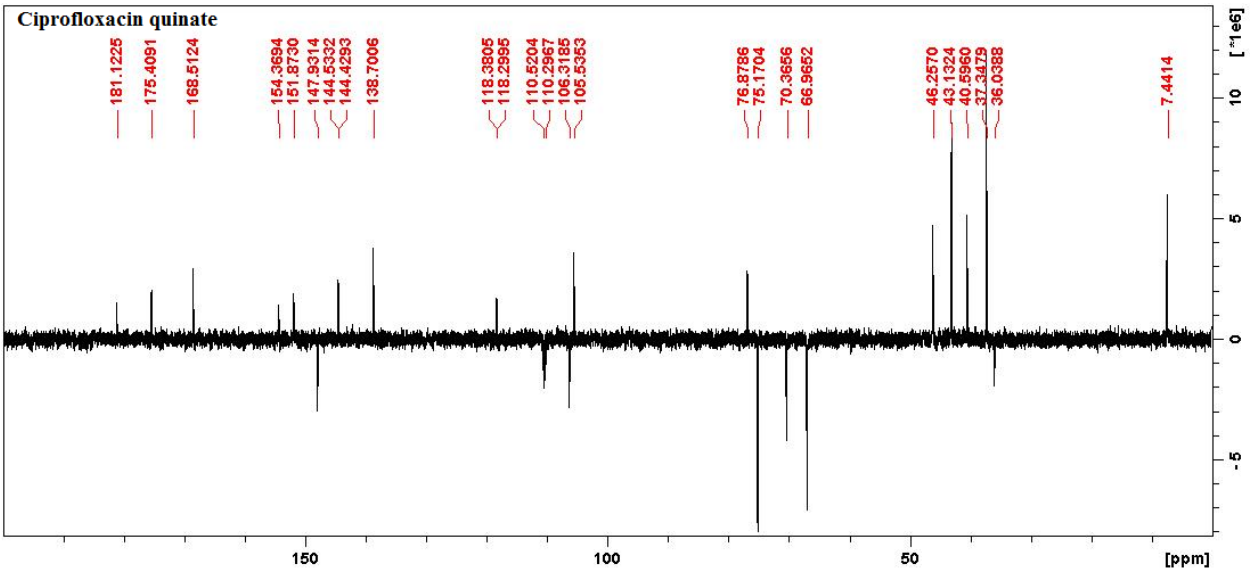
Ciprofloxacin quinate
181.1225
175.4091
168.5124
154.3694
151.8730
147.9314
144.5332
144.4293
138.7006
118.3805
118.2995
110.5204
110.2967
106.3185
105.5353
76.8786
75.1704
70.3656
66.9652
46.2570
43.1324
40.5960
37.3479
36.0388
7.4414
[*1e6]
[ppm]

Ciprofloxacin quinate

Elemental Composition Report

Single Mass Analysis

Tolerance = 5.0 PPM / DBE: min = -1.5, max = 100.0
Element prediction: Off
Number of isotope peaks used for i-FIT = 3

Monoisotopic Mass, Even Electron Ions
4 formula(e) evaluated with 1 results within limits (up to 20 closest results for each mass)
Elements Used:
C: 5-10 H: 10-15 O: 5-10

Rnc-9 - 51 (1.688) Cm (1:61)
TOF MS ES-

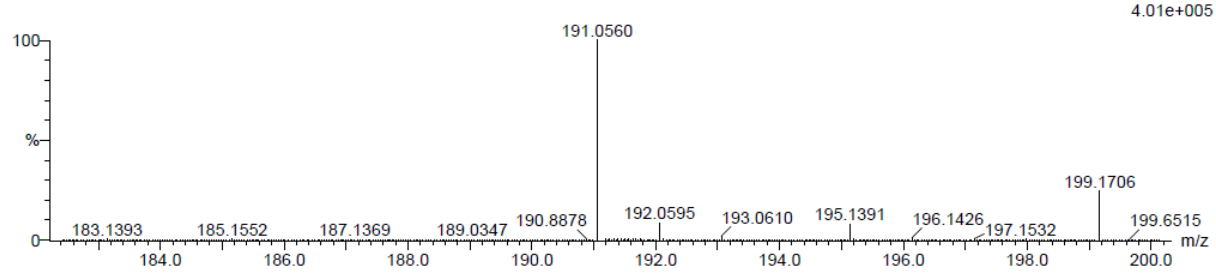

Minimum:				-1.5			
Maximum:		5.0	5.0	100.0			
Mass	Calc. Mass	mDa	PPM	DBE	i-FIT	i-FIT (Norm)	Formula
191.0560	191.0556	0.4	2.1	2.5	719.3	0.0	C7 H11 O6

Elemental Composition Report **Ciprofloxacin quinate** Page 1

Single Mass Analysis

Tolerance = 5.0 PPM / DBE: min = -1.5, max = 100.0
Element prediction: Off
Number of isotope peaks used for i-FIT = 3

Monoisotopic Mass, Even Electron Ions
14 formula(e) evaluated with 1 results within limits (up to 20 closest results for each mass)
Elements Used:
C: 15-20 H: 15-20 N: 0-5 O: 0-5 F: 1-1

Rnc-9 + 58 (1.923) Cm (1:61)
TOF MS ES+

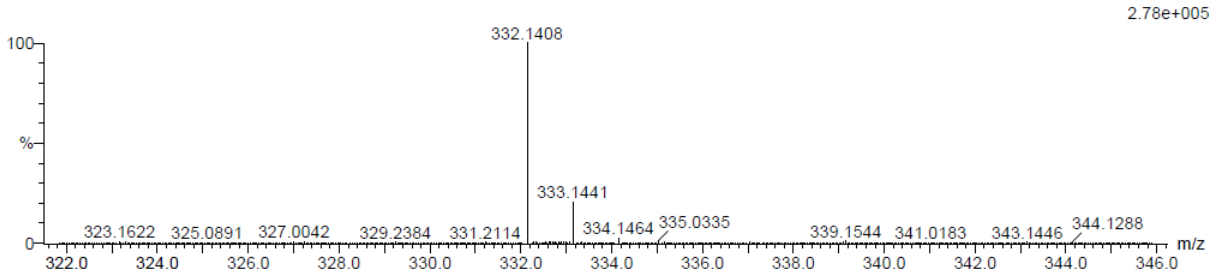

Minimum:				-1.5			
Maximum:		5.0	5.0	100.0			
Mass	Calc. Mass	mDa	PPM	DBE	i-FIT	i-FIT (Norm)	Formula
332.1408	332.1410	-0.2	-0.6	9.5	638.7	0.0	C17 H19 N3 O3 F

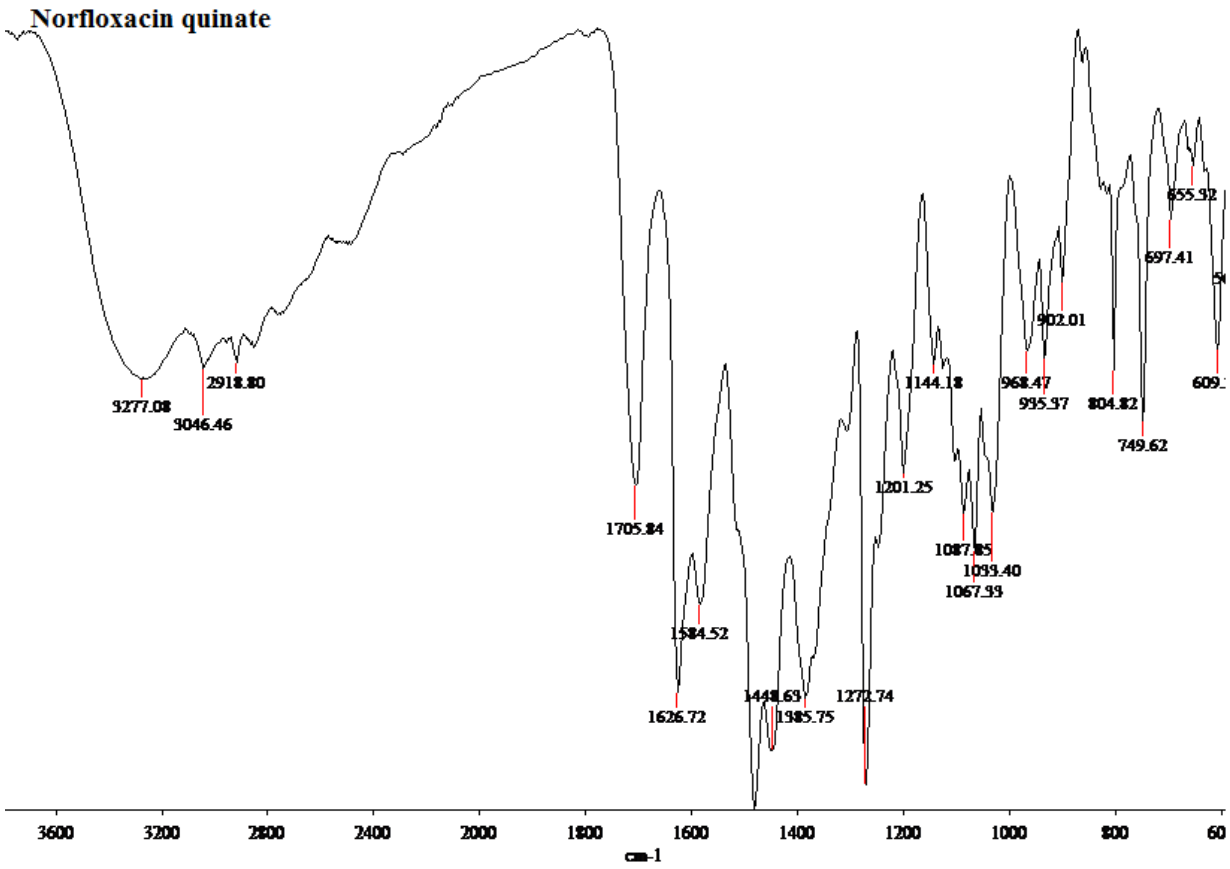
Norfloxacin quinate
3277.08
3046.46
2918.80
1705.84
1626.72
1584.52
1385.75
1272.74
1201.25
1144.18
1087.85
1067.33
968.47
935.97
902.01
804.82
749.62
697.41
655.32
3600
3200
2800
2400
2000
1800
1600
1400
1200
1000
800
cm-1

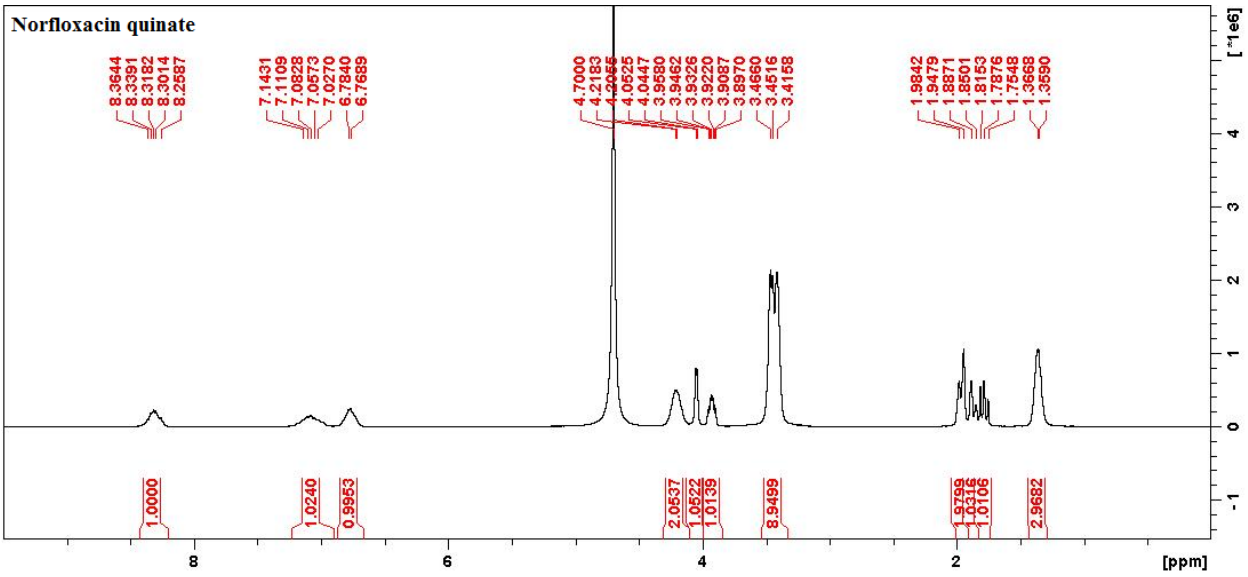
Norfloxacin quinate
8.3644
8.3391
8.3182
8.3014
8.2587
7.1431
7.1109
7.0828
7.0573
7.0270
6.7840
6.7689
4.7000
4.2183
4.0525
4.0447
3.9580
3.9462
3.9326
3.9220
3.9087
3.8970
3.4660
3.4516
3.4158
1.9842
1.9479
1.8871
1.8501
1.8153
1.7876
1.7548
1.3668
1.3590
1.0000
1.0240
0.9953
2.0537
1.0522
1.0139
8.9499
2.9682
[*1e6]
[ppm]

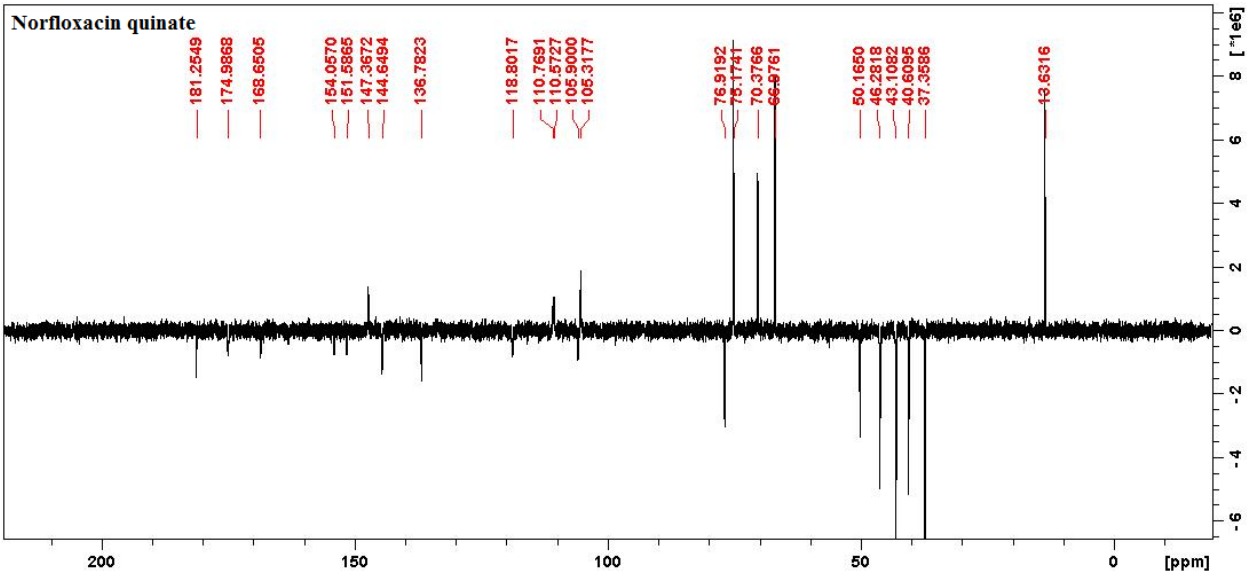
Norfloxacin quinate
181.2549
174.9868
168.6505
154.0570
151.5885
147.3672
144.6494
136.7823
118.8017
110.7691
110.5727
105.9000
105.3177
76.9192
73.1741
70.3766
66.9761
50.1650
46.2818
43.1082
40.6095
37.3586
13.6316
[*1e6]
[ppm]

Elemental Composition Report

Norfloxacin quinate

Page 1

Single Mass Analysis

Tolerance = 5.0 PPM / DBE: min = -1.5, max = 100.0
Element prediction: Off
Number of isotope peaks used for i-FIT = 3

Monoisotopic Mass, Even Electron Ions
4 formula(e) evaluated with 1 results within limits (up to 20 closest results for each mass)
Elements Used:
C: 5-10 H: 10-15 O: 5-10

QNP-10 - 61 (2.024) Cm (1:61)
TOF MS ES-

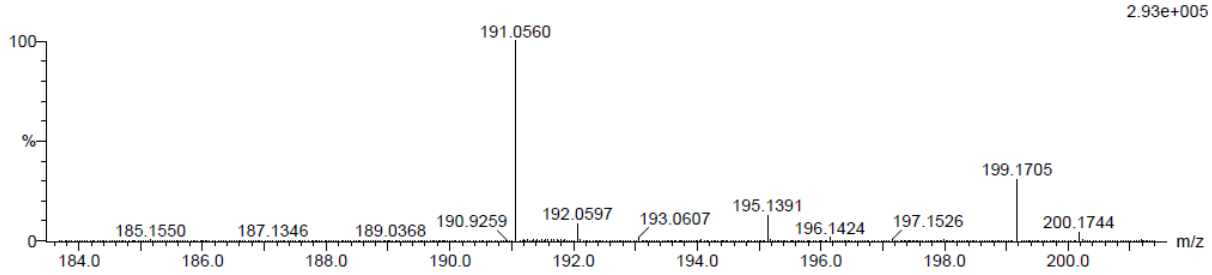

Minimum:				-1.5			
Maximum:		5.0	5.0	100.0			
Mass	Calc. Mass	mDa	PPM	DBE	i-FIT	i-FIT (Norm)	Formula
191.0560	191.0556	0.4	2.1	2.5	695.0	0.0	C7 H11 O6

Elemental Composition Report

Norfloxacin quinate

Page 1

Single Mass Analysis

Tolerance = 5.0 PPM / DBE: min = -1.5, max = 100.0
Element prediction: Off
Number of isotope peaks used for i-FIT = 3

Monoisotopic Mass, Even Electron Ions
17 formula(e) evaluated with 1 results within limits (up to 20 closest results for each mass)
Elements Used:
C: 15-20 H: 15-20 N: 0-5 O: 0-5 F: 1-1

QNP-10 + 24 (0.776) Cm (1:61)
TOF MS ES+

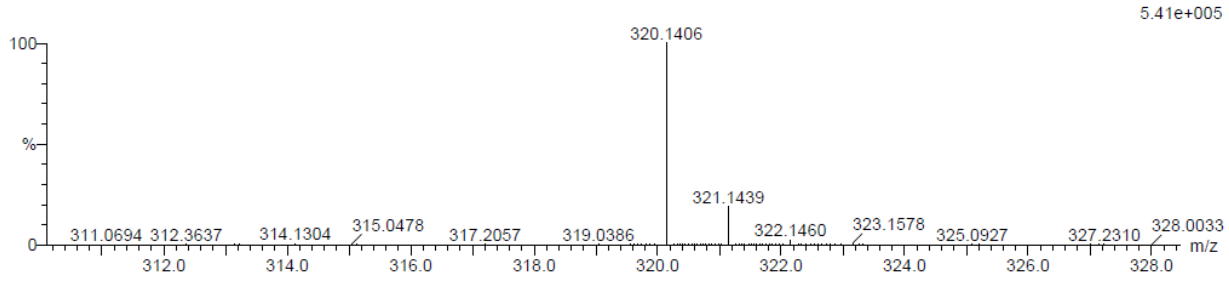

Minimum:				-1.5			
Maximum:		5.0	5.0	100.0			
Mass	Calc. Mass	mDa	PPM	DBE	i-FIT	i-FIT (Norm)	Formula
320.1406	320.1410	-0.4	-1.2	8.5	664.5	0.0	C16 H19 N3 O3 F